

RESEARCH REPORTS
OF THE
FACULTY OF ENGINEERING
MIE UNIVERSITY

V o l . 3 2

D e c e m b e r 2 0 0 7

PUBLISHED BY
FACULTY OF ENGINEERING
MIE UNIVERSITY
TSU, MIE, JAPAN

三重大学工学部研究報告

第32巻

2007年12月

目 次

論 文

佐野和博, 大野義章:

2バンドハバードモデルの強磁性と超伝導…………… 1

博士論文梗概 (2006年度 博士(工学)の学位取得者)…………… 24

論文抄録 (2006年掲載)…………… A-1

著書・編書・訳書・総説抄録 (2006年発行および掲載)…………… A-64

三 重 大 学

工学部研究報告

平成19年12月1日発行

編集兼発行者

三重大学工学部

三重県津市栗真町屋町1577

Research Reports of the Faculty of Engineering
Mie University

Vol.32

December 2007

CONTENTS

Original Papers

Kazuhiro Sano, Yoshiaki Ono

Ferromagnetism and Superconductivity in Two-band Hubbard Models 1

Abstracts of Doctor's Theses (Received The Degree of Doctor of Engineering in 2006)

..... 2 4

Abstracts of Papers (Published in 2006) A - 1

Abstracts of Books and Reviews (Published in 2006) A - 6 4

Research Reports of the Faculty of Engineering, Mie University

Publication Committee(*Chairman)

Naoki ISU*	Professor,Department of Information Engineering
Yasuo TAKEDA	Dean, Faculty of Engineering
Yasuyuki SUZUKI	Professor,Department of Mechanical Engineering
Hiroshi KAWAKAMI	Associate Professor,Department of Mechanical Engineering
Hideki SATOU	Associate Professor,Department of Electrical and Electronic Engineering
Yusuke AOKI	Assistant Professor,Department of Electrical and Electronic Engineering
Toshikazu KITAGAWA	Professor,Department of Chemistry for Materials
Atsushi HIRANO	Assistant Professor,Department of Chemistry for Materials
Satoshi ASANO	Associate Professor,Department of Architecture
Hiroyuki TAKAI	Associate Professor,Department of Architecture
Kazuhiko ONO	Associate Professor,Department of Information Engineering
Ichiro TAKEUCHI	Assistant Professor,Department of Information Engineering
Takashi TAKEO	Professor,Department of Physics Engineering
Yuuji HUJIWARA	Assistant Professor,Department of Physics Engineering

Ferromagnetism and Superconductivity in Two-band Hubbard Models

Kazuhiro Sano and Yoshiaki Ōno*
(Department of Physics Engineering)

(Received July 18, 2007)

Abstract

We investigate ferromagnetism and superconductivity in two types of two-band Hubbard models: the multi-orbital Hubbard model and the d - p model, with particularly paying attention to effect of the interplay between the electron correlation and the band splitting. As strong correlation plays a crucial role for these phenomena, we employ two complementary approaches: the numerical diagonalization method for one-dimensional models and the dynamical mean-field theory for the infinite-dimensional model. These approaches give us reliable results beyond the perturbative approximation or the usual mean-field like approximation. For the one-dimensional models, we calculate the critical exponent K_ρ based on the Tomonaga-Luttinger liquid theory and determine phase diagram of superconducting(SC) region by the condition $K_\rho > 1$. The SC region appears near partially polarized ferromagnetic region in the multi-orbital Hubbard model with finite band splitting. Analysis of pairing correlation functions for the ground state indicates that the triplet pairing is relevant to the superconductivity. In the one-dimensional d - p model, we find enhancements of the singlet and triplet pairing correlations at the SC region. Although only the singlet pairing is relevant to superconductivity near half-filling, the triplet pairing increases with electron filling and is relevant to the superconductivity as well as the singlet pairing near full-filling. In the infinite-dimensional d - p model, we calculate the local green's function on the basis of the dynamical mean-field theory, where the effective impurity Anderson model is solved using the numerical diagonalization method. It shows the phase diagrams of the metal-insulator transition on the ground state at half-filling and quarter-filling as functions of the Coulomb interaction and the band splitting. We obtain the transition temperatures for the ferromagnetism and the superconductivity as functions of the Coulomb interaction, the band splitting and the electron filling. It indicates that the transition temperature of the triplet superconductivity is higher than that of the singlet superconductivity near the ferromagnetic state. These results suggest a close relationship between the ferromagnetism and the superconductivity as a common feature of the two-band Hubbard models.

1 Introduction

The strongly correlated electron systems with multi-band (multi-orbital) have attracted much interest due to various interesting phenomena such as colossal magnetoresistance in manganites $\text{La}_{1-x}\text{Sr}_x\text{MnO}_3$ [1], triplet-pairing superconductivity in the ruthenate Sr_2RuO_4 [2], metal-insulator transition in alkali-doped fullerenes A_xC_{60} [3] and one-dimensional superconductivity of CuO_2 double chain in $\text{Pr}_2\text{Ba}_4\text{Cu}_7\text{O}_{15-\delta}$ [4]. Among them, spin-state transition of cobalt oxides in $\text{La}_{1-x}\text{Sr}_x\text{CoO}_3$ [5, 6, 7] give a good example displaying the effect of multi-orbital. Since the Hund's rule coupling and the crystal-field splitting between the t_{2g} and e_g orbitals are close to each other, the spin state of the cobalt ion depends on temperature, doping concentration and crystal structure. With increasing temperature, the low-spin state ($t_{2g}^6 e_g^0$, $S = 0$) of the Co^{3+} ($3d^6$) ion gradually changes into an intermediate-spin state ($t_{2g}^5 e_g^1$, $S = 1$) and/or a high-spin (HS) state ($t_{2g}^4 e_g^2$, $S = 2$)[6, 7, 8, 9]. With Sr doping, $\text{La}_{1-x}\text{Sr}_x\text{CoO}_3$ shows a spin-glass state for $x < 0.18$ and a ferromagnetism for $x > 0.18$ [10, 11].

Layered cobalt oxides such as Na_xCoO_2 also show a variety of interesting properties as multi-band systems. For example, large thermoelectric power is discovered in $\text{Na}_{0.5}\text{CoO}_2$ [12]. Weak ferromagnetism has been observed in $\text{Na}_{0.75}\text{CoO}_2$ [13]. The discovery of the superconductivity[14] in $\text{Na}_x\text{CoO}_2 \cdot y\text{H}_2\text{O}$ with $T_c \approx 5\text{K}$ for $x \approx 0.35$ and $y \approx 1.3$ has stimulated considerable attention on these materials. It has been suggest that large degeneracy of electronic states due to a competition

*Department of Physics, Niigata University

between the Hund's rule coupling and the crystal-field splitting plays a key role in the electronic states of Na_xCoO_2 as well as of $\text{La}_{1-x}\text{Sr}_x\text{CoO}_3$ [15].

With the new findings of these interesting materials, theoretical studies on the interplay between Coulomb interactions including the Hund's rule coupling and band splitting by crystal-field are highly desirable. The orbitally degenerate Hubbard model, which can be regarded as a kind of multi-band system, has been extensively investigated to clarify the effect of orbital degrees of freedom in the presence of intra-atomic Coulomb interaction. Many authors[16, 17, 18, 19, 20, 21, 22, 23, 24, 25, 26] have studied the ferromagnetism of this model and revealed that Hund's rule coupling plays a crucial role in ferromagnetism.

On the other hand, multi-band Hubbard model, which includes the effect of band splitting explicitly, has also been extensively studied for a long time. In particular, there has been much theoretical interest in the d - p model as a model of the copper oxide high-temperature superconductor. The model contains hopping t_{pd} between the Cu (d -orbital) site and the O(p -orbital) site and strong repulsive interactions at the d and p site (U_d and U_p , respectively). In addition, it can contain the nearest-neighbor d - p interaction U_{pd} and/or hopping t_{pp} between the nearest-neighbor p sites. It is widely accepted as a basic model describing the electronic structure of the Cu-O network. Many theoretical studies have been performed on this model to explain the superconductivity and/or the antiferromagnetism of the copper oxides. A few work has been discussed the possibility of so called flat band ferromagnetism in a type of d - p model[27].

In the present work, we address the multi-orbital Hubbard model in one-dimension and the d - p model in one- and infinite-dimension, while particularly paying attention to the effect of the interplay between the Coulomb interactions and the band splitting Δ . At the point of view of ferromagnetism and superconductivity in itinerant electron systems, we discuss these two models in detail. As the strong correlation effect plays crucial roles in these interesting phenomena, a nonperturbative and reliable approach is required. We employ the numerical diagonalization method for the multi-orbital Hubbard model and the d - p model with finite system sizes in one-dimension, and the dynamical mean field theory for the infinite-dimensional d - p model. These approaches are complementary for each other in dimensionality and expected to give us reliable results beyond the perturbative or the mean-field like approximations.

Numerical diagonalization approach has already been applied for the multi-orbital Hubbard model at $\Delta = 0$ case[17, 18]. Although the available system size is fairly small, the results are in good agreement with the strong coupling analysis[18] and the results from the density-matrix renormalization-group method[23]. To examine the superconductivity, we calculate the critical exponent of the correlation functions K_ρ based on the Luttinger liquid theory[28, 29, 30, 31]. The reliability of this approach has been extensively tested for various one-dimensional models such as the Hubbard model[32], the t - J model[33] and the U - V model[34]. We can thus expect that this approach is reliable for the multi-orbital Hubbard model and the d - p model as well.

In the limit of infinite dimensions, the self-energy becomes purely site-diagonal and the dynamical mean field theory (DMFT) becomes exact. The local Green's function is given by the impurity Green's function of an effective single impurity Anderson model. This effective one-site problem is calculated by the numerical diagonalization of the finite size clusters. By using this method, Momoi et al. studied the multi-orbital Hubbard model at $\Delta = 0$ [17]. They show the phase diagram of the ferromagnetism, but superconductivity was not discussed there. By calculating the magnetization and the pairing susceptibility at finite temperature, we show the transition temperatures for the ferromagnetism and the superconductivity as functions of the Coulomb interaction, the band splitting and the electron filling.

2 Luttinger Liquid Relation

At first, we briefly discuss a general argument for 1D-electron systems based on the Luttinger liquid theory. In the Luttinger liquid theory[28, 29, 30, 31], an effective Hamiltonian of 1D models in the Tomonaga-Luttinger regime is generally given by

$$H = \frac{v_\sigma}{2\pi} \int_0^L dx [K_\sigma (\partial_x \theta_\sigma)^2 + K_\sigma^{-1} (\partial_x \phi_\sigma)^2] + \frac{v_\rho}{2\pi} \int_0^L dx [K_\rho (\partial_x \theta_\rho)^2 + K_\rho^{-1} (\partial_x \phi_\rho)^2], \quad (1)$$

where v_σ , v_ρ , K_σ and K_ρ are the velocities and coupling parameters of spin and charge parts, respectively. According to the Luttinger liquid theory, some relations have been established as universal

relations in one-dimensional single band models[30, 31]. In the model which is isotropic in spin space, the coupling constant K_σ is renormalized to unity in the low energy limit and the critical exponents of various types of correlation functions are determined by a single parameter K_ρ .

For single band model, it is predicted that SC correlation is dominant for $K_\rho > 1$ (the correlation function decays as $\sim r^{-(1+\frac{1}{K_\rho})}$ in the Tomonaga-Luttinger (TL) regime and as $\sim r^{-\frac{1}{K_\rho}}$ in the Luther-Emery (LE) regime), whereas the CDW or SDW correlations are dominant for $K_\rho < 1$ (the correlation functions decay as $\sim r^{-(1+K_\rho)}$ in the TL regime and as $\sim r^{-K_\rho}$ in the LE regime). Here, the LE regime is characterized by a gap in the spin excitation spectrum, while in the TL regime, the excitation is gapless[28, 31]. In the case of non-interacting fermion systems, the exponent K_ρ is always unity. Thus, the effective interaction between quasi-particles is attractive for $K_\rho > 1$ whereas that is repulsive for $K_\rho < 1$.

The critical exponent K_ρ is related to the charge susceptibility χ_c and the Drude weight D by

$$K_\rho = \frac{1}{2}(\pi\chi_c D)^{1/2}, \quad (2)$$

with $D = \frac{\pi}{N_u} \frac{\partial^2 E_0(\phi)}{\partial \phi^2}$, where $E_0(\phi)$ is the total energy of the ground state as a function of magnetic flux $N_u \phi$ [31]. Here, the flux is imposed by introducing the following gauge transformation: $c_{m\sigma}^\dagger \rightarrow e^{im\phi/N_u} c_{m\sigma}^\dagger$ for an arbitrary site m . When the charge gap vanishes in the thermodynamic limit, the uniform charge susceptibility χ_c is obtained from

$$\chi_c = \frac{4/N_u}{E_0(N_e + 2, N_u) + E_0(N_e - 2, N_u) - 2E_0(N_e, N_u)}, \quad (3)$$

where $E_0(N_e, N_u)$ is the ground state energy of a system with N_u unit sites(cells) and N_e electrons. The filling n is defined by $n = N_e/N_u$, where N_u is the total number of unit cells or sites. The values of D and χ_c are calculated from the ground state energy of the finite size system through eq.(2) and (3).

It is noted that the situation is complicated for two-band models. When both bands have been occupied by electrons simultaneously, Fermi points appear in both bands. In this case, the electronic state of the low energy is completely changed and we can not use the above relations[35, 36, 37, 38]. On the other hand, if the electron density is sufficiently small and/or the band splitting is sufficiently large, electrons occupy only lower band. In this case, Fermi level exists in only lower band and the low energy effective Hamiltonian is considered to be equivalent to that of the single band model. Therefore, we can adopt the above Luttinger liquid relations of the single band model for even two-band model.

We numerically diagonalize the model Hamiltonian and obtain the value of K_ρ from the ground state energy of finite size systems using the standard Lanczos algorithm. In addition to the numerical diagonalization method, we use mean-field(MF) approximation to calculate the ground state energy and obtain the approximate value of K_ρ of the infinite system. This approximation has been confirmed to be reliable at least in the weak coupling regime[39].

3 Multi-orbital Hubbard Model

Previous works[17, 18, 19, 20, 21, 22, 23, 24] have studied the multi-orbital Hubbard model in the case of the crystal-field splitting $\Delta = 0$. In one dimension, some rigorous results are shown in the strong coupling limit $U \rightarrow \infty$: the ground state is a fully polarized ferromagnetism for $0 < n < 2$ except for $n = 1$ when U' and $J = J'$ are positive and finite[21]. The numerical result suggests that the ferromagnetism is stable also for $n = 1$ in the strong coupling region[23]. In infinite dimensions, the dynamical mean-field theory shows the existence of the ferromagnetism in the same parameter region observed in one dimension[22]. They revealed that Hund's rule coupling J plays a crucial role in ferromagnetism. However, possible mechanisms of superconductivity and the effect of crystal-field splitting Δ was not considered in these studies.

In this section, we examine ferromagnetism and related superconductivity in the multi-orbital Hubbard model, while particularly paying attention to the effect of the interplay between J and Δ [40, 41, 42].

3.1 Model Hamiltonian

We consider the following Hamiltonian for the one-dimensional multi-orbital Hubbard model:

$$\begin{aligned}
 H = & -t \sum_{i,m,\sigma} (c_{i,m,\sigma}^\dagger c_{i+1,m,\sigma} + h.c.) + U \sum_{i,m} n_{i,m,\uparrow} n_{i,m,\downarrow} \\
 & + U' \sum_{i,\sigma} n_{i,u,\sigma} n_{i,l,-\sigma} + (U' - J) \sum_{i,\sigma} n_{i,u,\sigma} n_{i,l,\sigma} + \frac{\Delta}{2} \sum_{i,\sigma} (n_{i,u,\sigma} - n_{i,l,\sigma}) \\
 & - J \sum_{i,m} (c_{i,u,\uparrow}^\dagger c_{i,u,\downarrow} c_{i,l,\downarrow}^\dagger c_{i,l,\uparrow} + h.c.) - J' \sum_{i,m} (c_{i,u,\uparrow}^\dagger c_{i,u,\downarrow}^\dagger c_{i,l,\uparrow} c_{i,l,\downarrow} + h.c.), \quad (4)
 \end{aligned}$$

where $c_{i,m,\sigma}^\dagger$ stands for the creation operator of an electron with spin σ in the orbital m ($= u, l$) at site i and $n_{i,m,\sigma} = c_{i,m,\sigma}^\dagger c_{i,m,\sigma}$. Here, t represents the hopping integral between the same orbitals and we set $t = 1$ in this study.

The interaction parameters U , U' , J and J' stand for the intra- and inter-orbital direct Coulomb interactions, the exchange (Hund's rule) coupling and the pair-transfer, respectively. Δ denotes the energy difference between the two atomic orbitals, that is, crystal-field splitting. For simplicity, we impose the relations, $J = J'$ and $U = U' + 2J$; the latter holds exactly in $3d$ -orbitals for $\Delta = 0$ and is a good approximation for $\Delta \neq 0$. The model in eq. (4) is schematically represented by Fig. 1(a). We numerically diagonalize the above model Hamiltonian up to 9 sites. In the noninteracting case ($U = U' = J = 0$), the Hamiltonian eq. 4 yields a dispersion relation $\epsilon^\pm(k) = -2t \cos(k) \pm \frac{\Delta}{2}$, where k is the wave vector and $\epsilon^+(k)$ ($\epsilon^-(k)$) represents the upper (lower) band energy. This band structure is schematically represented by Fig. 1(b).

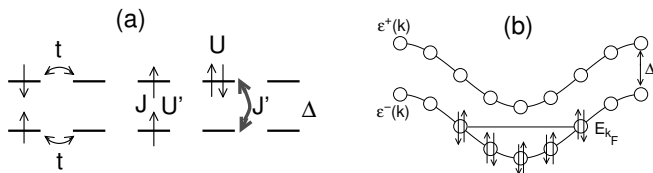


Figure 1: Schematic diagrams of (a) the model Hamiltonian and (b) the band structure in the noninteracting case.

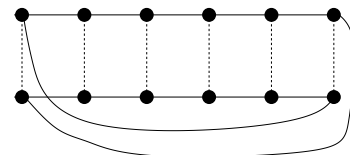


Figure 2: Schematic diagram of Moebius boundary condition at $\Delta = 0$.

3.2 Result for degenerate case

We first exhibit the result at $\Delta = 0$ and compare it with the previous works. At $\Delta = 0$, two bands are doubly degenerate and the finite size effect of the ordinary periodic boundary condition is fairly large. To reduce it, we use the Moebius boundary condition, which has been already used in t - J ladder models[43]. The Moebius boundary condition as shown in Fig.2, is a kind of the periodic boundary condition and efficiently reduces the finite size effect of the systems than the ordinary periodic boundary condition.

Figure 4 shows the phase diagram of the ground state for the $N_u = 8$ system at $n = 0.5$ (4electrons/8sites) with the result of the DMRG method by Sakamoto et al.[23] on the U' vs. J parameter plane. A ferromagnetic ground state with full spin polarization($S = max$) appears around $J \simeq U'$ for $U' \gtrsim 3$. The parameter regions $J/U' \gg 1$ and $J/U' \ll 1$ are paramagnetic($S = 0$). No partially polarized state was found at this filling. Figure also shows that the difference between our result and the DMRG result is small. The present result is similar to those by previous studies employing the periodic or the anti-periodic boundary conditions, but the phase boundaries of their ferromagnetic phases seem to depend on the system size greatly. We also indicate the phase boundary of the ferromagnetic phase by using the mean-field(MF) approximation in Fig.4. In this approximation, the ground-state energy E_0 is calculated as

$$\begin{aligned}
 E_0 = & \langle H \rangle \\
 = & \sum_{k < k_F, m, \sigma} \epsilon^\pm(k) + U N_u \sum_m \langle n_{m,\uparrow} \rangle \langle n_{m,\downarrow} \rangle + U' N_u \sum_\sigma \langle n_{u,\sigma} \rangle \langle n_{l,-\sigma} \rangle \\
 & + (U' - J) N_u \sum_\sigma \langle n_{u,\sigma} \rangle \langle n_{l,\sigma} \rangle + \frac{\Delta}{2} N_u \sum_\sigma (\langle n_{u,\sigma} \rangle - \langle n_{l,\sigma} \rangle), \quad (5)
 \end{aligned}$$

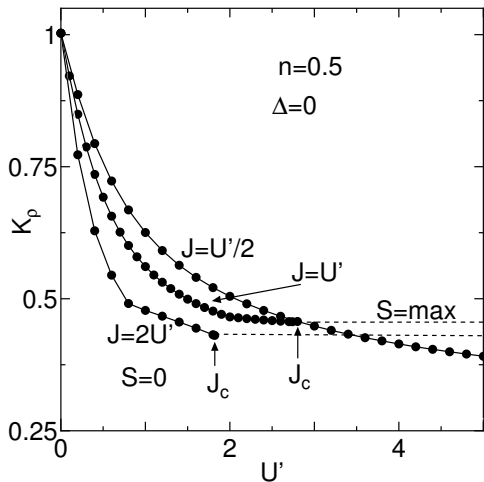


Figure 3: K_ρ as a function of U' in the cases of $J = U'/2$, $J = U'$ and $J = 2U'$ at $n = 0.5$ (4electrons/8sites). J_c indicates the critical point of the singlet ground state changing into the fully polarized ferromagnetic ($S=\max$) ground state.

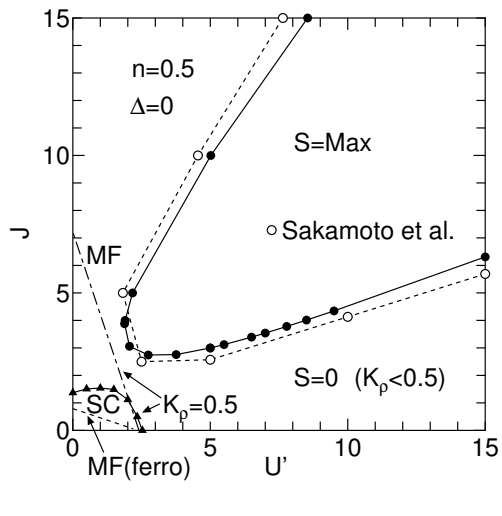


Figure 4: Phase diagram of the ferromagnetic state on the $U' - J$ parameter plane for $n = 0.5$ (4electrons/8sites) at $\Delta = 0$. The dashed line represents the phase boundary of the ferromagnetic state obtained by MF approximation. The solid triangle shows the point of $K_\rho = 0.5$ on the U' -axis.

where $\langle \rangle$ represents the expectation value of operators by the noninteracting ground state. Here, the terms $-J \sum_{i,m} (c_{i,u,\uparrow}^\dagger c_{i,u,\downarrow} c_{i,l,\downarrow}^\dagger c_{i,l,\uparrow} + h.c.)$ and $-J' \sum_{i,m} (c_{i,u,\uparrow}^\dagger c_{i,u,\downarrow}^\dagger c_{i,l,\uparrow} c_{i,l,\downarrow} + h.c.)$ are omitted since the expectation values of these terms are equal to zero. The result indicates that the ferromagnetic phase appears all over the region except the near the origin. Comparing with the numerical results, it seems to overestimate the ferromagnetic region.

Figure 5 shows the value of K_ρ as a function of U' for $J = 0$ at quarter filling $n = 1$ (4electrons/4sites). We also show the result of the Green's function Monte Carlo method obtained by Assaraf et al.[44] and the MF approximation for K_ρ [39], which are represented by the broken and the dashed lines in fig.5, respectively. Here, K_ρ of the MF approximation is estimated by the Luttinger liquid relation as well as Numerical diagonalization method and the ground state is restricted to the singlet state, that is, the condition $\langle n_{m,\uparrow} \rangle = \langle n_{m,\downarrow} \rangle$ is imposed. It shows good agreement with the numerical result in the weak coupling regime, ensuring the small finite-size effect of the numerical calculation. As U' increases, K_ρ decreases from unity to ~ 0.42 . For $J = 0$, the model Hamiltonian is equivalent to the SU(4) Hubbard model and the metal-insulator(MI) transition occurs at $K_\rho = 0.5$ [44]. When U' is larger than a critical value $U'_c \sim 3$, the MI transition is expected. Sakamoto et al. show the n -dependence of the chemical potential at quarter filling and the existence of large charge gap in the strong coupling region. Although the finite size effect does not allow the correct estimation of the transition point, they claim that the metal-insulator transition occurs at finite positive value of $U' = J \sim 3$.

Figure 6 gives the value of K_ρ as a function of U' in several conditions of $J = U'/2$, $J = U'$ and $J = 2U'$ at $n = 1$. As U' increases, K_ρ decreases, while it increases for a large U' in the condition $J = 2U'$. In the region $K_\rho > 0.5$, the SC correlation is expected to be the most dominant compared with the CDW and SDW correlations. To confirm the SC state, we calculate the lowest energy of the singlet state $E_0(\phi)$ as a function of an external flux ϕ . As shown in Fig.7, the anomalous flux quantization occurs in the region $K_\rho > 0.5$, where the signature of it increases with J . It indicates that the SC state is surely realized in this parameter region.

In Figure 8, we give the phase diagram of the ground state for $N_u = 4$ at the electron density $n = 1$ (4electrons/4sites) with the result of DMRG method[23] on the U' vs. J parameter plane. A complete ferromagnetism with $S=\max$ appears around $J \simeq U'$ in the strong coupling regime. This result is in good agreement with the DMRG result obtained by Sakamoto *et al.*[23]. The dashed line presents the boundary between the ferromagnetic state and the singlet state by using the mean-field approximation. It seems to be fairly overestimate for the ferromagnetic region. It also indicates that

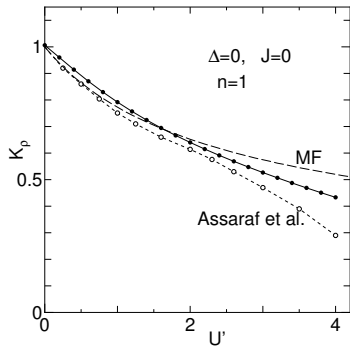


Figure 5: K_ρ as a function of U' in the cases of $J = 0$ for $n = 1.0$ (4electrons/4sites) at $\Delta = 0$. The dashed line represents a MF estimation for K_ρ . The broken line indicates the GFMC result obtained by Assaraf et al.

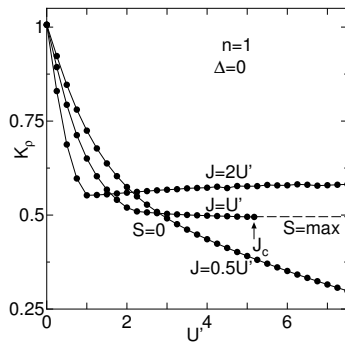


Figure 6: K_ρ as a function of U' in the cases of $J = U'/2$, $J = U'$ and $J = 2U'$ for $n = 1.0$ (4electrons/4sites) at $\Delta = 0$.

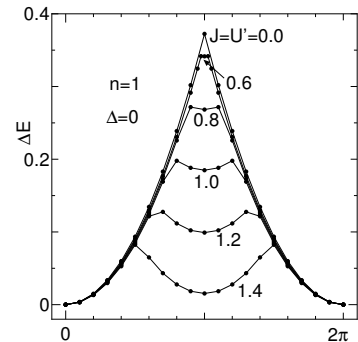


Figure 7: The energy difference $E_0(\phi) - E_0(0)$ as a function of an external flux ϕ at $n = 1.0$ (6electrons/6sites) at $\Delta = 0$.

the ferromagnetic region is smaller than the case of $n = 0.5$. In this ferromagnetic region, Sakamoto *et al.* also claimed that the system shows the triplet SC for $J > U'$, while it becomes insulator for $J < U'$. The SC phase boundary in the ferromagnetic region is smoothly connected to that in the paramagnetic region as shown in Fig. 8. These results tell us that the Hund's rule coupling J plays important roles not only for the ferromagnetism but also for the superconductivity. In the paramagnetic state ($S=0$), we plot the phase boundary separating the SC region with $K_\rho > 0.5$ and the insulating region with $K_\rho < 0.5$. As mentioned above, this SC phase is confirmed by the anomalous flux quantization, while this quantization disappears in the insulating region with large U' (not shown). Within the bosonization method, the SC state has been identified as the triplet SC with spin gap[25]. However, very recent work claims that the relevant symmetry of the pairing is not

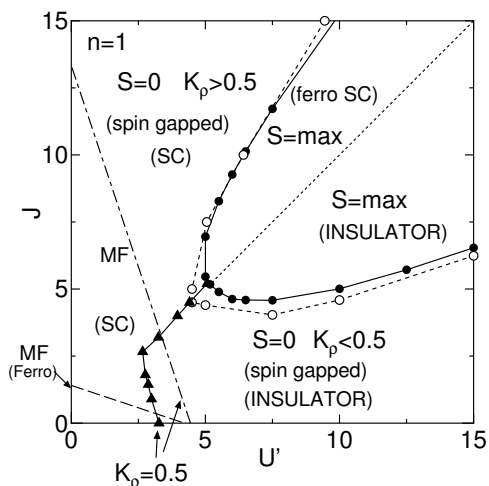


Figure 8: Phase diagram of the ferromagnetic state on the $U' - J$ parameter plane for $n = 1$ (4electrons/4sites) at $\Delta = 0$. The dashed line represents the phase boundary of the ferromagnetic state obtained by MF approximation. The solid triangle shows the point of $K_\rho = 0.5$ on the U' -axis.

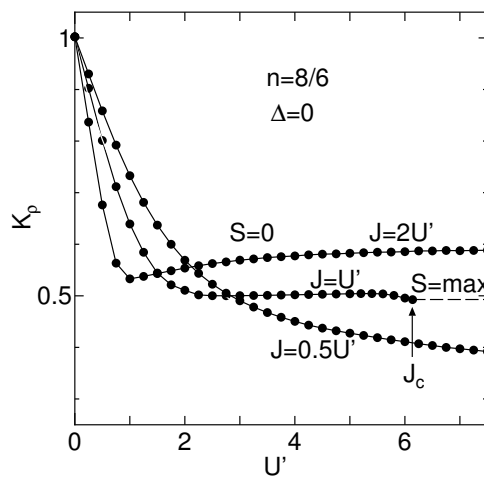


Figure 9: K_ρ as a function of U' for $n = 4/3$ (8electrons/6sites) at $\Delta = 0$.

' p -' wave like triplet but ' d_{xy} -' like singlet by using the bosonization method and DMRG method within the model at $U' = 0$ [26].

To examine the case of over the quarter-filling($n=1$), we calculate the value of K_ρ as a function of U' in several conditions of $J = U'/2$, $J = U'$ and $J = 2U'$ at $n = 4/3$ (8electrons/6sites). As shown in Figure 9, it seems to be similar to the case of ($n \leq 1$). This result suggests that the overall aspect of the electronic state dose not much depend on n .

3.3 Case for finite Δ

Next, we consider the case of $\Delta > 0$. When the lowest energy of the upper band, $\epsilon^+(0)$, is larger than the Fermi energy, E_{k_F} , electrons occupy only the lower band with $k_F = \frac{\pi n}{2}$ and the model is regarded as a "single component" electron system. Hereafter, we mainly treat the case with $\epsilon^+(0) > E_{k_F}$. In this case, we can not adopt the Moebius boundary condition, since the symmetry of inter-band is broken by finite Δ . In the case $n < 1$, we find the following boundary conditions are suitable, that is, the periodic(antiperiodic) boundary condition for the lower(upper) band at $N_e = 4m + 2$ and the antiperiodic(periodic) boundary condition for the upper(lower) band at $N_e = 4m$, where N_e is the total electron number and m is an integer. This boundary condition can be regard as an extension of the Moebius boundary condition for the finite Δ .

For $n > 1$, on the other hand, our experience indicates that the usual boundary conditions, that is, the periodic boundary condition at $N_e = 4m + 2$ and the antiperiodic boundary condition at $N_e = 4m$ for the both bands, are little better. This choice of the boundary conditions is rather empirical, but it seems to lead better results.

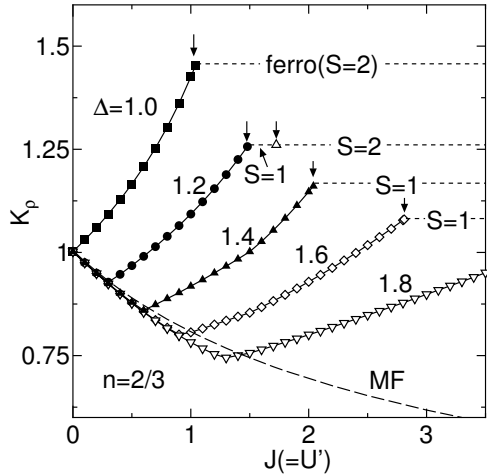


Figure 10: K_ρ as a function of $J(=U')$ for $n = 2/3$ (6electrons/9sites) at $\Delta = 1.0, 1.2, 1.4, 1.6,$ and 1.8 . The down arrows indicate the critical points of $J(=U')$. The dashed line represents a weak coupling estimation for K_ρ .

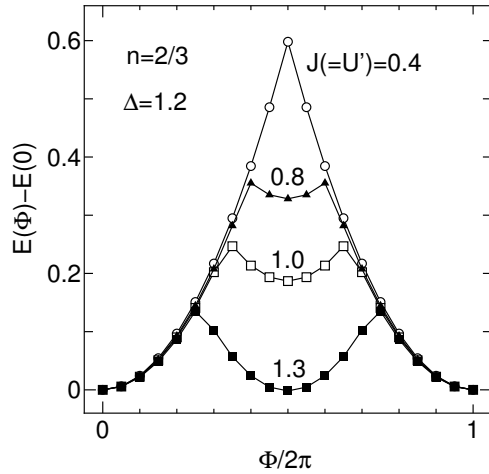


Figure 11: The energy difference $E_0(\phi) - E_0(0)$ as a function of an external flux ϕ for $J(=U') = 0.4, 0.8, 1.0$ and 1.3 at $n = 2/3$ (6electrons/9sites) and $\Delta = 1.2$.

Figure 10 shows the value of K_ρ as a function of $J(=U')$ for several values of Δ at the electron density $n = 2/3$ (6electrons/9sites). As J increases, K_ρ decreases for a small J , while it increases for a large J , and then becomes larger than unity. Since we consider the single component system, the SC correlation is expected to be the most dominant compared with the CDW and SDW correlations in the region $K_\rho > 1$. To confirm the superconducting state, we calculate the lowest energy of the singlet state $E_0(\phi)$ as a function of an external flux ϕ . As shown in Fig. 11, the anomalous flux quantization occurs clearly at $J \sim 1.3$, where K_ρ is about 1.1. When $J = 0.4$, K_ρ is less than unity and the anomalous flux quantization is not found.

When J is larger than a certain critical value, the ground state changes into the partially ferromagnetic state with $S=1$ or $S=2$ from the singlet state. In Fig. 10, the broken line represents the MF approximation for K_ρ . This approximation depends upon only the noninteracting ground state where the lower band is exclusively occupied, as shown in Fig. 1. Therefore, the effect of the upper

band is omitted and the result is independent of Δ . This approximation breaks down when the effect of the upper band becomes crucial. In this regime, K_ρ rapidly increases with increasing J , and finally becomes larger than unity indicating the superconducting state. The critical values of J with $K_\rho = 1$ are $J_c \approx 0.3, 1.0, 2.4$ and 4.0 for $\Delta = 1.0, 1.2, 1.6$ and 1.8 , respectively.

In Fig.12, we show the phase diagram of the superconducting state with $K_\rho > 1$ together with the partial ferromagnetic state with $S = 1$ and $S = 2$ on the U' vs. J parameter plane for $n = 2/3$ (6electrons/9sites) at $\Delta = 1.2$, where the $S = 2$ state is depicted by the bunch of thin solid circles(shadowed region). The superconducting phase appears near the partially polarized ferromagnetic region. It extends from the attractive region with $J < 0$ and $U' < 0$ to the realistic parameter region for $3d$ transition-metals with $U' > J > 0$. We have confirmed that the superconducting region increases as Δ decreases, as shown in Fig.10.

Figure 13 shows the global phase diagram on the $U' - J$ plane for $n = 4/3$ (8electrons/6sites) at $\Delta = 4.0$. When $U' \gtrsim J \gtrsim \Delta$, the fully polarized ferromagnetism with $S = S_{\max}$ appears. It accompanies the partially polarized ferromagnetism with $0 < S < S_{\max}$ for $J \lesssim \Delta$. Inset shows the magnification of the phase diagram near the origin. As well as $n < 1$, the superconducting state with $K_\rho > 1$ appears near the partially polarized ferromagnetic region and it extends to the realistic parameter region with $U' > J > 0$. The configuration of the partially polarized ferromagnetic state and the superconducting state is similar to the case $n < 1$. When J exceeds $\epsilon^+(0) - E_{k_F}$, the inter-band excitation develops and the occupation number of the upper band increases, which results in a large orbital fluctuation accompanied by the fluctuation between the low-spin and the high-spin states. The mechanism of superconductivity may be related to this orbital fluctuation. We note that superconductivity is also observed for the $J' = 0$ ($J \neq 0$) case in contrast to the previous study[45, 46], where the pair-transfer J' is crucial to superconductivity. The existence of the partially polarized ferromagnetism for $\Delta > 0$ has been reported in a different type of two-band Hubbard model[40].

In Fig. 14, we show the doping dependence of the critical values of J for the superconductivity and the ferromagnetism at $\Delta = 4$ with $J = U'$, where we use $n=4/3, 10/7, 3/2, 8/5$ and $12/7$ systems. We determine the critical values on condition that $K_\rho > 1$ for the superconductivity and $S > 0$ for the ferromagnetism. Although the finite size effect is considerably large, the phase boundary for the superconductivity can be approximately given by the phenomenological equation, $J_c = \epsilon^+(0) - E_{k_F}$. Here, $\epsilon^+(0) - E_{k_F}$ corresponds to the lowest energy of the single-particle excitation from the lower band to the upper band. This equation was found to be a good approximation for various $n > 1$ [41].

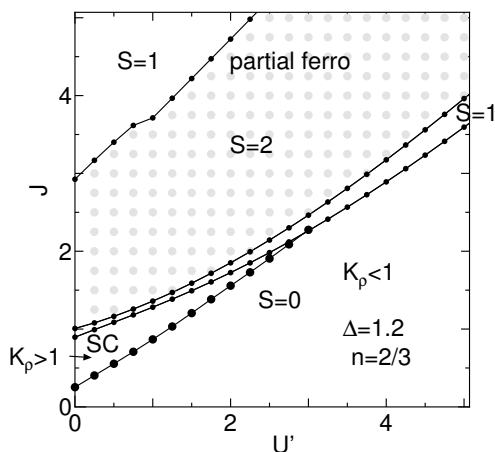


Figure 12: Phase diagram of the superconducting state with $K_\rho > 1$ and the ferromagnetic states with $S = 1$ and $S = 2$ (shaded region depicted by the bunch of thin solid circles) on the $U' - J$ parameter plane for $n = 2/3$ (6electrons/9sites) at $\Delta = 1.2$.

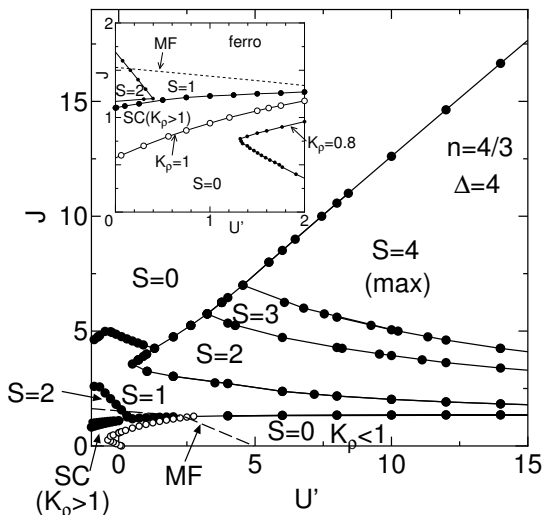


Figure 13: Global phase diagram on the $U' - J$ plane for $n = 8/6$ at $\Delta = 4.0$. The dashed line indicates the phase boundary of the complete(partial) ferromagnetic state obtained by the MF approximation. Inset shows the magnification of the phase diagram near the origin.

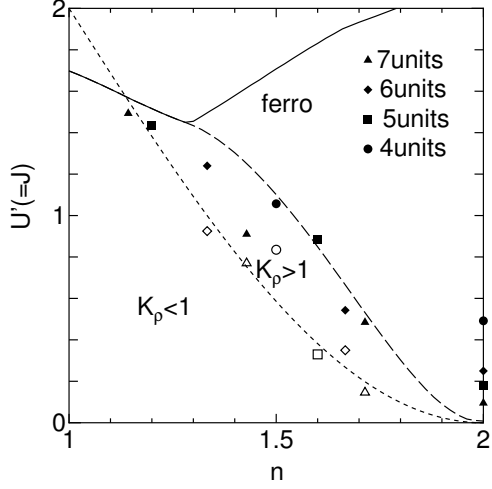


Figure 14: Phase diagram on the $n - J$ plane $\Delta = 4.0$. The broken line represents the phenomenological equation $J_c = \epsilon^+(0) - E_{k_F}$ (see text) as a function of n . The solid(dashed) line indicates the phase boundary of the complete(partial) ferromagnetic state obtained by the MF approximation.

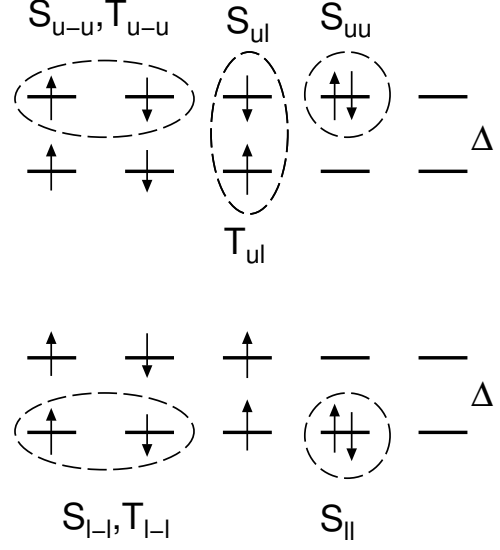


Figure 15: Schematic diagrams of various types of superconducting paring; $S_{||}$, S_{uu} , $S_{|-|}$, S_{u-u} and S_{ul} (singlet paring) and $T_{|-|}$, T_{u-u} and T_{ul} (triplet paring)

We also show the phase boundary of the ferromagnetic state obtained by the MF approximation. It seems to consist with the numerical result.

3.4 Paring correlation functions

Next, we consider superconducting paring of the system, as shown in Fig. 15. In Fig.16, we show various types of superconducting paring correlation functions $C(r)$ in detail for $n = 2/3$ (6electrons/9sites) at $\Delta = 1.0$ and $J(=U') = 1.04$. The paring correlation functions are defined by

$$S_{||}(r) = \frac{1}{N_u} \sum_i \langle c_{i,l,\uparrow}^\dagger c_{i,l,\downarrow}^\dagger c_{i+r,l,\downarrow} c_{i+r,l,\uparrow} \rangle, \quad (6)$$

$$S_{uu}(r) = \frac{1}{N_u} \sum_i \langle c_{i,l,\uparrow}^\dagger c_{i,u,\downarrow}^\dagger c_{i+r,u,\downarrow} c_{i+r,u,\uparrow} \rangle, \quad (7)$$

$$S_{|-|}(r) = \frac{1}{2N_u} \sum_i \langle (c_{i,l,\uparrow}^\dagger c_{i+1,l,\downarrow}^\dagger - c_{i,l,\downarrow}^\dagger c_{i+1,l,\uparrow}^\dagger) (c_{i+r+1,\downarrow} c_{i+r,l,\uparrow} - c_{i+r+1,l,\uparrow} c_{i+r,l,\downarrow}) \rangle, \quad (8)$$

$$S_{u-u}(r) = \frac{1}{2N_u} \sum_i \langle (c_{i,u,\uparrow}^\dagger c_{i+1,u,\downarrow}^\dagger - c_{i,u,\downarrow}^\dagger c_{i+1,u,\uparrow}^\dagger) (c_{i+r+1,u,\downarrow} c_{i+r,u,\uparrow} - c_{i+r+1,u,\uparrow} c_{i+r,u,\downarrow}) \rangle, \quad (9)$$

$$S_{ul}(r) = \frac{1}{2N_u} \sum_i \langle (c_{i,l,\uparrow}^\dagger c_{i+1,u,\downarrow}^\dagger - c_{i,l,\downarrow}^\dagger c_{i+1,u,\uparrow}^\dagger) (c_{i+r+1,u,\downarrow} c_{i+r,l,\uparrow} - c_{i+r+1,u,\uparrow} c_{i+r,l,\downarrow}) \rangle, \quad (10)$$

$$T_{|-|}(r) = \frac{1}{2N_u} \sum_i \langle (c_{i,l,\uparrow}^\dagger c_{i+1,l,\downarrow}^\dagger + c_{i,l,\downarrow}^\dagger c_{i+1,l,\uparrow}^\dagger) (c_{i+r+1,\downarrow} c_{i+r,l,\uparrow} + c_{i+r+1,l,\uparrow} c_{i+r,l,\downarrow}) \rangle, \quad (11)$$

$$T_{u-u}(r) = \frac{1}{2N_u} \sum_i \langle (c_{i,u,\uparrow}^\dagger c_{i+1,u,\downarrow}^\dagger + c_{i,u,\downarrow}^\dagger c_{i+1,u,\uparrow}^\dagger) (c_{i+r+1,u,\downarrow} c_{i+r,u,\uparrow} + c_{i+r+1,u,\uparrow} c_{i+r,u,\downarrow}) \rangle, \quad (12)$$

$$T_{ul}(r) = \frac{1}{2N_u} \sum_i \langle (c_{i,l,\uparrow}^\dagger c_{i+1,u,\downarrow}^\dagger + c_{i,l,\downarrow}^\dagger c_{i+1,u,\uparrow}^\dagger) (c_{i+r+1,u,\downarrow} c_{i+r,l,\uparrow} + c_{i+r+1,u,\uparrow} c_{i+r,l,\downarrow}) \rangle, \quad (13)$$

where $C(r) = S_{\parallel}(r)$, $S_{uu}(r)$, $S_{l-l}(r)$, $S_{u-u}(r)$ and $S_{ul}(r)$ denote the singlet paring correlation functions on the same site in the lower orbital, on the same site in the upper orbital, between the nearest neighbor sites in the lower orbital, between the nearest neighbor sites in the upper orbital, between lower and upper orbitals on the same site, respectively. Further, $T_{l-l}(r)$, $T_{u-u}(r)$ and $T_{ul}(r)$ are the triplet paring correlation functions between the nearest neighbor sites in the lower orbital, between the nearest neighbor sites in the upper orbital and between lower and upper orbitals on the same site, respectively. The absolute value of $T_{u-u}(r)$ is small, but the correlation of it is the slowest to decay. This result

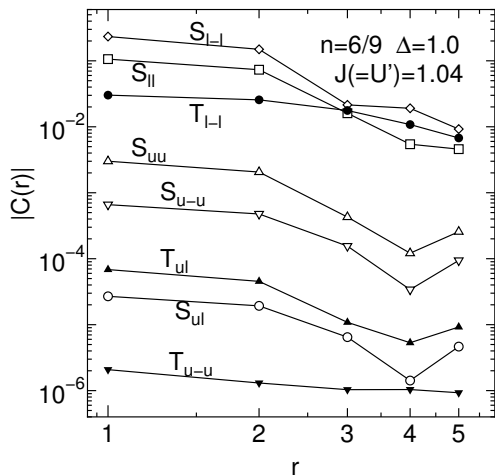


Figure 16: The singlet paring correlation functions $C(r) = S_{\parallel}(r)$, $S_{l-l}(r)$, $S_{uu}(r)$, $S_{u-u}(r)$, $S_{ul}(r)$ and the triplet correlation functions $T_{l-l}(r)$, $T_{u-u}(r)$, $T_{ul}(r)$, respectively(see text). Here we show the absolute value of the correlation functions at $\Delta = 1$ and $J(= U') = 1.04$ for $n=2/3$ (6electrons/9sites).

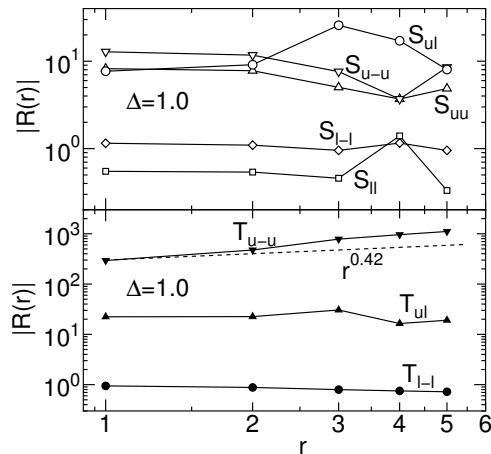


Figure 17: The ratio of the singlet paring correlation functions $R(r) = C(r)_{J=1.04}/C(r)_{J=0.2}$ for $S_{l-l}(r)$, $S_{uu}(r)$, $S_{u-u}(r)$ and $S_{ul}(r)$ and that of the triplet correlation functions for $T_{l-l}(r)$, $T_{u-u}(r)$, $T_{ul}(r)$ with the power-low $r^{0.42}$, respectively(see text). The broken line represents the power-low $r^{0.42}$ predicted by the Luttinger liquid relation.

seems to suggest that the relevant paring of the superconductivity is the *triplet paring* between *lower* and *upper* orbitals on the same site and the ferromagnetic fluctuation near the ferromagnetic phase may cause the paring. To clarify the behavior of the correlation functions, we calculate the ratio $R(r)$ of the paring correlation functions at $J(= U') = 1.04$ and that of $J(= U') = 0.2$ as

$$R(r) = \frac{C(r)_{J=1.04}}{C(r)_{J=0.2}}. \quad (14)$$

Although the correlation function $C(r)$ decays as distance r increases, the function $R(r)$ for relevant paring is expected to increase with r , because the value of K_ρ at $J = 1.04$ is larger than that at $J = 0.2$, where K_ρ is about at 1.4 and 0.98, respectively. Then, the behavior of $R(r)$ is expected to $\sim r^{0.42}$. In fig.17, we show $R(r)$ for $S_{\parallel}(r)$, $S_{l-l}(r)$, $S_{uu}(r)$, $S_{u-u}(r)$ and S_{ul} , (upper panel) and the triplet paring correlation functions $T_{l-l}(r)$, $T_{u-u}(r)$ and $T_{ul}(r)$ with the power-low $r^{0.42}$ predicted by the Luttinger liquid relation (lower panel), respectively. It indicates that that function $R(r)$ for the triplet paring, T_{u-u} , is much enhanced for long range paring correlation. On the other hand, the remains are not enhanced or decay as r increases. These results suggest that the paring correlation function $T_{u-u}(r)$ is most relevant paring to the superconductivity. Although the system size is too small to compare the slope of the function $R(r)$ with the power-low enhancement $\sim r^{0.42}$ directly, the behavior of $R(r)$ for $T_{u-u}(r)$ seems to be roughly consistent with the result of the Luttinger liquid relation.

4 d - p Chain Model

In the previous works[47, 48, 49, 50, 51, 52], the present authors and many other authors studied the one-dimensional d - p model with large on-site Coulomb repulsion U_d at Cu sites and intersite re-

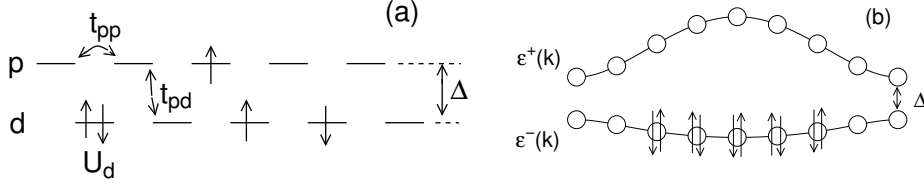


Figure 18: Schematic diagrams of (a) the model Hamiltonian and (b) the band structure in the noninteracting case.

pulsion U_{pd} , by using the numerical method. They claimed that the superconducting (SC) correlation is found to be dominant compared with the charge density wave (CDW) and spin density wave (SDW) correlations and the parameter U_{pd} is central in inducing a SC state. However, we found that if the hopping term t_{pp} is added to the model, the situation will be completely changed[53]. It enhances the fluctuation of charge and spin, and increases the exponent K_ρ as parameter U_{pd} does. Therefore, the repulsive interaction U_{pd} is not always necessary for the SC state.

In this section, we reexamine the one-dimensional d - p model in the presence of the hopping term t_{pp} to clarify the electronic structure of the SC state, especially paying attention to the symmetry of the pairing correlation.

4.1 Model Hamiltonian

We consider the following model Hamiltonian for the Cu-O chain in the hole picture;

$$\begin{aligned}
 H = & t_{pd} \sum_{\langle ij \rangle, \sigma} (p_{i\sigma}^\dagger d_{j\sigma} + h.c.) + t_{pp} \sum_{\langle ij \rangle, \sigma} (p_{i\sigma}^\dagger p_{j\sigma} + h.c.) \\
 & + \epsilon_d \sum_{j, \sigma} d_{j\sigma}^\dagger d_{j\sigma} + \epsilon_p \sum_{i, \sigma} p_{i\sigma}^\dagger p_{i\sigma} + U_d \sum_j \hat{n}_{dj\uparrow} \hat{n}_{dj\downarrow},
 \end{aligned} \tag{15}$$

where $d_{j\sigma}^\dagger$ and $p_{i\sigma}^\dagger$ stand for creation operators of a hole with spin σ in the Cu(d) orbital at site j and of a hole with spin σ in the O(p) orbital at site i , respectively, and $\hat{n}_{dj\sigma} = d_{j\sigma}^\dagger d_{j\sigma}$. Here, t_{pd} stands for the transfer energy between the nearest-neighbor d and p sites and will be set at unity ($t_{pd}=1$) hereafter in this study. The atomic energy levels of d orbital and p orbital are given by ϵ_d and ϵ_p , respectively. The charge-transfer energy Δ is defined as $\Delta = \epsilon_p - \epsilon_d$.

For the noninteracting case ($U_d = 0$), the Hamiltonian in eq. (15) is easily diagonalized to yield a dispersion relation

$$E^\pm(k) = \frac{1}{2} \left\{ \epsilon_d + \epsilon_p + 2t_{pp} \cos k \pm \sqrt{(\Delta + 2t_{pp} \cos k)^2 + 16(t_{pd} \cos(k/2))^2} \right\}, \tag{16}$$

where k is a wave vector and $E^+(k)(E^-(k))$ represent an upper (lower) band energy. For $t_{pp} > 0$, the width of the lower band $E^-(k)$ decreases with decreasing Δ and becomes perfectly flat at $\Delta_{flat} = 2t_{pp} - t_{pd}^2/t_{pp}$. When $\Delta < \Delta_{flat}$, the band bends with a peak at $k = 0$. To investigate the electronic structure of the interacting case, we numerically diagonalize the Hamiltonian up to 14 sites (7 unit cells). To carry out a systematic calculation, We use the periodic boundary condition for $N_h = 4m + 2$ and the antiperiodic boundary condition for $N_h = 4m$, where N_h is the total hole number and m is an integer.

4.2 Critical exponent K_ρ

In Fig. 19, we show the numerical results of K_ρ obtained through eq. 2 as a function of U_d for $n = 4/3$ (8holes/6units) at $\Delta = 2$ and $t_{pp} = 0.5$. We also plot K_ρ obtained through the mean field (MF) approximation, respectively. In the MF approximation, the renormalized bands $\tilde{E}^\pm(k)$ are given by eq. 16 in which Δ is replaced by

$$\tilde{\Delta} = \Delta - \frac{1}{2} U_d \langle n_d \rangle, \tag{17}$$

where $\langle n_d \rangle$ is the hole density at a d site and is determined by solving the self-consistent equation in the MF approximation. Using the renormalized band $\tilde{E}^-(k)$, we can calculate the charge susceptibility

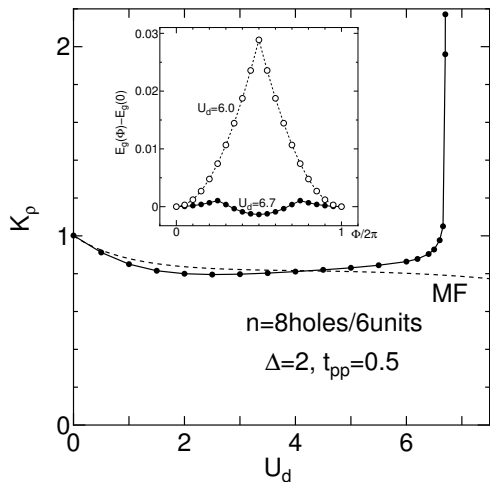


Figure 19: The critical exponent K_ρ as a function of U_d at $\Delta = 2$ and $t_{pp} = 0.5$ for $n = 4/3$ (8holes/6units). The dashed lines represent the results of the MF approximation (See in the text) Inset shows the energy difference $E_0(\phi) - E_0(0)$ as a function of an external flux ϕ

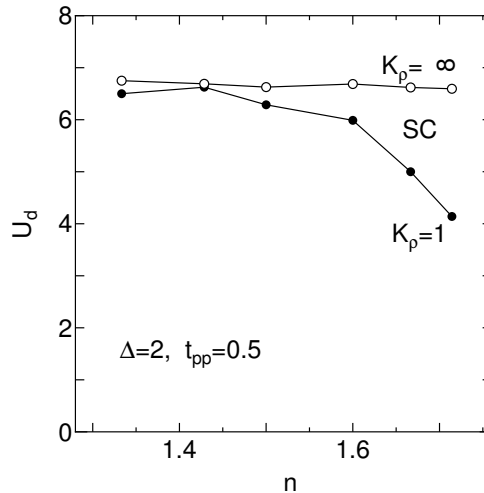


Figure 20: The SC region sandwiched between the two lines of $K_\rho = 1$ and $K_\rho = \infty$ on the $n-U_d$ parameter plane at $\Delta = 2$ and $t_{pp} = 0.5$. Here, we use $n = 8/6, 10/7, 6/4, 8/5, 10/6$ and $12/7$ systems.

χ_c and the Drude weight D . Substituting those values into eq. (2), we obtain K_ρ within the MF approximation. In the weak coupling regime, the results of the numerical diagonalization are in good agreement with the MF approximation. It also seems to be roughly consistent with the numerical results even in the strong coupling regime except for $U_d \gtrsim 6$.

When $U_d \lesssim 3$, K_ρ decreases as U_d increases. For sufficiently large U_d , K_ρ increases with increasing U_d and diverges at $U_d \sim 6.8$ when the charge susceptibility diverges. The region where K_ρ is larger than unity appears at $6.5 \lesssim U_d \lesssim 6.8$. When $K_\rho > 1$, the SC correlation is expected to be most dominant compared with the CDW and SDW correlations. Inset shows the energy difference $E_0(\phi) - E_0(0)$ as a function of an external flux ϕ . It shows that the anomalous flux quantization occurs at $U_d = 6.7$, when K_ρ is about 2.0. While, at $U_d = 6.0$, $K_\rho \simeq 0.86$ and the anomalous flux quantization is not found. These result also confirms the SC phase at $U_d = 6.7$. The divergence of K_ρ suggests that the effective bandwidth is close to zero. In fact, if we use the numerical value of $\langle n_d \rangle \simeq 0.83$ with $U_d = 6.7$ in eq. (7), we obtain $\tilde{\Delta} \sim -0.8$ and the effective bandwidth is nearly equal to 0.1. It is very small compared with the noninteracting band. The result of the anomalous flux quantization shows that the variation of $|E_0(\phi) - E_0(0)|$ at $U_d = 6.7$ is much smaller than that at $U_d = 6.0$. It also indicates that the effective bandwidth is small.

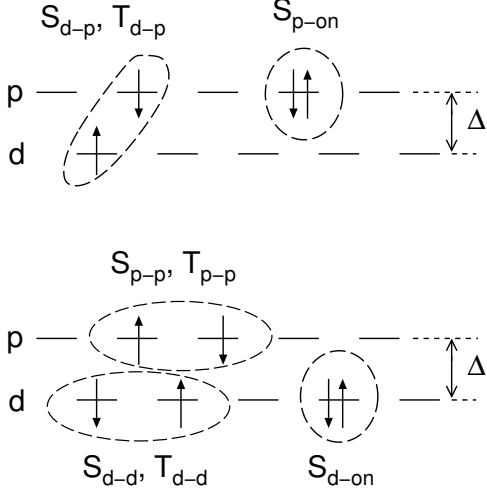
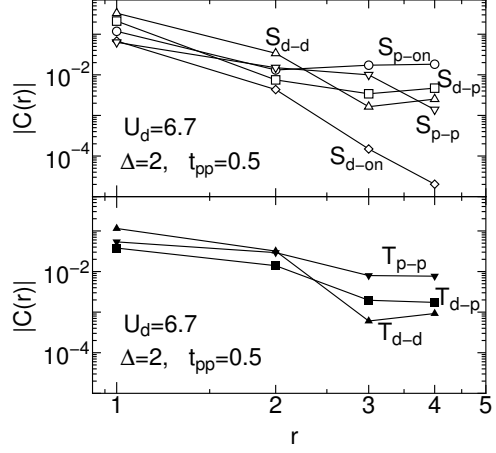
Figure 20 shows the SC region where $1 < K_\rho < \infty$ on the $n - U_d$ parameter plane at $\Delta = 2$ and $t_{pp} = 0.5$. We use $n = 8/6, 10/7, 6/4, 8/5, 10/6$ and $12/7$ systems, where numerator and denominator correspond to numbers of electrons and unit cells, respectively. The region sandwiched between the two lines of $K_\rho = 1$ and $K_\rho = \infty$ corresponds to the SC region. It is narrow near $n = 1.4$, however, it increases with increasing n .

4.3 Pairing correlation functions

We investigate various types of superconducting pairing in detail. as shown in Fig. 21. Figure 22 shows the pairing correlation functions $C(r)$ defined by

$$S_{p\text{-on}}(r) = \frac{1}{N_u} \sum_i \langle p_{i\uparrow}^\dagger p_{i\downarrow}^\dagger p_{i+r\uparrow} p_{i+r\downarrow} \rangle, \quad (18)$$

$$S_{d\text{-on}}(r) = \frac{1}{N_u} \sum_i \langle d_{i\uparrow}^\dagger d_{i\downarrow}^\dagger d_{i+r\uparrow} d_{i+r\downarrow} \rangle, \quad (19)$$


 Figure 21: Schematic diagrams of various pairing for d - p model.

 Figure 22: The singlet pairing correlation functions $C(r) = S_{p-on}(r)$, $S_{p-p}(r)$, $S_{d-on}(r)$, $S_{d-d}(r)$ and $S_{d-p}(r)$ (upper panel) and the triplet pairing correlation functions $T_{p-p}(r)$, $T_{d-d}(r)$ and $T_{d-p}(r)$ (lower panel), respectively (see text). Here we show the absolute value of the correlation functions at $\Delta = 2$, $t_{pp} = 0.5$ and $U_d = 6.7$ for $n=4/3$ (8holes/6units).

$$S_{p-p}(r) = \frac{1}{2N_u} \sum_i \langle (p_{i\uparrow}^\dagger p_{i+1\downarrow}^\dagger - p_{i\downarrow}^\dagger p_{i+1\uparrow}^\dagger)(p_{i+r+1\downarrow} p_{i+r+1\uparrow} - p_{i+r+1\uparrow} p_{i+r\downarrow}) \rangle, \quad (20)$$

$$S_{d-d}(r) = \frac{1}{2N_u} \sum_i \langle (d_{i\uparrow}^\dagger d_{i+1\downarrow}^\dagger - d_{i\downarrow}^\dagger d_{i+1\uparrow}^\dagger)(d_{i+r+1\downarrow} d_{i+r+1\uparrow} - d_{i+r+1\uparrow} d_{i+r\downarrow}) \rangle, \quad (21)$$

$$S_{d-p}(r) = \frac{1}{2N_u} \sum_i \langle (d_{i\uparrow}^\dagger p_{i\downarrow}^\dagger - d_{i\downarrow}^\dagger p_{i\uparrow}^\dagger)(p_{i+r\downarrow} d_{i+r\uparrow} - p_{i+r\uparrow} d_{i+r\downarrow}) \rangle, \quad (22)$$

$$T_{p-p}(r) = \frac{1}{2N_u} \sum_i \langle (p_{i\uparrow}^\dagger p_{i+1\downarrow}^\dagger + p_{i\downarrow}^\dagger p_{i+1\uparrow}^\dagger)(p_{i+r+1\downarrow} p_{i+r+1\uparrow} + p_{i+r+1\uparrow} p_{i+r\downarrow}) \rangle, \quad (23)$$

$$T_{d-d}(r) = \frac{1}{2N_u} \sum_i \langle (d_{i\uparrow}^\dagger d_{i+1\downarrow}^\dagger + d_{i\downarrow}^\dagger d_{i+1\uparrow}^\dagger)(d_{i+r+1\downarrow} d_{i+r+1\uparrow} + d_{i+r+1\uparrow} d_{i+r\downarrow}) \rangle, \quad (24)$$

$$T_{d-p}(r) = \frac{1}{2N_u} \sum_i \langle (d_{i\uparrow}^\dagger p_{i\downarrow}^\dagger + d_{i\downarrow}^\dagger p_{i\uparrow}^\dagger)(p_{i+r\downarrow} d_{i+r\uparrow} + p_{i+r\uparrow} d_{i+r\downarrow}) \rangle, \quad (25)$$

where $S_{p-on}(r)$, $S_{d-on}(r)$, $S_{p-p}(r)$, $S_{d-d}(r)$ and $S_{d-p}(r)$ denote the singlet pairing correlation functions on a same p site, on a same d site, between the nearest neighbor p sites, between the nearest neighbor d sites and between the nearest neighbor p and d sites, respectively. Further, $T_{p-p}(r)$, $T_{d-d}(r)$ and $T_{d-p}(r)$ denote the triplet pairing correlation functions between the nearest neighbor p sites, between the nearest neighbor d sites and between the nearest neighbor p and d sites, respectively. Here, we show the absolute value of the correlation functions at $\Delta = 2$, $t_{pp} = 0.5$ and $U_d = 6.7$ for $n=4/3$ (8holes/6units). The orders of the absolute value of these correlation functions are almost equal to one another.

However, the correlation functions $C(r)$ for $S_{p-on}(r)$ and $S_{p-p}(r)$ seem to decay slower than that of the remains. It suggests that these pairing play an important role in the superconductivity. We also examine the ratio of the pairing correlation functions $R(r)$ at $U_d = 6.7$ and $U_d = 6.0$ as $R(r) = C(r)_{U_d=6.7} / C(r)_{U_d=6.0}$, where $K_\rho \sim 2.0$ at $U_d = 6.7$ and $K_\rho \sim 0.86$ at $U_d = 6.0$. The function $R(r)$ for relevant pairing is expected to behave as $r^{1.1}$. In fig.23, we show the ratio of the pairing correlation functions $R(r)$ for $S_{p-on}(r)$, $S_{p-p}(r)$, $S_{d-on}(r)$, $S_{d-d}(r)$ and $S_{d-p}(r)$ with the power-low $r^{1.1}$ (upper panel) and that of the triplet pairing correlation functions for $T_{p-p}(r)$, $T_{d-d}(r)$

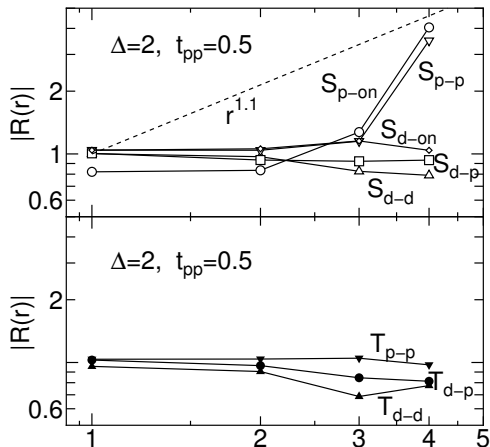


Figure 23: The ratio of the singlet paring correlation functions $R(r) = C(r)_{U_d=6.7}/C(r)_{U_d=6.0}$ for $S_{p-on}(r)$, $S_{p-p}(r)$, $S_{d-on}(r)$, $S_{d-d}(r)$ and $S_{d-p}(r)$ with the power-low $r^{1.1}$ depicted the broken line (upper panel) and that of the triplet paring correlation functions for $T_{p-p}(r)$, $T_{d-d}(r)$ and $T_{d-p}(r)$ (lower panel), respectively. Here we show the absolute value of $R(r)$ at $\Delta = 2$, $t_{pp} = 0.5$ for $n=4/3$ (8holes/6units).

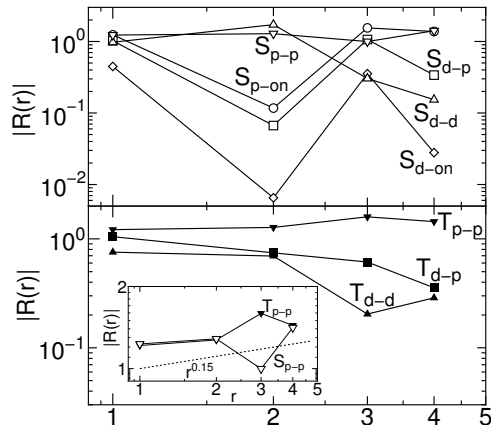


Figure 24: The ratio of the singlet paring correlation functions $R(r) = C(r)_{U_d=6.59}/C(r)_{U_d=4.14}$ for $S_{p-on}(r)$, $S_{p-p}(r)$, $S_{d-on}(r)$, $S_{d-d}(r)$ and $S_{d-p}(r)$ (upper panel), and that of the triplet paring correlation functions for $T_{p-p}(r)$, $T_{d-d}(r)$ and $T_{d-p}(r)$ (lower panel), respectively. Here we show the absolute value of $R(r)$ at $\Delta = 2$, $t_{pp} = 0.5$ for $n=12/7$ (12holes/7units). Inset shows $R(r)$ for $S_{p-p}(r)$ and $T_{p-p}(r)$ with the power-low $r^{0.15}$.

and $T_{d-p}(r)$ (lower panel), respectively. It indicates that that $R(r)$ for $S_{p-on}(r)$ and $S_{p-p}(r)$ are much enhanced at long range paring correlation and seem to be roughly consistent with the power-low obtained by the Luttinger liquid relation. On the other hand, the remains decay as distance r increases or are almost constant. These results suggest that the singlet paring correlation functions $S_{p-on}(r)$ and $S_{p-p}(r)$ are most relevant to the superconductivity and the triplet paring is irrelevant.

On the other hand, the situation is changed for large hole density. In this case, the triplet paring correlation is enhanced as well as the singlet paring correlation. In fig.24, we show the ratio of the singlet paring correlation functions $R(r) = C(r)_{U_d=6.59}/C(r)_{U_d=4.14}$ for $S_{p-on}(r)$, $S_{p-p}(r)$, $S_{d-on}(r)$, $S_{d-d}(r)$ and $S_{d-p}(r)$ (upper panel), and that of the triplet paring correlation functions for $T_{p-p}(r)$, $T_{d-d}(r)$ and $T_{d-p}(r)$ (lower panel), respectively, where we show the absolute value of $R(r)$ for $n=12/7$ (12holes/7units). Here, $R(r)$ of the relevant paring is expected to behave as $r^{0.15}$ since $K_\rho \sim 1.15$ at $U_d = 6.59$ and $K_\rho \sim 1.0$ at $U_d = 4.14$. Inset shows $R(r)$ for $S_{p-p}(r)$ and $T_{p-p}(r)$ with the power-low $r^{0.15}$. It shows that $R(r)$ for $T_{p-p}(r)$ increases with r as well as that for $S_{p-p}(r)$, which seems to be roughly consistent with the power-low $r^{0.15}$ predicted by the Luttinger liquid relation. suggests that the triplet paring becomes relevant to the superconductivity as well as the singlet paring near $n = 2$.

5 d - p Model in Infinite Dimensions

Recently, some significant progress has been achieved in understanding the strongly correlated electron systems by using the dynamical mean-field theory (DMFT)[54, 55]. In this approach, the lattice problem is mapped onto an effective impurity problem where a correlated impurity site is embedded in an effective uncorrelated medium that has to be determined self-consistently. To solve the effective impurity problem, several methods have been applied including the iterated perturbation theory[55], the non-crossing approximation[56], the quantum Monte Carlo (QMC) method[57], the exact diagonalization (ED) method[58] and the numerical renormalization group (NRG) method[59, 60]. The DMFT becomes exact in the limit of infinite spatial dimensions ($d = \infty$)[54] and believed to be a good approximation in high dimensions.

In the $d = \infty$ single-band Hubbard model at half-filling, the Mott metal-insulator transition is found to occur as a first-order phase transition at finite temperature below a critical temperature T_{cr} [55]. Below T_{cr} , a coexistence of the metallic and insulating solutions is found for the same value of the on-site Coulomb interaction U in the range $U_{c1} < U < U_{c2}$ [55, 60]. The magnetic phase diagram was obtained as a function of doping, temperature and U . A commensurate antiferromagnetic order changes to an incommensurate state at a value of the doping which depends on U [61]. The ferromagnetism was observed for an intermediate interaction strength $U \gtrsim 2$ in non-bipartite lattices such as the fcc-type lattice[62] but was completely suppressed for $U \lesssim 20$ in bipartite lattices such as the hypercubic lattice[63]. The superconducting phase is absent in the $d = \infty$ single-band Hubbard model[64].

The DMFT has also been applied to the multi-band Hubbard model to elucidate the effect of the Hund's rule coupling on the Ferromagnetism[20, 22] and the Mott transition[65, 66]. Several authors have extensively studied the d - p model using the DMFT[58, 67, 68, 69, 70, 71, 72, 73, 74, 75]. The Mott transition was found to occur at $n = 1$ (or $n = 3$)[67, 68, 69, 70, 71, 73, 74], where n is the total electron number per unit cell and given by the sum of p - and d -electron numbers: $n = n_p + n_d$. The phase diagram of the Mott transition was obtained over the whole parameter regime including the Mott-Hubbard type ($U < \Delta$) and the charge-transfer type ($U > \Delta$)[69, 70]. When the carrier is doped with $n > 1$, the superconductivity was observed in the charge-transfer regime[58, 67, 69], while it was not observed in the Mott-Hubbard regime. The antiferromagnetism was also observed at and near $n = 1$ [75]. More recently, the present authors discussed the ferromagnetism which was found to occur at and near $n = 2$ in the intermediate interaction strength $U \approx 2\Delta \gtrsim 2$ [72]. Therefore it is interesting to discuss the relationship between the magnetism and the superconductivity in the d - p model in infinite dimensions and to obtain the phase diagram as functions of the parameters such as the interaction, the electron filling and the temperature.

5.1 Model and formulation

We consider the d - p model on a Bethe lattice with infinite connectivity $z \rightarrow \infty$. The Hamiltonian is written as

$$H = \sum_{i,j,\sigma} (t_{i,j} d_{i\sigma}^\dagger p_{j\sigma} + h.c.) + \epsilon_p \sum_{j,\sigma} p_{j\sigma}^\dagger p_{j\sigma} + \epsilon_d \sum_{i,\sigma} d_{i\sigma}^\dagger d_{i\sigma} + U_d \sum_i n_{i\uparrow}^d n_{i\downarrow}^d, \quad (26)$$

where $d_{i\sigma}^\dagger$ and $p_{j\sigma}^\dagger$ stand for creation operators of a electron (or a hole) with spin σ in the d -orbital at site i and in the p -orbital at site j , respectively. $n_{i,\sigma}^d = d_{i\sigma}^\dagger d_{i\sigma}$. $t_{i,j} = \frac{t_{pd}}{\sqrt{z}}$ represents the transfer energy between the nearest neighbor site and the parameter t_{pd} will be set to unity in the present study. The atomic energy levels of d -orbital and p -orbital are given by ϵ_d and ϵ_p , respectively. The charge-transfer energy Δ is defined as $\Delta = \epsilon_p - \epsilon_d > 0$.

In the DMFT, the effective action of the impurity problem is given by

$$S = U_d \int_0^\beta d\tau n_{d\uparrow}(\tau) n_{d\downarrow}(\tau) - \int_0^\beta \int_0^\beta d\tau d\tau' \sum_\sigma d_\sigma^\dagger(\tau) D_{0\sigma}^{-1}(\tau - \tau') d_\sigma(\tau'), \quad (27)$$

where the Weiss function $D_{0\sigma}$ includes effects of the interaction at all the sites except the impurity site. This action is derived by tracing out the fermionic degrees of freedom in the original lattice model except the impurity site. The local Green's function $D_\sigma(\tau - \tau') = -\langle T d_\sigma(\tau) d_\sigma^\dagger(\tau') \rangle_S$ is calculated with this action. Using $D_{0\sigma}$ and D_σ , we introduce the local self-energy $\Sigma_\sigma(i\omega_n) = D_{0\sigma}(i\omega_n)^{-1} - D_\sigma(i\omega_n)^{-1}$, where ω_n is the Matsubara frequency, $\omega_n = (2n + 1)\pi/\beta$. The self-consistency condition for the local Green's functions gives the relations

$$D_\sigma(i\omega_n) = \int d\varepsilon N(\varepsilon) \times \frac{i\omega_n + \mu - \varepsilon_p}{(i\omega_n + \mu - \varepsilon_d - \Sigma_\sigma(i\omega_n))(i\omega_n + \mu - \varepsilon_p) - \varepsilon^2}, \quad (28)$$

$$P_\sigma(i\omega_n) = \int d\varepsilon N(\varepsilon) \times \frac{i\omega_n + \mu - \varepsilon_d - \Sigma_\sigma(i\omega_n)}{(i\omega_n + \mu - \varepsilon_d - \Sigma_\sigma(i\omega_n))(i\omega_n + \mu - \varepsilon_p) - \varepsilon^2}, \quad (29)$$

where μ is the chemical potential and $P_\sigma(\tau - \tau') = -\langle T p_\sigma(\tau) p_\sigma^\dagger(\tau') \rangle_S$ is the local Green's function at p -site. For the Bethe lattice with $z = \infty$, the density of states is given by a semi-circular function,

$N(\varepsilon) = \sqrt{4 - (\varepsilon/t_{pd})^2}/2\pi t_{pd}$. Using the semi-circular density of states in eqs.(28) and (29) and eliminating $\Sigma_\sigma(i\omega_n)$, we obtain the simple form of the self-consistency equations

$$D_{0\sigma}(i\omega)^{-1} = i\omega_n + \mu - \varepsilon_d - t_{pd}^2 P_\sigma(i\omega_n), \quad (30)$$

$$P_\sigma(i\omega)^{-1} = i\omega_n + \mu - \varepsilon_p - t_{pd}^2 D_\sigma(i\omega_n). \quad (31)$$

To calculate the local Green's function $D_\sigma(i\omega_n)$ for a given $D_{0\sigma}(i\omega_n)$, we use the numerical diagonalization method (DMFT-ED method). The self-consistency equations (30) and (31) lead a new $D_{0\sigma}(i\omega)$ and we repeat the calculation of the local Green's function. This process is iterated until the solutions converge.

In the DMFT-ED method, we approximately solve the impurity Anderson model of a finite-size cluster;

$$H_{And} = \varepsilon_{0\sigma} \sum_\sigma n_{d\sigma} + \sum_{l=2,\sigma}^{N_s} \varepsilon_{l\sigma} c_{l\sigma}^\dagger c_{l\sigma} + \sum_{l=2,\sigma}^{N_s} V_{l\sigma} (d_\sigma^\dagger c_{l\sigma} + c_{l\sigma}^\dagger d_\sigma) + U_d n_{d\uparrow} n_{d\downarrow}, \quad (32)$$

where $\varepsilon_{0\sigma}$ is the impurity level and $\varepsilon_{l\sigma}$ ($l = 2, 3, \dots, N_s$) are levels of the 'conduction electron' hybridized with the impurity by $V_{l\sigma}$. We regard the non-interacting Green's function $G_{0\sigma}^{And}(i\omega_n)$ as the Weiss function $D_{0\sigma}(i\omega)$ in the action eq.(27). Then, the interacting Green's function $G_\sigma^{And}(i\omega_n)$ corresponds to the local Green's function $D_\sigma(i\omega)$ in the original lattice problem. Here, $G_{0\sigma}^{And}(i\omega_n)$ is defined by

$$G_{0\sigma}^{And}(i\omega_n) = \frac{1}{i\omega_n - \varepsilon_{0\sigma} - \sum_{l=2}^{N_s} \frac{V_{l\sigma}^2}{i\omega_n - \varepsilon_{l\sigma}}}. \quad (33)$$

For a given $D_{0\sigma}(i\omega)$, we determine $2N_s - 1$ parameters $\varepsilon_{0\sigma}, \varepsilon_{l\sigma}, V_{l\sigma}$ ($l = 2, 3, \dots, N_s$) to make $G_{0\sigma}^{And}(i\omega_n)$ as close to $D_{0\sigma}(i\omega)$ as possible. Using these parameters, we diagonalize the finite cluster of the impurity Anderson model, and calculate $G_{0\sigma}^{And}(i\omega_n)$ ($D_{0\sigma}(i\omega_n)$). At finite temperature, the Green's function is straightforwardly calculated from the full set of states $|i\rangle$ with eigenvalues E_i according to

$$D_\sigma(i\omega_n) = \frac{1}{Z} \sum_{i,j} \frac{|\langle i|d_\sigma^\dagger|j\rangle|^2}{i\omega_n - E_i + E_j} (e^{-\beta E_i} + e^{-\beta E_j}). \quad (34)$$

Using the Lanczos method with the continued-fraction expansions, we also calculate the zero temperature Green's functions. In this case, we replace the Matsubara frequencies by a fine grid of imaginary frequencies, $\tilde{\beta}$ ($i\omega_n = (2n + 1)\pi/\tilde{\beta}$), where the fictitious inverse temperature $\tilde{\beta}$ determines a low-frequency cut-off.

5.2 Metal-Insulator transition at $n = 2$

First, we consider the paramagnetic state at zero temperature for $n = n_d + n_p = 2$. In the non-interacting case $U_d = 0$, the system is a band-insulator with the energy gap Δ for $\Delta \neq 0$ while it is a semimetal for $\Delta = 0$. Within the restricted Hartree-Fock (HF) approximation, the energy gap is given by $\Delta - \frac{U_d n_d}{2}$. Then the system is metallic for $U_d = 2\Delta$, otherwise it is insulating. We note that $n_d = n_p = 1$ for $U_d = 2\Delta$ due to the particle-hole symmetry. In the inset in Fig. 25, we show the chemical potential μ as functions of n for $U_d = 7, 8, 9, 10$ at $\Delta = 6$ and $T = 0$ calculated from the DMFT-ED method with the system size $N_s = 8$ [72]. In this calculation, the solution is restricted to the paramagnetic state with $\varepsilon_{0\sigma} = \varepsilon_0$, $\varepsilon_{l\sigma} = \varepsilon_l$ and $V_{l\sigma} = V_l$ for $l = 2, 3, \dots, N_s$. When U_d increases from $U_d = 0$, the discontinuity in the chemical potential at $n = 2$ decreases and finally becomes zero at a critical value, where a transition from the band-insulator to the correlated semimetal occurs[67]. The critical values for the metal-insulator transition are plotted in Fig. 25. In contrast to the HF approximation, the metallic state is found in the wide parameter region due to a correlation effect considered in the DMFT.

5.3 Ferromagnetism

At low temperature, the correlated semimetal mentioned above becomes unstable compared to a ferromagnetic state. In Fig. 26, we plot the magnetization for the d -electron M_d , that for the p -electron M_p and the total magnetization $M = M_d + M_p$ as functions of the temperature T at $n = 2$ for $U_d = 8$

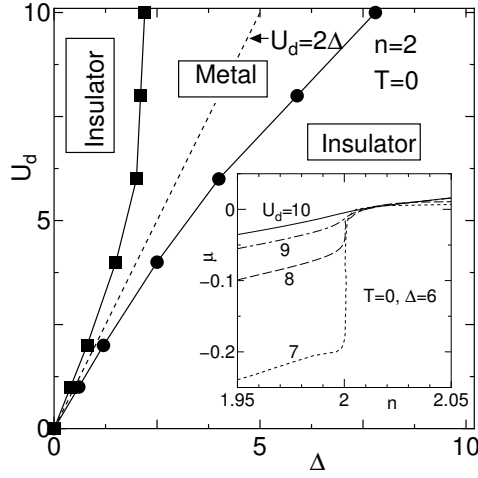


Figure 25: The phase boundary separating the metallic and insulating regimes as a function of U_d and Δ at $n = 2$ and $T = 0$. The inset shows the chemical potential as functions of n for $U_d = 7, 8, 9, 10$ at $\Delta = 6$ and $T = 0$ calculated from the DMFT-ED method with $N_s = 8$.

and $\Delta = 4$ calculated from the DMFT-ED method with $N_s = 6$ [72]. As shown in Fig. 26, M_d and M_p have opposite sign to each other. In the low temperature limit, both of M_d and M_p become constant, while the sum of them M becomes zero. The feature of the ferromagnetism from the DMFT is similar to that from the HF approximation as shown in Fig. 26. However, the transition temperature T_c from the HF approximation is much higher than that from the DMFT (see also Fig. 29). In Fig. 27, we plot the magnetization as functions of U_d with keeping $\Delta = \frac{U_d}{2}$ at $n = 2$ and $T = 0.01$ calculated from the DMFT-ED method together with those from the HF approximation. When U_d increases, the each component of the magnetization monotonically increases. In both approximations, the ferromagnetism is observed for the intermediate interaction strength $U_d \gtrsim 2$. This is a striking contrast to the single-band Hubbard model where the ferromagnetism is observed only for the strong

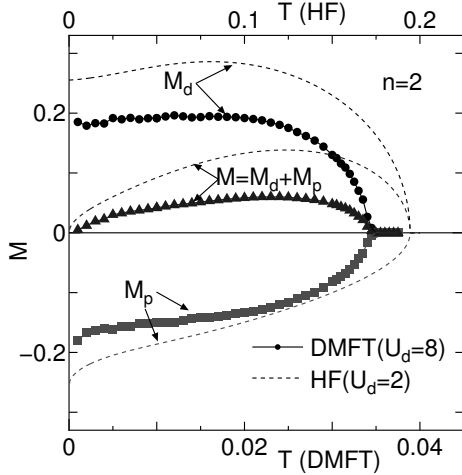


Figure 26: The magnetization for the d -electron M_d , that for the p -electron M_p and the total magnetization $M = M_d + M_p$ as functions of the temperature T at $n = 2$, obtained from the DMFT-ED method for $U_d = 8$ and $\Delta = 4$ with $N_s = 6$ and from the HF approximation (dashed lines) for $U_d = 2$ and $\Delta = 1$.

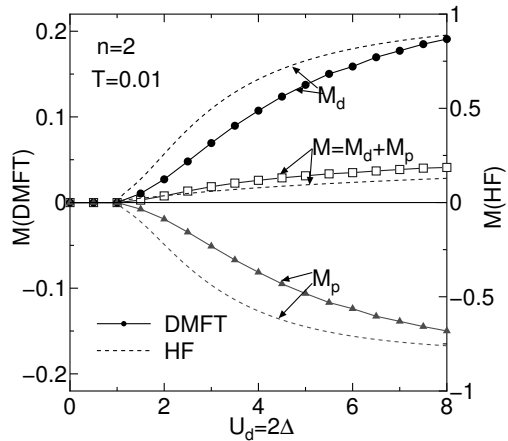


Figure 27: The magnetization for the d -electron M_d , that for the p -electron M_p and the total magnetization $M = M_d + M_p$ as functions of U_d with $\Delta = U_d/2$ at $n = 2$ and $T = 0.01$, obtained from the DMFT-ED method and from the HF approximation (dashed lines).

coupling region $U \gtrsim 20$ in bipartite lattices within the DMFT[63]. We note that the value of the magnetization from the DMFT is about five times smaller than that from the HF for the same values of U_d and Δ .

Fig. 28 shows the total magnetization M as a function of the electron filling n . When n decreases, M continuously becomes zero at a critical value of n for high temperatures (see for $T = 0.025$), while it discontinuously becomes zero for low temperatures (see for $T = 0.01$). The similar properties are also observed within the HF approximation as shown in Fig. 28. At low temperatures, however, the HF approximation also predicts a metastable state where M decreases with increasing n and continuously becomes zero at a critical n (see for $T = 0.025$). By calculating the thermodynamic potential, we find that the phase separation of the ferromagnetic state and the paramagnetic state occurs at the low temperatures (see Fig. 29).

Fig. 29 shows the transition temperature for the ferromagnetism T_c as a function of n for several values of $U_d (= 2\Delta)$ [72]. T_c monotonically decreases with decreasing n . The closed circles show the second-order phase transition, while the open circles show the discontinuous transition as seen in Fig. 28. Within the HF approximation, the second-order phase transition occurs at the high temperature (solid line), while the phase separation occurs at the low temperature (area between the dotted lines). In the DMFT, it is difficult to calculate the thermodynamic potential directly from the local Green's function. But we may expect that, within the DMFT, the similar phase separation takes place at low temperatures where the magnetization shows a discontinuous transition as shown in Fig. 28.

5.4 Superconductivity

Finally, we discuss the superconductivity in the d - p model (26). In infinite dimensions, the on-site paring susceptibility χ of this model is given by[55, 67]

$$\begin{aligned} \chi &= \frac{1}{N} \int_0^\beta d\tau \sum_{ij} \langle T d_{i\uparrow}(\tau) d_{i\downarrow}(\tau) d_{j\downarrow}^\dagger(0) d_{j\uparrow}^\dagger(0) \rangle \\ &= T \sum_{\nu, \nu'} [\alpha^{-1/2} \{I - \Lambda\}^{-1} \cdot \Lambda \cdot \alpha^{-1/2}]_{\nu, \nu'}, \end{aligned} \quad (35)$$

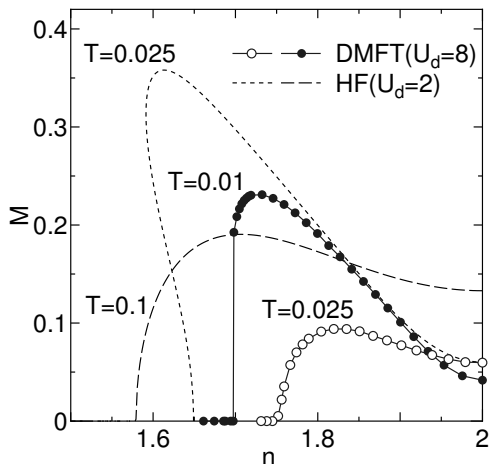


Figure 28: The total magnetization M as a function of the electron number n , obtained from the DMFT-ED method for $U_d = 8$ and $\Delta = 4$ at $T = 0.01$ (closed circles), 0.025 (open circles), and from the HF approximation for $U_d = 2$ and $\Delta = 1$ at $T = 0.025$ (dotted line), 0.1 (dashed line).

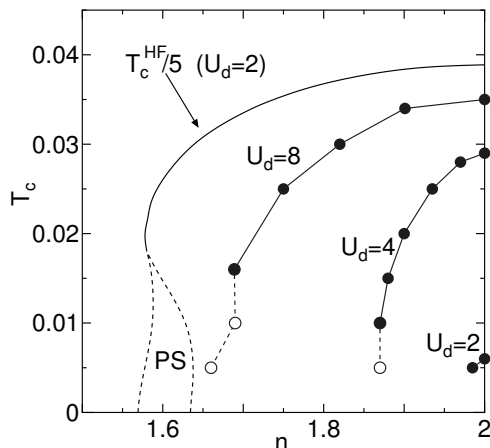


Figure 29: The transition temperature T_c for the ferromagnetism as a function of the electron filling n , obtained from the DMFT-ED method (closed and open circles) for $U_d = 2\Delta = 8, 4, 2$, and from the HF approximation (solid and dotted lines) for $U_d = 2\Delta = 2$.

with

$$\Lambda_{\nu,\nu'} = t_{pd}^4 |P(i\nu)| [\tilde{\chi}_{loc}]_{\nu,\nu'} |P(i\nu')|, \quad (36)$$

$$\alpha_{\nu,\nu'} = t_{pd}^4 |P(i\nu)|^2 \delta_{\nu,\nu'}, \quad (37)$$

where, $\tilde{\chi}_{loc}$ is the local pairing susceptibility at a d -site given by

$$[\tilde{\chi}_{loc}]_{\nu,\nu'} = T^2 \int_0^\beta d\tau_1 \int_0^\beta d\tau_2 \int_0^\beta d\tau_3 \int_0^\beta d\tau_4 e^{i\nu(\tau_1-\tau_2)} e^{i\nu'(\tau_3-\tau_4)} \langle T d_\uparrow(\tau_1) d_\downarrow(\tau_2) d_\downarrow^\dagger(\tau_3) d_\uparrow^\dagger(\tau_4) \rangle. \quad (38)$$

To calculate $\tilde{\chi}_{loc}$ within the DMFT-ED method, we use a spectral representation of r.h.s. in eq.(38) by inserting a complete set of eigenstates $|i\rangle$.

When the largest eigen value of Λ , λ_{max} , approaches unity, the pairing susceptibility diverges. It signals the transition into the superconducting state from the normal state. In Fig.30, we show the value of λ_{max} as a function of the temperature T for $U_d = 8$ and $\Delta = 4$ at $n = 1.3$ and 1.7 obtained from the DMFT-ED with the system size $N_s = 5$. The value of λ_{max} increases with decreasing T and exceeds unity at a certain critical temperature. For $n = 1.3$, the critical temperature for the spin-singlet pairing, T_{SS} , is higher than that for the spin-triplet pairing, T_{TS} , while, for $n = 1.7$, T_{TS} is higher than T_{SS} [76]. This tendency is consistent with the zero-temperature DMFT-ED result with the system size $N_s = 6 - 8$ [58].

We note that the triplet superconductivity is on-site pairing and the gap function is odd in the Matsubara frequency as first proposed by Berezinskii in the superfluid ^3He [77]. In the present calculation, the eigen function corresponding to the largest eigen value of Λ for the triplet-pairing, is proportional to the gap function at the critical temperature, and is confirmed to be odd in the Matsubara frequency.

In Fig.31, the superconducting transition temperature for the triplet pairing T_{TS} and that for the singlet pairing T_{SS} , obtained from the DMFT-ED method mentioned above, are plotted as functions of n for $U_d = 8$ and $\Delta = 4$. We also plotted the transition temperature for the ferromagnetism T_c (see Fig. 29) together with that for the antiferromagnetism T_N calculated from the DMFT-ED method with $N_s = 6$. As seen in Fig.31, the singlet superconductivity is realized for $n \lesssim 1.4$ near the antiferromagnetic phase, where the antiferromagnetic fluctuation is considered to be responsible for the singlet pairing. On the other hand, the triplet superconductivity is realized for $T \gtrsim 1.4$ near the ferromagnetic phase, where the ferromagnetic fluctuation is considered to be responsible for the triplet pairing. Significantly, a reentrant superconducting transition is observed for $1.4 \lesssim n \lesssim 1.5$. The reentrant transition has also been observed in the $d = \infty$ periodic Anderson model[78]. Therefore, the

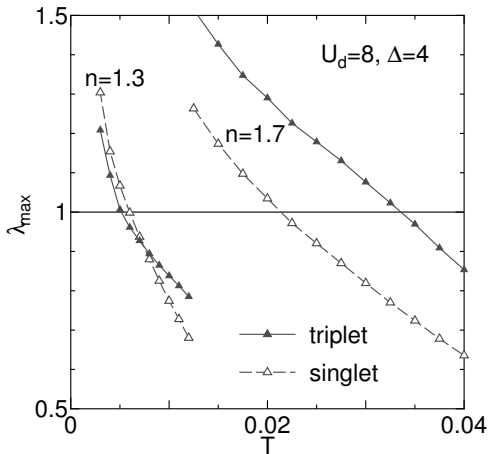


Figure 30: The largest eigen value λ_{max} as a function of the temperature T for $U_d = 8$ and $\Delta = 4$ at $n = 1.3$ and 1.7 obtained from the DMFT-ED with $N_s = 5$.

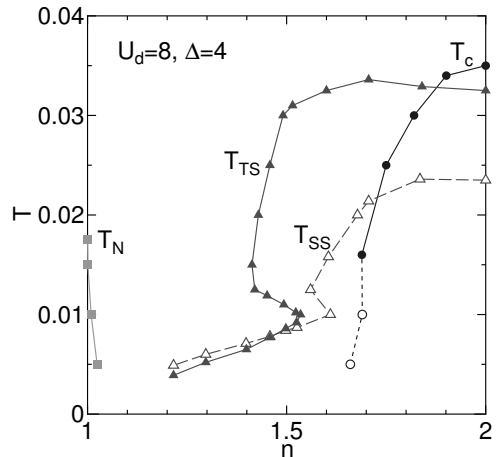


Figure 31: Transition temperatures for the ferromagnetism T_c , the spin-triplet superconductivity T_{TS} , the spin-singlet superconductivity T_{SS} and the antiferromagnetism T_N , obtained from the DMFT-ED for $U_d = 8$ and $\Delta = 4$.

reentrant superconducting transition is considered to be a specific feature of two-band type models including d - p model and the periodic Anderson model.

6 Summary and Discussion

We have investigate the ferromagnetism and the related superconductivity of the Hubbard model with two-fold orbital degeneracy and the d - p model with paying attention to the effect of the interplay between the Coulomb interactions and the band splitting. To obtain reliable results beyond the perturbative or the mean-field like approximations, we use the numerical diagonalization method for the one-dimensional models and the dynamical mean-field theory for the infinite-dimensional model. For one-dimensional models, we calculate the critical exponent K_ρ based on the Luttinger liquid theory and the paring correlation functions of the ground state.

In the one-dimensional multi-orbital Hubbard model, we have obtained various phase diagrams including the ferromagnetic and the superconducting state on the $U' - J$ parameter plane. The fully polarized ferromagnetism has been found in the strong coupling regime with $U' \gtrsim J \gtrsim \Delta$. For $1 < n < 2$, the ferromagnetism is metallic and mainly caused by the double-exchange mechanism[23]. Crystal-field splitting destroys the fully polarized ferromagnetism resulting in a partially polarized one for $J \lesssim \Delta$. In the vicinity of the partially polarized ferromagnetism, we have found the triplet superconducting phase, when J exceeds the lowest energy of the inter-band excitation. It extends to the realistic parameter region for $3d$ transition-metals with $U' > J$.

Sakamoto *et al.*[23] claimed that the metallic ferromagnetism for $\Delta = 0$ appears in a similar parameter region in any dimension by comparing the results from one dimension with those from infinite dimensions. It is natural to think that this ferromagnetism will appear in two and three dimensions even in the presence of Δ . Then, we expect that a partially polarized (weak) ferromagnetism appears in real materials, in which Hund's rule coupling and crystal-field splitting compete with each other, such as in cobalt oxides. In fact, a weak ferromagnetism has been observed in the layered $\text{Na}_{0.75}\text{CoO}_2$ [13] as well as in the perovskite $\text{R}_{1-x}\text{A}_x\text{CoO}_3$ [79]. The orbital degeneracy of $3d$ electrons is considered to play a crucial role in Na_xCoO_2 as well as in $\text{La}_{1-x}\text{Sr}_x\text{CoO}_3$ [15].

In our calculation, we can not find any sign of the superconductivity near the fully polarized ferromagnetic state at the realistic parameter region $U' > J$. It suggests that not the complete ferromagnetic state but the weak ferromagnetic state can be a key to the superconductivity of real materials. The competition between Hund's rule coupling and crystal-field splitting causes the large orbital fluctuation, accompanied by the fluctuation between the low-spin and the high-spin states at each Co ion. This fluctuation is expected to mediate the superconductivity near the weak ferromagnetism. Since the orbital fluctuation has a local character, the mechanism for the superconductivity could be common in all dimensions. We therefore think that exploration of the superconductivity in the vicinity of the weak ferromagnetism in the perovskite $\text{R}_{1-x}\text{A}_x\text{CoO}_3$ [79] may be promising.

In the one-dimensional d - p model, we have calculated the critical exponent K_ρ and the various types of the paring correlation functions. Using the Luttinger liquid relations, we have found that the SC correlation is dominant in the parameter region where the renormalized band becomes almost flat. Since the narrowing of the effective bandwidth leads to the enhancement of the fluctuation, it can cause the superconductivity. The behavior of the paring correlation functions suggests that the singlet paring on a same p site and between the nearest neighbor p sites are most relevant to the superconducting state near half-filling. This result can be interpreted that the antiferromagnetic fluctuation meditates the singlet paring as similar as the t - J model. However, in large doping case $n = 12/7$, the triplet paring between the nearest neighbor p sites becomes relevant to the superconductivity as well as the singlet paring between the nearest neighbor p sites. This result suggests that the low energy physics of the d - p model can not well described by the t - J model near $n = 2$. We think that the existence of multi-band might be crucial to understand the triplet paring superconductivity.

We also examine infinite-dimensional d - p model based on the dynamical mean-field theory. The dynamical mean-field theory becomes exact in the limit of infinite spatial dimensions and believed to be a good approximation in high dimensions. The result is expected to be complementary to the result of the one-dimensional d - p model. We obtain the phase diagrams of the metal-insulator transition on the ground state at half-filling and quarter-filling. We also calculate the magnetization and the pairing susceptibility to obtain the transition temperatures for the ferromagnetism and the superconductivity. It shows that the singlet superconductivity is realized for $n \lesssim 1.4$ near the antiferromagnetic phase, where the antiferromagnetic fluctuation is considered to be responsible for the singlet pairing. On

the other hand, the triplet superconductivity is realized for $T \gtrsim 1.4$ near the ferromagnetic phase. We think that the ferromagnetic fluctuation is responsible for the triplet pairing as well as the one-dimensional case near $n = 2$.

Ferromagnetism and superconductivity has been studied for a long time as a central argument in itinerant electron systems. In this paper, we have presented the electron correlation and the band splitting to be crucial for the ferromagnetism and the related superconductivity in the two types of the two-band Hubbard models. We hope that our work would yield an insight into the deep relationship between these interesting phenomena.

References

- [1] For a review, see, for example, Y. Tokura, Ed., *Colossal Magnetoresistive Oxides* (Gordon and Breach Science, New York, 2000).
- [2] Y. Maeno, H. Hashimoto, K. Yoshida, S. Nishizaki, T. Fujita, J. G. Bednorz and F. Lichtenberg, *Nature* (London) **372** 532 (1994).
- [3] O. Gunnarsson, E. Koch and R. M. Martin, *Phys. Rev.* **B54** R11026 (1996).
- [4] M. Matsukawa, Yuh Yamada, M. Chiba, H. Ogasawara, T. Shibata, A. Matsushita and Y. Takano, *Physica C* **411** 101 (2004).
- [5] G. H. Jonker and J. H. Van Santen, *Physica* **19** 120 (1953).
- [6] R. R. Heikes, R. C. Miller and R. Mazelsky, *Physica* **30** 1600 (1964).
- [7] P. M. Raccach and J. B. Goodenough, *Phys. Rev.* **155** 932 (1967).
- [8] K. Asai, P. Gehring, H. Chou, and G. Shirane, *Phys. Rev.* **B40** 10982 (1989).
- [9] M. Itoh, M. Sugahara, I. Natori and K. Motoya, *J. Phys. Soc. Jan.* **64** 3967 (1995).
- [10] M. Itoh, I. Natori, S. Kubota and K. Motoya, *J. Phys. Soc. Jpn.* **63** 1486 (1994).
- [11] D. Louca, J. L. Sarrao, J. D. Thompson, H. Roder and G. H. Kwei, *Phys. Rev.* **B60** 10378 (1999).
- [12] I. Terasaki, Y. Sasago and K. Uchinokura, *Phys. Rev.* **B56** R12685 (1997).
- [13] T. Motohashi, R. Ueda, E. Naujalis, T. Tojo, I. Terasaki, T. Atake, M. Karppinen and H. Yamauchi, *Phys. Rev.* **B67** 064406 (2003).
- [14] K. Takada, H. Sakurai, E. Takayama-Muromachi, F. Izumi, R. A. Dilanian and T. Sasaki, *Nature* **422** 53 (2003).
- [15] W. Koshibae, K. Tsutsui and S. Maekawa, *Phys. Rev.* **B62** 6869 (2000).
- [16] K. Kusakabe and H. Aoki, *Physica. B* **194-196** 217 (1994).
- [17] W. Gill and D. J. Scalapino, *Phys. Rev.* **B35** 215 (1987) .
- [18] J. Kuei and R. T. Scalettar, *Phys. Rev.* **B55** 14968 (1997) .
- [19] J. E. Hirsch, *Phys. Rev.* **B56** 11022 (1997).
- [20] K. Held and D. Vollhardt, *Eur. Phys. J. B* **5** 473 (1998).
- [21] S. Q. Shen, *Phys. Rev.* **B57** 6474 (1998).
- [22] T. Momoi and K. Kubo, *Phys. Rev.* **B58** R567 (1998).
- [23] H. Sakamoto, T. Momoi and K. Kubo, *Phys. Rev.* **B65** 224403 (2002).
- [24] K. Sano and Y. Ōno, *J. M. M. M.* **310** (2) e319 (2007).
- [25] H. C. Lee, P. Azaria and E. Boulat, *Phys. Rev.* **B69** 155109 (2004).

- [26] T. Shirakawa, Y. Ohata, S. Nishimoto, J. M. M. M. **310 (2)** 663 (2007)
- [27] H. Tasaki, Prog. Theor. Phys. **99** 489 (1998).
- [28] J. Sólyom, Adv. Phys. **28**, 201 (1979).
- [29] V. J. Emery, in *Highly Conducting One-Dimensional Solids*, edited by J. T. Devreese, R. Evrand and V. van Doren, (Plenum, New York, 1979), p.327.
- [30] F.D.M. Haldane, J. Phys. **C14** 2585 (1981).
- [31] J. Voit, Rep. Prog. Phys. **58** 977 (1995).
- [32] H. J. Schulz, Phys. Rev. Lett. **64** 2831 (1990).
- [33] M. Ogata, M. U. Luchini, S. Sorella and F. F. Assaad, Phys. Rev. Lett. **66** 2388 (1991).
- [34] K. Sano and Y. Ōno, J. Phys. Soc. Jpn. **63** 1250 (1994); J. Phys. Chem. Solids. **62** 281 (2001); **63** 1567 (2002).
- [35] L. Balentz and M.P.A. Fisher, Phys. Rev. **B53** 12133 (1996).
- [36] M. Fabrizio, Phys. Rev. B **54** 10054 (1996).
- [37] V. J. Emery, S. A. Kivelson and O. Zachar, Phys. Rev. **B59** 15641 (1999).
- [38] In this case, the electronic state is described by two-component charge degrees of freedom, while the single band model has a single component charge degree of freedom. The bosonization method for the two-chain model with a small interchain hopping[32, 35, 36, 37] shows that the model has a spin-gaped phase and SC and CDW correlations decay as $\sim r^{-\frac{1}{2K_\rho}}$ and $\sim r^{-2K_\rho}$ respectively (SDW correlations decay exponentially). Hence, SC correlation is dominant for $K_\rho > 0.5$. In this case, one of the charge degree of freedom has a charge gap and the remain has gapless excitations.
- [39] K. Sano, Physica **B281&282** 829 (2000); J. Phys. Soc. Jpn. **69** 1000 (2000).
- [40] K. Kusakabe, S. Watanabe and Y. Kuramoto, J. Phys. Soc. Jpn. Suppl. **71** 311 (2002).
- [41] K. Sano and Y. Ōno, J. Phys. Soc. Jpn. **72** 1847 (2003).
- [42] K. Sano and Y. Ōno, J. Phys.: Condens. Matter **19** 14528 (2007).
- [43] Detail of the Moebius boundary condition is discussed by T.F.A. Muller and T. M. Rice, Phys. Rev. **B58** 3425 (1998).
- [44] R. Assaraf, P. Azaria, M. Caffarel and P. Lecheminant, Phys. Rev. **B60**, 2299 (1999).
- [45] M. Imada, J. Phys. Soc. Jpn. **70** 1218 (2001).
- [46] K. Yamaji, J. Phys. Soc. Jpn. **70** 1476 (2001).
- [47] K. Sano and Y. Ōno, Physica **C205** (1993) 170; Phys. Rev. **B51** (1995) 1175; Physica **C242** 113 (1995).
- [48] X. Zotos, W. Lehr and W. Weber, Z. Phys. **B74** 289 (1989).
- [49] A. Sudbø, C.M. Varma, T. Giamarchi, E.B. Stechel and T. Scalettar, Phys. Rev. Lett. **70** 978 (1993).
- [50] W. Barford and E. R. Gagliano Physica **B194-196**, 1455 (1994); see also, C. Vermeulen, W. Barford and E. R. Gagliano, Europhys. Lett. **28** 653 (1994).
- [51] E.B. Stechel, A. Sudbø, T. Giamarchi and C.M. Varma, Phys. Rev. **B51** 553 (1995).
- [52] A. W. Sandvik and A. Sudbø, Phys. Rev. **B54** R3746 (1996).
- [53] K. Sano and Y. Ōno, J. Phys. Soc. Jpn. **67** 389 (1998); **67** (1998) 4151.

- [54] W. Metzner and D. Vollhardt, Phys. Rev. Lett. **62** 324 (1989).
- [55] A. Georges, G. Kotliar, W. Krauth and M. J. Rozenberg, Rev. Mod. Phys. **68** 13 (1996).
- [56] Th. Pruschke, M. Jarrell and J.K. Freericks, Adv. Phys. **44** 187 (1995).
- [57] M. Jarrell, Phys. Rev. Lett. **69** 168 (1992).
- [58] M. Caffarel and W. Krauth, Phys. Rev. Lett. **72** 1545 (1994).
- [59] O. Sakai and Y. Kuramoto, Solid State Commun. **89** 307 (1994).
- [60] R. Bulla, Phys. Rev. Lett. **83** 136 (1999).
- [61] J.K. Freericks and M. Jarrell, Phys. Rev. Lett. **74**, 186 (1995).
- [62] M. Ulmke, Eur. Phys. J. B **1** 301 (1998).
- [63] T. Obermeier, T. Pruschke and J. Keller, Phys. Rev. **B56** R8479 (1997).
- [64] M. Jarrell and T. Pruschke, Z. Phys. **B 90**, 187 (1993).
- [65] A. Koga, Y. Imai and N. Kawakami, Phys. Rev. **B66** 165107 (2002).
- [66] Y. Ōno, M. Potthoff and R. Bulla, Phys. Rev. **B67** 035119 (2003).
- [67] A. Georges, G. Kotliar and W. Krauth, Z. Phys. **B 92** 313 (1993).
- [68] T. Mutou, H. Takahashi and D. S. Hirashima, J. Phys. Soc. Jpn. **66** 2781 (1997).
- [69] Y. Ōno and K. Sano, J. Phys. Chem. Solids **62** 285 (2001).
- [70] Y. Ōno, R. Bulla and A. C. Hewson, Eur. Phys. J. B **19** 375 (2001).
- [71] Y. Ōno, R. Bulla, A. C. Hewson and M. Potthoff, Eur. Phys. J. B **22** 283 (2001).
- [72] Y. Ōno and K. Sano, J. Phys. Soc. Jpn. Suppl. **71** 356 (2002).
- [73] Y. Ohashi and Y. Ōno, J. Phys. Soc. Jpn. **70** 2989 (2001).
- [74] Y. Ohashi and Y. Ōno, J. Phys. Soc. Jpn. Suppl. **71** 217 (2002).
- [75] H. Watanabe and S. Doniach, Phys. Rev. **B57** 3829 (1998).
- [76] In our previous paper[69], we reported that T_{SS} is close to T_{TS} and is slightly higher than T_{TS} for all n , but the calculation was done with a smaller system size $N_s = 4$.
- [77] V. Berezinskii, JETP Lett. **20** 287 (1974).
- [78] A. Tahvildar-Zadeh, M. Hettler and M. Jarrell, Phil. Mag. B **78** 365 (1998).
- [79] H. Masuda, T. Fujita, T. Miyashita, M. Soda, Y. Yasui, Y. Kobayashi and M. Sato, J. Phys. Soc. Jpn. **72** 873 (2003).

Theoretical Study on Nematic Liquid Crystalline Ordering in Thin Confined Systems

Muniriding YASEN[†]

(Department of Physics Engineering, Division of Material Science)

Keywords: Nematic Phase, Maier-Saupe Model, Phase Transition, Effective Field,
Anchoring Wall, Uniaxial and Biaxial Order, Crossover

1. Introduction

An order of nematic is generally soft and reacts sensitively to an external field and also is affected to a condition of boundary walls which confine the liquid crystal. The direction of the order is changed by an electric field under suitable anchoring condition due to walls, and competition between both agents is applied to liquid crystal displays. Therefore, it is important to understand how the ordering and direction are controlled by anchoring conditions.

In this thesis, nematic crystalline ordering in thin confined systems under various type of anchoring conditions are investigated in the framework of the Maier-Saupe model based on statistical mechanism method. In order to clarify the mechanism of continuous change of phase, non-uniformity due to boundary effect is described in terms of effective field which is conjugate to the order parameters, and behavior of the system is analyzed by observing loci of the effective fields on the phase diagram of the bulk.

2. Nematic ordering in a homeotropic cell

The nematic ordering in a thin system under the homeotropic anchoring condition is studied. As the system that correspondent to the homeotropic system, the surface molecule orientation that fixed into a wall surface normal was introduced. The first order transition disappears and continuous change of phase occurs in the system with thickness smaller than a certain critical thickness. The mechanism of this continuous change occurring at the thickness just smaller than a critical thickness is disclosed; a metastable high-temperature phase changes to a metastable low-temperature one continuously via an unstable phase between them. On the other hand, at the extremely thin system, the effective fields do not cross the transition line nor the bound lines of the metastable states and move in an analytic domain, and the system undergoes the usual continuous change.

[†] Product Development Center, Optical Business Headquarters, Nitto Denko Corporation

3. Nematic ordering under external fields

Another type of anchoring wall, that is the state in which the molecule aligns to a substance in parallel is studied. The bulk systems under external field corresponding to this are nematic phase having negative magnetic anisotropy. So, nematic phase transition with both uniaxial and biaxial order parameters is studied in the two kind of external fields where are conjugate to the order parameters, respectively. Figure 1 shows a global phase diagram on the fields versus temperature space is obtained first in the mean field theory, which is similar topologically to the phase diagram of the three-state Potts in three dimensions. Based on this diagram, the ordering phenomenon in the system with planer anchoring walls is predicted, where the first order phase transition changes to the second order one as the thickness of the system becomes small.

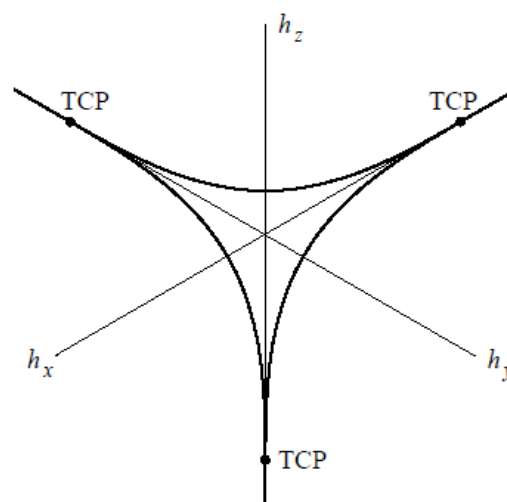


Fig. 1 Phase diagram on the oblique $h_x - h_y - h_z$ plane. TCP is the tricritical point.

4. Effects of Biaxial Anchoring Wall on Nematic Ordering

Nematic Ordering in the system with biaxial anchoring walls are investigated as the correspondent to a bulk nematic system exposed two kinds of external fields. The analyses are carried out in the framework of the mean field theory. The wall condition is given by a probability density function of the long axis orientation of molecule on the wall and by a parameter denoting strength of interaction between a nematic molecule and a molecule on the wall. And Landau unfolding method was used in this study to do a numerical calculation simply. It is shown that the biaxial order suppresses the uniaxial order and the crossover between the homeotropically and homogeneously anchored phases is proved to occur under the condition which is strictly similar to that at bulk in the fields. Also, when the interaction of molecule on wall was strong, it is shown that a wetting phenomenon is caused even under biaxial walls.

Author's publications

- [1] M.Yasen, M. Torikai, M.Yamashita: *J. Phys. Soc. Jpn.*, **73**, (2004) 2453-2457.
- [2] M. Yasen, M. Torikai and M. Yamashita: *Mol. Cryst. Liq. Cryst.* **438** (2005) 77.
- [3] M. Yasen, M. Torikai and M. Yamashita: *2nd Japanese-Italian Workshop on Liquid Crystals* (Tsu (Japan), 2004.9.5-8), Book of Abstracts, P5.

A Study of Positive Active Materials for Lithium Ion Rechargeable Battery

Kenji Shizuka †
(Energy Conversion Chemistry, Division of Materials Science)

Keywords: Lithium-ion battery, Positive active materials, Cathode

1. The objective of this study

The objective of this study is to characterize the positive active materials for lithium ion rechargeable battery and to identify the relationship between the properties and the electrochemical performances, and to bring these results to develop the excellent materials.

2. Summary

【Spinel Li-Mn-O materials】 $\text{Li}(\text{Mn}_{2-x}\text{Li}_x)\text{O}_{4-\delta}$ have been extensively studied for cathode material in large capacity rechargeable Li-ion batteries for EV. However, it has large capacity fading upon charge and discharge cycling. It is important to clarify the mechanism of capacity loss in order to improve the cycle life. Oxygen nonstoichiometry of $\text{LiMn}_2\text{O}_{4-\delta}$ has been reported, however, only qualitative relationship between the cycle life and oxygen deficiency ' δ ' has been reported so far. Therefore, the quantitative details of relationship between the cycle life and the oxygen deficiency were studied. δ was precisely determined by chemical analysis. The capacity retention is linearly decreased with increasing δ . The changes in lattice parameter at the end of discharged state after the cycle depended on δ . They were in good accordance with the degradation in the low voltage region of potential curve, which was strongly affected by oxygen loss and rapidly saturated within about the 100th cycle. These results implied the influence of Jahn-Teller ion Mn^{3+} introduced with oxygen deficiency.

In addition, the mechanisms of manganese spinels dissolution and capacity fade at high temperature were studied. Tests on the stability of spinels stored at different states of charge were performed. Mn dissolution took place irreversibly from the charged state with formation of MnF_2 , ramsdellite- $\text{Li}_{0.5}\text{MnO}_2$. In the discharged state, the Mn at the surface of the LiMn_2O_4 was in equilibrium with a soluble species, which leads to an increase in the cathode resistance. The amount of the dissolved Mn increased with increasing LiPF_6 concentration and that 2 equiv. of PO_2F_2^- were generated. Concurrent formation of carbonate decomposition products suggests the mechanism of Mn dissolution from the charged state was composed of three steps as shown in Fig. 2.

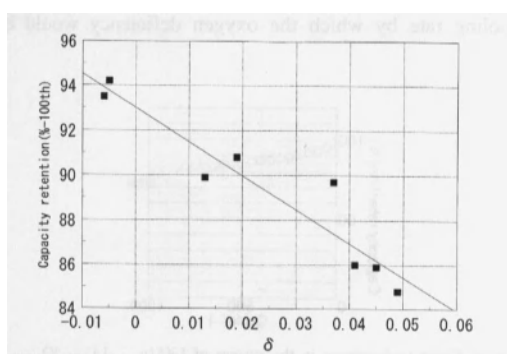


Fig. 1. The relationship between oxygen deficiency δ and capacity retention rate after the 100th cycle.

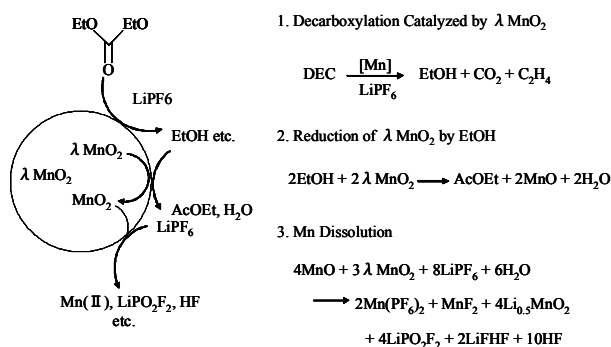


Fig. 2. Proposed mechanism of Mn dissolution from λMnO_2 .

【Layered Li-Ni-O materials】 The effect of CO_2 on layered $\text{Li}_{1+z}\text{Ni}_{1-x-y}\text{Co}_x\text{Mn}_y\text{O}_2$ ($\text{M} = \text{Al}, \text{Mn}$) materials was studied. $\text{Li}_{1+z}\text{Ni}_{(1-x)/2}\text{Co}_x\text{Mn}_{(1-x)/2}\text{O}_2$ ($\text{Ni}/\text{Mn} = 1$) singularly exhibit high storage stability. On the other hand, $\text{Li}_{1+z}\text{Ni}_{0.80}\text{Co}_{0.15}\text{Al}_{0.05}\text{O}_2$ were very unstable. The surface of CO_2 -treated sample is overspread with passivation which might be Li_2CO_3 . The relationship between degree of carbonation and cell performance revealed the discharge capacity was not decreased and the capacity retention was improved during the consumption of excess lithium ' z ', and then deteriorated rapidly above ' z ' in $\text{Li}_{1+z}\text{Ni}_{0.80}\text{Co}_{0.15}\text{Al}_{0.05}\text{O}_2$.

† Mitsubishi Chemical Group Science and Technology Research Center, Inc.

【Layered Li-Ni-Mn-Co-O materials】 $\text{Li}_{1+y}\text{Ni}_x\text{Co}_{1-2x}\text{Mn}_x\text{O}_2$ materials were characterized by various methods. The cell performance depended on the composition. The rate performance deteriorated as Co content decreased, and improved as excess Li content increased. The change of cell performance associated with composition variations was closely related to both the cation mixing (structural disorder) and the volume resistivity (electrical conductivity). The degree of cation mixing depended greatly on Co content, and the volume resistivity depended greatly on excess Li content.

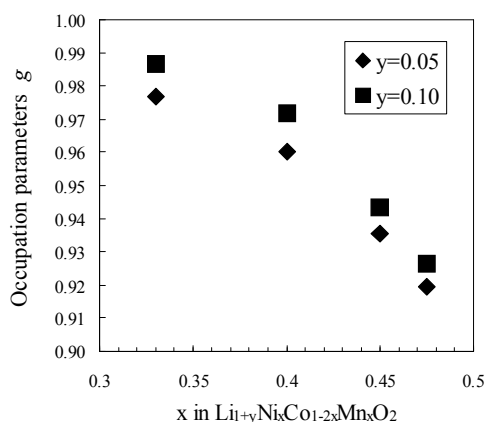


Fig. 3. Relationship between composition and occupation parameter $g(\text{Li})$ for $\text{Li}_{1+y}\text{Ni}_x\text{Co}_{1-2x}\text{Mn}_x\text{O}_2$ ($y=0.05$ and 0.10).

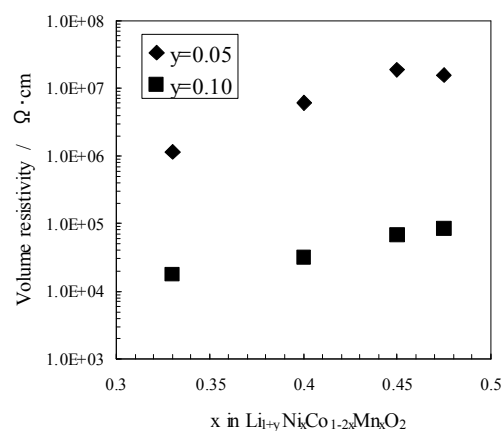


Fig. 4. Relationship between composition and volume resistivity for $\text{Li}_{1+y}\text{Ni}_x\text{Co}_{1-2x}\text{Mn}_x\text{O}_2$ ($0.33 \leq x \leq 0.475$, $y=0.05$ and 0.10).

X-ray absorption fine structure on layered $\text{Li}(\text{Ni}, \text{Mn}, \text{Co})\text{O}_2$ materials was studied. This study revealed that Li contributes to the rate capability through the concentration of Ni^{3+} in the transition metal layers, which is closely related to the volume resistivity of the material. On the other hand, Co contributes to the Li-ion conductivity through the less cation mixing rather than to the electronic conductivity of the pristine powder.

The electrochemical analysis of $\text{Li}_{1+y}\text{Ni}_{5/12}\text{Co}_{1/6}\text{Mn}_{5/12}\text{O}_2$ ($y = 0.04, 0.13$) materials was performed to elucidate how the change of the volume resistivity of the pristine powder contributes to the cell performance. Electrochemical impedance measurements indicated the charge transfer resistance decreased with increased excess Li content 'y'. The equivalent circuits' model considering the volume resistivity was proposed.

【Li-Cu-Ni-O materials】 The solid solution materials between Li_2CuO_2 and Li_2NiO_2 were studied with respect of the electrochemical performance and the crystal structure. Pure Li_2CuO_2 shows only 100 mAh/g of capacity, but nickel substituted compositions delivered reversible capacity of 250 mAh/g corresponding one equivalent of lithium. The enhancement of reversible capacity is attributed to the stability of Ni^{3+} state compared to Cu^{3+} . Li_2CuO_2 undergoes phase change to monoclinic during lithium deintercalation, while the nickel-rich compositions show a new phase different from either original orthorhombic or monoclinic structure. The latter phase shows two-step voltage profile at 2 and 4 V. The middle composition in the solid solutions, e.g. $\text{Li}_2\text{Cu}_{0.6}\text{Ni}_{0.4}\text{O}_2$, indicates high capacity and high resistance against the structural degradation under high rate lithium intercalation.

3. Concluding remarks

The present study has identified the relationship between the properties and the electrochemical performances about the positive active materials, and brought these results to develop the excellent materials.

Author's publications

- [1] Y. Chida, H. Wada, K. Shizuka, Relationship between cycle life of $\text{Li}(\text{Mn}_{2-x}\text{Li}_x)\text{O}_{4-\delta}$ and oxygen deficiency δ , *J. Power Sources*, **81-82** (1999) 454.
- [2] T. Aoshima, K. Okahara, C. Kiyohara, K. Shizuka, Mechanisms of manganese spinels dissolution and capacity fade at high temperature, *J. Power Sources*, **97-98** (2001) 377.
- [3] K. Shizuka, C. Kiyohara, K. Shima, Y. Takeda, Effect of CO_2 on layered $\text{Li}_{1+z}\text{Ni}_{1-x-y}\text{Co}_x\text{M}_y\text{O}_2$ ($M = \text{Al}, \text{Mn}$) cathode materials for lithium ion batteries, *J. Power Sources*, accepted for publication.
- [4] K. Shizuka, T. Kobayashi, K. Okahara, K. Okamoto, S. Kanzaki, R. Kanno, Characterization of $\text{Li}_{1+y}\text{Ni}_x\text{Co}_{1-2x}\text{Mn}_x\text{O}_2$ positive active materials for lithium ion batteries, *J. Power Sources*, **146** (2005) 589
- [5] K. Okamoto, K. Shizuka, T. Akai, Y. Tamaki, K. Okahara, M. Nomura, X-ray absorption fine structure study on layered LiMO_2 ($M=\text{Ni}, \text{Mn}, \text{Co}$) cathode materials, *J. Electrochem. Soc.*, **153** (2006) A1120.
- [6] K. Shizuka, S. Takano, K. Okahara, Relationship between physical properties and electrochemical performances for $\text{Li}_{1+y}\text{Ni}_x\text{Co}_{1-2x}\text{Mn}_x\text{O}_2$ positive active materials, *J. Power Sources*, submitted for publication.
- [7] N. Imanishi, K. Shizuka, T. Matsumura, A. Hirano, Y. Takeda, Preparation and electrochemical properties of Li_2CuO_2 - LiNiO_2 solid solutions as lithium intercalation electrode, *Solid State Ionics*, **177** (2006) 1341.

Estimation, Parameter Learning and Prediction of Time-Varying

Communication Channels

Gagik Mkrtychyan †

Keywords: Digital communication systems, time-varying signal propagation channels, inter-carrier interference cancellation, channel estimation, dynamic parameter learning, model-based prediction.

1. The purpose

The aim of this research is feasibility study of high data rate communication in time varying signal propagation channels. The targets of research are the effective inter-carrier interference cancellation method and provision of the estimation, dynamic parameter learning and prediction of time varying channel response.

2. The related prior arts

There is the known bound for communication systems performance, but that bound is mostly unattainable because of the channel response knowledge error and the interference in time varying channels. The time varying channel response estimation is required for many wireless communication systems because of the user mobility. In some mobile wireless applications, such MC-CDMA, the precise channel estimation is not satisfactory and each user must predict the uplink channel response in the time varying fading channel. The main problem of linear regression based prediction methods is the requirement of the channel's statistics knowledge, or otherwise the large number of known data transmission (pilot symbols or pilot tones) must be done for the precise calculation of the statistical characteristics, which leads to the significant loss of the communication efficiency. The inter-carrier interference (ICI) can become the strong degradation factor for channel estimation and data detection, due to the carrier frequency offset and Doppler frequency spread. While the problem of the carrier frequency offset is comparatively unsophisticated and has multiple suitable methods for the offset correction; the ICI caused by Doppler spread has very complex representation and there is no fully satisfying solution. The ICI occurs because when using IDFT, the spectral density function of n -th subcarrier is zero on the frequencies of all other subcarriers, but it is not zero even very near to them.

3. Proposed methods abstract

This research provides the detail representation of the temporal and spatial characteristics of the time varying channel models. The employed in this thesis dynamically quantized parameter based models describe the time varying channel by limited number of parameter set, which are assumed to be constant during some quantized period of the time, but has random behavior from one time step to another transition. The transition between sets of the parameters depends only from the previous state of the parameters by the Markov chain rule, and the statistics of the time varying channel model is given by the transition probabilities. The conventional preamble symbol based channel estimation methods calculate the channel response separately for the each of preambles and then use linear and nonlinear interpolation for channel response calculation during the data symbols, transmitted between them. In this research is employed a different approach, based on the quantized limited number of the channel parameters, so the received information from the multiple preamble symbols is directly combined for maximum likelihood (ML) channel estimation results calculation.

The conventional pilot tones based channel estimation, widely used in the orthogonal frequency division multiplexing (OFDM) and the multi carried code division multiple access (MC-CDMA), employs the orthogonality of subcarriers for separate sub channels responses estimation and then linearly or nonlinearly interpolates the response through the whole communication channel. This method has two drawbacks for time varying channel: it suffers from introduced inter carrier interference (ICI) and it has a loss of the estimation precision during the interpolation. For solution of these problems in thesis is proposed the time domain correction of the subcarriers to reduce effect of ICI and frequency-time domain estimation for improving the

† Division of Systems Engineering, Department of Electrical and Electronic Engineering, Mie University

precision. In many of the wireless communication systems it is not only required the precise channel estimation but also it's near future prediction. For example the orthogonality of the MC-CDMA uplink transmission can be ensured only by means of the pre-equalization, and for the time varying channels the pre-equalization coefficients must be predicted using the estimation results of the downlink. In this thesis the quantized model based prediction approach is provided, which doesn't use the knowledge of channel statistics. The conventional methods based on the Wiener, Kalman or other filtering techniques need the channel response's autocorrelation knowledge, which is not known for the most of the practical propagation channel conditions.

The final part of the thesis is dedicated to the time varying channel's parameters dynamic learning. Due to the strong tendency to the unification of the mobile communication systems, the software-defined radio (SDR) with reconfigurable signal processing devices becomes the new standard for future generation of the wireless communication systems. SDR requires the learning of the multiple unknown parameters to realize the potential capabilities of the cognitive communication. The dynamic learning of the time varying channel parameters is valuable for SDR because it doesn't employ any knowledge about temporal and spatial characteristics of the propagation paths distribution. The dynamic parameter learning can be executed by means of the evolutionary algorithms in combination with the complex weighted neural networks. Evolutional algorithms are optimal multi dimensional search techniques, and are well known as the effective methods for the parameter learning. Evolutional algorithms can be conditionally divided into the three categories: evolution strategies, genetic algorithms and evolutionary programming. While the neural networks and genetic algorithms were widely used for the time invariant channel response learning, they were not applied to the time varying channel's parameters learning. The problem actually was that both pure neural networks and genetic algorithms couldn't be directly applied to the time varying conditions because the convergence time is too long and small fluctuation can create the chaotic behavior. In this thesis is proposed the usage of the evolutional strategy based method instead of the genetic algorithm. The proposed method controls the fit result of the nonlinearly dependent parameters by means of the choosing the principal components from both of the parents during the "crossover" and keeps the "elitism" of the "population set" by means of introducing the minimal "learning and crossover ages". The complex weighted neural networks, which are employed for learning of the propagation paths amplitudes, are simplified to the single layer perceptrons with the linear activation functions. This allows employing of the direct error gradient based learning of linear parameters, which decreases the number of the required learning steps and is more robust to the fluctuations due to the noise. The convergence problem is solved by the separation of the dynamic learning process for the nonlinearly and linearly dependent parameters. The first is realized by means of the evolutional algorithm, while the second is realized by means of the complex weighted neural network.

4. Concluding remarks

Unfortunately the degradation of data communication performance in time varying channels is inevitable, and all the channels are time varying to a greater or less extent. But in the most of the actual cases it is possible to strongly minimize the degradation effect if precisely to know channel response dependence in time. This thesis proposed the novel methods of ICI cancellation, dynamic learning and prediction of channel.

- 1) The proposed time domain signal form correction method can effectively compensate the ICI without significant increase of the signal processing complexity and is applicable up to the very high vehicle mobility.
- 2) Next contribution of the thesis is in the time varying channel's parameters learning by means of the adaptive quantization and the model based prediction of time varying channel, which allows compensation of the MUI in the uplink transmission of TDD MC-CDMA systems.
- 3) The finally proposed dynamic learning method combines the complex weighted neural networks with evolutionary learning algorithm for simultaneous learning and prediction of channel response, and it provides good accuracy for nearly ideal compensation of the degradation due to the time varying channel.

5. Publications

- [1] Gagik Mkrтчyan, Kazuo Mori and Hideo Kobayashi, "Correction of OFDM Signal Form in Time Domain to Reduce ICI Due to the Doppler Spread and Carrier Frequency Offset," IEICE Transactions on Communications, Vol.E88-B, no.1 pp.122-133, Jan. 2005.
- [2] Gagik Mkrтчyan, Katsuhiko Naito, Kazuo Mori and Hideo Kobayashi, "Doppler Spread Estimation Method for OFDM Signal Using Mean Square of Channel Impulse Response's Time Derivative," IEICE Transactions on Communications, vol.E89-B, No.10, pp2961-2966, Oct. 2006.
- [3] Gagik Mkrтчyan, Katsuhiko Naito, Kazuo Mori and Hideo Kobayashi, "Evolutional Algorithm Based Learning of Time-Varying Multipath Fading Channels for Software Defined Radio," IEICE Transactions on Communications, Vol.E89-B, No.12 pp.3269-3273, Dec. 2006.

Study on Improvement and Application of Titanium Dioxide-Based Photocatalysts

Naomi Nishikawa †

(Advanced Inorganic Chemistry, Division of Materials Science)

Keywords : Photocatalysts, TiO₂, sol-gel method, visible-light-driven

1. Introduction

Semiconductor-based photocatalysts which create electrons and holes by absorbing light have been applied to the design of environmental photocatalytic systems and dye-sensitized solar cells (DSSC). TiO₂ has been extremely focused on its variety of applications, because it shows a number of attractive characteristics such as high photoreactivity, low cost, non-toxicity and chemical stability. Recently, many attempts have been made to improve and apply of titanium dioxide-based photocatalysts.

In this research, it was aimed to prepare an improved photocatalyst based on the titanium dioxide by using the sol-gel method under the environment-friendly condition, and to evaluate their photocatalytic activity. In addition, visible-light-driven TiO₂ thin films were applied to a dye-sensitized solar cell system.

2. Adsorption and Photocatalytic Characteristics of Activated Carbon Made from TiO₂-Coated Woody Waste

Composite powder materials consisting of activated carbon and TiO₂ were prepared through the carbonization of woody waste powders coated with TiO₂ gel by using the sol-gel method. The effect of the conditions for preparing TiO₂ sols and the carbonization process on the properties of the resulting composites was examined. It was found that the addition of diethanolamine (DEA) to the TiO₂ sol was effective for achieving a smooth coating on woody waste-derived activated carbon. The composites obtained by heat-treating the wood powders coated with DEA and polyethylene glycol (PEG)-added TiO₂ gel with at 530 °C and 700 °C exhibited both the adsorption and the photocatalytic decomposition of methylene blue in water.

3. Preparation of Visible-Light-Driven Photocatalysts by Sol-Gel Method and Their Photocatalytic Activity

The Pr-doped photocatalytic thin films were prepared by the sol-gel method. The photocatalytic activity of the films under visible light irradiation was evaluated.

(1) Doping of Pr was very effective to shift the absorption edge of TiO₂ thin film toward the long wavelength. This means that the absorption edge shift toward visible wavelength side in the Pr-doped TiO₂ thin film, probably through the formation of an impurity level due to Pr³⁺ or Pr⁴⁺ in the band gap. For degradation of methylene blue solution, the Pr-doped TiO₂ thin film showed excellent photocatalytic activity under visible light (>400nm) irradiation, especially in the range of 400-500nm, while TiO₂ thin film showed no activity under the same condition (Fig.1). In other words, it was found that Pr-doped TiO₂ thin films acted as visible-light-driven photocatalyst.

(2) Pr-doped titanophosphate glass thin films were prepared by the sol-gel method. Under full arc irradiation of Xe lamp, the photocatalytic activity was observed for all samples. But, under visible light irradiation of Xe lamp, it was only seen for Pr-doped samples.

† Mie Science and Technology Promotion Center, Industrial Research Division, Mie Prefectural Government

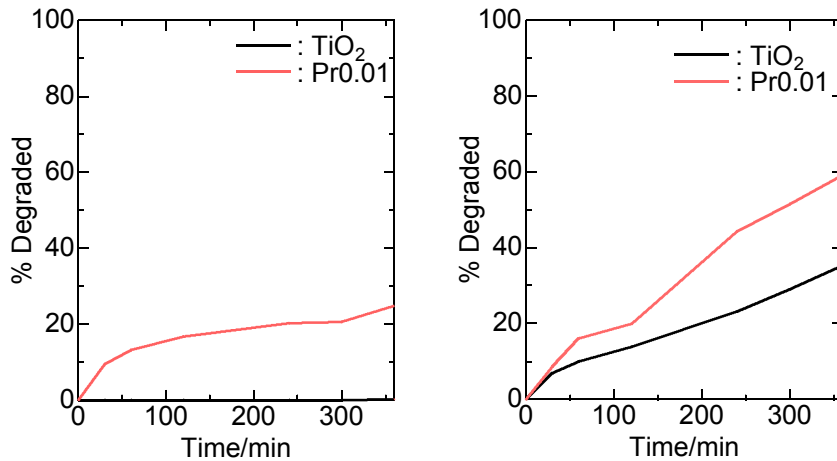


Fig.1 Photocatalytic activity of Pr-TiO₂ film under visible light ($\lambda > 400$ nm) irradiation of Xe lamp.

4. Reduction of Mite Allergen Activities by Photocatalytic Treatment with Titanium Dioxide for a Cleaner Indoor Environment

The reduction of mite allergen activities by photocatalytic treatment with titanium dioxide (TiO₂) was investigated for a cleaner indoor environment. Degussa P25 TiO₂ and recombinant Derf 1 protein were used as the photocatalyst and the mite allergen, respectively. With increasing the amounts of photocatalyst, the rate for the reduction of allergen activities increased gradually. At the irradiation time of 60 min, the reduction efficiencies of allergen activities were more than 96.9%, when the photocatalyst TiO₂ of more than 1 mg was used. As a consequence, the photocatalytic treatment with TiO₂ was very effective for the reduction of allergen activities. Since aspartic acid and glycine concentrations increased during the initial degradation, the destruction of amino acid may become a main reason for the reduction of allergen activities by the photocatalytic treatment. The photocatalytic treatment for the reduction of allergen activities is simple, easy handling and low cost.

5. Application of Visible-Light-Driven Pr-Doped TiO₂ Thin Films to a Dye-Sensitized Solar Cell System

Since it has been expected that absorption in a visible region by the Pr-doped TiO₂ layer was effective to enhance the conversion efficiency of dye-sensitized solar cell (DSSC), the photovoltaic properties of the Pr-doped TiO₂ thin film were evaluated for the DSSC system under the simulated sun light.

As a consequence, the light conversion efficiency (η) of DSSC using the Pr-doped TiO₂ thin film was 1.07%, although the efficiency was 0.71% for DSSC using the pure TiO₂ thin film.

6. Conclusion

In the present study, an improved TiO₂ photocatalyst were prepared by using the sol-gel method under the environment-friendly condition.

Author's Publications

[1] Naomi Nishikawa, Masaki Murayama, Kanichi Kamiya : " Adsorption and Photocatalytic Characteristics of Activated Carbon Made from TiO₂-coated Woody Waste", Mokuza Gakkaishi, Vol.52, No.1, pp.50-54, 2006

[2] Naomi Nishikawa, Satoshi Kaneco, Hideyuki Katsumata, Tohru Suzuki, Kiyohisa Ohta, Yasuo Takeda, Masaki Murayama, Eiji Yamazaki, Noritsugu Hashimoto, Kazuaki Masuyama and Masashi Shoyama : "Fabrication of Visible Light Response Praseodymium-doped TiO₂ Photocatalysts and Its Application to Dye-sensitized Solar Cells", Photo/ Electrochemistry & Photobiology in the Environment, Energy & Fuel, pp.311-319, 2006

[3] Naomi Nishikawa, Satoshi Kaneco, Hideyuki Katsumata, Tohru Suzuki, Kiyohisa Ohta, Eiji Yamazaki, Kazuaki Masuyama, Tadanori Hashimoto and Kanichi Kamiya : "Photocatalytic Degradation of allergen in water with Titanium Dioxide", Fresenius Environmental Bulletin (FEB), accepted,

Investigation of novel asymmetric reactions and synthetic study of a gastrin receptor antagonist, AG-041R

Takashi Emura[†]
(Organic chemistry, Chemistry for materials)

Keywords: Gastrin, Antagonist, Asymmetric synthesis, Diastereoselective, Menthol

1. The purpose

The aim of the research is to establish an efficient synthetic route for the novel anti gastrin agent AG-041R **1**, which has a tetra-substituted chiral center in the structure. The synthesis has to meet the requirement for the manufacturing cost and scalability, therefore efficient construction of the chiral center was investigated.

2. The substantiation of the synthesis

The approach taken for the retrosynthetic analysis (Scheme 1) revealed that a strategy based on the alkylation of the oxindole derivatives would be the most straightforward in order to obtain the basic framework of our target compound. From the outset it was realized that one of the synthetic challenges would be the asymmetric alkylation of oxindole derivative **2**. Therefore, the focus was on identifying an efficient method for the asymmetric alkylation reaction.

Asymmetric alkylation using a phase transfer catalyst is one of the choices for construction of the tetra-substituted chiral center. However, this method still requires a relatively large amount of chiral catalyst, which has a complicated structure and is difficult to obtain.

Due to availability and ease of control of the reaction process, it was decided to investigate the stoichiometric alkylation of oxindole enolates with haloacetic acid esters using a commercially available chiral alcohol such as *l*-menthol as an auxiliary. Reaction of this type has rarely been studied to date, even though a substantial amount of effort in using *l*-menthol as a chiral auxiliary has been demonstrated. To the best of our knowledge, only a single report has been published in which poor stereoselectivity was shown in the alkylation of oxindole derivatives with *l*-menthyl chloroacetate as a chiral electrophile.

3. The results of the asymmetric reaction

The alkylation reaction of urea **2** proceeded efficiently in aprotic polar solvents such as DMF and DMSO and the racemic AG-041 was synthesized from the alkylation of urea **2** with 2-bromo-*N-p*-tolylacetamide, and so we first tried the alkylation reaction with *l*-menthyl bromoacetate in DMF. The resulting diastereoselectivity of the reaction was low (Table 1, entry 1). Even at lower temperatures in DMF, only a slight degree of improvement in the stereoselectivity was observed (Table 1, entries 2 and 3). By using solvent THF, the selectivity showed a slight increase with *t*-BuOK as the base (Table 1, entry 4). When the reaction was performed in a less polar solvent with a lithium cation base, the

SCHEME 1. Retrosynthetic Analysis

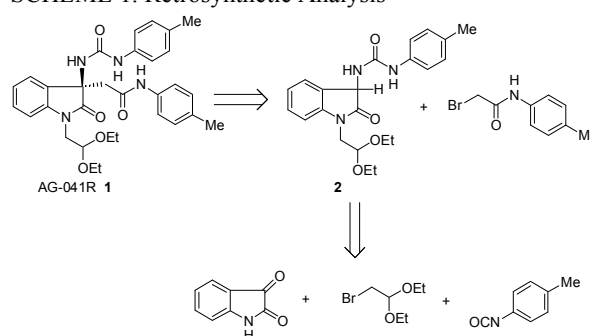


TABLE 1. Diastereoselective Alkylation of the Urea **2**

Entry ^a	Solvent	Base	Equiv of base	Temp. (°C)	Ratio (9 : 10)
1	DMF	<i>t</i> -BuOK	1.1	-10	60:40 ^e
2	DMF	<i>t</i> -BuOK	1.1	-60	75:25 ^e
3	DMF - Toluene	<i>t</i> -BuOK	1.1	-78	80:20 ^e
4	THF	<i>t</i> -BuOK	1.1	-10	75:25 ^e
5 ^b	THF	LiHMDS	1.0	20	90:10 ^e
6 ^{b, c}	Dioxane	LiHMDS	1.0	20	92:8 ^e
8	THF	LiHMDS	1.0	0	92:8 ^f
9	THF	LiHMDS	1.1	0	93:7 ^f
10 ^d	THF	LiHMDS	1.2	0	94:6 ^f
11	THF	LiHMDS	1.1	-15	94:6 ^f

^aUnless otherwise noted, the reaction was carried out with 1.2 equiv of *l*-menthyl bromoacetate. ^b1.1 equiv of *l*-menthyl bromoacetate was used. ^cLiHMDS in hexane was used. ^d1.3 equiv of *l*-menthyl bromoacetate was used. ^eDetermined by ¹H-NMR analysis of the crude reaction mixture. ^fDetermined by HPLC analysis of the crude reaction mixture.

[†]Chugai Pharmaceutical CO., LTD.

diastereoselectivity was greatly increased even at rt (Table 1, entry 5). Although dioxane showed the best results in terms of diastereoselectivity for the reaction (Table 1, entry 6), it requires special handling because of its possible carcinogenic activity. Therefore, THF was selected for further study. The diastereoselectivity increased when the reaction was performed at lower temperature (Table 1, entry 8) and was improved by the use of a slight excess of base (Table 1, entries 9 and 10).

Finally, we selected the reaction conditions shown above (Table 1, entry 9) for further scale-up. We have successfully performed the reaction on a scale of 100 g with a 91.8:8.2 diastereoselectivity ratio.

Recrystallization of the crude product from a methanol/water solution gave a diastereomerically pure product in 55% yield.

The transformation from the menthyl ester **3** to the final compound **1** was performed by the hydrolysis and amidation by using EDC-HCl as a coupling agent, the efficient total synthesis was achieved (Scheme 2).

SCHEME 2.

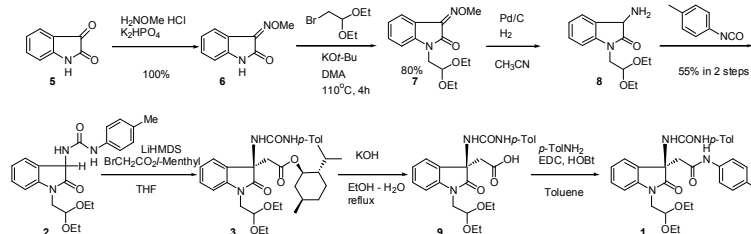


FIGURE 1. *l*-Menthyl Bromoacetate

4. Stereochemistry of the reaction

From the results shown in Table 1 and because the use of a more coordinatable lithium base gave the best stereoselectivity, there is possible coordination of *l*-menthyl bromoacetate with the lithium enolates at its carbonyl group in the transition state. In the most stable conformer of the *l*-menthyl bromoacetate the carbonyl group should be directed downward as depicted in Figure 1, which suggests that the oxindole enolates should approach from the down side of the conformer coordinating with the lithium cation, and thus the approach of the enolates from the upper side would be eliminated. And the results with the other type of oxindole derivatives indicate that the carbonyl group in the nitrogen protective group of the oxindole enolates should participate in the coordination with the lithium cation. Based on these results, the two transition states shown in Figure 2 are possibilities. Of the two, transition state A is preferable due to the steric interaction between the isopropyl group in the *l*-menthyl group and the nitrogen protective group in transition state B.

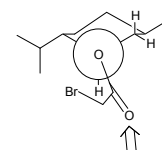
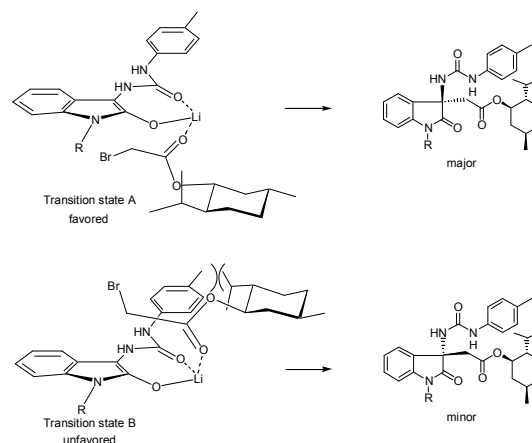


FIGURE 2. Plausible Favored and Unfavored Transition States



5. Conclusion

A highly efficient asymmetric alkylation of oxindole derivatives has been demonstrated by using commercially inexpensive *l*-menthol as a chiral auxiliary. The use of lithium cation is essential for the high diastereoselection. A six-step chromatography-free synthesis of the optically pure oxindole derivative **1** was successfully achieved by the finding of the diastereoselective reaction in overall yield of 26%.

Author's publication

T. Emura, T. Esaki, K. Tachibana, M. Shimizu. Efficient Asymmetric Synthesis of Novel Gastrin Receptor Antagonist AG-041R via Highly Stereoselective Alkylation of Oxindole Enolates. *J. Org. Chem.* **2006**, *71*, 8559.

Fundamental Research on Mechanical Evaluation of Cardiac Function Using Numerical Simulation

Masakazu Tsutsumi
(Material Science, Graduate School of Engineering)

Keywords: Biomechanics, Biomechanics, Human left ventricle, Myocardial wall motion, Finite element method, Mechanical evaluation, Cardiac function

1. Introduction

It is extremely important to estimate quantitatively the mechanical functions of the left ventricle from a viewpoint of the medical diagnosis of heart disease. In order to estimate the ventricular functions, the authors have constructed a fundamental numerical simulation system based on a finite element ventricle model connected with both an electric stimulus transmission model and a blood circulation system model.

2. Mathematical model of left ventricle and finite element simulation

The mathematical models of the left ventricle are composed of the mechanical model of the myocardial fiber, the electric stimulus transmission model and the blood circulation system model. The myocardium consists of numerous contractile muscle fiber elements called "sarcomere" which produce an active tensile force and contract by themselves after receiving the electric stimulus sent from the so-called pacemaker of the heart. The magnitude of active tensile force produced by the sarcomeres may be approximated through a set of simple relations proposed by Beyar and Sideman. The relationships of the magnitude of active tensile force against time and length are indicated in Fig. 1a and 1b, respectively. The installation of the fiber orientation into the finite element model is realized by transforming the standard element in the local coordinate system to the real element in the global coordinate system. As the circulation system model, a simplified electric circuit analogy model is employed in the present numerical simulation. The 3-dimensional geometry of the left ventricle is here assumed to be a prolate spheroid for simplicity. The isoparametric parallelepiped finite elements (198 elements in total) are arranged along the ventricular wall. The mechanical properties of the myocardial fiber and the other various material constants are not determined for a specific individual, but chosen on the basis of studies up to the present as well as the experience and knowledge of medical doctors.

To confirm the reliability of proposed simulation system, the numerical results were compared with the measurements results obtained by the corresponding MR-tagging technique. Fig. 2 shows three strain components in myocardium at end systole for normal heart. As recognized from this figure, the simulated results may reproduce well the corresponding results obtained by MR-tagging technique.

3. Numerical results and discussion

The dynamics changes and biomechanical properties are analyzed through a complete cardiac cycle. The reliability of the obtained numerical results is verified through the comparison with the measurement results obtained from the corresponding MR-tagging technique.

In the research work, the analysis of the cardiac functions supposed the following three heart diseases were performed using the proposed simulation system.

- (1) HHD (Hypertensive Heart Disease)
- (2) DCM (Dilated Cardiomyopathy) accompanied with LBBB (Left Bundle Branch Block)
- (3) MI (Myocardial Infarction)

From simulated results (HHD), it is considered that the amount of contraction of the myocardium decreases when the heart becomes the elevated blood pressure condition. It is also considered that the hypertrophy of the myocardial wall in HHD is one of acclimatization developments to compensate a reduction of the stroke volume.

From simulated results (DCM accompanied with LBBB), it is predicted that deformation of the myocardial wall during early systole is affected by the change of electric stimulus transmission pathway due to LBBB, and that during late systole is affected by the decrease of active force due to DCM.

From simulated results (MI), it is assumed that that the blood pressure is kept to some degree when the amount of contraction of the myocardium decreases 50% compared to normal heart.

4. Conclusion

The numerical system to analyze the mechanical properties and functions of the left ventricle has been constructed in this study by combining the mechanical model of the left ventricle with the circulatory

system model. The proposed simulation system can reproduce the generally well-accepted properties and functions of the left ventricle, and also makes it possible to estimate, for example, the stress distributions which are quite difficult to measure, while all of the basic elements of the system are very simple and fundamental. By substituting higher-grade models for the present fundamental models, the more complicated performance of the left ventricle could be reproduced in a more precise and reliable manner. Hence, in the future we can expect objective and quantitative diagnoses for heart diseases by improving the present numerical system.

There are still many problems to solve before we can realize the ideal simulation system. One of them is that there is a shortage of reliable invivo information about the mechanical properties of the bio-tissues and organ. And even if we could obtain such information, the characteristic complexity, the time dependence and the individual differences of organisms are turned to considerable barriers for the numerical simulation. However, it is expected that numerical simulators like those presented here will pay a major role in overcoming these difficulties.

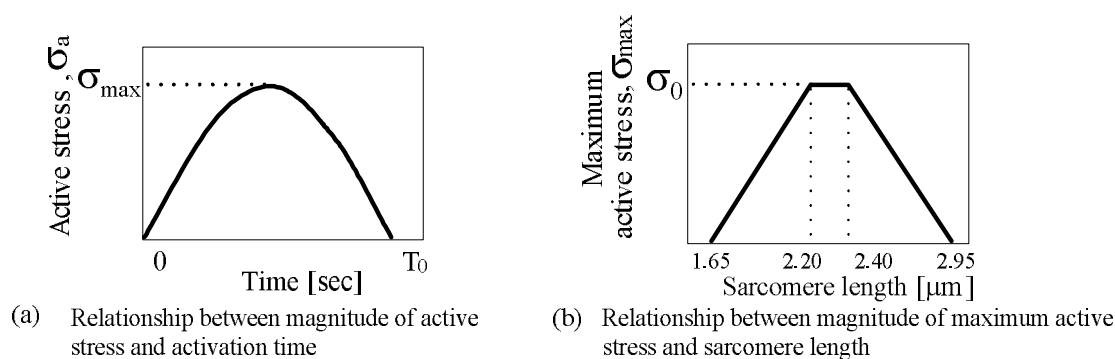


Fig. 1 Mechanical model of myocardium

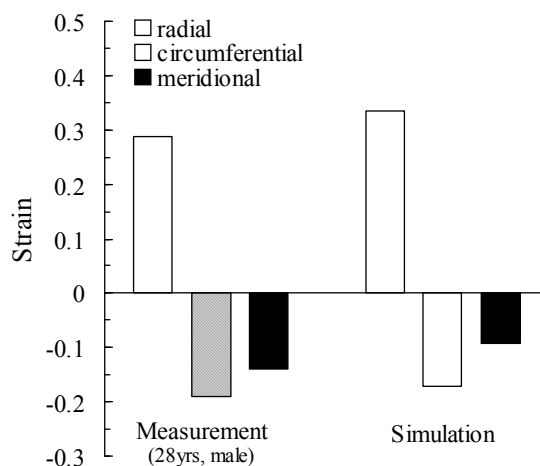


Fig. 2 Comparison between measurements by MR-tagging and numerical results (FEM) for normal heart

Author's publications

[1] Tadashi INABA, Takahiro NAKANO, Masakazu TSUTSUMI, Shingo KAWASAKI, Yasutomi KINOSADA, Masataka TOKUDA, Quantitative Evaluation of Left Ventricular Wall Motion in Patient with Coronary Artery Bypass Grafting Using Magnetic Resonance Tagging Technique, JSME International Journal, Series A, Vol.49, No.4, pp. 597-603, 2006.

[2] Masakazu TSUTSUMI, Akiyoshi SHIOMI, Tadashi INABA, Yutaka SAWAKI, Masataka TOKUDA, Finite Element Analysis of Cardiac Function in Hypertensive Heart Disease, Proceedings of 4th World Congress of Biomechanics, Proceedings CD, 2002.

[3] Masakazu TSUTSUMI, Kazuyuki YANAGISAWA, Tadashi INABA, Masataka TOKUDA, Mechanical Evaluation of Cardiac Function in Heart with Disease by Numerical Simulation, Proceedings of 5th World Congress of Biomechanics, pp.563-566, 2006.

Experimental Research on Mechanical Properties of Zr based Bulk Metallic Glass

Takamasa Yoshikawa

(Mechanical Properties of Materials, Division of Materials Engineering)

Keywords: Zirconium based bulk metallic glass, Amorphous, Mechanical properties, Thermoplastic deformation, Crystallization

1. Introduction

Bulk metallic glasses (BMGs) are alloys that have various features that are not observed in conventional metallic materials. BMGs consist of metallic elements with amorphous structures. It has the thickness and size enough to be applied to a structural material, i.e. bulk size, and exhibits the specific glass transition phenomenon different from conventional amorphous alloys. The BMGs show the excellent mechanical properties, high corrosion resistance and exhibit a low magnetic coercive force. In particular, Zirconium-based BMGs have not only high mechanical properties but also high glass forming ability. Due to these remarkable properties, it is expected that Zr-based BMGs will be applied to new structural materials. However, BMGs must be worked and formed at high temperatures into the desired shape for mechanical applications, because it is difficult to plastically deform BMGs at room temperature (RT).

In this study, the influence of thermoplastic deformation on the mechanical properties of BMGs at RT is investigated. In particular, the effects of temperature, strain, and strain rate in thermoplastic deformation on the fracture stress of BMGs at RT is focused on. A comprehension of the dependence of these parameters under hot conditions on the material strength at RT will expedite the industrial use of BMGs.

2. Experimental method

The strength properties of $Zr_{55}Al_{10}Cu_{30}Ni_5$ and $Zr_{60}Al_{10}Cu_{25}Ni_5$ BMGs were investigated at RT (293 K). To study the influence of heat alone on the mechanical and atomic structural properties of these BMGs at RT, specimens were heated in a muffle furnace. Subsequently, mechanical loading tests and analysis of atomic structure by using a XRD were performed at RT after cooling. Moreover the plastic deformation behavior of these BMGs at high temperature was studied by using a hot loading machine to which an electrical furnace is attached. The tensile tests were performed at various temperature conditions and strain rates. All the thermoplastic deformation experiments were stopped before the fracture of the specimens. After thermoplastic deformation, the strength properties were studied at RT, and compared with the as-cast materials. To investigate the thermal properties of the $Zr_{55}Al_{10}Cu_{30}Ni_5$ and $Zr_{60}Al_{10}Cu_{25}Ni_5$ BMGs, a DSC was used.

3. Result and discussion

The fracture stresses of as-cast $Zr_{55}Al_{10}Cu_{30}Ni_5$ and $Zr_{60}Al_{10}Cu_{25}Ni_5$ BMGs at RT were more than 1500 MPa. These materials exhibited a large elastic strain, extending up to 2.0%. On the other hand, it was difficult to plastically deform these BMGs at RT. The stress-strain curves of these BMGs are similar to those of so-called brittle materials, particularly for the tensile tests. However, several experimental results indicated that the BMGs have mechanical properties similar to those of ductile materials such as steel, although no plastic strain appears in their stress-strain curves at RT.

When the $Zr_{55}Al_{10}Cu_{30}Ni_5$ BMGs were heated at a temperature greater than 685 K in the muffle furnace, this material was crystallized. Furthermore, the fracture stress of crystallized material drastically decreased at RT after cooling. The material undergoing heating above 685 K is embrittled and loses the ductile properties that the as-cast materials possess. However, the $Zr_{55}Al_{10}Cu_{30}Ni_5$ BMG after being heated below 685 K was not crystallized and its mechanical strength can be maintained at levels similar to that of the as-cast samples. On the other hand, the $Zr_{60}Al_{10}Cu_{25}Ni_5$ BMG also maintains the as-cast strength properties after being heated at a temperature below 710 K. Therefore, these temperatures can be considered as the upper limit temperature in order to maintain the as-cast strength after a heating process.

These materials exhibited plastic strain at a high temperature although no plastic deformation appeared at RT. The temperature to allow the plastic deformation lied over not only a higher but also a lower temperature than the upper limit temperature. The property of plastic deformation of these BMGs at a high temperature depended strongly on not only the temperature but also the strain rate.

The three parameters—strain, temperature, and strain rate of the thermoplastic deformation—can be considered to have an effect on the structure of the BMG, and thus on the strength after the deformation, even if the environmental temperature is lower than the upper limit temperature. Therefore, the influence of each parameter on the mechanical properties of the $Zr_{60}Al_{10}Cu_{25}Ni_5$ BMG at RT was studied. The experimental results showed that the strength of this BMG at RT after the thermoplastic deformation depends strongly on the amount of thermoplastic strain, the temperature and the strain rate during deformation. When the strain rate is comparatively low, the strength of this material at RT gradually decreases with increasing the thermoplastic strain. On the other hand, a higher strain rate prevents the strength after thermoplastic deformation from decreasing. Furthermore, the decrease of the strength of this BMG at RT is significant at a higher temperature even if the temperature is lower than the upper limit temperature.

From the thermal analysis by using a DSC, the crystallization temperature of the specimens deformed under various hot conditions changed with the thermoplastic strain. The tendency of the change coincided with those of the strength at RT after the deformation depending on the three parameters. The decrease of crystallization temperature is considered to imply that the material changes into the state to be more easily crystallized because the crystalline phase is precipitated and then a local free volume increases inside the amorphous phase.

4. Conclusion

From the experimental results of Zr-based BMGs, the influence of the thermoplastic deformation on the mechanical properties at RT was clarified. It is important and useful from the industrial viewpoint that these BMGs can be freely deformed and the excellent strength properties can be maintained after thermoplastic deformation.

Author's publications

- [1] T. Yoshikawa, M. Tokuda and T. Inaba, Key Engineering Materials, Vols. 340-341, (2007) pp.113-118
- [2] T. Yoshikawa, M. Tokuda and T. Inaba, Journal of The Society of Materials Science Japan, Vol. 56, No.2, (2007) pp.171-177

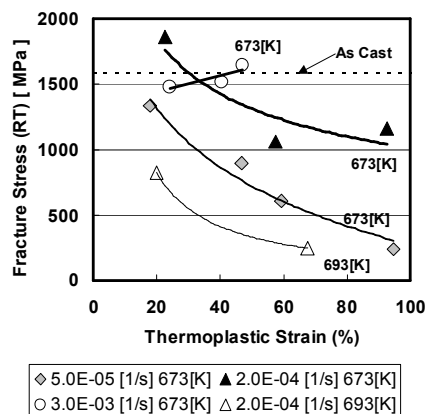


Fig. 1 Influence of thermoplastic strain at 673 K corresponding to strain rate and temperature on fracture stress of $Zr_{60}Al_{10}Cu_{25}Ni_5$ BMG at RT

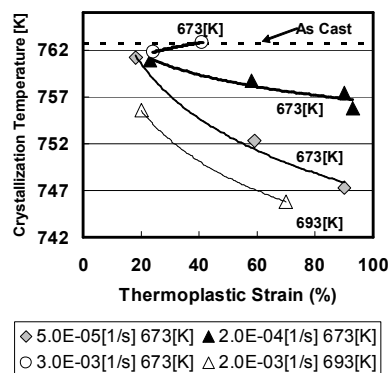


Fig. 2 Influence of thermoplastic deformation parameters on crystallization temperature of $Zr_{60}Al_{10}Cu_{25}Ni_5$ BMG at RT

A Study on the Modification of the Engineering Plastics to the Advanced High-Performance Materials

Hatsuhiko Harashina[†]
(Materials Chemistry, Division of Materials Science)

Keywords: Engineering plastics, Poly(oxymethylene), Poly(ethylene terephthalate), Poly(ester amide), Ethanolamine, Flame retardancy, Thermal properties, Thermal analysis, Molecular orbital calculation

1. Introduction

Engineering plastics, including Poly(oxymethylene)s (**POMs**) and poly(ethylene terephthalate) (**PET**), have superior physical, mechanical, thermal, electrical and chemical properties, and they have been used in many industrial fields such as the automotive, electrical/electronic, construction and consumer markets. Moreover, in order to apply **POM** and **PET** to various industrial fields as the further advanced materials, the progressive and drastic improvement of the fundamental issues having **POM** and **PET** needs to be performed. As a design methodology for the advanced high-performance engineering plastics, the formulation design by packaging of the optimized functional additives (ex. flame retardants) or the structural modification by introducing of hydrogen-bondable amide groups to the polymer main chain can be expected.

The present paper describes the results of a study on the modification of the engineering plastics to the advanced high-performance materials, including **POM** and **PET**, the objective of which was to produce new advanced plastic compositions and polymers, characterize them, and obtain the fundamental design methodology to create the advanced high-performance materials.

2. Results and Discussion

2.1. A Study on Design Methodology for High-Performance (flame retardancy) of POM [1]

New flame retardant combination system for **POM** was investigated. It was found that **POM** is synergistically flame-retarded by the combination of red phosphorus with novolac as a phenolic resin and melamine as an aminotriazine compound. Furthermore, the detailed combustion behavior of the flame retarded **POM** has been studied to confirm its flame retarding mechanism by using thermal and FTIR analyses. The results of cone calorimetry, thermogravimetry and FTIR analysis suggested that the flame retarding mechanism is the intumescent char formation in the condensed phase. Novolac having a phenolic hydroxyl group is miscible with **POM**, and in the flaming process, red phosphorus yields phosphine and its acidic product such as phosphoric acid due to hydrolysis and oxidation reactions.

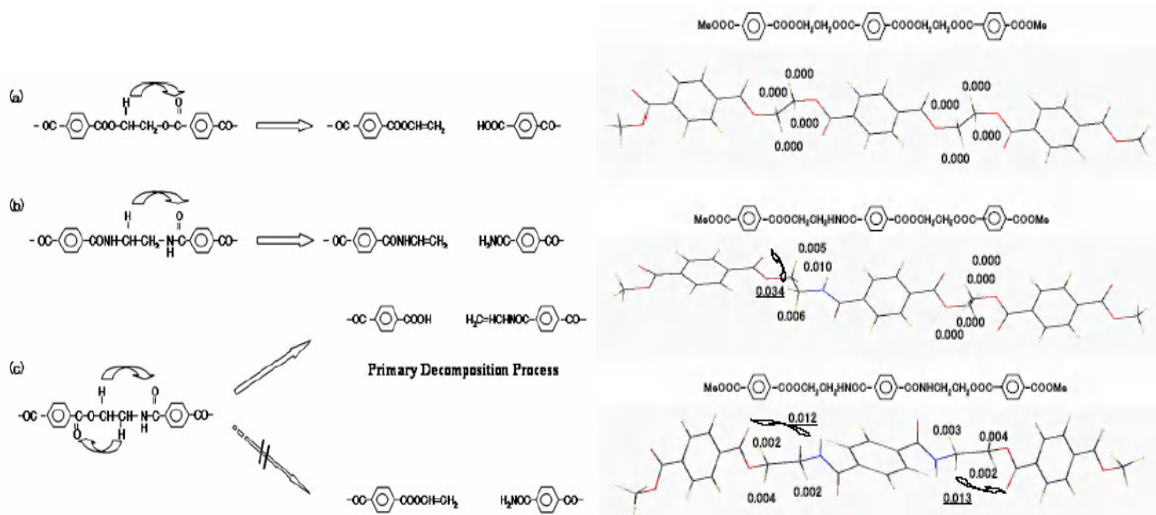
In addition, all of novolac, melamine and phosphine are able to readily react with formaldehyde generating from **POM** during burning to give the reinforced and cross-linked char network through the polyaddition and polycondensation reactions. Therefore, the red phosphorus/novolac/melamine ternary combination system could synergistically promote the high flame retardancy of **POM** without the flaming drips.

2.2. A Study on Design Methodology for High-performance of semiaromatic polyesters [2, 3]

Semiaromatic poly(ester amide)s (**PEAs**) were synthesized by the melt polycondensation of ethanolamine (**EA**)-derivatives with dimethyl terephthalate (**DMT**) and ethylene glycol (**EG**) in the presence of tetrabutyl titanate as a catalyst, and their crystallization and thermal properties were investigated.

[†] Polyplastics Co., Ltd.

Introduction of an amide group into the semiaromatic polyesters such as poly(ethylene terephthalate) (**PET**) gave the **PEAs** (**EA**-modified **PET** polymers) having an increase of melting point. Interestingly, these **PEAs** were found to decompose at a lower temperature than **PET** on the basis of the TGA analysis. Moreover, the direct pyrolysis/mass spectrometry suggested that an initial step of the thermal decomposition was a β -CH hydrogen transfer reaction via a six-member ring transition state at the ester-ethylene-amide unit, at which the carbon-oxygen bond scission takes place to yield carboxyl and *N*-vinylamide end groups (Scheme 1). Furthermore, molecular orbital calculations using trimer model molecules supported strongly that the β -CH hydrogen transfer reaction in the thermal decomposition of **PEAs** occur more easily at the methylene group next to the amide group in an ester-ethylene-amide unit rather than at the methylene group next to the ester group in an ester-ethylene-ester one (Figure 1).



Scheme 1.

The β -CH hydrogen-transfer reactions of (a) **PET**, (b) poly(ethylene terephthalamide), and (c) **PEAs**.

Figure 1.

Frontier electron densities on ethylene protons for trimer models of **PET** and **PEAs**.

3. Conclusions

i) The red phosphorus/novolac/melamine ternary combination system could promote the high flame retardancy of **POM** without the flaming drips. The flame retarding mechanism was the intumescent char formation to give the reinforced and cross-linked char network through the polyaddition and polycondensation reaction in the condensed phase.

ii) Semiaromatic poly(ester amide)s (**PEAs**) were synthesized by the melt polycondensation of ethanolamine derivatives with **DMT** and **EG**. The primary thermal decomposition of **PEAs** was a β -CH hydrogen transfer reaction via six-member ring transition state in the ester-ethylene-amide unit to form carboxyl and *N*-vinylamide end groups. The thermal decomposition behavior of **PEAs** was explained well by semiempirical molecular orbital calculations on the basis of trimer model molecules.

Author's Publications

- [1] H. Harashina, Y. Tajima, T. Itoh, "Synergistic effect of red phosphorus, novolac and melamine ternary combination on flame retardancy of poly(oxymethylene)", *Polymer Degradation and Stability*, vol.91, 1996-2002 (2006).
- [2] H. Harashina, T. Nakane, T. Itoh, "Synthesis of Poly(ester amide)s by the Melt Polycondensation of Semiaromatic Polyesters with Ethanolamine and Their Characterization", *Journal of Polymer Science Part A: Polymer Chemistry*, vol.45, No.11, 2184-2193 (2007).
- [3] H. Harashina, T. Nakane, T. Itoh, "Synthesis and Properties of Semi-aromatic Polyesteramides Using Ethanolamine", *Polymer Preprints, Japan* vol.53, No.2, 4119 (2004).

A Study of the Reception Space Planning of Homes for the Elderly

Hideki FUJIEDA

(Architecture and planning, Division of Systems Engineering)

Keywords: Visitor, Residents, Change of receptions, State of receptions, Setting, Nursing home

1. The significance of setting reception space of a nursing home as a research theme

The act of receiving guests in a homelike environment has been considered to be an important act that ties people inside the house and those outside, and various types of reception space have been created in the private homes. However, in spite of its importance, the reception space of nursing homes has never been discussed in detail, nor even the actual situation is grasped yet. Current national policy for the preparation of the nursing homes is to attain the continual homelike environment before and after entering them. Thus, more and more attention is to be paid to the reception space. In this sense, it is necessary to grasp the current conditions of the reception space of the nursing homes and to propose a guideline to them.

2. Purpose of the Study

A study of the reception space planning is a new perspective. Therefore, there are almost no previous studies of this matter. This study aims to set up some guidelines for the nursing homes to become a place where both the residents and the visitors feel at home. This is done by (1) overviewing the current trends in order to extract their characteristics, and (2) analyzing the reception space in detail.

3. Definition of the reception at a nursing home

It is defined as residents and visitors "sharing time comfortably."

4. Status of visitors

There are two types of visitors to nursing homes: one is those who come to see the residents individually; the other is those administrating the programs of the nursing homes.

5. The institutions investigated

In order to grasp the current situation of various types of homes for the elderly, the institutions investigated are those covered by the public nursing care insurance set by the Ministry of Health, Labor and Welfare. The author sent out a questionnaire to a total of 55 institutions: 19 special nursing homes, 9 group homes, 10 care houses, 2 private nursing homes, 13 geriatric health care institutions, 2 geriatric medical care hospitals. In addition, the author visited 11 institutions: 4 special nursing homes, 3 geriatric health care institutions, 1 geriatric medical care hospital, 1 group home, 2 care houses.

6. The method of this study and its results

This study is carried out in five phases through "interviews and questionnaires to people involved in the act of reception" and "the observations of the receptions space of the institutions."

[Issues of the Reception at the Homes for the Elderly]

Processes and problems involving the act of reception (chapter 2) aim to grasp the actual situation of the reception at the institutions, to organize the significance of reception and the problems of reception at institutions, and to propose the topics to be discussed in the following chapters. What is clarified here is that the act of reception is necessary for residents of the institutions since it facilitates psychologically affirmative effects and that the institutional programs are necessary especially at the institutions for the aged since it leads to heartwarming mingling at various places in the site of the institutions. Following matters are to be considered for individual visits: frequencies of the visits, location of the institutions, equipment of the rooms, reception at the common space, and the awareness of the people involved in the act of reception. As to the institutional programs, environments that generate conversations and the awareness of the people involved in the act of reception are to be considered.

As to the changes of reception after moving into institutions (chapter 5), some specific characteristics of the life in the NAITO Architects Co.,Ltd,Dr.Eng.

institutions are extracted in contrast to those found in the private homes. What is clarified to be of importance as to the location of the institutions is the accessibility by private cars. This is because many of the visitors visit the institutions by car regardless of the distance from their residence. Next, reception at the common space and the attitudes of the inmates and the guests are investigated. The act of reception is found to be performed not only in the private rooms but also at various places inside and outside the institutions. The private rooms are preferred because in there both the guests and the inmates are able to enjoy private conversations in an intimate atmosphere. On the other hand, the guests have to care a lot about the health condition of the inmates and the inmates are sometimes reluctant to show their private space to the guests. That is why they go outside the private rooms for a walk or for a change of mood. In order for the inmates to enjoy the reception outside the private rooms "without feeling any constraints," following places are preferred: half-private living rooms, dining rooms, corridors, entrance halls, meeting rooms, bathrooms and outside institutions. Of course, different institutions have different facilities (i.e., presence or absence of certain equipment) and these also affect the details and frequencies of the act of reception.

[Extraction of the Conditions of the Reception Space Planning]

As to the equipment of the reception space of the institutional program (chapter 3), observation and analysis are done in order to grasp the conditions in which the act of reception through the program prepared by each institution becomes successful by the visitors who take part in the program and to clarify the condition for the preparation of the reception space. As a result, six types of institutional programs (i.e., viewing-type, circle-type, service-type, luncheon-type, conversation-type, and festival-type) are proved to be used differently in the care space, in the common space outside the care units in the building, and outside the building. Also, necessary conditions for each space division are clarified.

As to the case study of how the change of the reception space affects the atmosphere of the reception space (chapter 4), in order to clarify the factors that may improve the quality of life (QOL), observation and analysis from the point of view of the relationship between the improvement of the living conditions and the reception circumstances are done through the cases of reconstruction of the hospitals for long-stay inpatients. As a result, necessary conditions for the preparation of the space in the private rooms, necessity of the places for the visitors to have a rest and exchange information and their requirements are extracted.

As to the equipment of the reception space of the institutions (chapter 6), in order to clarify the factors that bring about the reception, observation and analysis of the equipment are done by comparing the equipment of the places where reception is done. As a result, conditions for the staff members' ease of assistance and environmental conditions of private rooms, dining rooms, living rooms, and the space for residents and visitors to move together are clarified.

Lastly, a reception space planning checklist is proposed by summing up the results obtained by analyzing the situation and factors of reception, the conditions necessary for the preparation of the reception space, and the program conditions necessary for the preparation of the reception space. Furthermore, the checklist is applied to the two institutions (new KT hospital for long-stay inmates, and Y special nursing home) of which the author involved in designing and the designing concept is "the actualization of the homelike atmosphere." The problems of the design concept are in conformity with the ones drawn from the reception space planning checklist. This demonstrates that the reception space planning checklist obtained as a result of this study is effective in the actual design of the construction.

The reception space planning checklist proposed in this study is useful not only in designing an institution that aims to fulfill homelike atmosphere but also in administrating an institution since it gives us beneficial information on the improvement of the residents' facial expressions and physical conditions. The author, therefore, expects it to be widely accepted.

Although this study focuses on the reception space planning for the institutions of the elderly, its concept is applicable to the institutions where the mentally and/or physically malfunctioning people live or receive medical care as well as to the institutions for the elderly who require nursing care since the act of reception is an indispensable activity for a human to live.

Author's publications

- (1)H.FUJIEDA,S.IMAI,S.KINOSHITA:A Study of the Spatial Conditions of the Reception in Nursing homes, Journal of Architecture and Planning,No616,pp39-46,June.,2007
- (2)H.FUJIEDA,S.IMAI,S.KINOSHITA:A Study on Scenes of Reception in Nursing home, Regional Community Facilities Planning and Design,AIJ,Vol.23,pp251-258,Jul.,2005
- (3)N.OCHI,H.FUJIEDA,S.IMAI,S.KINOSHITA:Programed Reception to Neighborhood in Nursing homes, Regional Community Facilities Planning and Design,AIJ,Vol.23,pp259-264,Jul.,2005

A quantitative study on the camera calibration error

Takashi Fujimoto*

(Machine vision, Division of system engineering)

Keyword: camera parameter calibration, camera parameter, formulization, optimization, quantification

1. Purpose

The object's position on the image taken by the camera gives the information on the direction of a visual line cast by the camera on the object. Like a triangular surveying where the number of observing points is two, by using the information on the direction of a visual line from two or more observing points, 3-D position for the target can be presumed by fusing these. In order to perform this with high accuracy, we require the directions of visual lines with sufficient accuracy. Here, cameras involve some important camera parameters such as the principal point that is the intersection of the optical axis of camera with the image plane, the principal distance that is the distance between the center of lens and the image plane, and the length of 1-pixel on the image plane. So, these parameters are used for transforming image coordinates into visual lines with respect to the camera, not only measuring the image coordinates of object's feature points, but also we have to calibrate the camera parameters. So, camera parameter calibration is the basic and practical technique in the field of 3-D measurement based on visual information. So, in this research, we focus on the 2-plane calibration method is one of the simplest calibration methods, in the field of calibration technique, that use the reference such as the points and lines whose configuration are known, and conduct a study of following 3 perspectives.

1. Raising the precision of camera parameter calibration
2. Quantification of the calibration error to the true value of camera parameter
3. Evaluation of 3-D estimation error due to the calibration error

The outline of each viewpoint is as follows.

1. The accuracy of 2-plane calibration method calibrates the camera parameters by taking a picture of the calibration fiducial chart moving in the depth direction is affected by following factors.

- Amount of movement in depth direction of the calibration fiducial chart
- Imaging condition while photographing the calibration fiducial chart

So, we propose a new imaging condition from the perspective improving the accuracy of calibration, and optimize the amount of movement in the depth direction of the calibration fiducial chart.

2. New imaging condition and traditional imaging condition, in addition, we suppose the imaging condition that is possible in practical use, and formulized the accuracy of camera parameter calibration into the amount of movement in depth direction of the calibration fiducial chart.

3. So, the essential information obtained from 2-D image is visual angle that is the angle in which observing the object from camera, and is 3-D information, it is important to evaluate the accuracy of camera parameter calibration by using visual angle. In this research, we suppose the method to evaluate the error of visual angle accurately, and ascertain the characteristics between camera parameter calibration error and visual angle.

1. The candidate in this research

As before, in this research, we focus on the 2-plane calibration method. And, the parameters to be calibrated are following camera parameters.

- Principal point : the intersection of the optical axis of camera with the image plane
- Principal distance : the distance between the center of lens and the image plane
- The length of 1-pixel on the image plane

Suzuka Fuji Xerox Co.,Ltd *

And, we are premised on pinhole model as camera model. In addition, the 2-plane calibration method is the calibration method calibrating the camera parameters by taking a picture of the calibration fiducial chart moving in the depth direction.

2. Calculational procedure

In this research, We assume that the error is caused from the observation error of image coordinates of the fiducial points arisen in which we observe the fiducial points arranged on the calibration fiducial chart. Therefore, we calculate the error from camera to object calculated based on value of camera parameter calibration by using law of error propagation.

3. The influence of the imaging condition on the accuracy of calibration

The accuracy of 2-plane calibration method is affected by the imaging condition in which we take a photo of the calibration fiducial chart. So, we optimize the distance of the calibration fiducial chart, and formulize the calibration error of principal distance under the condition that the number of fiducial points are photed at the position of the calibration fiducial chart is near and far from camera is same (imaging condition.1). In addition, we formulize the calibration error of principal distance and the length of 1-pixel on the image plane under the condition that the additional fiducial points are photed at the position of the calibration fiducial chart is far position(imaging condition.2). By taking a photo of more fiducial points, we can advance the accuracy of calibration in 2-plane calibration method.

4. The influence of the setting error of the calibration fiducial chart on the accuracy of calibration

In actual use, there is a possibility that the position and the angle of the calibration fiducial chart. So, we formulize the accuracy of calibration if the position and the angle of the calibration fiducial chart involve errors.

5. The evaluation of the camera parameter calibration error by using visual angle

The essential information obtained from 2-D image is visual angle that is 3-D information and is the angle in which observing the object from camera. So, it is important to evaluate the accuracy of camera parameter calibration by using visual angle. In this research, we suppose the method to evaluate the error of visual angle accurately, and ascertain the characteristics between camera parameter calibration error and visual angle. And finally, we formulize the error of visual angle.

6. Conclusion

In this research, we focused on the 2-plane calibration method is one of the simplest calibration methods in the field of calibration technique. And, we examined the accuracy of calibration under the imaging condition.1 and imaging condition.2. Then, we optimized the amount of movement in depth direction of the calibration fiducial chart, and ascertained accuracy of calibration is improved under the imaging condition.2, and formulized the calibration error of camera parameters under each imaging condition. In addition, in practical use, there is a possibility that the position and the angle of the calibration fiducial chart, so that we formulize the accuracy of calibration if the position and the angle of the calibration fiducial chart involve errors. And finally, so the essential information obtained from 2-D image is visual angle that is 3-D information and is the angle in which observing the object from camera, we ascertained the characteristics between camera parameter calibration error and visual angle, and formulize the error of visual angle.

Author's publications

- [1] Y.NOMURA, T.FUJIMOTO, and D.ZHANG, "A Formulization of Camera-Parameter Calibration Errors and Resultant Visual-Line Estimation Errors" *Transactions of the JSME(Series C)* Vol.71, No.706(2005) pp.147~ 155
- [2] T.FUJIMOTO, Y.NOMURA, " Relationships between the camera calibration accuracy and the imaging condition" *Transactions of the JSME(Series C)* Vol.72, No.717(2006)
- [3] Takashi Fujimoto, Yoshihiko Nomura, "A formulation of camera parameter calibration error due to reference point setup error", *PROCEEDINGS of Asia International Symposium on Mechatronics (AISM)* 2006, December 12-15, (2006), CD-ROM
- [4] T.FUJIMOTO, Y.NOMURA, and D.ZHANG, "Theoretical Error Analysis with Camera Parameter Calibration" *PROCEEDINGS OF SPIE in Machine Vision and its Optomechatronic Applications*, Vol.5603(2004), pp.182~190.
- [5] T.FUJIMOTO, Y.NOMURA, and D.ZHANG, "A formulation of camera parameter calibration considering all errors about reference points " *PROCEEDINGS OF JSME in Mechanical Engineering Congress* ,Japan(2006), Vol.VII, pp.327~ 328.

Study on Systematization of Porous Concrete with Small to Large Size Aggregates

Akihiro Maegawa †
(Architecture, Division of Systems Engineering)

Keywords : Porous concrete, Aggregate, Particle size, Environment, Geometrical model

1. INTRODUCTION

Porous concrete is environmentally friendly material that has continuous voids inside to be used widely in various fields. The performance of porous concrete is largely determined by the size and quantity of the internal pores, and pore size is controlled and adjusted by the aggregate grain diameter used as well as the volume of bonding material. However, according to the past papers, most of studies on the porous concrete, the aggregate of the particle size 2 - 20 mm has been used. Therefore, in this study, to expand the usage of porous concrete, manufacturing method and fundamental properties of porous concrete with small to large size aggregates have been examined. With small size aggregate (particle size: 0.6 - 2.5 mm), it was defined as small particle size porous concrete, while with large one (particle size: 40 - 400 mm), it was defined as large particle size porous concrete. **Table 1** shows the placement of this study in porous concrete. In addition, to analyze the theory of compressive strength of porous concrete, a geometric model with ideally spherical aggregates was proposed.










2. EXPERIMENTAL STUDY ON FUNDAMENTAL PROPERTIES OF SMALL PARTICLE SIZE POROUS CONCRETE

Basic properties of small particle size porous concrete (hereafter referred to as “SPOC”) were examined. According to the test results, SPOC was superior in water retention and pumping compared to normal particle size porous concrete (particle size: 5 - 13 mm). **Fig. 1** shows that the smaller the aggregate grain, the higher the water retention and pumping rate. It should be noted, however, that permeability of SPOC is rather low.

3. EXPERIMENT AND MODELING ON RELATIONSHIP BETWEEN COMPRESSIVE STRENGTH AND VOID RATIO OF POROUS CONCRETE

There was little theoretical examination on the relationship between void ratio and compressive strength

Table 1 The placement of this study in porous concrete

Classification		The object of this research		Area investigated in the past			The object of this research	
								
		Small particle size porous concrete (Porous mortar)		Porous concrete			Large particle size porous concrete	
Aggregate	Particle size	0.6~1.2mm	1.2~2.5mm	2.5~5mm	5~13mm	13~20mm	20~40mm	40~400mm
	Kinds of material	Crushed fine stone, Molten fine slag		Crushed stone, Recycle aggregate			Crushed stone, Concrete rubble	
Construction method		Mixing by mixer  Tamping vibration / Spraying		Mixing by mixer  Tamping vibration			Integration of coarse aggregate by spraying binder	
Application field		Water retentive and pumping pavement Water penetration pavement Base for greenery		(Grasses)			(Trees) (Fishing reef)	

† Mie Science and Technology Promotion Center, Industrial Research Division, Mie Prefectural Government

of porous concrete. Therefore, a simple geometrical model concerning compressive strength was proposed, and the calculated values were compared with the experimental ones. From the result, it is possible to predict the experimental results by means of the proposed model. Especially, in the case of direction 1, orthorhombic lattice array showed an excellent presumption accuracy (Fig. 2).

4. FUNDAMENTAL STUDY ON MANUFACTURING METHOD OF LARGE PARTICLE SIZE POROUS CONCRETE

Manufacturing method of large particle size porous concrete (hereafter, referred to as "LPOC") using concrete rubble was examined. As the aggregate grain diameter was large, it was difficult to mix LPOC by means of a normal mixer. Therefore, in stead of manufacturing with a mixer, a binder was splayed on the upper surface of the concrete rubbles of every layer. By the experiment, it was confirmed that LPOC was producible by the spraying method.

5. APPLICABILITY AS FISHING REEF OF LARGE PARTICLE SIZE POROUS CONCRETE

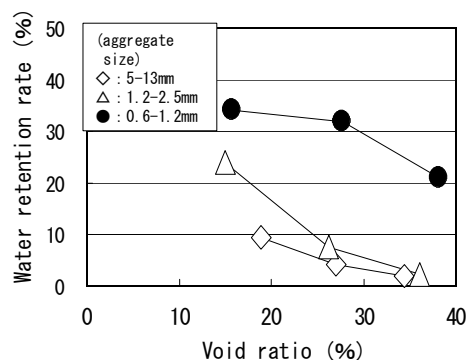
Experiments have been carried out to confirm applicability of LPOC as the fishing reef. Firstly, to confirm stability of fishing reef placed in a sea, LPOC was sunk in the large-scale waterway where waves and currents can be generated. It has been found that void of fishing reef decreases the power of current and wave, and the effect on wave is especially large. Next, to confirm applicability as a fishing reef for marine creatures, 70 LPOC blocks (size: 1 m × 1 m × 0.7 m) were sunk into Ise bay of Mie Prefecture. After six months, lobsters, abalones, sea cucumbers etc. were found to live in LPOC. Judging from the result, LPOC is useful to fishing reeves.

6. CONCLUSIONS

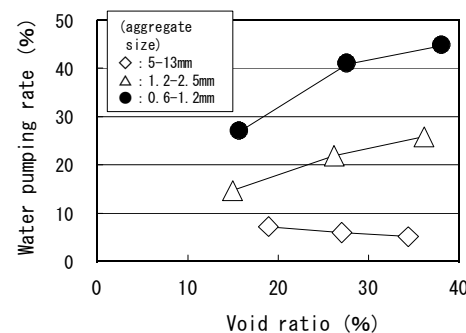
In the present study, a new performance of porous concrete was recognized. Moreover, a geometrical model concerning compressive strength of porous concrete was proposed. In the future, it is expected that results of this study contribute to the development for porous concrete.

Author's Publications

- [1] Akihiro Maegawa, Shigemitsu Hatanaka, Naoki Mishima and Yukihiisa Yuasa, *Fundamental study on manufacturing method of large particle porous concrete using concrete rubble and applicability as fishing bank*, Journal of Structural and Construction Engineering, AIJ, No. 589, 43-48, Mar., 2005
- [2] Akihiro Maegawa, Shigemitsu Hatanaka, Naoki Mishima and Yukihiisa Yuasa, *Fundamental study on manufacture of large particle porous concrete using concrete rubble*, Proceeding of Japan Concrete Institute, Vol. 26, No. 1, 1455-1460, 2004
- [3] Akihiro Maegawa, Shigemitsu Hatanaka, Naoki Mishima and Moe Kuroda, *Fundamental study on bending fracture properties of large particle porous concrete*, Proceeding of Japan Concrete Institute, Vol. 27, No. 1, 1273-1278, 2005
- [4] Akihiro Maegawa, Toshihiko Shakouchi, Yukihiisa Yuasa, Naoki Mishima and Shigemitsu Hatanaka, *Research on stability of fishing bank made by large particle porous concrete placed under sea*, Journal of Technology and Design, AIJ, No. 22, 53-58, Dec., 2005
- [5] Akihiro Maegawa, Akira Yamamoto, Naoki Mishima and Shigemitsu Hatanaka, *Experimental study on manufacturing method of small particle size porous concrete*, Proceeding of Japan Concrete Institute, Vol. 28, No. 1, 1397-1402, 2006
- [6] Akihiro Maegawa, Shigemitsu Hatanaka, Naoki Mishima and Akira Yamamoto, *Experimental study on fundamental properties of small particle size porous concrete*, Cement Science and Concrete Technology, No. 60, 264-270, 2006



(a) Water retention rate



(b) Water pumping rate

Fig. 1 One example of test results of small particle size porous concrete

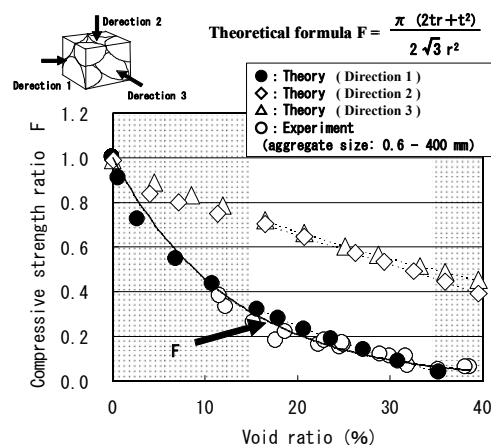


Fig. 2 Comparison between theoretical value and experimental value

(In the case of orthorhombic lattice array)

Flow Analysis of Particle Laden Two-Phase Jet Flow from Rectangular Nozzle and Its Application to Micro-Blasting Process

Masaki Sugimoto*
(Fluid Engineering, Division of Systems Engineering)

Keywords: Rectangular jet flow, Gas-solid two phase flow, Micro-blasting

1. Introduction

Micro-blasting process, MBP by particle laden impinging air jet flow with the order of 10mm particles has been increasing in order to process brittle materials, such as glass or ceramic, as the fine process for high accuracy and productivity. In MBP, a circular nozzle is used commonly, yet it takes a large number of scanning times to process a wide area, and then a long machining time. Recently, use of a two-dimensional rectangular nozzle has been considered to process a large area with high efficiency. However, it is difficult to obtain uniform and high accuracy for cutting depth over the nozzle width.

In this study, in order to improve the cutting performance of an MBP nozzle, a new rectangular nozzle with a large aspect ratio is proposed and the flow characteristics and cutting performance are examined precisely.

2. Experimental and results

Figure 1 shows the nozzles used. The first nozzle is considered in order to change a circular cross section to a rectangular one. The second nozzle has three bars in it to diffuse or spread the flow. The third and fourth nozzles are proposed to improve the cutting performance. Particle laden impinging jet is used to process the brittle material, glass plate. Particle used is silicon carbide, SiC of 50% diameter d_{p50} is $25\mu\text{m}$.

The particle behavior from each rectangular nozzle was measured by PIV. The cutting performance of nozzle was examined by evaluating the shape of cutting cross section of glass plate. The cutting efficiency was evaluated by comparison of cutting removals per supplied power with conventional circular nozzle.

Figure 2 shows the visualized flow pattern in the half right had the particle velocity vectors and in the half left had the particle concentration for the free jet of each nozzle, respectively. In the case of 1st nozzle, particle does not disperse to y direction, it concentrated at center of nozzle, $y/h=0$. However setting the vane in nozzle, particle dispersed to y direction, 2nd nozzle shows uniform concentration except edge of nozzle. The concentration of 3rd nozzle has uniform all over the nozzle width, then the velocity vector becomes uniform, too.

The cutting performance of each nozzle is shown in Fig.3. All of the case, cutting depth correspond with particle concentration, dense region becomes deep and thin region becomes shallow. Center of nozzle and near the both side edge in y direction the cutting depths of 1st and 2nd nozzle are considerably. On the other hand, the 3rd nozzle has a high cutting performance, the accuracy of cutting depth of it is within 10% in the wide range at $-70 < y/h < 70$ since particle flow is uniform.

Figure 4 shows the cutting efficiency of 3rd nozzle with conventional nozzle. The 3rd nozzle has the largest

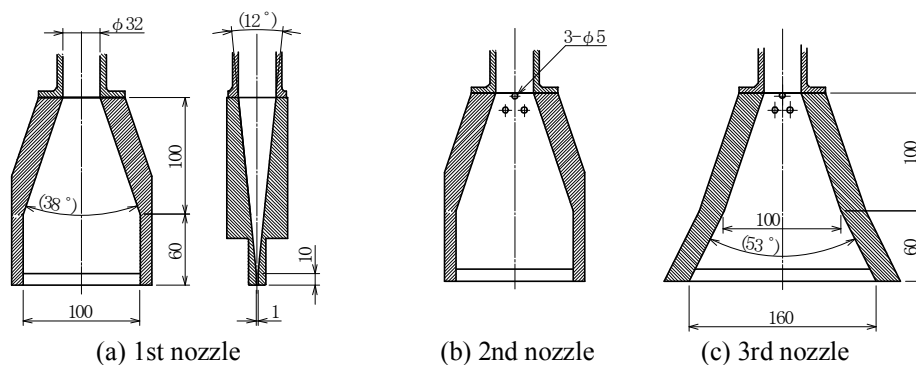


Fig. 1 Details of new rectangular nozzle

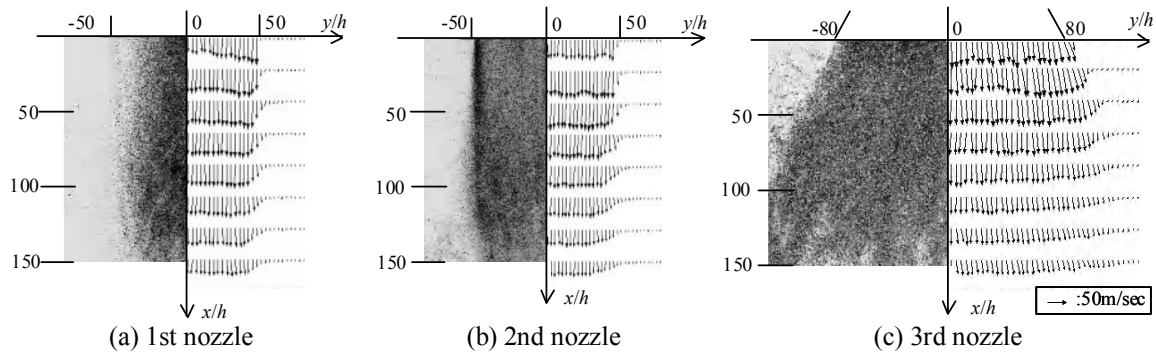


Figure 2 Particle flow image and particle velocity vector

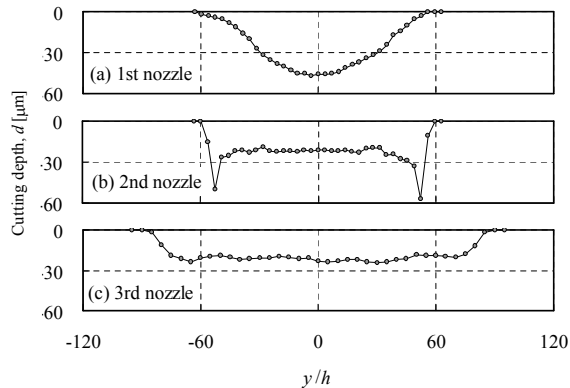


Figure 3 Cutting profile of work-piece

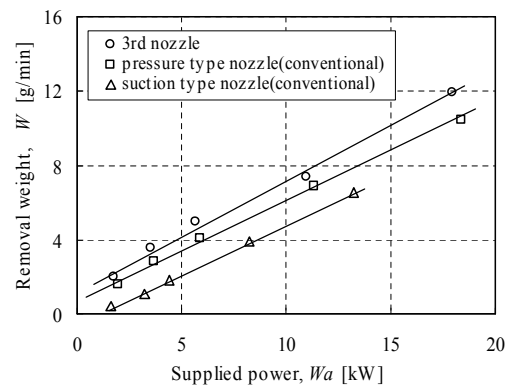


Figure 4 Cutting efficiency

cutting efficiency under the same supplied power. The cutting rate of the 3rd nozzle is almost 1.2 times of the conventional circular nozzle, and moreover it has a larger processing speed. It results from reduction of particle-particle interaction and improvement of particle discharging from impinging spot at work-piece.

3. Conclusion

Main results are as follows,

- (1) The circular vane is effective to uniform the particle flow. Also, uniform particle flow can be obtained by expanding the nozzle exit.
- (2) The cutting accuracy shows a high quality of within 10% at $-70 < y/h < 70$ for the 3rd nozzle.
- (3) The 3rd nozzle takes the largest removal weight compared to the conventional circular nozzles. For example, cutting efficiency of the 3rd nozzle improves by 20% of the pressure type nozzle at the supplied power of $W = 10$ kW.

Author's publications

- [1] M. Sugimoto, T. Shakouchi, K. Hayakawa, M. Izawa, Gas-Particle Two-Phase Jet Flow from Slot Nozzle and Micro-Blasting Process, Trans. of Jpn. Soc. Mech. Eng., Series B, Vol.71, No.710 (2005), pp. 2450-2457.
- [2] M. Sugimoto, T. Shakouchi, K. Hayakawa, M. Izawa, A study on Machining Characteristics of Two-Dimensional Rectangular Abrasive Jet Machining Nozzle, Journal of Jpn. Soc. Precis. Eng., Vol.72, No.1 (2006), pp. 121-126.
- [3] M. Sugimoto, T. Shakouchi, K. Hayakawa and M. Izawa, Gas-Particle Two-Phase Jet Flow from Slot Nozzle and Micro-Blasting Process, JSME Int. Journal, Series B, Vol.49, No.3 (2006), pp. 705-713.
- [4] M. Sugimoto, T. Shakouchi, M. Izawa, Behaviors of Particle Laden Jet Flow and Machining Characteristics of Micro-Blasting Process, Journal of Jpn. Soc. Abras. Technol., Vol.51, No.1 (2007), pp. 46-51.
- [5] M. Sugimoto, T. Shakouchi, K. Hayakawa, M. Okazaki and M. Izawa, Particle Laden Impinging Jet Flow from Rectangular Nozzle and Abrasive Jet Machining, Proc. of Int. Conf. on Jets, Wakes and Separated Flows, ICJWSF-2005, JSME No.05-201 (2005), pp. 325-330.
- [6] M. Sugimoto and T. Shakouchi, Development of Rectangular Microblasting Nozzle, Proc. of Int. Conf. on Precision Engineering, ICPE 11th, JSPE Publication Series No.5 (2006), pp. 181-186.

Investigations on a Vertical Upward Gas-Liquid Two-Phase Flow through Sudden Contraction or Expansion Pipe

Voutsinas Alexandros+

(Fluid and Thermo Engineering Laboratory, Division of Systems Engineering)

Keywords: Bubbly two-phase flow, Sudden expansion-contraction pipe, Fluctuating flow, Flow control

1. The purpose

The aim of this research is to study the pipe flow characteristics when a gas-liquid two-phase flow passes through a vertical abrupt contraction or expansion area. The effect of several parameters, such as Reynolds number and volumetric gas flow rate, are considered. Drag and fluctuating phenomena are investigated and simple plus economic flow control methods are proposed and their results are presented.

2. Related prior arts

Two-phase gas-liquid flow systems are frequently seen in the industrial field. Several studies have been conducted so far, such as Aloui et al. (1999), conducting experiments for the singularity pressure drop, void fraction, wall shear stress, bubble velocity and size, or Kondo et al. (2003) giving valuable information concerning flow regime difference, local void fraction flow observation on bubble deformation.

However, studies dealing with the fluctuating phenomena and drag of the expansion /contraction area, and methods of flow control are scarcely seen in the bibliography.

3. Results and discussion

3.1 Sudden contraction pipe flow

The present work is divided into two main parts. Part one, is the case of a sudden contraction and part two, the expansion case. In both cases flow parameters were varied and the effect on the flow pattern was investigated.

For the case of a sudden contraction, prior to and after the contraction area, vortices generate, affecting significantly the downstream flow. The flowing conditions affect the size and length of it and fluctuating phenomena were observed. When the flow control method was applied, it showed a remarkable suppression of the vortex generation downstream, which is closely related to drag and fluctuation phenomena. In the following, fig.1 shows the comparative results from FFT analysis conducted between the plain contraction and when a ring shaped obstacle (proposed method) is attached in two different upstream positions. It is clear that the PSD value, which represents the intensity of the fluctuation, is largely suppressed when the flow control method is applied. This verifies that flow control is been achieved.

Figure 2 shows the results from the drag reduction measurements. Pressure distribution along the vertical axis was measured and the pressure loss difference due to the contraction effect was investigated.

3.2 Sudden expansion pipe flow

After the positive results from the proposed flow control method, investigations on the sudden expansion case were conducted. Similar to the contraction, on the downstream, vortex area is generated. In addition, due to the buoyancy force of the bubbles a gas-free region exists just downstream the expanded area. The area of this region is strongly affected by the liquid velocity. In addition, even though an axisymmetric sudden expansion,

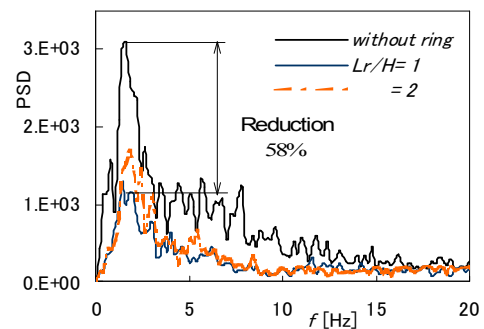


Fig.1 FFT analysis results
($A=0.18$, $Re=2 \times 10^4$, $\alpha_v=5\%$)

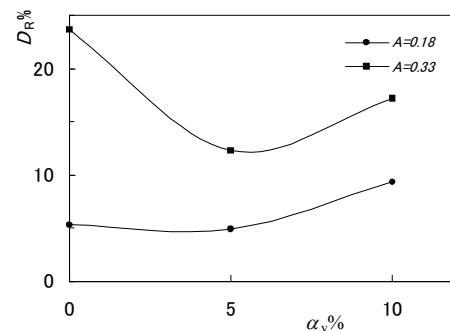


Fig.2 Drag reduction rate, $L_r/H=1$
($Re=1 \times 10^4$)

small changes in the force balance within the vortex region cause instabilities and fluctuating phenomena occur.

Two flow control methods were investigated. One, mounting the ring shaped obstacle at several downstream positions, dividing the vortex region into two parts and reducing its intensity. The second, installing a step-ring just after the expansion in order to reduce the recirculation area size.

It was found that two dominant frequency peaks exist. In addition, the second peak is strongly affected by the gas fraction as shown in fig.3. Increasing the volumetric gas fraction, it shows a tendency to shift its frequency to lower values even under different Reynolds number.

In fig.4, the FFT result between the plain expansion and the two suggested methods is illustrated. The fluctuation amplitude is considerably suppressed for both dominant peaks.

The drag reduction occurring due to the flow control method was also calculated and results are presented in fig.5. Reduction under all flow conditions was achieved, with values reaching up to 40% at its maximum.

4. Concluding remarks

- 1) From visualization results in both cases it was made apparent that the vortex region is strongly affected by the Reynolds number and volumetric gas fraction.
- 2) Fluctuation phenomena were investigated downstream the contraction/expansion. The dominant fluctuation frequency is affected significantly by gas fraction. Two dominant peaks were observed up to $\alpha_v=20\%$ for the sudden expansion, while just one was seen for higher values showing a tendency to shift its frequency to lower values in all cases.
- 3) When a ring is mounted, the frequency value did not change. This denotes that the geometric structure does not affect it. The most effective ring position shifts downstream for all Re number when increasing α_v .
- 4) Applying the flow control method, manages to suppress the vortex generation and reduces the fluctuation intensity, reaching values up to 70% depending on the flow conditions
- 5) The losses occurring due to sudden changes were investigated and by the proposed methods, drag reduction was achieved. Positive results could be retrieved at all conditions with values reaching up to 40%.

Author's Publications

- 1] A. Voutsinas., T. Shakouchi., k. Tsujimoto., T. Ando., "Flow Characteristics and Drag Reduction of Vertical Upward Gas-Liquid Two-Phase Flow through Sudden Contraction Pipe"(In Japanese), *Transactions of JSME, Series B*, Vol.72, No.720, (2006), pp.1888-1894.
- 2] A. Voutsinas., T. Shakouchi., J. Takamura., K. Tsujimoto and T. Ando., "Flow Characteristics and Control of Vertical Upward Gas-Liquid Two-Phase Flow Through a Sudden Contraction Pipe" *JSME-International Journal, Series B1*, November, (2006), No.06-4043.
- 3] A. Voutsinas., T. Shakouchi., J. Takamura., K. Tsujimoto., T. Ando., "Flow and Control of Vertical Upward Gas-Liquid Two-Phase Flow through Sudden Contraction Pipe", *Proceedings of the ICJWSF, International Conference on Jets, Wakes and Separated Flows*, CD-ROM (2005), pp.307-312, Toba, Mie, Japan.
- 4] A. Voutsinas., T. Shakouchi., T. Tsujimoto., T. Ando., "Gas-Liquid Two-Phase Oscillating, Fluctuating Flow through Vertical Sudden Contraction Pipe", *Transactions of JSME, Series B*, Vol.72, No.717, (2006), pp.1131-1136.
- 5] T. Shakouchi., T. Nakamura., J. Kawaguchi., A. Voutsinas., K. Tsujimoto and T. Ando., "PIV Measurement of Flow Characteristics Around Two-Tandem Square Cylinders in Gas-Liquid Bubbly Flow", *Proceeding of 4th International Symposium on Measurement Techniques for Multiphase Flows*, Sept. 10-12, (2003), Hangzhou, China.

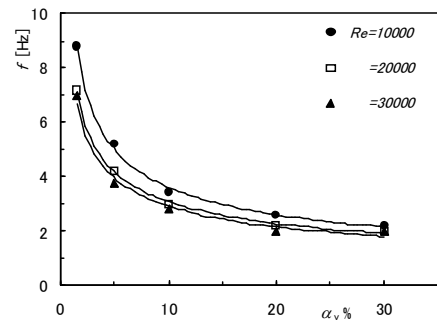


Fig.3 Second peak frequency variation under various Re number and gas fraction

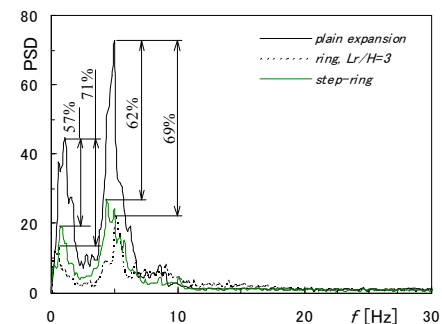


Fig.4 FFT analysis results
($Re=1 \times 10^4$, $\alpha_v=5\%$)

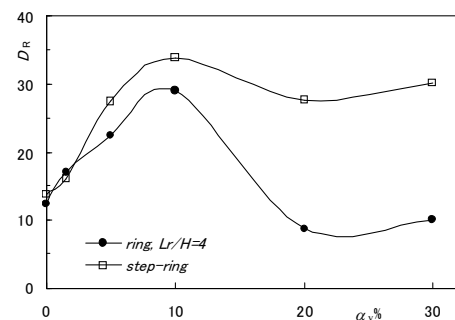


Fig.5 Drag reduction rate, D_R , ($Re=2 \times 10^4$)

A study of efficient downlink packet transmissions technique for CDMA cellular mobile communications

Abubaker Faraj Khumsi †

Keywords: Mobile communications, CDMA, Downlink, Transmit power control, Soft handoff, Transmission control, IP packets, Geographical unfairness, TPWC, MLPT, Downlink capacity

1. The purpose

The aim of this study is to improve the system capacity in CDMA cellular systems, especially in downlink communications. The focus on the applications which do not have stringent delay requirements such as web browsing and file transfer, the real time transmissions are not always necessary and time delay is tolerable such as IP packets. Since the CDMA cellular system is the major system and succeeded in the commercial application, the focus in this thesis is on this technique.

2. The related prior arts

The rapid growth in demand for mobile communications has led into intense research and development effort towards a new generation of cellular systems. The new system must be able to provide quality of service (QoS), support a wide range of services and improve the system capacity. In the cellular systems, the mobility causes dynamic variations in link quality and interference levels, sometimes requiring that a particular user change its serving base stations. This change is known as a handoff. Usually, continuous service is achieved by supporting handoff from one cell to another. The availability of cheap and reliable wireless Internet access will shift the service base traditionally found in mobile cellular networks toward emerging wireless Internet service. This will result in significant demand being placed on both existing and next generation cellular and IP networks. The key challenge in realizing an IP wireless network is how to support soft handoff in order to minimize the packet losses and enhance the system performance. Although the soft handoff is an effective way to increase channel capacity, reliability, and coverage of CDMA (Code Division Multiple Access) systems, it has some disadvantages especially in downlink channels. One of the main problems is that the simultaneous multiple base station transmissions will cause an increase in the interference that affects other radio links, and consequently limits the downlink capacity. The conventional scheme, Site Selection Diversity Transmission Power Control (SSDT), which realizes site selection transmission diversity instead of the full site transmission diversity during soft handoff mode has also some shortcomings. The disadvantage of this scheme is that in bad channel conditions the larger transmitted power is required to compensate the fading. As a result of this, the downlink interference increases.

3. Proposed methods abstract

This thesis focuses on the applications which do not have stringent delay requirements such as web browsing and file transfer, the real time transmissions are not always necessary and time delay is tolerable. The aim of this thesis is to enhance the system performance for the downlink IP packet transmission by improving the transmission delay and geographical unfairness in transmission quality.

This thesis divided into three parts; in the first part we propose a transmission control scheme to support IP packets transmission on CDMA wireless networks. The objective of this proposal is to improve the system capacity with maintaining the minimum service disruption during handoffs of the mobile stations. In this proposed scheme, if the channel condition is bad due to fading fluctuation, the base station delays the packet transmission until better channel conditions are available. In other words, the base station sends the packets only when the instantaneous attenuation from the transmitting base station is less than a threshold value. The performance assessment of the simulation results proved that by applying this proposed scheme the system throughput would be efficiently improved.

† Division of Systems Engineering, Department of Electrical and Electronic Engineering, Mie University

In the second part of this thesis; the location-based transmission power and window control scheme (location-based TPWC scheme) is proposed. The objective is to improve the transmission delay performance and the geographical unfairness in transmission quality. In the conventional TPWC and multi-link packet transmission (MLPT) scheme, the packets are sent only during a transmit time window according to the propagation conditions. Besides, MLPT scheme reduces the delay caused by TPWC. However, by applying this conventional scheme, there will be a considerable increase in the transmission delay under some circumstances owing to the delay packet transmission. To avoid these shortcomings, the proposed scheme offers the same transmission window size for all mobile stations in order to improve the delay and unfairness. By using the soft handoff status as an indicator of the mobile locations, the base station individually adjust the transmission window for each mobile station. By maintaining almost the same size of transmission window for all the mobile stations, which is attained by adjusting the required threshold value for each mobile station, the transmission delay performance and the geographical unfairness can be improved.

In the third part of this thesis; an adaptive transmission window control scheme based on soft handoff status and traffic load is proposed. This scheme is proposed to avoid the shortcomings of our previous proposed scheme (a location-based TPWC scheme). The location-based TPWC scheme improved the delay performance and geographical unfairness, but the selected threshold values which constrain the transmission window are not optimum for all traffic loads. In this proposed scheme the threshold values are controlled by taking into account not only the locations of the mobile stations but also the traffic load. The advantage of this scheme is that the optimum threshold values are chosen for each traffic load. The throughput and transmission delay performances for the proposed scheme were evaluated by computer simulations. Based on the simulation results, the proposed scheme can achieve the same throughput performance and improve the delay performance compared with the conventional schemes. Furthermore, the performance comparison concludes that the proposed scheme is better than the conventional ones for maintaining fairness of service to all mobile stations at different traffic loads. Accordingly, the proposed scheme is effective for packet transmissions in CDMA cellular packet communication systems.

4. Concluding remarks

This thesis investigated the packet transmission control in downlink CDMA cellular systems. Several techniques are proposed to cope with the recent trend in wireless communications. This trend is to provide the mobile users with ubiquitous access to the Internet, mobility and handoff. Mobility management is an important issue in the area of mobile communications. These proposed schemes reduced the service disruption during soft handoff phase and improved the system capacity. The techniques proposed in this thesis contribute to the development of the future mobile systems.

5. Publications

[1] Abubaker Khumsi, Kazuo Mori, Hideo KOBAYASHI, "Downlink Packet Transmission Control in Soft Handoff Status on CDMA Wireless IP Networks," ECTI-EEC Transactions on Electrical Eng., Electronics, and Communications, Vol. 3, No.2, pp125-131, August 2005.

[2] Abubaker Khumsi, Kazuo MORI, Hideo KOBAYASHI, "Downlink Packet Transmission Control Based on Soft Handoff Status in CDMA Cellular Packet Networks," IEICE Transactions on Communications, Vol. E90-B, No.5, to be published in May 2007.

[3] Abubaker Khumsi, Kazuo Mori, Hideo KOBAYASHI, "Soft Handoff Technique for Downlink IP Packet Transmissions in Cellular Environments," Proc. of ISCIT 2004, pp.1138-1143, Sapporo, Japan, Oct. 2004.

[4] Kazuo Mori, Khumsi ABUBAKER, Katsuhiko NAITO, Hideo KOBAYASHI, Hamid AGHVAMI, "Downlink Packet Transmission Control Based on Handoff Status in CDMA Cellular Packet Networks," Proc. of IEEE International Zurich seminar on communications, pp.62-65, Feb. 2006.

[5] Abubaker KHUMSI, Kazuo MORI, Katsuhiko Naito, Hideo KOBAYASHI, "Adaptive Transmission Window Control for Downlink Packet Transmission in CDMA Cellular Networks," Proc. of 2006 International Symposium on Intelligent Signal Processing and Communication Systems (ISPACS), pp. 743-746, Tottori, Japan, Dec. 2006.

Study on Mitigation Methods of Non-Linear Distortion for OFDM Based Wireless Communications Systems

Pisit Boonsrimuang †

Keywords: OFDM, PAPR, Non-Linear channel, Inter-modulation noise, WLAN channel, Satellite channel Clipping, DAR, IDAR and Dummy sub-carrier insertion.

1. The purpose

The purpose of this research achieves the high transmission data rate in the non-linear channel for Orthogonal Frequency Division Multiplexing (OFDM) based wireless communications systems. The targets of research are to achieve the best bit error rate (BER) performance with efficient usage of non-linear power amplifier at the transmitter. In this research proposes the several solutions of non-linear distortion, which could provide various practical solutions for next generation of multimedia wireless communications systems employing the OFDM technique.

2. The related prior arts

One of the limitations of using OFDM technique is the larger Peak to Averaged Power Ratio (PAPR) of its time domain signal. The larger PAPR signal would cause the severe degradation of BER performance and the undesirable frequency spectrum re-growth both due to the non-linear distortion occurring in the non-linear amplifier which is usually required at the transmitter in the wireless communications systems. The simple solution to overcome this problem is to operate the non-linear amplifier at the linear region with taking the enough larger input back-off (IBO). However, this approach leads the inefficient usage of non-linear power amplifier, and would lead a serious problem on battery consumption especially for the cases of mobile terminal and portable wireless LAN terminal. In order to maximize the usage of power efficiency, the non-linear amplifier is usually forced to operate at the near its saturation region. However this approach will lead to the severe degradation of BER performance and undesirable frequency spectrum re-growth for the larger PAPR signal due to the occurring of inevitably higher non-linear distortion.

3. Proposed methods abstract

The PAPR problem is currently recognized as one of the essential research topics when employing OFDM technique in the non-linear channel. Up to today, various kinds of methods were proposed in order to solve the PAPR problem. These proposed methods could be mainly categorized into two types of methods; 1) to reduce the PAPR to extend possible at the transmission side, and 2) to compensate the non-linear distortion at the receiver side.

As for the first type of methods, there are three major proposals which can improve the PAPR performance at the transmission side, that are the selected mapping method (SLM), partial transmit sequence method (PTS) and dummy sequence insertion method (DSI). All of these methods can provide the better PAPR performance by controlling the phase of data or dummy sub-carriers. The SLM and PTS methods control the phase of data sub-carrier and the DSI method controls the phase of dummy sub-carriers at the transmission side. First two methods are required to inform the phase information controlled for the data sub-carriers to the receiver as the side information. On the other hand, the DSI method requests no side information, because of using dummy sub-carriers, which could be discarded at the receiver. From this reason, the DSI method could be realized with almost the same system efficiency and less overall system complexity as compared with the PTS and SLM methods. Although the PAPR performance could be improved as increasing the number of predetermined discrete phases, the computation complexity would increase due to the necessity of larger number of iterations in the flipping algorithm.

From this fact, the conventional DSI method has a limitation on PAPR improvement when assuming the small number of predetermined discrete phases so as to keep the acceptable computational complexity.

To solve the above problem on the conventional DSI method, this research proposes two novel PAPR reduction methods both of which can achieve the better PAPR performance with less computation complexity than the conventional DSI method. The feature of the first proposed DSI method is to employ the time-frequency domain swapping algorithm in the determination of frequency data for dummy sub-carriers. In the proposed method, the larger amplitude levels are detected in the time domain and these amplitude levels are converted to the frequency domain to determine the frequency data for the dummy sub-carriers. These procedures are repeated up to reaching either of the predetermined PAPR performance or the number of

† Division of Systems Engineering,
Graduate School of Engineering, Mie University

predetermined iterations. The feature of second proposed method is to enable the determination of frequency data for each dummy sub-carrier theoretically by using the continuous phase. From this fact, the proposed method can achieve the better PAPR performance with less computation complexity than that for the conventional DSI method. From the computer simulation results, it is confirmed that these two proposed method can achieve much better PAPR performance and BER performance than the conventional method with less computation complexity in the non-linear channel.

As for the second type of methods, the clipping method in conjunction with the Decision Aided Reconstruction (DAR) method was proposed to compensate the clipping noise at the receiver side. The clipping method is well known simple method to enable the reduction of PAPR performance by clipping the larger amplitude level of transmission OFDM signal at the transmission side. Although the clipping method can achieve the better PAPR performance, this method produces newly the clipping noise which causes the degradation of BER performance. The DAR method was proposed to compensate the clipping noise in which the clipping noise is reconstructed at the receiver side by using the decision data information. However the DAR method can only mitigate the clipping noise and not for the non-linear distortion occurring in the non-linear amplifier.

To solve the above problem on the conventional DAR method, this research proposes the Improved DAR (IDAR) method, which can mitigate both the clipping noise and inter-modulation noise. In the proposed IDAR method, the characteristics of non-linear amplifiers are required to be known at the receiver for mitigating the inter-modulation noise. This research also proposes the estimation method for AM-AM and AM-PM conversions characteristics of non-linear amplifiers by using low PAPR (Peak to Averaged Power Ratio) preamble symbols. This research presents two example systems which employ the proposed IDAR method in the wireless LAN system and the broad band satellite communication systems. From the computer simulation results, it is concluded that the proposed IDAR method can achieve the higher transmission data rate and higher efficient usage of non-linear power amplifier with keeping the better BER performance even in the non-linear channel.

4. Concluding remarks

This research proposed the solutions for PAPR problems. These proposed methods could be mainly categorized into two types of methods; 1) to reduce the PAPR to extend possible at the transmission side, and 2) to compensate the non-linear distortion at the receiver side.

First type, the common name can be called by PAPR reduction methods. The PAPR performance is required to reduce as more as possible before inputted to the HPA at the transmitter side. All of PAPR reduction methods can improve both for the spectral growth and BER performance for OFDM technique in the wireless communications. This research proposes two PAPR reduction methods by using dummy sub-carriers. The proposed methods can achieve better PAPR and BER performances with less complexity than conventional method. These methods suitable for low cost receiver because it have no required additional circuits. The conventional OFDM receiver can work with these methods.

Second type, this research proposes the IDAR method that can work well both for WLAN and satellite channel. In the simulation results show that the proposed method can improve BER performance and efficient usage of HPA. The proposed method can achieve higher transmission data rate than single carrier modulation in the satellite channel by using multi-level QAM. To realize in the practical system, research also proposes the non-linear characteristic estimation method that the non-linear amplifier characteristics in the IDAR method is required to be known at the receiver.

The multi-level QAM have capability to improve the transmission data rate, however have very sensitivity to the non-linearity of HPA such as 64QAM. The last chapter proposed combination between PAPR reduction and IDAR methods. The proposed method can employ multi-level QAM in the satellite channel. The simulation results show that the proposed methods show the higher data transmission rate and better BER performance than single carrier modulation.

As a conclusion of researches in this research, the proposed PAPR reduction methods and mitigation methods of non-linear distortion noise could provide various practical solutions for next generation of multimedia wireless communications systems employing the OFDM technique.

5. Publications

- [1] Pisit Boonsrimuang, Kazuo Mori, Tawil Paungma and Hideo Kobayashi, "Proposal of Clipping and Inter-Modulation Noise Mitigation Method for OFDM Signal in Non-linear Channel," IEICE Transactions on Communications, Vol.E88-B, No.2, pp.427-435, February 2005.
- [2] Pisit Boonsrimuang, Pornpawit Boonsrimuang, Kazuo Mori, Tawil Paungma and Hideo Kobayashi, "Mitigation of Non-linear Distortion using PTS and IDAR Method for Multi-Level QAM-OFDM system," ECTI Transactions on Computer and Information Technology, Vol.1, No.2, pp 84-90, Nov 2005.
- [3] Pisit Boonsrimuang, Katsuhiko Naito, Kazuo Mori, Tawil Paungma and Hideo Kobayashi, "PAPR Reduction of OFDM Signal by Use of DSI Method with Time-Frequency Domain Swapping Algorithm," IEICE Transactions on Communication, Vol.E90-B, No.4, pp.1001-1006, April 2007.

Ergonomic Study on VDT Workstation Design for Decreasing Workload

Shin Saito†

(System Design, Division of System Engineering)

Keywords: VDT, Workstation, System design, Multi display, Display height, Workload

1. Introduction

In this study, the height and the number of the liquid crystal display (LCD) were discussed to propose the ergonomic design for visual display terminal (VDT) workstation that is able to decrease the workload of VDT operators. There were two kinds of studies in the doctor's thesis. The first study was to decide the appropriate height of LCD, and the second study was to discuss the number of the LCD, with using multi display type VDT.

In order to design the ideal VDT workstation, these VDT operations were analyzed by work efficiency, work posture, electromyogram (EMG) activities and subjective assessment in ergonomic aspects.

2. Appropriate height of LCD in VDT work

The appropriate heights of LCD, including a notebook personal computer (NPC), were discussed by analyzing of work posture and EMG activities of neck muscles of VDT operators. The comparative experiments were carried out in each experimental condition.

Results were as follows. It is necessary to separate the display of NPC from the keyboard and central processing unit (CPU). The position of the NPC display prevents the head from inclining forward, while maintaining an adequate viewing distance. The height of the display should be adjusted to each user with 1200 mm as an upper limit. The appropriate height can be estimated by summing of the sitting height and the chair height of each user. Moreover, a manuscript stand should be attached to the display in data entry tasks to prevent poor posture.

3. Characteristics of multi LCD type VDT

The characteristics of multi display VDT was evaluated by the analyses of work performance, subjective assessment, work posture, EMG activities, critical fusion frequency (CFF), NASA Task Load Index (NASA-TLX) and subjective symptoms of fatigue.

Results were as follows. Work efficiency of the single LCD was inferior compared to multi LCD and large one. The multi display type VDT workstation was evaluated highly, in visibility and operability, than the single display. A head moved wider for the system with multi LCD than those with a single LCD and large one. EMG activities did not differ significantly in all experiment conditions. Fatigue and workload of multi LCD did not differ significantly than single LCD.

4. Conclusion

The appropriate height of LCD and the multi LCD were examined to design the comfortable VDT workstation for decreasing workload. These design requirements are going to obtain ergonomic data applicable to the guidelines and recommendation for VDT operations.

†: Mie Prefectural College of Nursing, JAPAN

Development of A Flexible Structural Force Sensor and Application to A Robot Hand

Naoki Saito

(System Engineering, Division of Mechanical Engineering)

Keywords: Flexible structure, Force sensor, Robot hand,

1. The purpose

The aim of this research is to develop a flexible structural force sensor which is mounted on a surface of a fingertip of a robot hand and to examine feasibility of new dexterous tasks by the sensor. The sensor's flexibility is modeling on a human finger cushion. This research describes a structure and fundamental characteristics of measurement of the flexible sensor and several applications about object grasping by a robot hand which installed the sensor on its finger.

2. Outline of the flexible structural force sensor

In this research, we propose a new type of force sensor. This sensor can measure a contact location ϕ_c and four-axis contact forces which are consisted of a vertical force F_z , two-axis shearing forces F_x , F_y and a rotational moment around the contact point M_c . This sensor structure is shown in Figure 1. This sensor consists of two parts: a contact part and a measurement part. The contact part is an arch beam that is made of silicon rubber. Silicon rubber is an elastic material, so the contact part is easily deformed.

On the other hand, the measurement part consists of four beams and a support part. When a contact force is transmitted from the contact part to the measurement part, these beams are deformed depending on the amount of contact force or the direction of the contact force.

Four-axis contact forces are calculated in terms of the amount of these deformations which are measured by strain gages ϵ_{x1} , ϵ_{x3} , ϵ_{z1} and ϵ_{z3} on the beam of the measurement part.

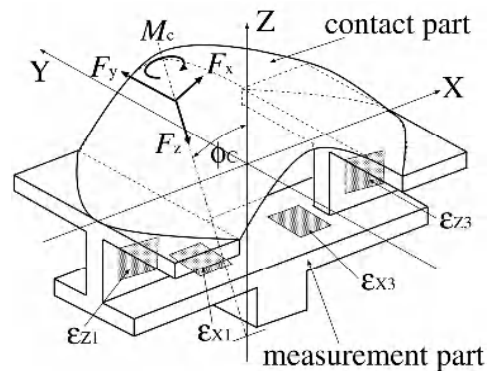


Figure 1: Structure of the flexible force.

3. Characteristics of measurement

A contact location and four-axis contact forces are determined with the use of some equations which are derived based on Castigliano's theorem and simple analysis model of the contact part which is included all of dimensions and material characteristics of the sensor. Validity of equations for determines these information and measurement accuracy are confirmed experimentally. One of the experimental results is shown as Figure 2. This result shows that desired values and experimental results are advisable agreement.

In addition, this sensor can also calculate four-axis deformations of the flexible contact part of the sensor. Deformations of the contact part are determined with the use of measurement result of each contact force.

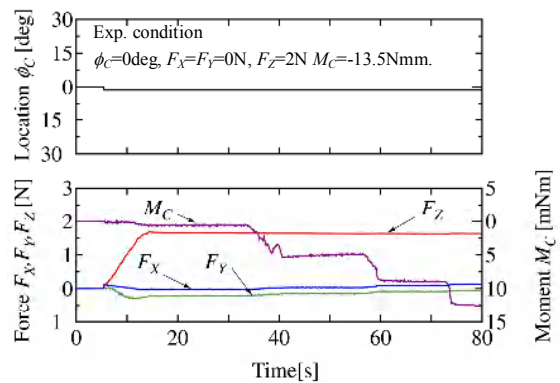


Figure 2: Experimental results of a contact location and four-axis contact force measurement.

4. Applications

4-1. Object grasping against translational and rotational slippage

The issue of translational and rotational slippage that occurs when a robot hand grasps an object is discussed. To grasp an object against each directional slippage is important for a dexterous task realization. In this application, a sufficient conditional expression to grasp an object against translational and rotational slippage is presented. This expression is derived based on the consideration of a contact area between a flexible contact part and object's surface such as Figure 3 which occurs the sensor is pressed to the object. An effectiveness of the expression is confirmed experimentally with the use of a translational gripper where the flexible contact sensor is mounted. Figure 4 shows experimental result of object grasping. From this result, it is confirmed that grasping force is increasing with increasing translational force and rotational moment. On the other hand, object's position does not change approximately. Therefore, it is confirmed that the robot hand can grasp against translational and rotational slippage.

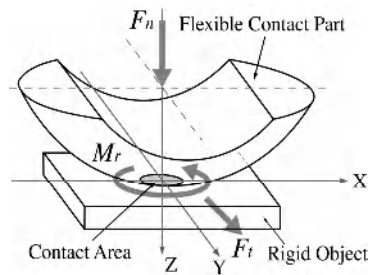


Figure 3: A contact area between the flexible contact part of the sensor and an object.

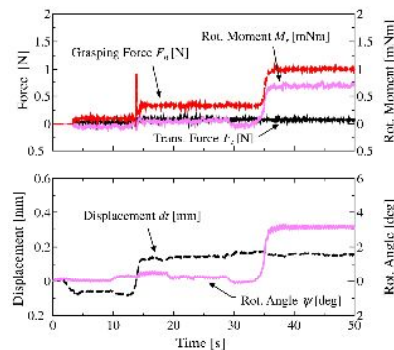


Figure 4: Experimental results of object grasping against translational and rotational slippage.

4-2. Object placing with a low impulsive force

A placing motion of a grasped object by a robot hand equipped with the sensor on the finger is discussed. The aim of this application is to realize a quick placing motion with the impulsive force between the object and the floor small. To derive a dynamic model of the motion, we consider the deformation of the flexible sensor occurring when the hand grasps the object. The dynamic model represents the relationship between the impulsive force and an approaching trajectory of the robot hand to the floor. From this model, we can obtain the trajectory of the hand which ensures that the impulsive force is less than the object's own weight.

Figure 5 and Figure 6 show that the experimental results of placing motion. From Figure 5, it is confirmed that the robot hand position is approximately same as a desired trajectory which is obtained by the model, and the sensor deformation is decreased. From Figure 6, it is confirmed that a reaction force is less than the object's weight. Therefore, it is confirmed that the hand equipped the flexible sensor can put down the grasping object with low impulsive force.

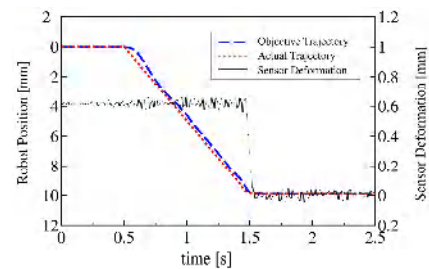


Figure 5: Experimental result of robot position and sensor deformation.

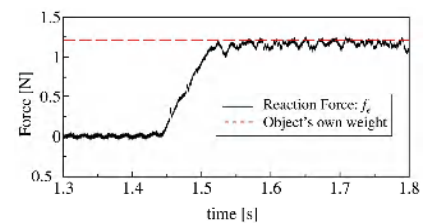


Figure 6: Experimental result of reaction force from the floor.

5. Conclusion

In this research, we proposed a new type of force sensor which has a flexible contact mechanism. This sensor can measure a contact location and four-axis contact forces.

An effectiveness of this flexible structural force sensor demonstrated through two applications. These results of application suggest that the robot hand which has a flexible contact part on its finger surface can perform dexterous tasks.

Author's publications (in part)

- [1]N. Saito, T. Satoh, S. Kajikawa, H. Okano, *Development of Four-Axis Contact Force Sensor with a Flexible Contact Part*, IEEJ Trans. SM, Vol.125, No.1, pp.7-14, 2005.
- [2]N. Saito, T. Satoh, H. Okano, *Grasping Force Control in Consideration of Translational and Rotational Slippage of an Object by a Flexible Contact Sensor*, IEEJ Trans. EIS, Vol.126, No.8, pp.990-996, 2006.
- [3]N. Saito, T. Satoh, Y. Suzuki, H. Okano, *Placing Motion of an Object by a Robot Hand with a Flexible Sensor*, Trans. of JSME C, Vol.73, No.725, pp.206-213, 2007.

Estimation on The Amount of Movement Lines of Material Transportation with Systematization of The Information and Material Management

- A study on the facility management of hospital architecture -

Shinsuke Kawai*

(Architectural Design and Planning, Division of Systems Engineering)

Keywords: hospital architecture, facility management, connection with departments, ordering system, material management and supply systems, model, amount of movement lines, material transportation, estimation, nursing activities locations, gradual composition

This paper aims at the hospital architecture offering essential medical services. The foremost tasks of hospital architecture are to contribute to the sound management and to maintain the high functional levels in the long run. To settle these issues, facility management is thought to be quite effective.

Medical services by doctors and nurses include not only treatment directly for patients but also consequential chores. Increasing the latter means decreasing the quality of medical treatment. Under the financial pressure, hospital managers must save life cycle cost. When hospital architecture is planned, flows of people, articles and information are considered to be indicators. These flows need to be investigated closely, and to be improved so that medical staff can take more time in the direct medical treatment. They have to reduce the burden of moving around, to diminish the stress of indirect consequential chores, and to save and simplify their labors. It can be also successful in financial management. Targeting material transportation, the medical information system and the material management and supply system, to systematize the movement of materials and information enables hospitals to control effectively. This means achieving greater efficiencies in management and medical treatment.

The purpose of this study is as follows; one is to organize a hospital supporting system and to suggest what to evaluate; another is to estimate the amount of movement lines, which have been made more efficient by a hospital supporting system and a department arrangement. Some previous work have reported the flows of materials, the movement of the transporter, the amount of transportation, the department arrangements, and the estimation of plan type and so on. Generally speaking, the contents of the most previous work can be divided into hospital management and architectural space. In this study, the medical information system and material management and supply system are treated systematically. Considering the movement lines as an indicator, hospital management and architectural space are treated comprehensively in the Chapter 1.

In the first half of the second chapter and in the third chapter, the first purpose of this study is achieved. One example of hospital supporting system, i. e. ordering system has been investigated in the survey questionnaires. The results of the survey show that the interlock of the doctor's processing order and accounting procedure is distinguishing. Two difficulties are still left; how to make it a standard and how to abolish many kinds of tickets and vouchers. The evolution items concerning what to introduce first are as follows; first, where many systems are adopted-[B: prescription and checkup], [C' : B plus medical radiation], [C: C' plus injection], and [E: C plus interlocking accounting]; second, how many tickets and vouchers are eliminated-[I: many], [II: few], and [III: none]. A pattern of [E-III] is the most systematic. Also interviews are conducted at four hospitals. As a result, it is revealed that plural systems are introduced. The types of the material management and supply system are depend on the combination of supply methods, management methods, and planar forms of supplying section. From the actual conditions of those four hospitals, three typical models are derived. Making an allowance for the introduction of the POS system and the material management at consumption of each model are simulated.

The latter half of the second chapter and the Chapter 4 treat the connection with departments. The patterns of department arrangement have developed with systemization of the medical information system. In the pattern of E-III, characteristically the flow of job cards has replaced that of web orders. The common materials are pick up from a flow chart of supplying operation and presented as a flow modeling. Examined qualitatively, the flows of articles and supplies in three models are estimated.

In the Chapter 5, the amount of transportation between each department is figured out. Another research on transportation is conducted at the hospitals for three days. The results shows that the conveyance during the

* Redeveloping Project Team on Univ.Hospital and School of Medicine, Mie Univ.

daytime on weekdays occupies 70 % of the whole, and that increase in scheduled transport makes the number of transporting operations decrease. The rate of transportation load by the types of transportation is demonstrated.

The amount of movement lines of materials are calculated in the Chapter 6. That of each hospital is different, but by establishing the medical information system, it can be reduced by about 25 to 50 %, and when the material management and supply systems are added, it can be cut by more 39 %, and when the POS system is added, by 50 %. It is concluded that the material management and supply systems are effective in providing the easy access, and that three models are successful in helping the medical staff to shorten the walking distance and the POS system in helping the administrative staff. More two points are clarified; an intensive supplying sections needs ingenuity of department arrangement in order to lessen the movement lines; and dispersive supplying section should systematize the material management service.

The seventh chapter deals with the flow of staff and patients in hospital ward. Another inquiry has done at the foregoing hospitals. According to the results of the survey, it is determined that nurses walk around more than 4 kilometer during the working hours. Most of the destinations are nurse station to exchange information, document the nursing record, and so on. At the other destinations, they give patients treatment and talk with their families. And it has revealed that the locations of nursing activities are in a gradual composition. The combinations of the materials and facilities are examined and the results show that the hospital supporting system can decentralize working locations and shorten the movement lines. Moreover, even the existing hospitals can make improvements.

The position in facility management (FM) of this research product is considered in the next chapter and estimated through the viewpoints of space and systems, which is one of the methods for evaluation of FM productivity. One characteristic of hospital architecture is that a hospital has plural systems. Systematization not only in each department but also between departments can make the flows and transportation easier. In each department, nursing service and the hospital supporting system are connected closely and the system should be typical and customized. In the hospitals used for a long term, which needs more flexible systems, the model 3 and the POS system are promising. The space arrangement under the influence of systematization is the positional relation between demanding spaces and supplying spaces. Scattering the supplying spaces can cut down the amount of movement lines. On the other hand, concentrating them make it easier to upgrade systems and renovate. In the case of the POS system, because out-of-hospital carriers are involved in the transporting service, hospitals needs high security and the simple and quick access to demanding places from the outside.

Another example of FM in hospital architecture is functional estimation. In order to maintain the level of systems, periodical and uncomplicated checking is significant. When the material arrangement is not considered for nursing service in a unit of a hospital ward, it might not be consistent with its hospital supporting system and need to reassemble the whole system.

Three points are left for the future investigation; first, exploration in the United States about the development of the POS system; second, simulation of the changing service in a nursing ward by grading the hospital supporting system; third, establishment of screening self-diagnosis in a practical way.

Author's publications

[1]S.Kawai and S.Imai, The Developing Pattern of Ordering System's Introduction - A study on the informational connection with departments of Hospital Architecture, Hospital Administration, Journal of the Japanese Society on Hospital Administration, Vol.40 No.2, pp.5-12, 2003.4

[2]S.Kawai and S.Imai, A Study of Stock Management and Supply Systems through Modeling and Estimation on the Changes with Advancements in Information Technology, Hospital Administration, Journal of the Japanese Society on Hospital Administration, Vol.43 No.1, pp.23-34, 2006.1

[3]S.Kawai and S.Imai, Evaluation of The Material Management and Supply Systems' Modeling through The Material Flow - A study on the connection with departments of hospital vol.1, Journal of Architecture and planning, Transactions of Architectural Institute of Japan, No.605, pp.55-62, 2006.7

[4]S.Kawai and S.Imai, The Amount of Material Transportation through The Material Management and Supply Systems - A study on the connection with departments of hospital vol.2, Journal of Architecture and planning, Transactions of Architectural Institute of Japan, No.613, pp.45-52, 2007.3

[5]S.Kawai, K.Katsuno and S.Imai, A Basic Study on Gradual Composition of Locations for Nursing Activities in Wards in Relations to The Locations of Materials, Journal of Architecture and planning, Transactions of Architectural Institute of Japan, No.614, 2007.4

Motion tracking of left ventricular myocardium using ultrasound

Wataru OHYAMA *

Keyword: Ultrasonic diagnosis system, Myocardial motion tracking

1 Introduction

The echocardiogram is an essential tool for diagnosis and treatment of cardiovascular diseases. The use of echocardiograms for clinical diagnosis serves clinicians and doctors with multifold advantages including noninvasiveness of diagnosis and real-time imaging. Recent technical innovations of ultrasonic diagnosis equipment reclaim their new availabilities in clinics. These novel modalities require to track a specific tissue of myocardium to keep their focus on a relevant tissue to evaluate. In this research, four novel algorithms, that aim to contribute for these new availabilities of ultrasonic in diagnosis, are investigated.

2 Automatic Extraction of Left Ventricular Endocardium

Automatic extraction of left ventricular endocardium in echocardiograms is required for quantitative evaluation of the functional performance of the left ventricle. In this section, a novel automatic extraction method based on double thresholding for echocardiograms is proposed, and its effectiveness and the accuracy are evaluated. B-mode echocardiograms are first binarized with a threshold determined by the discriminant analysis for the gray level histogram. Then the binary images are contracted n times to remove small regions and to disconnect the region of cardiac cavity from the other false regions. Among the obtained regions which corresponds to the cardiac cavity is selected and dilated $2n$ times to create a mask which restricts the region of the second thresholding operation. The size and the location of the cardiac cavity in the preceding frame are utilized to select the corresponding region. The masked image of each frame is binarized in the restricted area in the same way as in the first thresholding operation. The evaluation test is carried out using the scatter diagram of radius of contours extracted by two observers and automatic extraction method. These results showed that the accuracy of the extracted contours was favorably compared to the accuracy of manually traced contours.

3 Automatic Tracking for Regional Myocardial Motion

In this section, an automatic tracking method for 2-D motion of Regional myocardial motion in high-frame rate echocardiography by using the correlation method with connective multiple ROIs is proposed. The proposed method is a combination method of maximization for correlation of brightness distribution and optimization the geometric location of ROIs. A comparison test of tracking accuracies between the

* Mie University

conventional method and proposed one is carried out. Results of these tests shows that proposed method is able to derive more accurate trajectories from echocardiography than conventional method.

4 Local Myocardial Motion Tracking Using Ultrasonic Doppler Signal

In this section, a new method for automatically tracking the motion of local region in left ventricular myocardium by means of ultrasonic pulsed Doppler signal is proposed. This method consists of a velocity detection procedure based on correlation weighted mean instantaneous phase difference and a motion tracking procedure employing a elastic model. Most of ultrasonic pulsed Doppler signals contain considerable amount of speckled noise, which causes detection error of velocity. The procedure of correlation weighted mean velocity is aimed to reduce the velocity detection error, and the elastic model is used to avoid the accumulation of the error to keep track of the motion of the myocardium in reasonable accuracy.

5 Local Myocardial Motion Tracking Using Ultrasonic RF Signal

This section describes a new algorithm to track identical myocardium accurately through a few cardiac cycles. Hierarchical correlation is used with wide correlation window as first and narrow one as second. Then, to increase the reliability of the estimated position of myocardial motion, neighboring points are weighted by correlation coefficients of ultrasonic waveforms between sequential pulses and are summed up. This method was applied to normal and diseased hearts. Tracking error during one cardiac cycle decreased to one-fifth of simple method and the stability increased substantially. Regional myocardial strains in the wall were estimated and color-coded using this tracking method. Result: this strain image revealed clearly the differences of myocardial function between endocardium and epicardium, and the specific characters of myocardial diseases. Moreover, the cyclic variation of integrated backscatters is automatically obtained using this tracking method. This cyclic variation also indicated the myocardial tissue characters of diseased heart in terms of ultrasonic backscatter intensity.

6 Conclusions

In this research, new modalities to track the myocardial motion from echocardiogram. The proposed approaches are able to increase the performance of motion tracking. These methods contribute to provide new applications of ultrasonic for diagnosing cardiovascular diseases.

Author's publications

1. W.Ohyama, T.Wakabayashi, F.Kimura, S.Tsuruoka, and K.Sekioka: "Automatic Extraction of Left Ventricular Endocardium in Echocardiograms Using Double Thresholding Method (in Japanese)": The Transactions of The Institute of Electrical Engineers of Japan: Vol. 121-C, No. 9, pp. 1448-1456
2. W. Ohyama, N. Ismail, T. Wakabayashi, F. Kimura, S. Tsuruoka, and K. Sekioka: "Local Myocardial Motion Tracking Based on Correlation Phase Difference Method (In Japanese)":IEICE Transactions Vol. J86-A No.9 pp.917-928
3. W.Ohyama, M.Inami, T.Wakabayashi, F.Kimura, S.Tsuruoka, and K.Sekioka: "Automatic Tracking for Regional Myocardial Motion by Correlation Method with Connecting Multiple ROIs (in Japanese) " : The Transactions of The Institute of Electrical Engineers of Japan: Vol. 124-C, No. 10, pp. 2079-2086

Abstracts of Papers (2006)

Department of Mechanical Engineering

*nonmember

Tips on Using Vacuum Techniques, Yasuyuki SUZUKI, Seimitsukougakkaishi, Vol.72 No.2 pp.191-194, 2006.

Evaluation of Fracture Surface of 11/4Cr-1/2Mo Steel by Residual Magnetization Induced from Inverse-Magnetostrictive Effect, Hiroichi HASE, Shigeo KOTAKE, Mitsuhiko OHOTA, Hiroshi KAWAKAMI and Yasuyuki SUZUKI; Key Engineering Materials (Engineering Plasticity and its Application from Nanoscale to Microscale), 340-341, pp.549-554, 2006.

A Fingertip Guiding Manipulator for Mental Image Creation of Multi-Stroke Drawings, Yoshihiko Nomura, Yuki Yagi, Tokuhiko Sugiura, Hirokazu Matsui, Norihiko Kato, Microsystem Technologies, Vol. 13, No. 8-10, pp. 905-910, (Apr. 2007), ISSN 0946-7076 (Published Online: Nov. 2006)

Relationships between the Camera Calibration Accuracy and the Imaging Condition, FUJIMOTO Takashi 1 NOMURA Yoshihiko 2 ZHANG Dili, Trans. of JSME PartC,72(706), pp. 1695-1700, 2006

A Fingertip Guiding Manipulator for Mental Image Creation of Multi-Stroke Drawings, Yoshihiko Nomura, Yuki Yagi, Tokuhiko Sugiura, Hirokazu Matsui, Norihiko Kato, CD-ROM Proc. of ASME/JSME Joint Conference on Micromechatronics for Information and Precision Equipment (MIPE 2006), 2006

Fingertip Guiding Manipulator: Haptic Graphic Display for Mental Image Creation, Yoshihiko Nomura, Yuki Yagi, Tokuhiko Sugiura, Hirokazu Matsui, and Norihiko Kato, Proc. of 9th Annual International Conference ICCHP 2006 (Computers Helping People with Special Needs) 2006

High-quality and small-capacity e-learning video featuring lecturer-superimposing PC screen images, Yoshihiko Nomura, Michinobu Murakamia, Ryota Sakamoto, Tokuhiko Sugiura, Hirokazu Matsui, and Norihiko Kato, Proc. of SPIE Conference on Intelligent Robots and Computer Vision XXIV: Algorithms, Techniques, and Active Vision 2006 "High-Quality and Small-Capacity Lecture-Video-File Creating System for Chalk-and-Talk Based Lecture," Ryota Sakamoto, Yoshihiko Nomura, Norihiko Kato, Proc. of E-Learn 2006

A formulation of camera parameter calibration error due to reference point setup error, Takashi Fujimoto, Yoshihiko Nomura, Proc. of Asia International Symposium on Mechatronics (AISM) 2006

Automatic control of a monitoring camera for remote manipulator operation”, Masahiko Niwa, Naoaki Tsuda, Norihiko Kato, Yoshihiko Nomura and Hirokazu Matsui, Proc. of the 15th IEEE International Symposium on Robot and Human Interactive Communication (RO-MAN06), pp.151-156, 2006

An ergonomic study on multi screen type VDT work, Shin SAITO*, Norikazu OHNISHI*, Zojiro KATOH*, Masaru MIYAO*, Kaoru ITO*, Ryojun IKEURA and Kazuki MIZUTANI, Journal of Society for Occupational Safety, Health and Ergonomics, 7, 1, pp.17-22, 2006.

The aim of this study was to evaluate the characteristics of multi screen type visual display terminals (VDT) work by the analyses of work performance and subjective assessment. The comparative study, multi screen and single screen type VDT workstation, was carried out to get some ergonomic data which would be applicable to the guidelines and recommendation for VDT operations using multi screens. Seventy healthy persons, 32 males and 38 females, whose ages ranged from 18 to 47 years (average age: 23.4) were selected as subjects. They performed data search and entry task for 5 minutes using both word processing and spread sheet software in each workstation. The work efficiency and the subjective assessment of multi screens were significantly superior in comparison with a single screen. The reason why a multi screen type workstation was evaluated highly is that visibility and operability are better than with a single screen. The characteristic of multi screen type VDT work is operation method and increased efficiency by dividing software into two screens. It is necessary to examine workload, sense of incongruity and skill of operation, and other possible problems before spreading widely to many work places.

Impedance control for an industrial power assist device considering contact operations, Hiroyuki KATO, Ryojun IKEURA, Shinpei NOGUCHI, Kazuki MIZUTANI, Hisashi NAKAMURA* and Tomohiro HONDA*, Transactions of the Japan Society of Mechanical Engineers, 72, 714, pp.214-221, 2006.

This paper describes a control method for a power assist device used in factories. An adaptive control scheme is employed to control the power assist device and to estimate its dynamic parameters. Using the adaptive control, the maneuverability of the system is good in free space but it is very dangerous in the task of which an object supported by system contacts on a floor or a wall. Therefore, we propose an improved system controlled by an adaptive control in which the local control method changes to a feedback or a feed forward control in the contact condition. The improved system detects collisions based on the difference between the actual input torque to the power assist device and reference input torque, which is calculated based on the estimated parameters of the manipulator dynamics. Then, the effectiveness of the system is shown.

Ergonomic evaluation of multi display type VDT, Shin Saito, Takahiro NAKATSUKASA, Ryojun IKEURA and Kazuki MIZUTANI, The 9th Korea-Japan Joint Symposium on Ergonomics Osaka, pp.524-525, 2006.

The aim of this study was to evaluate working conditions using multi display VDTs in terms of work performance, head movement and EMG activities of the neck. A comparative study using single, multi and large display type VDT workstations, was undertaken to obtain ergonomic data applicable to the guidelines and recommendation for VDT operations using multi displays. Subjects comprised 10 healthy volunteers

who performed data search and entry tasks for 5 min on each workstation. Work efficiency of the single display was inferior compared to multi and large displays. Head movement was greater with multi and large displays than with a single display. EMG activities did not differ significantly between multi and large displays. The characteristics of a multi display type VDT work is increased efficiency by dividing software into 2 displays. Workload, sense of incongruity, skills required for operation and other possible problems must be examined before spreading this approach becomes widespread in workplaces.

A rating method for the vehicle steering based on the impedance of human arms , Ryojun IKEURA, Hiroyuki HOSHINO, Daisuke YOKOI, Yoji KANEHARA*, Mitsuhiro HOSHINO* and Kazuki MIZUTANI, Transactions of Society of Automotive Engineers of Japan, 37, 4, pp.33-38, 2006.

The relationship between the stiffness of human arms and the subjective evaluation in the operation of a steering wheel is investigated. First, the estimation and its normalization method of the arm stiffness is proposed for avoiding the difference among individuals. Next, the experiments using the steering control device are conducted to obtain the arm stiffness and the subjective rating under the several conditions. Finally, it is verified that the value of the normalized arm stiffness correlates strongly to the subjective evaluation.

Allocation of Three Control Forces to Four Actuators for 3-DOF Hybrid Vibration Isolation System, Kazuki MIZUTANI, Keisuke ITO and Ryojun IKEURA, Proceedings of the 13th International Congress on Sound and Vibration, pp.CDROM, RS-03_509, 1-8, 2006.

This paper treats a hybrid type vibration isolation system for 3-DOF vibrations, that is, bouncing, pitching and rolling vibrations. The hybrid type system is composed of passive spring-damper system and active system with electromagnetic actuators. The controller for the vibration isolation system derives one control force for bounce and two control moments for pitch and roll in regard to the center of gravity. Usually, an actuator to supply vibration control force is set in each supporting part at the four corners of the loading platform. The allocation of three control outputs to four actuators is not unique because of redundancy. In this paper, the allocation of the control output is discussed in detail.

Optimal Vibration Control for Overhung Rotor System Using Actively Flexible Pedestal, Kazuki MIZUTANI, Yukinobu NISHIYAMA*, Kazuhiro IIDA* and Ryojun IKEURA, Proceedings of the ACTIVE 2006, pp.CDROM, No.26, 1-11, 2006.

This paper describes an active vibration control to effectively reduce the unbalanced vibration of an overhung rotor system. A flexible bearing pedestal supporting the overhung rotor is installed in four pairs of U-shaped electromagnets as a control device. The electromagnets give a flexible pedestal the control force to effectively reduce unbalanced vibrations of the overhung rotor indirectly. The optimal regulator theory is applied to decide the control gain suppressing the vibrations of the overhung rotor. Frequency response curves are simulated numerically, and the optimal feedback gains to give the effective vibration suppression performance are provided. For practical use, the simplification of the rotor model for controller design and the application of the Kalman filter are also examined. The numerical results are compared with experimental ones for the overhung rotor system with the vibration control device, and both results show

the similar tendency in our study.

Characteristic of 2 DOF cooperation task by two humans, Shahrman Bin Abu Bakar, Yuichiro HANDA, Ryojun IKEURA and Kazuki MIZUTANI, Proceedings of SICE-ICASE Internation Joint Conference 2006, pp.296-301, 2006.

In this research, we propose to analyze the characteristic of human-to-human cooperation in vertical motion. The experiment subject is divided into master and slave category where the slave is required to close their eyes during the experiment. Experiment devices are equipped with 3D position sensors and Force sensors to measure the position, angle and force value. By differentiating those values, speed, angular velocity and torque value are known. This research is concentrating the special characteristic that occurs to the slave side during human-to-human cooperative work where the weight, distance and speed are varied.

Development of 6-Axis Material Tester for Measuring Mechanical Spine Properties, M. Fujiwara*, T. Masuda*, T. Inaba, T. Katoh, Y. Kasai, S. Ito*: Journal of Robotics and Mechatronics, Vol.18, No.2, pp.160-165, 2006.

Because mechanical spine properties having multiple degrees of freedom (DOF) are generally difficult to measure, we developed a parallel 6-axis material tester with hybrid position/force control. We give examples of 6-axis testing and results of material tests using polyurethane rubber and animal spines.

Quantitative Evaluation of Left Ventricular Wall Motion in Patient with Coronary Artery Bypass Grafting Using Magnetic Resonance Tagging Technique, T. Inaba, T. Nakano, M. Tsutsumi, S. Kawasaki*, Y. Kinoshita*, M. Tokuda: JSME International Journal, Series A, Vol.49, No.4, pp.597-603, 2006.

Left ventricular wall motions during systole were investigated from a mechanical perspective by using a magnetic resonance tagging technique. Subjects were 7 patients with coronary artery bypass grafting (CABG). First, by analyzing strain in the left ventricular wall, cardiac contractility was evaluated in the patients with CABG. Next, by calculating displacement in the myocardial wall, paradoxical movements following CABG were quantitatively evaluated. Strain analysis showed local decreases in circumferential strain in 4 of 7 subjects. The results of displacement analysis clarified that following CABG, the degree of radial displacement was small in the septal wall and large in the lateral wall, and circumferential displacement towards the septal wall occurred in the anterior and posterior walls. Since this behavior was seen in both reduced and normal cardiac contractility groups, paradoxical movements in the present patients were not caused by reduced cardiac contractility, but rather by rigid-body motion of the entire heart.

Shape Memory Characteristics of TiNi Casting Alloys Made by Using Self-propagating High-temperature Synthesis, K. Kitamura*, T. Kuchida, T. Inaba, M. Tokuda, Y. Yoshimi*: Materials Science and Engineering A, Vols.438-440, pp.675-678, 2006.

Self-propagating high-temperature synthesis (SHS) is a new method of making an ingot of TiNi. This method shows little gravity segregation. The purpose of this study is to investigate the difference of the shape memory characteristics of the TiNi casting alloys made from a SHS ingot and from a conventional melt cast ingot. The samples used in this study were rods made by centrifugal casting. Differential scanning calorimetry (DSC), X-ray diffraction, and tensile test were used to examine the shape memory characteristics on the samples. The heat treatment conditions were 773 K–1.8 ks and 1073 K–3.6 ks, respectively. The DSC samples were both ends (the top and bottom area) of the rod samples. The results

of the XRD measurements showed that TiNi phase was obtained in all the samples. In contrast, the result of the DSC test showed that more gravity segregation effect happened in the melt cast sample than in the SHS sample. As the conclusion of this study, gravity segregation had little effect in the SHS ingot sample.

Superelastic Property of Ti-Ni Alloy Produced by Casting After SHS, K. Kitamura*, T. Kuchida, T. Inaba, M. Tokuda, Y. Yoshimi*: *Materials Transactions*, Vol.47, No.11, pp.2867-2870, 2006.

The superelastic properties of cast Ti-Ni shape memory alloy (SMA) were studied. Base materials were prepared as a melting method ingot and as a self-propagating high-temperature synthesis (SHS) ingot. The composition of these ingots was Ti-50.8 at%Ni. Each ingot was cast into a rod shape by centrifugal casting. The heat-treatment conditions were 773 K for-1.8 ks and 773 K-1.8 ks → 873 K-3.6 ks. Shape memory characteristics were measured by differential scanning calorimetry (DSC), X-ray diffraction (XRD) and a tensile test. All casting specimens have good shape memory characteristics. According to DSC measurements, the melt method specimens show gravity segregation.

Mechanical Evaluation of Cardiac Function in Heart with Disease by Numerical Simulation, M. Tsutsumi, K. Yanagisawa, T. Inaba, M. Tokuda: *Proceedings of 5th World Congress of Biomechanics*, pp.563-566, 2006.

A numerical simulation system using the three-dimensional finite element method (3D-FEM) is established to reproduce the performance of the left ventricle during one cardiac cycle, which may ultimately provide useful information for medical diagnosis. In this study, the diseased human heart is analyzed by using the proposed numerical simulation system and the numerical results are composed with measurements results.

Bonding Process of Al/Cu bonding with liquefaction after solid state diffusion in air,

Hiroshi Kawakami, Junya Nakajima, Jippe Suzuki

Proc. of 2nd JWS-KWS Joint Symposium of Young Researchers, Preprints of the National Meeting of J. W. S., Vol.79, pp.140-141(2006)

Effect of Bonding Conditions on Al/Cu Diffusion Liquefaction Bonding, Hiroshi Kawakami, Junya Nakajima, Toshiharu Kawabe, Jippe Suzuki, *Proc. of Sino-Japanese Young Researchers Forum*, pp.1-4(2006)

Fundamental Studies on Remote Laser Cutting for an ALIMS Robot, Muneharu KUTSUNA*, Jippe SUZUKI, Hiroshi KAWAKAMI, *Documents of International Institute of Welding*, No.IE-413-06, pp.1-8, (2006)

Behavior of Mg in Al/Cu Diffusion Liquefaction Bond, Hiroshi Kawakami, Masanori Fujiwara, Junya Nakajima, Toshiharu Kawabe, Jippe Suzuk, *Proc. of The First South-East Asia International Institute of Welding Congress*, pp.232-243(2006)

Bonding for Aluminum in Air using Some Insert Metals, Hiroshi Kawakami, Keiko Kimura, Jippe Suzuki, *Proc. Advance Technology in Welding Work(CD-ROM)*, pp.1-7(2006)

Application of Resistance Heating Technique to Hot Stamping of High-Strength Steel Sheet, Seijiro MAKI, Yuuki TANAKA*, Ken-ichiro MORI*: Journal of the Japan Society for Technology of Plasticity, 47(544), pp.394-398, 2006 (in Japanese)

Improvement of Product Strength and Press Formability of Al-Mg-Si Alloy Sheets by Resistance Heat Treatment and Artificial Aging, Minoru ISHIGURO*, Seijiro MAKI, Ken-ichiro MORI*: Journal of Japan Institute of Light Metals, 56(6), pp.313-316, 2006 (in Japanese)

Thermo-Mechanical Treatment Using Resistance Heating for Production of Fine Grained Heat-Treatable Aluminum Alloy Sheets, S. Maki, M. Ishiguro*, K. Mori*, H. Makino*: J. Mater. Process. Technol., 177, pp.444-447, 2006

Mechanism of Improvement of Formability in Pulsating Bulging Hydroforming of Tubes, Ken-ichiro MORI*, Tomoyoshi MAENO*, Seijiro MAKI: Journal of the Japan Society for Technology of Plasticity, 47(548), pp.835-839, 2006 (in Japanese)

Mushy-State Forging of Aluminum Alloy Using On-Site Resistance Heating, S. Maki, T. Shibata*, H. Shibata*, K. Mori*: Proceedings of the International Conference on Advances in Materials and Processing Technologies, AMPT 2006, Las Vegas, NV, July 30-Aug. 3, CD-ROM, 2006

Improvement of Formability and Shape Accuracy in Pulsating T-Shape Hydroforming of Tube, Ken-ichiro Mori*, Loh-mousavi Mohsen*, Kentaro Hayashi*, Seijiro Maki: Proceedings of the 2006 Japanese Spring Conference for the Technology of Plasticity, pp.5-6, 2006 (in Japanese)

Press Quenching Using Resistance Heating of Ultra High Strength Steel Sheet, Seijiro Maki, Atsushi Hamamoto*, Shouichi Saitou*, Ken-ichiro Mori*: Proceedings of the 2006 Japanese Spring Conference for the Technology of Plasticity, pp.45-46, 2006 (in Japanese)

Oxidation Preventing in Hot Press Forming of Ultra High Strength Steel Sheet, Makoto Kishimoto*, Syouichi Saitou*, Seijiro Maki, Ken-ichiro Mori*, Tatsushi Hayashi*, Toshihiko Okamura*: Proceedings of the 2006 Japanese Spring Conference for the Technology of Plasticity, pp.47-48, 2006 (in Japanese)

Hot Blanking of Ultra High Strength Steel Sheets, Syouichi Saitou*, Makoto Kishimoto*, Seijiro Maki, Ken-ichiro Mori*, Tatsushi Hayashi*, Toshihiko Okamura*: Proceedings of the 2006 Japanese Spring Conference for the Technology of Plasticity, pp.49-50, 2006 (in Japanese)

Resistance Heating Characteristics of Tubular Blank for Hot Press Forming of Ultra High Strength Steel Sheets, Seijiro Maki, Makoto Kishimoto*, Naotaka Arisawa*, Ken-ichiro Mori*: Proceedings of the 2006 Japanese Spring Conference for the Technology of Plasticity, pp.137-138, 2006 (in Japanese)

Decrease of Surface Cracks in Hot Shear Spinning of Cast Aluminum Alloy Castings, Minoru Ishiguro*, Yuuta Isomura*, Ken-ichiro Mori*, Osamu Ebihara*, Daigo Sugiyama*, Takayuki Nonaka*, Seijiro Maki: Proceedings of the 2006 Japanese Spring Conference for the Technology of Plasticity, pp.211-212, 2006 (in Japanese)

Mashy-State Forging of Cast Iron Using Resistance Heating, Kazuhito Suzuki*, Seijiro Maki, Ken-ichiro Mori*: Proceedings of the 2006 Japanese Spring Conference for the Technology of Plasticity, pp.345-346, 2006 (in Japanese)

Semi-Solid Forming of Titanium Alloy Using Resistance Heating, Seijiro Maki, Kazuhito Suzuki*, Ken-ichiro Mori*: Proceedings of the 57th Japanese Joint Conference for the Technology of Plasticity, pp.135-136, 2006 (in Japanese)

Resistance Heating Characteristics in Local Heating Blanking of Ultra High Strength Steel Sheets, Shoichi Saito*, Seijiro Maki, Ken-ichiro Mori*, Kanji Ueno*, Yasuji Hokazono*, Takuya Yamazaki*: Proceedings of the 57th Japanese Joint Conference for the Technology of Plasticity, pp.139-140, 2006 (in Japanese)

Blowing of Aluminum Compact in Dies by Resistance Heating, Minoru Ishiguro*, Seijiro Maki, Ken-ichiro Mori*, Hikaru Nisikawa*: Proceedings of the 57th Japanese Joint Conference for the Technology of Plasticity, pp.241-242, 2006 (in Japanese)

Modelings of Fiber Deformation During Machining Aramid-FRP, Eitoku Nakanishi, Masao Fukumori*, Yutaka SAWAKI*, Kiyoshi Isogimi*: Proceedings of 16th European Conference of Fracture, CD-ROM, 2006

“Wind tunnel study on the velocity profile over roughness hill” Takao MAEDA, Yasunari KAMADA, Nobutoshi NISIO, Keita NAKANO: WIND ENERGY, Vol. 30, No3, pp. 113, pp. 113-1163, 2006.

In this paper, the experimental results of velocity measurements around hill are described for various slopes. Three types of hill model are tested. The model hill has the equivalent roughness of the actual hill's surface. As the results, the flow pattern around hill shape is described. Also, it is shown that the separating point to the hill surface depends on the upstream shape.

“Study on aerodynamic forces of HAWT” Takao MAEDA, Yasunari KAMADA, Hideyasu FUJIOKA, Jun SUZUKI, Masami KAMIBAYASHI: Proceedings of JSME Fluids Engineering Division 84th Annual meeting, No.06-21, CD-ROM, 2006.

The horizontal axis wind turbines are operated under skew inflow condition and it has tilt angle to keep the

distance between tower and blade tip. Therefore, it is important to analyze the forces and moment of rotor with yawed and tilted inflow condition. In this study, the wind turbine was placed with yaw miss alignment or changing the distance between tower and rotor in a wind tunnel. Through measuring the forces and moments of HAWT with six-component detector, the characteristics of rotor performance with yaw and tilt angle condition and influence of tower position are considered.

“Study on Performance Improvement of Micro Wind Turbine with a Combination of Nosecone and Diffuser Casing” Takao MAEDA, Yasunari KAMADA, Kenta ADACHI: Proceedings of RENEWABLE ENERGY 2006, P-W-29, pp. 909-912, CD-ROM, 2006.

This study is related to use wind turbines that installed in urban area. Such area has low annual wind speed with strong turbulence. The purpose of this study is to enlarge the wind turbines output power and to improve the power curve shape with a combination of nosecone and diffuser. In this study, the utilization of diffuser for wind turbines is considered for increasing the avail ability of wind turbine. Otherwise, the nosecone with aerodynamic form was introduced. The nosecone has effect of improving the flow inside diffuser and performance of wind turbine when operating in low tip speed ratio.

“Field Measurement of Unsteady Aerodynamics Load on the Blade of Field Horizontal Axis Wind Turbine” Takao MAEDA, Yasunari KAMADA, Keita NAITO: Proceedings of RENEWABLE ENERGY 2006, P-W-17, pp. 865-868, CD-ROM, 2006.

This paper describes the experimental results of field wind turbine rotor. The experiments are carried out with 10mdiameter of HAWT. The pressure distributions on the rotating blade are measured by the pressure transducers. The blade root moment are measured simultaneously by the strain gauges. The mean wind speed are measured by a sonic anemometer, the local velocity of the test section is measured by 7 holes Pitot tubes. The relation between the aerodynamic forces from pressure distribution and the blade root moment from strain gauges are discussed. The measured moment from strain gauges show the similar fluctuation.

“Wind Tunnel Study on Velocity Profile over Hill” Takao MAEDA, Yasunari KAMADA, Nobutoshi NISHIO: Proceedings of RENEWABLE ENERGY 2006, P-W-17, pp. 861-864, CD-ROM, 2006.

This paper shows the experimental results of the velocity profile over hill in wind tunnel. The experiments are carried out with various two-dimensional hill models that contains of various slope shapes. 3 types of slopes are tested as hill model, and they are divided for model upstream and downstream slopes at the top. In the measurements, the equivalent roughness to the ground is set on the hill surface. The velocity profiles are measured by two-dimensional PIV. As the result, the velocity distribution around hill is shown for various hill shapes and the energy density in the wind is discussed from the viewpoint.

“Experimental studies on the wind turbine airfoils with dynamic state” Takao MAEDA, Yasunari KAMADA, Masayoshi SAITO: Proceedings of JSME Annual meeting 2006 (2) No.06-1, pp. 255-256, 2006.

In generally, the two-dimensional airfoil characteristics in the static state are used for the wind turbine blade

design. However, the wind turbines are operated in the natural wind with continuously changing in both speed and direction. So, the attack angle of the blade element is fluctuating. Specially, in the inboard section attack angle have big amplitude of fluctuation caused by the yaw misalignment. The airfoil characteristics in the dynamic state are important for the inboard section. In this paper, the airfoil characteristics are investigated experimentally by the surface pressure measurement. Also the dynamic characteristics with sinusoidal pitching motion are measured. As the results, it is found that the dynamic characteristics depend on the amplitude of stall angle. Furthermore, at low Reynolds number the stall angle for wind turbine airfoils is depend in both leading edge radius and suction side curvature.

“Experimental Study on unsteady aerodynamics effect on the blade root Load of HAWT field rotor”

Takao MAEDA, Yasunari KAMADA, Kei TANAKA, Keita NAITO, Yuu OUCHI: Proceedings of IEEE ISEM 2006, CD-ROM, 2006.

This paper describes the experimental results of field wind turbine rotor. The experiments are carried out with 10m diameter of HAWT. The pressure distributions on the rotating blade are measured by the pressure transducers. The blade root moment are measured simultaneously by the strain gauges. The mean wind speed are measured by a sonic anemometer, the local velocity of the test section is measured by 7 holes Pitot tubes. The relation between the aerodynamic forces from pressure distribution and the blade root moment from strain gauges are discussed. The aerodynamic force shows the fluctuation by the local wind speed and direction change. The measured moment from strain gauges show the similar fluctuation. That includes the short period vibration of the blade natural frequency.

“Studies on small scale generation plant by woody biomass gasification (Operation by upper type)”

Yasunari KAMADA, Takao MAEDA, Norio WATANABE: The 11th National Symposium on Power and Energy Systems, No, 06-8, pp. 81-82, 2006.

The experimental results of the up-draft type gasification system are described. In the experiments, the small reactor is operated in up-draft configuration. The operational condition of the reactor is described in detail.

“Studies on unsteady characteristic of field horizontal-axis wind turbine blade” Takao MAEDA, Yasunari KAMADA, Kei TANAKA, Yuu OUCHI, Keita NAITO: The 11th National Symposium on Power and Energy Systems, No, 06-8, pp. 47-48, 2006.

This report describes a experimental study related to the pressure distributions on a field horizontal axis wind turbine. It was known that a dynamic stall was occurred on a wind turbine blade. A cross-correlation function is used for the data reduction to analyze the occurrence condition of the dynamic stall. As a result, when local angle of attack is kept at the high angle, it turned out that dynamic stall occurs. The parameter of judgment for occurrence condition of dynamic stall is also suggested.

“Japanese Wind Energy Prospect and Recent Technology” Takao MAEDA (invited lecture), Proceedings of 2006 Spring Conference of KWEA General Meeting & International Symposium, pp. 83-98, 2006.

There are many barriers to development of wind energy. Japan’s climate condition is different from EU countries. It often experiences typhoons and lightning strikes due to its meteorological

characteristics. Wind has a stronger turbulence level due to complex terrain. There are many endeavors being undertaken to find the best solution for these problems. This paper reviews the wind energy activities in Japan. This includes wind resources, market, trends, environment, prospects and R&D.

“WIND TUNNEL STUDY ON SURFACE PRESSURE MEASUREMENT ON ROTATING BLADE OF HAWT” Takao MAEDA, Yasunari KAMADA, Hideyasu FUJIOKA: Proceedings of the European Wind Energy Conference & Exhibition, BL3-138 CD-ROM, 2006.

Experimental results of the surface pressure distribution on a blade of a horizontal axis model rotor for the rotating and non-rotating status are shown. The experiments were carried out in a wind tunnel with a 2.4m diameter three-bladed rotor. The pressure distribution at $r/R > 0.7$ showed good agreement between the rotating and the non-rotating situations. The pressure distribution for the inboard section of $r/R < 0.5$ showed a stall delay. The method of determining the effective angle of attack for a rotating blade from LDV measurements is also discussed.

“The wind tunnel experiments for wind turbines” Takao MAEDA, Yasunari KAMADA: JSME Fluids Engineering Division, News Letter, http://www.jsme-fed.org/newsletters/2006_9/no3.html#ctop, 2006.

The wind tunnel experiments for wind turbines are described. The wind turbines are aerodynamic device which extracts the kinematical energy from wind. The performance of turbines strongly depends on the aerodynamics of the rotor. To investigate the aerodynamics of the rotor, many experiments are carried out in wind tunnel. The velocity measurements and pressure measurements techniques are explained in detail.

A Study on Machining Characteristics of Two-Dimensional Rectangular Abrasive Jet Machining Nozzle, Masaki SUGIMOTO, Toshihiko SHAKOUCHI, Kohei HAYAKAWA and moriyasu IZAWA, *Journal of the Japan Society for Precision Engineering*, 72-1, pp.121-126, 2006.

Control of Flow Separation and Drag Reduction of Abrupt Expansion Pipe, Toshitake ANDO, Toshihiko SHAKOUCHI, Hiroyuki YAMAMOTO and Koichi TSUJIMOTO, *Transaction of the Japan Society of Mechanical Engineers*, 72-717 B, pp.1125-1130, 2006.

Gas-Liquid Two-Phase Oscillating Flow, Fluctuating Flow through Vertical Sudden Contraction Pipe, Alexandros VOUTSINAS, Toshihiko SHAKOUCHI, Koichi TSUJIMOTO, and Toshitake ANDO, *Transaction of the Japan Society of Mechanical Engineers*, 72-717 B, pp.1131-1136, 2006.

Flow Characteristics and Drag Reduction of Vertical Upward Gas-Liquid Two-Phase Flow through Sudden Contraction Pipe, Alexandros VOUTSINAS, Toshihiko SHAKOUCHI, Koichi TSUJIMOTO and Toshitake ANDO, *Transaction of the Japan Society of Mechanical Engineers*, 72-720 B, pp.1888-1894, 2006.

Effect of Throat Surface Roughness on Jet Pump, Yukitaka YAMAZAKI, Tomonori NAKAYAMA, Tadashi NARABAYASHI, Hidetoshi KOBAYASHI and Toshihiko SHAKOUCHI, *Transaction of the Japan Society of Mechanical Engineers*, 72-720 B, pp.1895-1900, 2006.

Flow Control of Turbulent Round Jet using a Resonance Nozzle, Toshihiko SHAKOUCHI, *Journal of Aeronautics, Astronautics and Aviation*, Ser. A, 38-1, pp.1-9, 2006.

Behaviors of Particle Laden Jet Flow and Machining Characteristics of Micro-Blasting Process, Masaki SUGIMOTO, Toshihiko SHAKOUCHI and Moriyasu IZAWA, *Journal of the Japan Society for Abrasive Technology*, 51-1, pp.46-51, 2005.

Effect of Surface Roughness on Jet Pump Performance, Yukitaka YAMAZAKI, Tomonori NAKAYAMA, Tadashi NARABAYASHI, Hidetoshi KOBAYASHI and Toshihiko SHAKOUCHI, *JSME International Journal*, Ser. B, 49-4, pp.928-932, 2006.

Flow Characteristics and Control of Vertical Upward Gas-Liquid Two-Phase Flow through a Sudden Contraction Pipe, Alexandros VOUTSINAS, Toshihiko SHAKOUCHI, Junichi TAKAMURA, Koichi TSUJIMOTO and Toshitake ANDO, *JSME International Journal*, Ser. B, 49-4, pp.1000-1007, 2006.

Flow Analysis for Single and Multi-Nozzle Jet Pump, Tadashi NARABAYASHI, Yukitaka YAMAZAKI, Hidetoshi KOBAYASHI and Toshihiko SHAKOUCHI, *JSME International Journal*, Ser. B, 49-4, pp.933-940, 2006.

Globular Formation of Fine Particle using a New High Temperature Air-Jet-Flow System, Hirokazu NAKAMURA and Toshihiko SHAKOUCHI, *Journal of Powder Technology*, 166, pp.14-23, 2006.

Gas-Particle Two-Phase Jet Flow from Slot Nozzle and Micro-Blasting Process, Masaki SUGIMOTO, Toshihiko SHAKOUCHI, Kohei HAYAKAWA and Moriyasu IZAWA, *JSME International Journal*, Ser. B, 49-3, pp.705-713, 2006.

Drag Reduction of Abrupt Expansion Pipe Flow, Toshitake ANDO, Toshihiko SHAKOUCHI, Hiroyuki YAMAMOTO and Koichi TSUJIMOTO, *Proc. of International Symposium on Advanced Fluid/Solid Science and Technology in Experimental Mechanics, ISEM06-Sapporo*, CD-ROM, 2006

Development of Rectangular Micro-blasting Nozzle, Masaki SUGIMOTO and Toshihiko SHAKOUCHI, *Proc. of International Conference on Precision Engineering, ICPE11-Tokyo*, CD-ROM, 2006.

Analysis of turbulent structures of natural convection in a vertical channel by using DNS, Koichi TSUJIMOTO, Naohiro Ohya, Toshihiko SHAKOUCHI and Toshitake ANDO, *Transaction of the Japan Society of Mechanical Engineers*, 72-719 B, pp.1666-1673, 2006.

Analysis of turbulent structures of natural convection in a vertical channel by using DNS , Koichi TSUJIMOTO, Naohiro Ohya, Toshihiko SHAKOUCHI and Toshitake ANDO, *Proc. Fifth International Symposium on Turbulence Heat and Mass Transfer*, CD-ROM, 2006.

Direct Numerical Simulation of Jet Mixing Control Using Combined Jets, Koichi TSUJIMOTO, Toshihiko SHAKOUCHI, Shuji SASAZAKI and Toshitake ANDO, *JSME International Journal*, Ser. B, 49-4, pp.966-973, 2006.

Department of Electrical and Electronic Engineering

*nonmember

Visual Servo of Active Camera and Manipulator with Simple On-line Calibration for Estimated Image Feature, Itsushi Kinbara, Satoshi Komada, and Junji Hirai : Proceedings of the 9th IEEE International Workshop on Advanced Motion Control AMC'06, vol.2, pp.636-640, 2006

In visual servo system, there are problems on time delay by image processing and difference between image processing period and control period. In order to overcome these problems, the estimated image feature applied to a fixed camera has been proposed. Since the compensation of delay utilizes image Jacobian matrices which represent geometric models of manipulator and camera, it is affected by their calibration error. Therefore, this paper proposes a new visual servo system for active camera using estimated image feature with a simple on-line calibration. In order to reduce estimation error of image feature, the proposed method is calibrating each element of image Jacobian matrices from error of the estimated image feature. It is simple algorithm and few calculation amount compared to calibrating each parameters correctly such as internal camera parameters and orientation of manipulator and camera. The effectiveness of the proposed strategy is confirmed by a moving object tracking by a manipulator and an active camera.

Study on parameters identification of dynamic equation of human lower limb for improved estimation of muscular tensions, Shohei Oda, Noboru Okuyama, Satoshi Komada, and Junji Hirai : Proceedings of the 9th IEEE International Workshop on Advanced Motion Control AMC'06, vol.1, pp.356-361, 2006

We have proposed a new rehabilitation support equipment that estimates the muscular tensions of lower limbs in order to offer it to the PTs and the patients in a comprehensible form to realize a biofeedback therapy. The muscular tension is estimated by solving the optimization problem from joint torque of each examinee's joint during training. This paper reports comparison and its discussion of joint torque of each joint derived by an examinee's identified parameters of dynamic equation and parameters determined by the average of about 100 peoples. The accuracy of the joint torque is improved by the identified parameters.

Visual Servo of Active Cameras and Manipulators by Time Delay Compensation of Image Features with Simple On-line Calibration, Itsushi Kinbara, Satoshi Komada, and Junji Hirai : Proceedings of SICE-ICASE International Joint Conference 2006, pp.5317-5322, 2006

In visual servo system, there are problems on time delay caused by image processing and difference between image processing period and control period. In order to overcome these problems, an estimation method of image features has been applied to a fixed camera, which realizes visual servo with control period. Since the compensation of delay utilizes image Jacobian matrices, it is affected by calibration error. Therefore, this paper proposes a new visual servo system for manipulators and active cameras using the estimated image features with a simple on-line calibration. In order to reduce estimation error of image feature, the proposed method is calibrating each element of image Jacobian matrices from error of the estimated image feature. It is simple algorithm and few calculation amount compared to calibrating each parameters correctly such as internal camera parameters, orientation of manipulator and camera, and so on. The effectiveness of the proposed strategy is confirmed by tracking simulation of a moving object by a manipulator and an active camera.

Development of a Biofeedback Therapeutic Exercise Supporting Manipulator for Lower Limbs, Yosuke Hashimoto, Satoshi Komada, and Junji Hirai : Proceedings of International Conference on Industrial Technology ICIT 2006, vol.2, pp.352-357, 2006

Although equipments that support physical therapy have been developed, there are few types of equipment to improve quality of physical therapy. This paper proposes a new concept of robotic biofeedback exercise equipment that displays human muscle force during training. The concept tries to have therapeutic value through grasping of condition for trainee during exercise and giving an incentive to perform training. The machine is not only for convalescent

patients but also for athletes and ordinary persons with a physical trouble. The manipulator is designed to support lower limb rehabilitation of knee and hip joints in sagittal plane where a three-degree-of-freedom manipulator is adopted in order to realize low height equipment. Since the manipulator has redundant degree-of-freedom, collision avoidance is performed based on acceleration control by disturbance observer. Moreover, simultaneous isokinetic movement for knee and hip joints that has an adjustment capability of maximum speed and acceleration degree is realized in order to realize safe training by isokinetic muscular contraction. Desired motion of the proposed manipulator is confirmed experimentally.

A Realization Method of Fault-tolerant Control of Flexible Arm under Sensor Fault by Using an Adaptive Sensor Signal Observer, Yu Izumikawa, Kazuhiro Yubai, and Junji Hirai : Journal of Power Electronics, vol.6, no.1, pp.8-17, 2006

In this paper, we propose a fault-tolerant control system for the position control and vibration suppression of a flexible arm robot. The proposed control system has a strain gauge sensor signal observer based on a reaction force observer and detects a fault by monitoring an estimated error. In order to improve the estimation accuracy, the plant parameters included in the sensor signal observer are updated by using the strain gauge sensor signal in normal time through the adaptive law. After fault detection, the proposed control system exchanges the faulty sensor signal for the estimated one and switches to a fault mode controller so as to maintain the stability and the control performance. We confirmed the effectiveness of the proposed control system through several experiments.

A Fundamental Study on Reconfigurable Robot System Construction with Central- and Local Intelligence, Nobuyasu Miwa, Kazuhiro Yubai, and Junji Hirai : Proceedings of the 9th IEEE International Workshop on Advanced Motion Control AMC'06, vol.1, pp.90-93, 2006

This paper deals with a study on reconfigurable robots. Firstly, the concept of the reconfigurable robot is described. Secondly, construction of the distributed robot control system consisting of Local- and Central Intelligence is explained. Then the authors propose Virtual Velocity Transmission Algorithm (VVTA) as the best-suited control scheme for this system, and finally confirm the effectiveness of the proposed algorithm by simulations.

A Joint Design Method for Achieving Robust Performance -Experimental Study in 2-mass System-, Naoya Wakayama, Kazuhiro Yubai, and Junji Hirai : Proceedings of the 9th IEEE International Workshop on Advanced Motion Control AMC'06, vol.2, pp.467-471, 2006

Joint design methods are based on an iterative scheme of model identification and controller design associated with each other. This paper proposes a new joint design method based on GIMC structure. The proposed joint design method evaluates the performance degradation from the nominal performance explicitly so as to achieve the nominal performance for the actual plant. The identification of dual Youla-parameter R and the design of Youla-parameter Q are related to each other under the same control objective. Youla parameter Q is implemented in GIMC structure proposed by Zhou. The effectiveness of the proposed design method is verified by an actual control system.

Fault-Tolerant Control of Flexible Arm Based on Dual Youla Parameter Identification, Tsubasa Sakuishi, Kazuhiro Yubai, and Junji Hirai : Proceedings of the 9th IEEE International Workshop on Advanced Motion Control AMC'06, vol.2, pp.452-455, 2006

In recent years, control system reliability has received much attention with increase of situations where computer-controlled systems such as robot control systems are used. In order to improve reliability, control systems

need to have abilities to detect faults (fault detection) and maintain the stability and the control performance (fault tolerance). In this paper, we address the strain gauge sensor fault of a flexible arm robot. In order to achieve a fault-tolerant control system, the effect of the fault is identified as dual Youla parameter by regarding the estimation error of the faulty sensor signal as the faulty plant output. Moreover, Youla parameter is designed so as to suppress the effect of dual Youla parameter. Youla parameter is implemented in GIMC structure proposed by Zhou. Since GIMC structure includes a conditional feedback, it is suitable for achieving a fault-tolerant control system. The effectiveness of the proposed fault-tolerant control system is confirmed by some experiments.

Design of Gain-Scheduling Controller Based on Interpolation of Loop Shaping H_∞ Controller, Yuki Maekawa, Kazuhiro Yubai, and Junji Hirai : Proceedings of the 9th IEEE International Workshop on Advanced Motion Control AMC'06, vol.1, pp.29-32, 2006

In this paper, we propose a design method of gain-scheduling controller. We extend LSDP to gain-scheduling version. The controllers designed according to LSDP consist of a state observer and a regulator. The observer-gain and regulator-gain at each design point determine the control performance, and they are interpolated by polynomial. The gain-scheduling controller varies these gains according to the operating point. We apply the design method of gain-scheduling controller to an inverted pendulum and confirm the effectiveness of the proposed controller by some experiments.

Stabilization of Rotary Inverted Pendulum by Gain-scheduling of Weight and H_∞ Loop Shaping Controller, Kazuhiro Yubai, Kazunori Okuhara, and Junji Hirai : Proceedings of the 32nd Annual Conference of the IEEE Industrial Electronics Society, pp.288-293, 2006

Gain-scheduling control is one of effective methods for plants whose dynamics changes significantly according to its operating point. A frozen parameter method is known to be a practical gain-scheduling controller synthesis, which interpolates the controllers designed at the prespecified (frozen) operating points according to the current operation point. Hyde et al. proposed a gain-scheduling control that H_∞ loop shaping procedure is adopted as a controller synthesis at each operating point. H_∞ loop shaping procedure is based on loop shaping of an open loop characteristic by frequency weights and is known to be effective for plants with bad condition number. However, weight selection satisfying control specifications is a hard job for a designer. This paper describes the design of a suboptimal weight and a controller by means of algorithm that maximizes the robust stability margin and shapes the open loop characteristic into the desired shape at each operating point. Moreover, we formulate a weight optimization problem as a generalized eigenvalue minimization problem, which reduces the designer's burden of weight selection. Finally, we realize robust and high performance control system by scheduling both weights and controllers. The effectiveness of the proposed control system is verified in terms of the achieved robust stability margin and experimental time responses of a rotary inverted pendulum, which involves strong nonlinear dynamics.

Gain-scheduling Control of Rotary Inverted Pendulum by Weight Optimization and H_∞ Loop Shaping Procedure [in Japanese], K. Yubai, K. Okuhara and J. Hirai: IEEJ Transactions on Electronics, Information and Systems, Vol.126, no.12, pp.1504-1513, 2006

Gain-scheduling control is one of effective methods for plants whose dynamics changes significantly according to its operating point. A frozen parameter method is known to be a practical gain-scheduling controller synthesis, which interpolates the controllers designed at the prespecified (frozen) operating points according to the current operation point. Hyde et al. proposed a gain-scheduling control that H_∞ loop shaping procedure is adopted as a controller synthesis at each operating point. H_∞ loop shaping procedure is based on loop shaping of an open loop characteristic by frequency weights and is known to be effective for plants with bad condition number. However, weight selection

satisfying control specifications is hard job for a designer. This paper describes the design of a suboptimal weight and a controller by means of algorithm that maximizes the robust stability margin and shapes the open loop characteristic into the desired shape at each operating point. Moreover, we formulate a weight optimization problem as a generalized eigenvalue minimization problem, which reduces the designer's burden of weight selection. Finally, we realize robust and high performance control system by scheduling both weights and controllers. The effectiveness of the proposed control system is verified in terms of the achieved robust stability margin and experimental time responses of a rotary inverted pendulum, which involves strong nonlinear dynamics.

Abstraction and Implementation of Human Skill by Hybrid Dynamical System Theory - Application to an Automatic Driving System -, ShangChang Ma, Tadanao Zanma, Muneaki Ishida: Vol.126-C, No.12, pp.1524-1530, 2006

In this paper, we propose a modeling method for drivers' driving skill with which automatic driving of the vehicle is realized. The method is to formulate the automatic driving system of a vehicle as a switched system with unknown switch points by using HHARX model, which can extract driving operation modes and their switch conditions simultaneously. To verify the effectiveness, we apply the proposed method to an automatic driving system of a small remote-controlled vehicle, instead of a real vehicle. Simulation results illustrate that obtained models can achieve functions such as start acceleration, normal traveling, stop deceleration and auto steering in the automatic driving system.

Automatic driving system using identification of switched systems with unknown switch points, ShangChang Ma, Tadanao Zanma, Muneaki Ishida: IEEJ Transactions on Electrical and Electronic Engineering, Vol.1, No.4, pp.426-437, 2006

In this paper, we propose an approach to abstract human manipulation skill, which can be useful in systems of machine intelligence and human operator assistance. Because of the lack of good physical models for human skill, it is impossible to model it by traditional methods - from physical or chemical principles of a system. Our approach is to consider human manipulation skill as a hybrid dynamical system (HDS). For the purpose, a hinging hyperplane autoregressive exogenous (HHARX) model is utilized as it is able to deal with manipulation modes and their switches simultaneously. We obtain the HHARX model by system identification via mixed-integer linear programming (MILP). As a typical example, we apply our approach to an automatic driving system of a small radio-controlled vehicle. Both simulation and experimental results illustrate the effectiveness of the proposed method.

Optimal control of DC-DC converter using mixed logical dynamical system theory, Nobuhiro Asano, Tadanao Zanma and Muneaki Ishida: Proceedings of 2006 IEEE International Conference on Industrial Technology, (ICIT), pp. 110-115, 2006

This paper presents an optimal control method of dc-dc converters. The method is based on hybrid dynamical system theory. Specifically, the input of the considered system is confined to discrete value whereas the output to be controlled is continuous value. The system is modeled as a mixed logical dynamical system. Then, the optimal control law is obtained by means of model predictive control. To illustrate the effectiveness of the proposed method, some numerical simulations are shown.

Simultaneous vibration suppression control of PMSM using repetitive control with Fourier series, Kenji Kawai, Tadanao Zanma and Muneaki Ishida: Proceedings of 2006 IEEE International Conference on Industrial Technology, (ICIT), pp. 854-859, 2006

This paper proposes a suppression control method of the motor frame vibration caused by the torque ripple of PMSM. The method utilizes the feedforward compensation signals by the repetitive control and the Fourier series expansion using a vibration signal obtained by an acceleration sensor which is attached to the motor frame. In order to realize on-line generation of the feedforward compensation signals to reduce the vibration, a novel parameter auto-tuning method for the repetitive control is proposed. The method enables to shorten time to suppress the torque ripple since simultaneous vibration suppression control can be achieved. The effectiveness of the proposed method is illustrated through some experimental results.

Speed Estimation Method utilizing Rotor Slot Harmonics Detected from Line Current for Speed Sensorless Drive of Ultra High Speed Induction Machine, Koichi Nishibata, Muneaki Ishida, Shinji Doki, Takashi, Masuzawa, Masami Fujitsuna: Proceedings of 2006 IEEE International Conference on Industrial Technology, (ICIT), pp. 1591-1596, 2006

Recently, development of power electronics technology has made it possible to realize ultra high speed machine and it has been expected in various applications. This research aims at sensorless control drive of induction machine in the ultra high speed region by utilizing rotor slot harmonics caused by structure of induction machine. In this paper, we proposed a novel speed estimation method utilizing rotor slot harmonics detected from line current for speed sensorless drive of ultra high speed induction machine. It is possible to detect the rotor slot harmonics with high signal-noise ratio by utilizing a harmonics model of IM and fast fourier transform (FFT) with limitation of a detection band. Moreover, the effectiveness of the proposed method is confirmed by experimental result.

Study for Small Size Wind Power Generating System Using Switched Reluctance Generator, Kazutoshi Ogawa, Naoki Yamamura, Muneaki Ishida: Proceedings of 2006 IEEE International Conference on Industrial Technology, (ICIT), pp. 1510-1515, 2006

Recently, problems such as air pollution and global warming become serious because of increasing consumption of the fossil fuel. Therefore, there have been many studies related to the natural energy generation system effective to cope with these problems. The small size wind power generating system is one of the most useful generation systems utilizing natural energy. Now, Permanent Magnet Type Synchronous Generator or Induction Generator is used for the wind power generating system. However, material cost of the Permanent Magnet Type Synchronous Generator is high, though the generation efficiency is high, and the efficiency of the Induction Generator is low, though it is tough and requires little maintenance. Therefore, we focus attention on SRM (Switched Reluctance Motor) which is characterized by simple structure, toughness, and high efficiency. And we studied a small size wind power generating system which uses the SRM as a SRG (Switched Reluctance Generator). In this paper, configuration of the small size wind power generating system using a SRG, the generation principle and an experimental set up and results are presented. We also propose a power control method by calculated the magnetization energy of the SRG. Also, we propose MPPT (Maximum Power Point Tracking) control method based on foregoing control method and constant resistance control method. And we show validity of the proposed control method by experimental results.

Identification of human skill and its application to an automatic driving system --an approach from hybrid dynamical

system-- Shangchang Ma, Tadanao Zanna, Muneaki Ishida: Proceedings of The 32nd Annual Conference of the IEEE Industrial Electronics Society (IECON06), pp. 400-405, 2006

In this paper, we propose an approach to model human skill, which can be useful in systems of machine intelligence and human operator assistance. The approach is to consider the model of human manipulation skill as a hybrid dynamical system (HDS), where, each continuous submodel deals with its related manipulation mode, while a discrete event model represents the switches between all the submodels. In particular, we express the HDS model as a hinging hyperplane autoregressive exogenous (HHARX) model as it is able to deal with manipulation modes and their switches simultaneously. Based on experimental data manipulated by an expert human operator, HHARX parameters are identified via mixed-integer linear programming (MILP). As a typical example, we apply our approach to an automatic driving system of a small radio-controlled vehicle. Both simulation and experimental results illustrate the effectiveness of the proposed method.

Smoothed-Power Output Supply System for Battery of Stand-alone Renewable Power System Using EDLC, Jia Yan, Ryosuke Shibata, Naoki Yamamura and Muneaki Ishida, Proceedings of Power Electronics and Motion Control Conference, Vol. 3, pp 1-5, 2006

A smoothed-power output topology for battery of stand-alone renewable power system (SARPS) using EDLC (electric double layer capacitor) is presented. To prolong the service life of battery, decrease maintenance cost and power loss of SARPS by realizing smoothed-power output supply, an EDLC is paralleled with battery as a part of storage system, and connected by a bi-directional buck/boost compensation topology. The EDLC stores fluctuant component and compensate battery current through proposed topology and switch control. Whereas the changeable natural condition and initial power condition, an appointed fluctuant power condition as an example to analyze the validity of proposed method in simulation and real-time experiment example firstly. The results show that smoothed-power output for battery can be obtained through proposed topology and satisfy the criterion of smooth precision. And then, the experiment result carried out in actual stand-alone wind power system further shows the feasibility of proposed topology.

Keywords Recognition of Handwritten Character String on Whiteboard Using Word Dictionary for e-Learning, Daisuke YOSHIDA, Shinji TSURUOKA, Hiroharu KAWANAKA, Tsuyoshi SHINOBI: Proc. of International Conference on Hybrid Information Technology (ICHIT 06), Vol.1, pp.140-145, 2006

We are developing an individual e-Learning system using two communication cameras and a pen capture tool on whiteboard for university students. In this research, keywords recognition for the written characters by the lecturer on the whiteboard is important for indexing the scene database. We are considering the handwritten keyword recognition. The whiteboard image captured by the pen capture tool is recognized to character strings and the string corresponds to keywords in a textbook to link to the explanation of the keyword in textbook. One of important problems in our learning system is that the accuracy of handwritten character recognition on whiteboard is not enough for keyword recognition. In this paper, we propose the new matching method of high accuracy keyword recognition using word dictionary and the distance of character recognition. We confirmed the usefulness using word dictionary for handwritten keyword recognition on whiteboard.

Heart Motion Evaluation Indexes Using Ultrasonic RF Signal, Yosuke.MIZUTANI, Shinji TSURUOKA, Hiroharu

KAWANAKA, Tsuyoshi SHINOGI, Wataru OHYAMA, Kiyotsugu SEKIOKA*: Proc. of International Conference on Hybrid Information Technology (ICHIT 06), Vol.2, pp. 62-67, 2006

Our research group has developed the tracking method of regional myocardium from ultrasonic radio frequency (RF) signal. The tracking method employs a hierarchical correlation method. In addition, we regarded the correlation coefficient as the confidence coefficient. If it is not high, the tracking position is corrected by neighbor points. The tracking method can detect the movement of myocardium very well if the RF signal is clear. In this research, we investigate the moving distance based on the tracking position that includes less error. As a result, the contributions of the distance are different between normal example and abnormal example. We propose three indexes defined by amounts of statistics for the evaluation of a heart motion. We compared the accuracy between indexes and thickening rate by ROC analysis. As a result, one of proposed indexes has higher accuracy than thickening rate.

3-D Display of the Wall Motion for Regional Cardiac Muscle from Ultrasonic B-mode Image –Wall Motion of Thickness, Thickening Rate using Contour of Inner and Outer Wall—, Soohyo YANG, Shinji TSURUOKA, Tsuyoshi SHINOGI, Hiroharu KAWANAKA, Wataru OHYAMA, Fumitaka KIMURA, Tetsushi WAKABAYASHI, Kiyotsugu SEKIOKA*: Proc. of International Conference on Hybrid Information Technology (ICHIT 06), Vol.2, pp.6-12, 2006

In this paper, we propose a new 3-D display method of the motion function on the endocardium to evaluate the motion of the myocardium objectively. Its method displays cardiac wall motion during one cardiac cycle or more, and it is colored the thickness or the thickening rate of the myocardium on the surface of the 3-D endocardium object. The endocardium and epicardium of the heart are extracted from a set of ultrasonic B-mode Images. We implemented 3-D display system using C language and DirectX 3D in MS-Windows. We determine the position of the points for 3-D display from the contour lines of the cardiac muscle. We define the thickness by the shortest distance between the endocardium and the epicardium, and we calculate the thickness rate from the obtained thickness. And in Experimental 3-D display, We confirmed the usefulness of our 3-D display.

Modeling Error Estimation of Mobile Robot Using Co-Evolutionary Computation and Image Processing, H. Chinthaka. N. PREMACHANDRA, Hiroharu KAWANAKA, Shinji TSURUOKA, Tsuyoshi SHINOGI: Proc. of Joint 3rd International Conference on Soft Computing and Intelligent Systems and 7th International Symposium on advanced Intelligent Systems (SCIS & ISIS 06), TH-E3-4, pp. 361-366, 2006

Recently, Evolutionary Computations (ECs) have been employed to minimize modeling errors between robotic movements on the computer simulation system and the trajectories of an actual mobile robot. Generally, this task is important but it is so difficult. In this paper, we propose the method to minimize the modeling error of between robotic movements and simulation results using co-evolutionary computations with image processing technique. In the proposed method, we employ the video camera system on the ceiling for capturing the robot movements, and the trajectories of the actual mobile robot are detected from captured images by image processing technique and the modeling error is estimated. We experimented using an actual mobile robot to validate the effectiveness of the proposed method, and the results shows that modeling errors are reduced effectively by the proposed method. Finally, this paper describes the problem and future works of this study.

3-D Display of the Wall Motion for Regional Cardiac Muscle from Ultrasonic B-mode Image –Wall Motion Display of Thickness, Thickening Rate—, Soohyo YANG, Shinji TSURUOKA, Tsuyoshi SHINOGI, Hiroharu KAWANAKA,

Wataru OHYAMA, Fumitaka KIMURA, Tetsushi WAKABAYASHI, Kiyotsugu SEKIOKA*, Fumio OKUYAMA*: Proc. of Proc. of Joint 3rd International Conference on Soft Computing and Intelligent Systems and 7th International Symposium on advanced Intelligent Systems (SCIS & ISIS 06), SA-D3-3, pp.1848-1853, 2006

We have developed extracting the inner and outer walls of the cardiac muscle from a set of ultrasonic B-mode images. In this paper, we propose a new 3-D (radius, angle and time) display method of the motion function on the inner wall to evaluate the motion of the myocardium objectively. Its method displays the time transition of a cardiac wall during one cardiac cycle, and it is colored the thickness or the thickening rate of the myocardium on the surface of the 3-D object. The inner and outer walls of the heart are extracted from a set of ultrasonic B-mode Images. We implemented 3-D display system using C language and DirectX 3D in MS-Windows. We calculate the position of the points for 3-D display from the contour lines of the cardiac muscle by the cubic spline curve. The curve connects smoothly between one point and the other one point. And we found the thickness and thickening rate by using the contour lines of the cardiac muscle. We define the thickness by the shortest distance between the outer wall and the inner wall, and we calculate the thickness rate from the obtained thickness. We add the rotation view of the 3-D object to see the every side of myocardium. We confirmed the usefulness of our 3-D display.

New Indexes on Heart Motion Evaluation Using Ultrasonic RF Signal, Yosuke MIZUTANI, Shinji TSURUOKA, Hiroharu KAWANAKA, Tsuyoshi SHINOGLI, Wataru OHYAMA, Kiyotsugu SEKIOKA*: Proc. of Joint 3rd International Conference on Soft Computing and Intelligent Systems and 7th International Symposium on advanced Intelligent Systems (SCIS & ISIS 06), SA-D4-2, pp.2001-2006, 2006

Our research group has developed the tracking method of regional myocardium from ultrasonic radio frequency (RF) signal. The tracking method employs a hierarchical correlation method. In addition, we regarded the correlation coefficient as the confidence coefficient. If it is not high, the tracking position is corrected by neighbor points. The tracking method can detect the movement of myocardium very well if the RF signal is clear. In this research, we investigate the moving distance based on the tracking position that includes less error. As a result, the contributions of the distance are different between normal example and disorder example. We propose three indexes defined by the amounts of statistics for the evaluation of a heart motion. The error rates for diagnosis with the proposed index (FP=4.8[%], FN= 9.5[%]) is lower than that with thickening rate (FP=13.6[%], FN=14.3[%]).

Telemedicine Imaging Collaboration System with Virtual Common Information Space, Fumio OKUYAMA*, Takenori HIRANO*, Yuusuke NAKABAYUASHI*, Hirohito MINOURA*, Shinji TSURUOKA, Yosuke OKAYAMA: Proc. of the Sixth IEEE International Conference on Computer and Information Technology (CIT'06), pp.1-6, 2006

The computerization of the clinical record and the realization of the multimedia have brought improvement of the medical service in medical facilities. It is very important for the patients to obtain comprehensible informed consent. Therefore, the doctor should plainly explain the purpose and the content of the diagnoses and treatments for the patient. We propose and design a Telemedicine Imaging Collaboration System which presents a three dimensional medical image as X-ray CT, MRI with stereoscopic image by using virtual common information space and operating the image remotely. This system can offer a comprehensible three-dimensional image of the diseased part. Therefore, the doctor and the patient can easily understand it, depending on their demand. In this paper, we described the examination situation of the system design.

Scan Chain Flip-Flop Reordering Method Considering Wiring Length for Test Response Test Vector Overlapping Testing, Tsuyoshi SHINOGLI, Tadao KYOTANI, Masakazu TOKAIRIN, Terumine HAYASHI, Hiroharu KAWANAKA, Shinji TSURUOKA : Proceedings of IEEE 7th Workshop on RTL and High Level Testing(WRTL06), pp.63-68, 2006

To reduce the test cost in full-scan testing, a method of "Test Response Test Vector Overlapping" without any additional built-in hardware has already been proposed. In this paper, we propose a method of restricted scan flip-flop reordering considering the wiring length of scan chain for reducing test cost of the Test Response Test Vector Overlapping testing further.

Test Data Sequence Generation Method for Test Response - Test Vector Overlapping [in Japanese], Hiroyuki YAMADA, Tsuyoshi SHINOGLI, Tadao KYOTANI, Terumine HAYASHI, Shinji TSURUOKA : The IEICE Transactions on Information and Systems [in Japanese], Vol.J89-D No.8, pp.1654-1662, 2006

To reduce the LSI testing cost in full-scan testing, various methods are proposed which utilize some additional built-in circuits dedicated for testing. In contrast, a previous method, called Reduced Scan Shift, does not utilize any additional hardware. However, the method totally relies on scan chain flip-flop reordering, which is not always applicable. In this paper, we propose a test data sequence generation method for Reduced Scan Shift without scan chain flip-flop reordering. It fully utilizes justification technique and don't-care bits in test vectors. Two rescue methods against fault coverage degradation are also discussed. Experimental results show its effectiveness.

Proposal of Residual Frequency Offset Compensation Method for OFDM Systems, Fang WANG, Masaaki YAMAMOTO, Katsuhiro NAITO, Kazuo MORI, Hideo KOBAYASHI: Journal of IITE, vol.60, No.5, pp.773-780, May 2006

Complexity Reduced Maximum Likelihood Detection for SDM-OFDM System, Yuanrun TENG, Katsuhiro NAITO, Kazuo MORI, Hideo KOBAYASHI: IEICE Transactions on Communications, vol.E89-B, No.7, pp2084-2087, July 2006

Doppler Spread Estimation Method for OFDM Signal Using Mean Square of Channel Impulse Response's Time Derivative, Gagik MKRTCHYAN, Katsuhiro NAITO, Kazuo MORI, Hideo KOBAYASHI: IEICE Transactions on Communications, vol.E89-B, No.10, pp2961-2966, Oct. 2006

Evolutional Algorithm Based Learning of Time Varying Multipath Fading Channels for Software Defined Radio, Gagik MKRTCHYAN, Katsuhiro NAITO, Kazuo MORI, Hideo KOBAYASHI: IEICE Transactions on Communications, vol.E89-B, No.12, pp.3269-3273, Dec. 2006

PAPR Reduction Method for OFDM Signal by Using Dummy Sub-carriers, Pongsakorn BOONSRIMUANG, Pisit BOONSRIMUANG, Kazuo MORI, Tawil PAUNGMA*, Hideo KOBAYASHI: Proc. of 1st International Symposium

on Wireless Pervasive Computing (ISPWC'2006), pp.70-74, Jan. 2006

Prediction of Time-Varying Multipath Fading Channel for Pre-Equalization of the Signal in Uplink Mobile MC-CDMA Communications, Gagik MKRTCHYAN, Katsuhiro NAITO, Kazuo MORI, Hideo KOBAYASHI: Proc. of IEEE The 8th International Conference on Advanced Communication Technology (ICACT2006), pp. 204-209, Feb. 2006

Downlink Packet Transmission Control Based on Handoff Status in CDMA Cellular Packet Networks, Kazuo MORI, Abubaker KHUMSI, Katsuhiro NAITO, Hideo KOBAYASHI, Hamid AGHVAMI*: Proc. of IEEE 2006 International Zurich Seminar on Communications (IZS2006), pp.62-65, Feb. 2006

Proposal of QAM-OFDM System with IDAR Method for Non-Linear Satellite Channel, Pisit BOONSRIMUANG, Katsuhiro NAITO, Kazuo MORI, Tawil PAUNGMA*, Hideo KOBAYASHI: Proc. of IEEE Vehicular Technology Conference (VTC 2006-Spring), May 2006

Asymmetric Traffic Accommodation Using Cell Sizing in CDMA/FDD Cellular Packet Communication Systems, Kazuo MORI, Katsuhiro NAITO, Hideo KOBAYASHI, Hamid AGHVAMI*: Proc. of IST Wireless & Mobile Communications Summit 2006, CD-ROM, Mykonos, Greece, June 2006

Proposal of Demodulation Method for OFDM System under Multi-path Fading Environment with Delay Spread Greater than Guard Interval, Kazuya MORIWAKI, Katsuhiro NAITO, Kazuo MORI, Hideo KOBAYASHI: Proc. of IEEE VTS Asia Pacific Wireless Communications Symposium (APWCS06), Aug. 2006

Proposal of Non-Linear Distortion Mitigation Method for MC-CDMA System, Naoki SAWADA, Katsuhiro NAITO, Kazuo MORI, Hideo KOBAYASHI: Proc. of IEEE VTS Asia Pacific Wireless Communications Symposium (APWCS06), Aug. 2006

Study of Media Access Control Protocol for Ad Hoc Networks under Slow Fading Channel, Shoko UCHIDA, Katsuhiro NAITO, Kazuo MORI, Hideo KOBAYASHI: Proc. of IEEE VTS Asia Pacific Wireless Communications Symposium (APWCS06), Aug. 2006

Study of Site Diversity System for Roadside to Vehicle Communication, Kouichi TERADA, Katsuhiro NAITO, Kazuo MORI, Hideo KOBAYASHI: Proc. of IEEE VTS Asia Pacific Wireless Communications Symposium (APWCS06), Aug. 2006

Simple PAPR Reduction Method for OFDM System By Using Dummy Sub-carriers, Pisit BOONSRIMUANG, Kazuo MORI, Tawil PAUNGMA*, Hideo KOBAYASHI: Proc. of 3rd International Conference on

Telecommunications and Computer Networks (IADAT-tcn 2006), Portsmouth, United Kingdom, pp.110-114, Sept. 2006

Dynamic Subband and Code Channel Assignment for Multicast Band Division MC-CDMA Systems, Kazuo MORI, Katsuhiko NAITO, Hideo KOBAYASHI, Hamid AGHVAMI*: Proc. of IEEE International Symposium on Personal, Indoor and Mobile Radio Communications (PIMRC2006), Helsinki, Finland, Sept. 2006

TCP Based Resource Allocation Method for Base Station Diversity System, Katsuhiko NAITO, Kazuo MORI, Hideo KOBAYASHI: Proc. of IARIA International Conference on Systems and Networks Communications (ICSNC 2006), Tahiti, French Polynesia, Oct.. 2006

Adaptive Transmission Window Control for Downlink Packet Transmission in CDMA Cellular Networks, Abubaker Faraj KHUMSI, Kazuo MORI, Katsuhiko NAITO, Hideo KOBAYASHI: Proc. of IEEE International Symposium on Intelligent Signal Processing and Communication Systems (ISPACS2006), Dec. 2006

Adaptive Slot and Bit Allocation Method for OFDMA Transmission Systems, Fang WANG, Yuanrun TENG, Katsuhiko NAITO, Kazuo MORI, Hideo KOBAYASHI: Proc. of IEEE International Symposium on Intelligent Signal Processing and Communication Systems (ISPACS2006), Dec. 2006

Study of local alternative ad hoc routing protocol for the exposed terminal problem, Takanori WATANABE, Katsuhiko NAITO, Kazuo MORI, Hideo KOBAYASHI: Proc. of IEEE International Symposium on Intelligent Signal Processing and Communication Systems (ISPACS2006), Dec. 2006

Evaluation of base station diversity system for reliable multicast delivery, Katsuhiko NAITO, Kazuo MORI, Hideo KOBAYASHI: Proc. of IEEE International Symposium on Intelligent Signal Processing and Communication Systems (ISPACS2006), Dec. 2006

Fault Tolerant Training Algorithm for Multi-Layer Neural Networks Focused on Hidden Unit Activities, Takase Haruhiko, Kita Hidehiko and Hayashi Terumine : Proceedings of International Joint Conference on Neural Networks 2006, pp. 2849-2854, Sheraton Vancouver Wall Centre Hotel, Vancouver, Canada, July 16-21, 2006

We propose a new training algorithm that enhances fault tolerance of multi-layer neural networks (MLNs). Faults mean physical defects or noise in MLNs. Some studies on fault tolerance pointed out that faults on the connections that connected to an output unit bring worse damage than other faults, and proposed training algorithms that enhance fault tolerance of MLNs based on this idea. In this paper, we reveal that it is not always true. Based on this idea, we improved our previous method (weight minimization algorithm).

Low Power Oriented Test Modification and Compression Techniques for Scan Based Core Testing, Terumine Hayashi,

Naotsugu Ikeda*, Tsuyoshi Shinogi, Haruhiko Takase, and Hidehiko Kita : Proceedings of the fifteenth Asian Test Symposium (ATS2006), pp.327-332, Nov. 2006

This paper proposes effective techniques for reducing not only test data volume but also scan-in transitions that are closely related to power dissipation. First, we adopt a new test smoothing algorithm that can reduce scan-in transitions through test vector modification. Second, we propose a test compression method that can reduce test data volume while keeping down the increase of transitions as small as possible. The effectiveness of the proposed techniques is shown through experiments for ISCAS'89 benchmark circuits.

Programming Exercise System with Automatic Test for Novice Programmers, Kenji KAWAMOTO, Hideyuki KANZA, Hidehiko KITA, Haruhiko TAKASE and Terumine HAYASHI : the 14th International Conference on Computers in Education (ICCE2006), Beijing, China, 2006

Programming exercises are essential for learning programming skills. However, they take a lot of time for teachers. So they cannot give their students enough advices on their programs. We have developed a programming exercise system assisting teachers. It checks students' programs syntactically and tests them automatically.

Influence of Si doping on the optical and structural properties of InGaN films, Da-bing LI, Takuya KATSUNO, Masakazu AOKI, Hideto MIYAKE and Kazumasa HIRAMATSU: Journal of Crystal Growth 290, pp.374-378, 2006

Simulation of InGaP Liquid Phase Epitaxy Including Convention, Hiromoto SUGAWA*, Toshihiro TSUJI*, Kazumasa HIRAMATSU, Takashi JINBO*, and Tetsuo SOGA*: THEORETICAL AND APPLIED MECHANICS JAPAN 55, pp.279-284, 2006

Enhanced emission efficiency of InGaN films with Si Doping, Da-bing LI, Yu-huai LIU, Takuya KATSUNO, Keisuke NAKAO, Kazuya NAKAMURA, Masakazu AOKI, Hideto MIYAKE and Kazumasa HIRAMATSU: Physica Status Solidi (c) 3, pp.1944-1948, 2006

Fabrication of thick AlN film by low pressure hydride vapor phase epitaxy, Yu-huai LIU, Tomoaki TANABE, Hideto MIYAKE, Kazumasa HIRAMATSU, Tomohiko SHIBATA* and Mitsuhiro TANAKA*: Physica Status Solidi (c) 3, pp.1479-1482, 2006

n-type conductivity control of AlGaIn with high Al mole fraction, Takuya KATSUNO, Yu-huai LIU, Dabing LI, Hideto MIYAKE, Kazumasa HIRAMATSU, Tomohiko SHIBATA* and Mitsuhiro TANAKA*: Physica Status Solidi (c) 3, pp.1435-1438, 2006

Enhancement of blue emission from Mg-doped GaN activated at low temperature in O₂/N₂ mixture, Da-Bing LI,

Katsuya NAKAMURA, Hideto MIYAKE, Kazumasa HIRAMATSU, Masaaki KOBAYASHI* and Shigeki KIKUTA*: *Physica Status Solidi (c)* 3, pp.2750-2753, 2006

Growth characteristics of carbon nanotubes on nanotip-formed substrate, Hideki SATO, Mai MATSUBAYASHI, Takamichi SAKAI, Koichi HATA, Hideto MIYAKE, Kazumasa HIRAMATSU, Akinori OSHITA and Yahachi SAITO*: *Journal of Vacuum Science & Technology B* 24, pp.1004-1007, 2006

Fabrication of high-quality nitride semiconductors by facet control technique, Hideto MIYAKE and Kazumasa HIRAMATSU: *OYO BUTURI* 75, pp.467-472, 2006 [in Japanese]

Fabrication of LSMO Single Layers and LSMO/YBCO Double Layers, Hong Zhu, Masanori Okada, Atsushi Kamiya, Ajay K. Sarkar, Masahito Matsui, Md. Motin Seikh, Tamio Endo: *International Journal of Nanoscience* Vol.5, No.4-5, pp.511-515, 2006

Interaction between Abrikosov and Josephson Vortices Induced by Microwave Magnetic Field in Bi2212 Crystal: Vortex Dynamics under Crossing Field, Tamio Endo, Ajay K. Sarkar, Hong Zhu, Ken-ichi Nakanishi, Ayumu Nishio, Masanori Okada, Kazuhiro Endo*: *Progress in Electromagnetics Research Symposium (Cambridge, USA)*, pp.583, 2006

Fabrication of YBCO and LBMO, and YBCO/LBMO Double Layers, Tamio Endo, Atsuya Akiba, Atsushi Kamiya, Hirokazu O-oka, Tatsuo Morimoto, Hong Zhu, Hirofumi Yamasaki*, Kazuhiro Endo*: *Beijing International Materials Week - International Conference on Superconducting Materials (Beijing, China)*, pp.79, 2006

Re-entrant Phase and Vortex Dynamics in Hi-Tc Superconducting Bi2212 Single Crystal, Tamio Endo, Ajay K. Sarkar, Ken-ichi Nakanishi, Ayumu Nishio, Atsuya Akiba, Hong Zhu, *International Conference on Composites/Nano Engineering (Boulder, USA)*, CDROM, 2006

Microwave Absorption in LCMO/YBCO Superlattice, Hong Zhu, Atsuya Akiba, Atsushi Kamiya, Hirokazu O-oka, Tatsuo Morimoto, Hirofumi Yamasaki*, Kazuhiro Endo*, Tamio Endo, Jacobo Santamaria*, Axel Hoffmann*, Suzanne te Velthuis*: *International Conference on Composites/Nano Engineering (Boulder, USA)*, CDROM, 2006

Tunneling Spectroscopy of Metallic Manganites with a Colossal Magnetoresistance Effect, Vladimir M. Svistunov*, V. N. Leonova*, M. A. Belogolovskii*, Yu. V. Medvedev*, Yu. F. Revenko*, Yuri M. Strzhemechny*, Tamio Endo: *International Conference on Composites/Nano Engineering (Boulder, USA)*, CDROM, 2006

Microwave Properties on Hi-Tc Superconductors, Tamio Endo, Hong Zhu, Ajay K. Sarkar, Atsuya Akiba, Atsushi Kamiya, Hirokazu O-oka, Tatsuo Morimoto, *Progress in Electromagnetics Research Symposium (Tokyo, Japan)*,

pp.263, 2006

Temperature Dependence of Microwave Absorption in Bi2212 Single Crystal, Hirokazu O-oka, Ajay K. Sarkar, Atsushi Kamiya, Ken-ichi Nakanishi, Tamio Endo, Md. Shahabuddin*: Progress in Electromagnetics Research Symposium (Tokyo, Japan), pp.264, 2006

Microwave Power Dependence of Microwave Absorption in Bi2212 Single Crystals, Tatsuo Morimoto, Ajay K. Sarkar, Atsuya Akiba, Ayumu Nishio, Tamio Endo, Md. Shahabuddin*: Progress in Electromagnetics Research Symposium (Tokyo, Japan), pp.265, 2006

Field Sweep-rate Dependence of Microwave Absorption in a-Oriented YBCO Superconductors: Atsuya Akiba, Hong Zhu, Tamio Endo, Masashi Mukaida*: Progress in Electromagnetics Research Symposium (Tokyo, Japan), pp.329, 2006

Microwave Absorption in Superconducting/Ferromagnetic YBCO/LCMO Superlattice, Hong Zhu, Atsuya Akiba, Tamio Endo, Jacobo Santamaria*, Axel Hoffmann*: Progress in Electromagnetics Research Symposium (Tokyo, Japan), pp.330, 2006

Magnetic Properties and FMR in LBMO and LSMO Thin Films, Atsushi Kamiya, Hong Zhu, Jose Colino*, Josep Nogues*, Tamio Endo: International Colloquium on Magnetic Films and Surfaces (Sendai, Japan), pp.50, 2006

Magnetoresistance and Magnetostriction of LBMO Thin Films, Hong Zhu, Ajay K. Sarkar, Hidetaka Nakashima, Atsuya Akiba, Ken-ichi Nakanishi, Josep Nogues*, Jose Colino*, Tamio Endo: International Colloquium on Magnetic Films and Surfaces (Sendai, Japan), pp.52, 2006

Fabrication of Single Layers of YBCO and LBMO, and Double Layers of YBCO/LBMO, Tamio Endo, Hong Zhu, Atsuya Akiba, Atsushi Kamiya, Hirokazu O-oka, Tatsuo Morimoto, IUMRS – International Conference in Asia (Jeju, Korea), pp.92, 2006

Effects of Substrate Surface Exposure to Oxygen-Plasma on a-c Orientation Growth of YBCO: Verification of Surface Migration Mechanism, Tamio Endo, Atsuya Akiba, Hong Zhu, Tatsuo Morimoto, Makio Ishikawa: International Conference on Solid Films and Surfaces (Bariloche, Argentina), Fr-Gro-1000, 2006

Fabrication of Nanostructured LBMO/YBCO Double Layers, Tamio Endo, Atsuya Akiba, Atsushi Kamiya, Hirokazu O-oka, Daichi Ashida, Tatsuki Machida, Hirofumi Yamasaki*, Kazuhiro Endo*: International Conference on Recent Trends in Nanoscience and Technology (Kolkata, India), pp.32, 2006

Growth Mechanism of Non c-axis Oriented Bi-2223 Superconducting Thin Films by MOCVD <Invited Talk>, Kazuhiro Endo*, Peter Badica*, Tamio Endo, Hisashi Kado*: International Conference on Recent Trends in Nanoscience and Technology (Kolkata, India), pp.29, 2006

Electron Paramagnetic Resonance Spectral Studies on Sapphire Mineral, S. Lakshmi Reddy*, Tamio Endo: International Conference on Recent Trends in Nanoscience and Technology (Kolkata, India), pp.260, (2006).

Growth control of carbon nanotubes by plasma- enhanced chemical vapor deposition and reactive ion etching, Hideki Sato, Takamichi Sakai , Mai Matsubayashi, Koichi Hata, Hideto Miyake, Kazumasa Hiramatsu, Akinori Oshita, Yahachi Saito*: Vacuum 80, No.7, pp.798-801, 2006

A novel process for growth of carbon nanotubes using plasma processes is reported. This process consists of formation of nanotips on substrate and growth of carbon nanotubes on it. The formation of the nanotips, which were formed under an intention to control formation of catalyst nanoparticles, was carried out on substrates by reactive ion etching. After the nanotips formation, the carbon nanotubes were grown on the substrate by plasma-enhanced chemical vapor deposition. Our results showed that the introduction of the nanotips on surface gave lower density and smaller diameter growth of carbon nanotubes than those without the structure.

Development of microfocused x-ray source by using carbon nanotube field emitter, Kunihiro Kawakita, Koichi Hata, Hideki Sato, Yahachi Saito*: Journal of Vacuum Science & Technology B 24, No.2, pp.950-952, 2006

To develop a microfocused x-ray source, field emission properties of a bundle of multiwalled carbon nanotubes were investigated under an ordinary vacuum pressure of 5×10^{-7} Torr for a practical use. Total emission current reached up to 1.3 mA at an applied voltage of -7 kV. An emitted electron beam was focused on a Cu anode by using a simple electrostatic lens and excited an x ray with the source size of less than 30 μ m. X-ray transmission images were taken as a preliminary demonstration for a microfocused x-ray source and clear images whose resolutions were nearly equal to the source size of x ray were easily obtained.

Growth of Carbon Nanotubes by Plasma-Enhanced Chemical Vapor Deposition, Hideki Sato, Koichi Hata: New Diamond and Frontier Carbon Technology, 16, No.3, pp.163-176, 2006

The growth of carbon nanotubes (CNTs) by plasma-enhanced chemical vapor deposition (PECVD) has attracted much attention because PECVD enables vertically aligned CNT growth and is applicable for CNT growth at low temperature. Large area growth of CNTs is also possible by PECVD. These are desirable features for the growth process of CNTs in nanoelectronics applications. Because of these features, it is expected that CNT growth has a variety of applications such as in field emission displays, interconnections in large-scale integrated circuits (LSIs) and optical devices. In this paper, we review studies of CNT growth by PECVD. Some examples of CNT growth by PECVD and selective CNT growth on substrates using semiconductor processes are described in this review.

Effect of catalyst oxidation on the growth of carbon nanotubes by thermal chemical vapor deposition, Hideki Sato,

Yasunori Hori, Koichi Hata, Kazuyuki Seko*, Hitoshi Nakahara*, Yahachi Saito*: Journal of Applied Physics, 100, No.10, pp.104321_1-6, 2006

We report a heat treatment of catalyst in air that drastically enhances a growth of carbon nanotubes (CNTs) by means of thermal chemical vapor deposition (CVD). An Fe catalyst film deposited on a Si substrate was heat treated at 700 degrees C in air before the acetylene CVD. The growth rate of the CNTs grown with the heat treatment was more than seven times higher than that of growth without the heat treatment. A scanning electron microscopy observation showed that the heat treatment in air promotes a granulation of the Fe catalyst. X-ray photoelectron spectroscopy and reflection high energy electron diffraction analyses showed that the heat treatment in air promotes an oxidation of the catalyst film and formation of Fe₂O₃ nanoparticles, suggesting that the heat treatment of Fe catalyst in air prevented the formation of Fe silicide that would deactivate the catalyst effect of Fe. The Fe₂O₃ nanoparticles do not agglomerate and can keep their original particles size. Thus the catalyst can maintain a catalyst activity during CNTs growth and, as a result, gives a growth enhancement of CNTs.

Desorption of Adsorbed Gas Molecule on a Pentagon at a Tip of Carbon Nanotube by Pulse Laser Irradiation, Shunsaku Waki, Koichi Hata, Hideki Sato, Yahachi Saito*: Technical Digest of 19th International Vacuum Nanoelectronics Conference & 50th International Field Emission Symposium, pp.263-264, 2006

Low Temperature Growth of Carbon Nanotubes by Alcohol Catalytic CVD for Field Emitter Applications, Hideki Sato, Koichi Hata, Ken Hiasa, Yahachi Saito*: Technical Digest of 19th International Vacuum Nanoelectronics Conference & 50th International Field Emission Symposium, pp.335-336, 2006

Development of Compact SEM Equipped with Carbon Nanotube Field Emission Cathode, Technical Ryosuke Yabushita, Koichi Hata, Hideki Sato, Yahachi Saito*: Technical Digest of 19th International Vacuum Nanoelectronics Conference & 50th International Field Emission Symposium, pp.427-428, 2006

Electron Optical System for Micro-Focused X-ray Source with Carbon Nanotubes Field Emitter, Technical Digest, Koichi Hata, Kunihiko Kawakita, Hideki Sato, Yahachi Saito*: Technical Digest of International Vacuum Nanoelectronics Conference & 50th International Field Emission Symposium, pp.429-430, 2006

Percolation Phenomena of Composites Made with Two Kinds of Filler and A New Potential Grading Materials, Tetsushi Okamoto*, Makoto Kawahara*, Toshimitsu Yamada*, Yoshiyuki Inoue* and Shuhei Nakamura: Trans. IEE of Japan, Vol. 126-A, pp. 1004-1012, 2006

During the last three decades, extensive and worldwide research has resulted in progress being made with respect to many aspects of percolation phenomena of composites with one kind of filler. However, composites made with two kinds of filler have not yet been investigated in depth. The percolation phenomena of the potential grading materials made up of silicon carbide, tri-iron oxide and high density polyethylene have been discussed in this study. As a result, a potential grading layer, which has a stable and excellent partial discharge suppression capability, has been developed.

Mechanical properties of composite materials made with PDMS-ethyl silicate hybrid and silica powder, S. Magara, F.

Imasato, A. Ohno, Y. Aoki, S. Nakamura, T. Shindo, T. Kawakita, T. Okamoto: Organic Materials for Electronics and Photonics, KOREA-JAPAN JOINT FORUM 2006, p. 167, 2006.

Application of a Hybrid Material Made with Ethoxy-Altered PDMS and TEOS to Thermostable Adhesives, A. Ohno, F. Imasato, S. Magara, Y. Aoki, S. Nakamura, T. Shindo, T. Kawakita, T. Okamoto: Organic Materials for Electronics and Photonics, KOREA-JAPAN JOINT FORUM 2006, p.168, 2006

Thermally Stable Proton Conductive Organic-Inorganic Hybrid Materials, Y. Aoki, T. Shindou: Organic Materials for Electronics and Photonics, KOREA-JAPAN JOINT FORUM 2006, p.169, 2006

Development of Thermally Conducting Sheet Made with PDMS-Based Organic-Inorganic Hybrid Material, Y. Aoki, S. Nakamura, T. Shindou: Organic Materials for Electronics and Photonics, KOREA-JAPAN JOINT FORUM 2006, p.170, 2006

CHANGE IN HEAT RESISTIVE, ELECTRICAL INSULATING AND MECHANICAL PROPERTIES OF HYBRID MADE WITH PDMS AND TEOS FOR THE MOLE RATIO OF THEM, Tetsushi OKAMOTO*, Takuya SHINDOU*, Makoto SUGIURA, Shuhei NAKAMURA: Conf. on Elect. Insul. Dielec. Phenom., pp.55-60, 2006

Electrical Insulating and Heat Resistive Properties of TEOS-PDMS Hybrid Materials [in Japanese], Tetsushi Okamoto, Fumitoshi Imasato, Takuya Shindou, Shuhei Nakamura: Proceedings of the 37th Symposium on Electrical and Electronic Insulating Materials and Applications in systems, pp.117-120, 2006

Preparation of Organic-inorganic Hybrid Materials by Sol-gel Method at Low Temperature and Their Application to Thermally Conducting Sheets [in Japanese], Yusuke Aoki, Shuhei Nakamura, Takuya Shindou: The papers of Technical Meetings on Dielectrics and Electrical Insulation, IEE Japan, pp.43-47, 2006.

Organic-Inorganic Hybrid Material and Its Application to Adhesive [in Japanese], Shuhei NAKAMURA, Atsushi OHNO, Yusuke AOKI, Takuya SHINDOU, Tadashi KAWAKITA: IEICE Technical Report OME2006-93 (2006-11), pp. 13-18, 2006

Department of Chemistry for Materials

* nonmember

Synthesis, Ionic Conductivity, and Thermal Properties of Proton Conducting Polymer Electrolyte for High Temperature Fuel Cell, Takahito ITOH, Yohei HAMAGUCHI, Takahiro UNO, Masataka KUBO, Yuichi AIHARA*, Atsuo SONAI* : Solid State Ionics 177, pp. 185-189, 2006

Hyperbranched polymer (poly-1a) with sulfonic acid groups at the end of chains was successfully synthesized. Interpenetration reaction of poly-1a with a hyperbranched polymer with acryloyl groups at the end of chains (poly-1b) as a cross-linker afforded a tough electrolyte membrane. The poly-1a and the resulting electrolyte membrane showed the ionic conductivities of 7×10^{-4} and 8×10^{-5} S/cm, respectively, at 150 °C under dry condition. The ionic conductivities of the poly-1a and the electrolyte membrane exhibited the VTF type temperature dependence. And also, both poly-1a and the resulting electrolyte membrane were thermally stable up to 200 °C.

Solid Polymer Electrolytes Based On Comblike Polymers, Takahito ITOH, Yukihiro MITSUDA, Katsumi NAKASAKA, Takahiro UNO, Masataka KUBO, Osamu YAMAMOTO* : Journal of Power Source 163, pp. 252-257, 2006

New comblike polymers such as a homopolymer (poly-4) of 3,5-bis[poly(ethylene glycol) methyl ether (350, $n=7.2$)]styrene (4) and an alternating copolymer (poly-4/TCNQ) of 4 with 7,7,8,8-tetracyanoquinodimethane (TCNQ) were prepared as a plasticizer for the poly(ethylene oxide) (PEO)-LiN(CF₃SO₂)₂ electrolyte, and the ionic conductivities, thermal property, electrochemical and thermal stabilities, and mechanical property for the comblike-based polymer electrolytes, composed of the comblike polymers, poly(ethylene oxide) (PEO), and LiN(CF₃SO₂)₂, were investigated. The polymer electrolytes containing an alternating copolymer poly-4/TCNQ showed the higher ionic conductivity, better thermal stability and better mechanical stability than that containing a homopolymer poly-4, due to the presence of an aromatic ring and a polar cyano group of the TCNQ unit.

Solid Polymer Electrolytes Based on Poly(1,3-diacetyl-4-imidazolin-2-one), Hiroyuki MITSUDA, Takahiro UNO, Masataka KUBO, Takahito ITOH : Polymer Bulletin 57, pp. 313-319, 2006

Solid polymer electrolytes composed of a homopolymer (poly(AcIM)) of 1,3-diacetyl-1,4-imidazolin-2-one (AcIM) and lithium bis(trifluoromethanesulfonimide) (LiTFSI) or of copolymers (poly(AcIM/VC)) of AcIM with vinylene carbonate (VC) and LiTFSI were prepared and their ionic conductivities and thermal properties were investigated. For the polymer electrolyte of the poly(AcIM) with LiTFSI, the highest ionic conductivity was found at the [Li]/[O] ratio of 1/3 with the values of 8.5×10^{-5} S/cm at 80 °C and 1.7×10^{-6} S/cm at 30 °C, respectively. In the polymer electrolyte of poly(AcIM/VC) with LiTFSI at the [Li]/[O] ratio of 1/3, the ionic conductivity increased with increasing VC unit content in the copolymers, and the highest ionic conductivity was found at the AcIM/VC ratio of 39/61 (mol%) with the values of 7.0×10^{-4} S/cm at 80 °C and 6.7×10^{-5} S/cm at 30 °C, respectively. This copolymer electrolyte showed a linear relationship between the ionic conductivity and the reciprocal of the temperature, indicative of the system decoupled from the segmental motion of the polymer.

Synergistic effect of red phosphorus, novolac and melamine ternary combination on flame retardancy of

poly(oxymethylene), Hatsuhiko HARASHINA, Yoshihisa TAJIMA*, Takahito ITOH : Polymer Degradation and Stability 91, pp. 1996-2002, 2006

New flame retardant system for poly(oxymethylene) (POM) has been studied. The combination of red phosphorus with novolac and melamine was found to act as an effective flame retardant of POM. The base POM exhibited very low limiting oxygen index (LOI) value of 15.3, while the flame retarded POM gave remarkably high LOI value of 37.5 and UL94 V-1 ranking without dripping at 0.8mm thickness. The results of cone calorimetry, thermogravimetry and FTIR analysis suggested that the flame retarding mechanism is the intumescent char formation in the condensed phase. Novolac having a phenolic hydroxyl group is miscible with POM, and in the flaming process, red phosphorus yields phosphine and its acidic product such as phosphoric acid due to hydrolysis and oxidation reactions. In addition, all of novolac, melamine and phosphine are able to readily react with formaldehyde generating from POM during burning to give the reinforced and cross-linked char network through the polyaddition and polycondensation reactions. Therefore, the red phosphorus/novolac/melamine ternary combination system could synergistically promote the high flame retardancy of POM without the flaming drips.

Topochemical Reaction of 7-Bromoethoxycarbonyl-7-cyano-1,4-benzoquinone Methide in the Solid State, Takahito ITOH, Kyoko TACHINO, Takahiro UNO, Masataka KUBO, Norimitsu TOHNAI*, Mikiji MIYATA* : Chemistry Letters 35(8), pp. 918-919, 2006

Topochemically controlled [2 + 2] photocycloaddition took place at the quinonid double bond of the 7-bromoethoxycarbonyl-7-cyano-1,4-benzoquinone methide (1) to afford its cyclobutane dimer.

Synthesis, Ionic Conductivity, and Thermal Properties of Hyperbranched Polymer with Phosphonic Acid Groups at the Chain Ends for High Temperature Fuel Cell, Takahito ITOH, Yohei HAMAGUCHI, Keita HIRAI, Takahiro UNO, Masataka KUBO, Yuichi AIHARA*, Atsuo SONAI* : ECS Transactions (Proton Exchange Membrane Fuel Cells 6) 3, pp. 113-121, 2006

Two different molecular weight hyperbranched polymers (HBP-PA(L) and HBP-PA(H)) with phosphonic acid groups at the chain ends were successfully synthesized. The ionic conductivities of the low molecular weight HBP-PA(L) and the high molecular weight HBP-PA(H) were found to be 1.3×10^{-4} and 6.4×10^{-5} S/cm, respectively, at 135 °C under dry condition, and showed the VTF type temperature dependence. And also, both polymers were thermally stable up to 300 °C, and they had suitable thermal stability as an electrolyte in the polymer electrolyte fuel cell operating under dry condition.

Emission from Silica Hybrid Containing RBG Fluorescent Conjugated Polymers, Yuya SUGIURA, Masashi SHOYAMA*, Koji INOUE*, Takahiro UNO, Takahito ITOH, Masataka KUBO : Polymer Bulletin 57, pp. 865-871, 2006

Red, green and blue fluorescent poly(arylene vinylene)s were prepared by Wittig reaction. Polycondensation of tetraethoxysilane (TEOS) was carried out in the presence of a mixed solution of these polymers to give a silica hybrid in which RBG fluorescent polymers were immobilized without phase separation. White light emission was observed from the ternary polymer blend/silica hybrid.

Nonbonding cross-linking agent, Masataka KUBO : Hyomen 44, pp. 337-344, 2006

Development of hybrid EL film by sol-gel method, Masataka KUBO, Masashi SHOYAMA* : Monthly DISPLAY 12, pp. 43-47, 2006

Titanium Tetraiodide Mediated Reductive Opening of Aziridines, Leading to the Aldol and Mannich-Type Reactions, Makoto SHIMIZU, Hiroshi KUROKAWA, Shuji NISHIURA, Iwao HACHIYA: Heterocycles, 70 (1), pp. 57-64, 2006

3,4,5,6-Tetrasubstituted-2-pyridone Synthesis via Nucleophilic Addition of Active Methine Compounds to Dialkynyl Imines Directed to the Synthesis of (-)-A58365A, Iwao HACHIYA, Shiho FUKUSHIMA, Makoto SHIMIZU: Heterocycles, 69 (1), pp. 43-48, 2006

Ring Expansion Reaction of Cyclic α -Keto Esters or α -Cyano Ketones via Conjugate Addition to Alkynyl Imines: The Synthesis of Functionalized Medium-Sized Carbocycles, Iwao HACHIYA, Wataru MAEHARA, Yasushi YAMADA, Toru KAMIKI, Makoto SHIMIZU: Synlett, (19), pp. 3271-3274, 2006

Efficient Asymmetric Synthesis of Novel Gastrin Receptor Antagonist AG-041R via Highly Stereoselective Alkylation of Oxindole Enolate, Takashi EMURA, Toru ESAKA*, Kazutaka TACHIBANA*, Makoto SHIMIZU: J. Org. Chem., 71 (22), pp. 8559-8564, 2006

Unexpected and Intriguing Reactivity of α -Imino Esters and Iminium Salts, Makoto SHIMIZU: Pure Appl.Chem., 78 (10), pp. 1867-1876, 2006

Efficient Pyrrole Synthesis Using Double Nucleophilic Addition to α,β -Unsaturated Imines with Plural Nucleophiles, Makoto SHIMIZU, Atsushi TAKAHASHI, Shiho KAWAI: Org. Lett., 8 (16), pp. 3585-3587, 2006

Remarkable Effects of Additives to Facilitate Aza-Mannich Type Reaction: A Rapid Access to α -Amino Ketone *O*-Alkyl Oximes, Makoto SHIMIZU, Mitsue TANAKA, Tomohiro ITOH, Iwao HACHIYA: Synlett, (11), pp. 1687-1690, 2006

New Synthetic Reactions Using Conjugate Addition Reactions of Active Methine Compounds to Alkynyl Imines and Ketones [in Japanese], Iwao HACHIYA, Makoto SHIMIZU, J. Synth. Org. Chem., Jpn., 64 (3), pp. 251-262, 2006

Synthesis of Bicyclic Compounds Containing a 2-Pyridone Structure by Addition of Malonic Esters to

Alkynylpyridines, Pyrimidine, and Thiazoles, Iwao HACHIYA, Masaki ATARASHI, Makoto SHIMIZU: *Heterocycles*, 67 (2), pp. 523-528, 2006

Rigid Molecular Tripod with an Adamantane Framework and Thiol Legs. Synthesis and Observation of an Ordered Monolayer on Au(111), Toshikazu KITAGAWA, Yuichi IDOMOTO*, Hiroaki MATSUBARA*, Daisuke HOBARA*, Takashi KAKIUCHI*, Takao OKAZAKI*, Koichi KOMATSU*: *J. Org. Chem.*, 71(4), pp. 1362-1369, 2006

Synthesis of Disubstituted Homodiamantanes by Acylative Ring Expansion Using Benzoyl Trifluoromethanesulfonate, Takao OKAZAKI*, Shusaku MANDAI*, Toshikazu KITAGAWA, and Ken'ichi TAKEUCHI*: *Sci. Tech. Adv. Mater.*, 7(6), pp. 531-535, 2006

Triplet Diphenylcarbenes Protected by Trifluoromethyl and Bromine Groups. A Triplet Carbene Surviving a Day in Solution at Room Temperature, Tetsuji ITOH, Yoshimaru NAKATA, Katsuyuki HIRAI*, and Hideo TOMIOKA*: *J. Am. Chem. Soc.*, 128(3), pp. 957-967, 2006

A Dendrimer Approach to High-Spin Polycarbenes. Conversion of Connectivity from Disjoint to Non-Disjoint by Perturbation of Nonbonding Molecular Orbital Coefficients, Katsuyuki HIRAI*, Eiko KAMIYA, Tetsuji ITOH, and Hideo TOMIOKA*: *Org. Lett.*, 8(9), pp. 1847-1850, 2006

Theoretical Study of Electronic Structures of [Peroxoporphinato]manganate $[\text{Mn}(\text{P})(\text{O}_2)]^-$ Anion, Yasunori YOSHIOKA, Hideaki SANO, Masaki MITANI: *Bull. Chem. Soc. Jpn.*, 79 (8), pp. 1201–1210, 2006

Geometries and electronic structures of the quintet and septet states of the $[\text{Mn}(\text{P})(\text{O}_2)]^-$ (P: porphinato) anion were theoretically investigated. Four local minimum geometries with two side-on additions of O_2 to MnP, **1** ($^5\text{B}_2$) and **3** ($^7\text{A}_2$), and two end-on additions of O_2 , **2** ($^5\text{A}''$) and **4** ($^5\text{A}'$), were found. One of the side-on forms, **1**, corresponds to that observed by X-ray crystallographic study. **3** is a septet state with higher spin than the quintet states of **1**, **2**, and **4**. Each of the two end-on forms has the corresponding transition state with the side-on geometry. Energy differences among **1**, **2**, and **3** are less than 1 kcal mol^{-1} . The electronic structures of four local minimum states were essentially different. **1** has an electronic structure presented as $[\text{Mn}^{\text{III}}(\text{O}_2^{2-})]^-$. **2** has antiferromagnetically coupled diradical character presented by the formal chemical formula of $[\text{Mn}^{\text{II}}(\text{O}_2^{\cdot-})]^-$. **3** has ferromagnetically coupled diradical character. **4** is presented by $[\text{Mn}^{\text{II}}(\text{O}_2^-)]^-$.

Electronic Structures of Heme(Fe)–Dioxygen Complex as an Intermediate Model of Dioxygen Reduction in Cytochrome *c* Oxidase, Yasunori YOSHIOKA, Masaki MITANI, Hiroyuki SATOH: *Internet Electron. J. Mol. Des.*, 5 (8), pp. 447–459, 2006

We have previously proposed the O_2 reduction mechanism that the protons transfer from the K-channel to the active site of CcO. The second proton transfer to the hydroperoxy intermediate FeOOH did not lead the OO bond cleavage. It has been recently reported that the addition of the proton induces the OO bond cleavage to yield the productive H_2O molecule and the oxo intermediate $\text{Fe}=\text{O}$, being inconsistent with our results. We have started this

study to confirm whether the OO bond cleavage occurs or not upon the proton addition. We concentrated our study to the changes of the electronic structures of the heme *a3* part throughout the sequential additions of the protons and an electron during the process of the O₂ reduction. We employed a model that is composed of porphyrin without any substituents, Fe, and an imidazole as His376. We added sequentially protons and an electron to the heme(Fe)–dioxygen complex. The geometrical parameters were fully optimized without any constraints. The unrestricted hybrid exchange–correlation functional B3LYP method was used. The Wachters double zeta basis set was employed for Fe atom. The 6–31G* basis set was used for C, N, and H atoms, and the 6–311+G* for O atom. All calculations were carried out using the program package Gaussian 98. The proton addition to FeOO (H2) to yield FeOOH (H3) causes the electron transfer from the porphyrin ring to FeOOH moiety, giving the porphyrin–radical cation. The additional proton to FeOOH (H4) leads to the OO bond cleavage, yielding the hydrogen bonded complex of an oxo heme (compound I) and a H₂O molecule. The bonding characters of FeOOH in H3 and H4 are identical, even though the electronic structures of the porphyrin rings in H3 and H4 are different. However, the proton addition to FeOOH (H3) does not lead to the OO bond cleavage. The protonated heme(Fe)–dioxygen complexes are effective models to investigate the reduction mechanism of a O₂ molecule in CcO.

A B3LYP Study of Proton Transfer Path within a Complex of Benzene Radical Cation and Water Cluster, Moriyuki SHIMIZU, Emi YAMASHITA, Masaki MITANI, Yasunori YOSHIOKA: *Chem. Phys. Lett.*, 432, pp. 22–26, 2006

We made a theoretical study of the proton transfer path from C₆H₆^{•+}(H₂O)₄ to C₆H₅[•](H₂O)₄H⁺ with a planar cyclic geometry of (H₂O)₄H⁺ by the hybrid density functional B3LYP method. The proton transfer proceeds in a three-step manner. In the first step, the proton in C₆H₆^{•+}(H₂O)₄ moves from the terminal H₂O molecule in the (H₂O)₄ cluster to yield a (H₂O)₃H⁺ cluster. In the last third step, one H₂O molecule leaves from C₆H₆(OH)[•] in C₆H₆(OH)[•](H₂O)₃H⁺ to yield a C₆H₅[•](H₂O)₄H⁺ complex through the H-abstraction by the OH radical. It is found that the proton transfer and redistribution from p to r of the radical electron proceed separately.

Highly Activated Vinyl Hydrogen in a Significantly Twisted Styrene, Hajime MORI*, Takafumi MATSUO*, Yasunori YOSHIOKA, Shigeo KATSUMURA*: *J. Org. Chem.*, 71 (24), pp. 9004–9012, 2006

The novel example of a vinylic hydrogen more reactive than a benzylic hydrogen was found by treatment of a twisted styrene derivative with a strong base followed by D₂O quenching. In this paper, the full details of the examples of the highly activated vinyl hydrogens in twisted styrene derivatives are described, with a discussion on the correlation between the reactivity of the vinyl hydrogens and the magnitude of the twist. The highly reactive vinyl hydrogens could be rationalized by considering the novel orbital interaction between the π^* orbital of the benzene ring and the σ orbital of the vinylic C–H bond in the twisted styrene derivatives.

Density Functional Study on Geometrical Features and Electronic Structures of Di- μ -oxo-Bridged [Mn₂O₂(H₂O)₈]^{q+} with Mn(II), Mn(III), and Mn(IV), Masaki MITANI, Yohei WAKAMATSU, Takeharu KATSURADA, Yasunori YOSHIOKA: *J. Phys. Chem. A*, 110 (51), pp. 13895–13914, 2006

We report the geometrical features and electronic structures of di- μ -oxo-bridged Mn–Mn binuclear complexes with H₂O ligands [Mn₂O₂(H₂O)₈]^{q+} in the iso- and mixed-valence oxidation states. All of the combinations among Mn(II), Mn(III), and Mn(IV) ions are considered the oxidation states of the Mn–Mn center, and the changes in molecular structure induced by the different electron configurations of Mn-based orbitals are investigated in relation to

the oxygen-evolving complex (OEC) of photosystem II. The stable geometries of complexes are determined by using the hybrid-type density functional theory for both of the highest- and lowest-spin couplings between Mn sites, and the lowest-spin-coupled states are energetically more favorable than the highest-spin-coupled states except in the case of the complexes with the Mn(II) ion. The coordination positions of H₂O ligands at the Mn(II) site tend to shift from the octahedral positions in contrast to those at the Mn(III) and Mn(IV) sites. The shape of the Mn₂O₂ core and the distances between the Mn ions and the H₂O ligands vary depending on the electron occupations of the octahedral eg orbitals on the Mn site with an antibonding nature for the Mn–ligand interactions, indicating the trend as Mn(II)–O > Mn(III)–O and Mn(IV)–O, O–Mn(II)–O > O–Mn(III)–O > O–Mn(IV)–O among the iso-valence Mn₂O₂ cores, and O–Mn(lower)–O < O–Mn(higher)–O within the mixed-valence Mn₂O₂ core, and as Mn(II)–OH₂ and Mn(III)–OH₂ > Mn(IV)–OH₂ for the axial H₂O ligand. The optimized geometries of model complexes are compared with the X-ray structure of the OEC, and it is suggested that the cubanelike Mn cluster of the active site may not contain a Mn(II) ion. The effective exchange integrals are estimated by applying the approximate spin projection to clarify the magnetic coupling between Mn sites, and the superexchange pathways through the di-oxo bridge are examined on the basis of the singly occupied magnetic orbitals derived from the singlet-coupled natural orbitals in the broken-symmetry state. The comparisons of the calculated results between [Mn₂O₂(H₂O)₈]⁹⁺ in this study and [Mn₂O₂(NH₃)₈]⁹⁺ reported by McGrady et al. suggest that the symmetric pathways are dominant to the exchange coupling constant, and the crossed pathway would be less important for the former than it would for the latter in the Mn(III)–Mn(III), Mn(IV)–Mn(IV), and Mn(III)–Mn(IV) oxidation states.

Synthesis, structure, and electrochemical properties of epitaxial perovskite La_{0.8}Sr_{0.2}CoO₃ film on YSZ substrate, Daisuke Mori*, Hideaki Oka*, Yoshitaka Suzuki*, Noriyuki Sonoyama*, Atsuo Yamada*, Ryoji Kanno*, Yoshiaki Sumiya, Nobuyuki Imanishi and Yasuo Takeda : Solid State Ionics 177, pp. 535-540, 2006

Epitaxial films of the perovskite, La_{0.8}Sr_{0.2}CoO₃ (LSC), for SOFCs cathode were deposited on yttria-stabilized zirconia (YSZ) single crystals by pulsed laser deposition method. The films were characterized by thin-film X-ray diffraction measurement, atomic force microscopy (AFM), transmission electron microscope (TEM), and ac impedance spectroscopy. The film orientations depend on the substrate planes. The LSC films on the YSZ (100) and (111) substrates showed the (110) orientation with different twin structures, while those on the YSZ (110) had (100) and (112) orientations. Surface morphology of the films also depends on the substrate orientations. These films showed different electrode properties depending on the orientations. The relationships between the properties, the film orientations, surface morphology, and lattice misfit are discussed.

An anomalous thermal expansion in the perovskite system, Gd_{1-x}Sr_xMnO₃ (0 ≤ x ≤ 0.3), A. Hirano, F. Hirano, T. Matsumura, N. Imanishi and Y. Takeda : Solid State Ionics 177, pp. 749-755, 2006

The thermal expansion behavior of sintered samples of Gd_{1-x}Sr_xMnO₃ (X=0.0–0.4) was studied. The sintered bodies in this system showed negative thermal expansion over a wide temperature range. The detailed crystal structure refinements with respect to temperature showed that the volume of the orthorhombic perovskite lattice monotonically increased with temperature, however, in addition to this, the release of distortion from the Jahn-Teller effect of Mn³⁺ ion occurred over a wide temperature range, which brought the negative expansion of the *a*-axis, although the *b*- and *c*-axes increased with temperature. The anomalous thermal expansion is explained by the sum of the effects of the shrinkage of the *a*-axis and absorption of the *b*- and *c*-axes' expansion by the pores in the sintered body.

Preparation and electrochemical properties of a $\text{Li}_2\text{CuO}_2\text{--Li}_2\text{NiO}_2$ solid solution as a lithium-intercalation electrode, N. Imanishi, K. Shizuka*, T. Ikenishi, T. Matsumura, A. Hirano and Y. Takeda : *Solid State Ionics* 177, pp. 1341-1346, 2006

Solid solution materials of Li_2CuO_2 and Li_2NiO_2 were studied with respect to their electrochemical performance and crystal structure. The $\text{Li}_2\text{CuO}_2\text{--Li}_2\text{NiO}_2$ system shows a solid solution over the whole composition range with the orthorhombic structure. Pure Li_2CuO_2 has a reversible capacity of only 100 mA h/g, and the capacity of $\text{Li}_2\text{Cu}_{1-x}\text{Ni}_x\text{O}_2$ increased with increasing the content of Ni. The maximum capacity of 250 mA h/g is obtained for $\text{Li}_2\text{Cu}_{0.5}\text{Ni}_{0.5}\text{O}_2$, and it exhibits a good reversibility for charge and discharge cycles. The orthorhombic Li_2CuO_2 undergoes a phase change to the monoclinic LiCuO_2 during lithium deintercalation, while nickel-rich compositions show a new phase that is different from either the original orthorhombic or monoclinic structure.

Impedance study and TEM characterization of a PLD perovskite air electrode, Nobuyuki Imanishi, Yoshiaki Sumiya, Ken Yoshimura, Tadaaki Matsumura, Atsushi Hirano, Yasuo Takeda, Daisuke Mori* and Ryoji Kanno* : *Solid State Ionics* 177, pp. 2165-2173, 2006

TEM observation and electron diffraction analysis of a laser ablation perovskite film was carried out. The film was deposited on a single-crystal substrate and showed epitaxial growth normal to the substrate. The crystal orientation of the perovskite film varies depending on the kind of single-crystal substrate. The surface structure of the atomic arrangement was investigated based on an analysis of electron diffraction patterns. Its relation to the kinetics of the reduction of molecular oxygen is discussed.

Novel Composite Anodes Consisting of Lithium Transition-Metal Nitrides and Transition Metal Oxides for Rechargeable Li-Ion Batteries, Y. Liu, Y. Takeda, T. Matsumura, J. Yang*, N. Imanishi, A. Hirano, and O. Yamamoto* : *J. Electrochem. Soc.*, 153 (2) , pp. A437-A444 , 2006

Lithium transition-metal nitrides are promising anode candidates for Li-ion batteries. However, lithium must be extracted from the nitrides in an initial anodic oxidation, indicating these compounds cannot directly combine with the current cathodes to constitute cells. This deterrent can be overcome by introducing a certain amount of Co_3O_4 , which shows large capacities and relatively high oxidation/reduction potentials, into the electrodes containing the above nitrides. A thermodynamically spontaneous reaction between these two active hosts results in a delithiated state of lithium metal nitrides. Under cycling within 1.4–0 V vs Li/Li^+ , Co_3O_4 is relatively inert to lithium and the nitrides become electrochemically active. The composite electrodes show high first-cycle efficiency of 100%, large capacities of 500 mAh g^{-1} , and excellent cyclability. Furthermore, research revealed that the composite electrodes demonstrated high cycling stability operating with polyethylene oxide (PEO) electrolytes at the elevated temperature. The reaction heating of the composite electrode under high Li utilization with PEO electrolytes via differential scanning calorimetry measurement was found to be extremely low compared with those of the lithium metal and the Li-alloy-based systems, suggesting that the composite electrodes could be promising anode candidates for all-solid-state PEO Li-ion batteries in terms of capacity, first-cycle charge efficiency, and thermal reliance.

Structural Changes and Electrochemical Properties of Chemically oxidized Na_xFeO_2 , Tadaaki Matsumura, Nobuyuki Imanishi, Atsushi Hirano, Ryoji Kanno* and Yasuo Takeda : *Journal of the Japan Society of Powder and Powder Metallurgy* 53 (11) , pp. 860-864, 2006

Na_xFeO_2 was obtained by chemical oxidization method using NO_2BF_4 and Br_2 which shows the redox potential of ca. 5.1 V and ca. 4.1 V vs Li / Li^+ , respectively. The oxidized products showed different X-ray diffraction patterns depending on the oxidizing species. In case of NO_2BF_4 , as soaking time progressed, new phase increased with decreasing of NaFeO_2 as starting material. The oxidized Na_xFeO_2 was possible to be inserted the Li ion electrochemically, and resulted in the crystal structure similar to the layered LiFeO_2 synthesized by the Li-ion-exchange method from NaFeO_2 . Reversible discharge-charge reactions were progressed for $\text{Na}_x\text{FeO}_2 // \text{Li}$ cell, and ac. 150 – 200 mAh/g of initial capacities were achieved although the capacities decreased with cycle numbers.

Effect of Silicon on the Formation of Graphitic Polyhedra and Balloon-like Particles, Fumio KOKAI, Noriko TAKAKUWA, Akira KOSHIO, Kunimitsu TAKAHASHI*: Applied Physics A, 84, pp. 391-394, 2006

Antibacterial Activity of Fluorine Incorporated DLC Films, Masatou ISHIHARA*, Tomomi KOSAKA*, Takako NAKAMURA*, Kazuo TSUGAWA*, Masataka HASEGAWA*, Fumio KOKAI, Yoshinori KOGA*: Diamond & Related Materials, 15, pp. 1011-1014, 2006

Electrochemical Reduction of CO_2 to Methane at the Cu Electrode in Methanol with Sodium Supporting Salts and Its Comparison with Other Alkaline Salts, Satoshi KANECO, Hideyuki KATSUMATA, Tohru SUZUKI, Kiyohisa OHTA: Energy Fuels, 20, pp. 409–414, 2006

Photoelectrochemical Reduction of Carbon Dioxide at p-Type Gallium Arsenide and p-Type Indium Phosphide Electrodes in Methanol, Satoshi KANECO, Hideyuki KATSUMATA, Tohru SUZUKI, Kiyohisa OHTA: Chem. Eng. J., 116, pp. 227–231, 2006

Sequential Molecular Vapor Elution Analysis for the Separation and Determination of LiCl and NaCl in River Waters, Yasutoshi SHIROTA, Md. Nurul AMIN, Yoshifumi WATANABE, Satoshi KANECO, Hideyuki KATSUMATA, Tohru SUZUKI, Kiyohisa OHTA: Anal. Chim. Acta, 560, pp. 159–163, 2006

Photoelectrocatalytic Reduction of CO_2 in LiOH/Methanol at Metal-modified p-InP Electrodes, Satoshi KANECO, Hideyuki KATSUMATA, Tohru SUZUKI, Kiyohisa OHTA: Appl. Catal. B: Environ., 64, pp. 139–145, 2006

Electrochemical Reduction of Carbon Dioxide to Ethylene at A Copper Electrode in Methanol Using Potassium Hydroxide and Rubidium Hydroxide Supporting Electrolytes, Satoshi KANECO, Hideyuki KATSUMATA, Tohru SUZUKI, Kiyohisa OHTA: Electrochim. Acta, 51, pp. 3316–3321, 2006

Electrochemical Reduction of High Pressure CO_2 at A Cu Electrode in Cold Methanol, Satoshi KANECO, Keiji IIBA, Hideyuki KATSUMATA, Tohru SUZUKI, Kiyohisa OHTA: Electrochim. Acta, 51, pp. 4880–4885, 2006

Electrochemical Reduction of CO₂ in Copper Particle-suspended Methanol, Satoshi KANEKO, Yosuke UENO, Hideyuki KATSUMATA, Tohru SUZUKI, Kiyohisa OHTA: Chem. Eng. J., 119, pp. 107–112, 2006

Fabrication of Visible Light Response Praseodymium-doped TiO₂ Photocatalysts and Its Application to Dye-sensitized Solar Cells, Naomi NISHIKAWA, Satoshi KANEKO, Hideyuki KATSUMATA, Tohru SUZUKI Kiyohisa OHTA, Yasuo TAKEDA, Masaki MURAYAMA*, Eiji YAMAZAKI*, Noritsugu HASHIMOTO*, Kazuaki MASUYAMA, Masashi SHOYAMA*: Photo/Electrochem. Photobiol. Environ. Energy Fuel, 5, pp. 311–319, 2006

Effect of Side-chain Structure on the Solar Photocatalytic Degradation of Phthalate Acid Esters, Satoshi KANEKO, Hideyuki KATSUMATA, Tohru SUZUKI, Kiyohisa OHTA: Photo/Electrochem. Photobiol. Environ. Energy Fuel, 5, pp. 347–359, 2006

Titanium Dioxide Mediated Photocatalytic Degradation of Dibutyl Phthalate in Aqueous Solution—Kinetics, Mineralization and Reaction Mechanism, Satoshi KANEKO, Hideyuki KATSUMATA, Tohru SUZUKI, Kiyohisa OHTA: Chem. Eng. J., 125, pp. 59–66, 2006

Removal of Arsenic in Aqueous Solutions by Adsorption onto Waste Rice Husk, Md. Nurul AMIN, Satoshi KANEKO, Taichi KITAGAWA, Aleya BEGUM, Hideyuki KATSUMATA, Tohru SUZUKI, Kiyohisa OHTA: Ind. Eng. Chem. Res., 45, pp. 8105–8110, 2006

Degradation of Polychlorinated Dibenzo-*p*-dioxins in Aqueous Solution by Fe(II)/H₂O₂/UV System, Hideyuki KATSUMATA, Satoshi KANEKO, Tohru SUZUKI, Kiyohisa OHTA, Yoshihiro YOBIKO*: Chemosphere, 63, pp. 592–599, 2006

Photo-Fenton Degradation of Alachlor in the Presence of Citrate Solution, Hideyuki KATSUMATA, Satoshi KANEKO, Tohru SUZUKI, Kiyohisa OHTA, Yoshihiro YOBIKO*: J. Photochem. Photobiol. A: Chem., 180, pp. 38–45, 2006

Determination of Atrazine And Simazine in Water Samples by High-performance Liquid Chromatography After Preconcentration with Heat-treated Diatomaceous Earth, Hideyuki KATSUMATA, Satoshi KANEKO, Tohru SUZUKI, Kiyohisa OHTA: Anal. Chim. Acta, 577, pp. 214–219, 2006

Degradation of Carbofuran by Cu/L-ascorbic acid/H₂O₂ System, Farzana FERDOUSH, Hideyuki KATSUMATA, Satoshi KANEKO, Tohru SUZUKI, Kiyohisa OHTA, Yoshihiro YOBIKO*: Photo/Electrochem. Photobiol. Environ. Energy Fuel, 5, pp. 321–334, 2006

Degradation of Diazinon in Aqueous Solution by V(IV)/H₂O₂ System, Hideyuki KATSUMATA, Hideyasu NAKAO, Farzana FERDOUSH, Satoshi KANECO, Tohru SUZUKI, Kiyohisa OHTA, Yoshihiro YOBICO*: *Photo/Electrochem. Photobiol. Environ. Energy Fuel*, 5, pp. 335–345, 2006

Membrane Fusion between a Giant Vesicle and Small Enveloped Particles: Possibilities for the Application to Construct Model Cells, Kanta TSUMOTO, Koki KAMIYA, Tetsuro YOSHIMURA: *Proceedings of the International Symposium on Micro-NanoMechatronics and Human Science, MHS 2005 Micro-Nano COE, IEEE*, pp. 7-12, 2006

Antigen-Based Immunofluorescence Analysis of B-Cell Targeting: Advanced Technology for the Generation of Novel Monoclonal Antibodies with High Efficiency and Selectivity, Masahiro TOMITA, Takatomi FUKUDA, Akira OZU, Keiichi KIMURA, Tian Yow TSONG*, Tetsuro YOSHIMURA: *Hybridoma*, 25(5), pp. 283-292, 2006

A New Technology for the Generation of Novel Monoclonal Antibodies Based on Short-Term Immunization, Masahiro TOMITA, Yoshiharu ASAOKA, Yasuhiko KATO, Shin OGATA*, Tian Yow TSONG*, Tetsuro YOSHIMURA: *Peptide Science 2005*, pp. 105-108, 2006

Controlled Self-Assembly of Amphiphilic Oligopeptides into Shape-Specific Nanoarchitectures, Tomoyuki KOGA*: Masahiro HIGUCHI, Takatoshi KINOSHITA*, Nobuyuki HIGASHI*: *Chem. Eur. J.*, 12 (5), pp.1360-1367, 2006

Polymer Adsorption Effects on Stabilities and Chemical Mechanical Polishing Properties of Ceria Particles, Norifumi SHIMONO, Naoyuki KOYAMA*, Masami KAWAGUCHI: *Jpn. J. Appl. Phys.*, 45 (5A), pp. 4196-4200, 2006

Buoyancy-driven Path Instabilities of Bubble Rising in Simple and Polymer Solutions of Hele-shaw Cell, Masami KAWAGUCHI, Sukehiro NIGA, Nobuaki GOU, Kazuo MIYAKE: *J. Phys. Soc. Jpn.*, 75 (12), pp.124401-1-124401-6, 2006

Ti³⁺-Free Multicomponent Titanophosphate Glasses as Ecologically Sustainable Optical Glasses, Tadanori HASHIMOTO, Hiroyuki NASU and Kanichi KAMIYA: *J. Am. Ceram. Soc.*, 89 (8), pp. 2521-2527, 2006

Tunable Localized-Surface-Plasmon-Resonance Characteristics of Independently Prepared Ag-TiO₂ Particles, Noritsugu HASHIMOTO, Tadanori HASHIMOTO, Hiroyuki NASU, Yoshitsugu YAMAMOTO and Seiji NIIJIMA: *e-J. Surf. Sci. Nanotech.*, 4 (7), pp. 566-569, 2006

Cycle Performance of Sol-Gel Optical Sensor Based on Localized Surface Plasmon Resonance of Silver Particles, Noritsugu HASHIMOTO, Tadanori HASHIMOTO, Taichi TERANISHI, Hiroyuki NASU and Kanichi KAMIYA:

Sens. Actuators B, 113 (1), pp. 382-388, 2006

Photocatalytic Degradation of Allergens in Water with Titanium Dioxide, Naomi NISHIKAWA, Satoshi KANECO, Hideyuki KATSUMATA, Tohru SUZUKI, Kiyohisa OHTA, Eiji YAMAZAKI, Kazuaki MASUYAMA, Tadanori HASHIMOTO and Kanichi KAMIYA: Fresen. Environ. Bull., 16 (3), pp. 310-314, 2006

Addition Effect of Phosphorus on Ni-Mo Catalysts in Hydrodenitrogenation, Weihua QIAN, Satoshi ABE, Akinobu NOJIMA, Kenji GUNJI, Atsushi ISHIHARA, Hiroyuki IKEDA: Prepr. Pap.-Am. Chem. Soc., Div. Petr. Chem. 51(2), pp.271, 2006

PVC Hydrocracking with Recovering of a Large Amount of H₂. Characterization of the Catalysts and the Products after Each Step of the Process, Thierry GIORNELLI, Franck DUMEIGNIL, Atsushi ISHIHARA: Energy Efficient Technologies I-ACS, Green Chem. Inst., pp. 63, 2006

Intercellular localization of occludins and ZO-1 as a solute transport barrier of the mesothelial monolayer, Kenichi KANEDA, Keiichi MIYAMOTO, Shinsuke NOMURA, Takashi HORIUCHI: J. Artif. Organs., 9(4), pp.241-50, 2006

Development of a new method for endovascular aortic repair: combination therapy of cell transplantation and stent grafts with a drug delivery system, Masaki KAJIMOTO, Takatsugu SHIMONO, Kouji HIRANO, Youichi MIYAKE, Yashuhiro SAWADA, Noriyuki KATO, Hitoshi HIRATA, Kyoko IMANAKA-YOSHIDA, Masakatsu NISHIKAWA, Toshimichi YOSHIDA, Hideto SHIMPO, Takashi HORIUCHI, Keiichi MIYAMOTO: CIRCULATION 114, pp.1378-83, 2006

Evaluation of Compliance and Stiffness of Decellularized Tissues as Scaffolds for Tissue-Engineered Small Caliber Vascular Grafts Using Intravascular Ultrasound, Yousuke MURASE*, Yuji NARITA*, Hideaki KAGAMI*, Keiichi MIYAMOTO, Yuichi UEDA*, Minoru UEDA*, Toyooki MUROHARA*: ASAIO, 52, pp.450-455, 2006

An image analysis algorithm for kinematics and morphology measurement of cells for the evaluation of tissue construction, Tomoko GESSEI, Chie OTSUKA, Masatoshi BANNO, Keiichi MIYAMOTO, Yuji OHTA, Takashi HORIUCHI: IFMBE Proceedings, 14:2006

Department of Architecture

*nonmember

City Planning Studies “Presents Situation and Prospects, District, Resort”, Satoshi ASANO, City Planning Review, No.263, pp.104-107, 2006

A Study on the Applying Circumstances and Roles of the Landscape Administrative Measures in the Landscape Ordinance about the Region Limitative type and the idea Active Type, the Present Condition of the Prefectures' landscape Administrative Measures Centered on the Landscape Ordinances Part 2, Yoshio BANDO, Satoshi ASANO and Shoji IMAI, Journal of Architecture and Planning, No.612, pp.99-105, 2006

In this study, we've made the hearing for 12 Prefectures and 12 municipalities of the total development type which occupies the Prefectures more than the others. So we've surveyed the situation bearing the landscape administrative measures of the total development type's Prefectures by making clear not only the applying circumstances of the hard measures of the wide-landscape region, the landscape-forming district, the large-scale activities etc. ,the important landscape structure etc. ,and the soft measures of the enlightenment etc. ,the landscape-forming agreement, the landscape-forming group, the support etc. ,but also the Prefectures' role for the municipalities. There're the 3 roles in the landscape administrative measures of the total development type

3D SPATIAL COMPOSITION OF CIVIC CENTER IN THE EARLY SHOWA ERA WITH BIRD' S-EYE VIEW PICTURES BY YOSHIDA HATSUSABURO IN CASES OF 18 PREFECTUAL CAPITAL CITIES BASED ON JAPANESE CASTLE-TOWNS.[in Japanese], Kenjiro MATSUURA : Journal of Architecture and Planning , Transactions of Architectural Institute of Japan, No. 602, p.p. 105-112, 2006.4

This paper aims to clarify 3D spatial composition of Civic Center in the early Showa era with bird's-eye view pictures by YOSHIDA Hatsusaburo in cases of 18 prefectural capital cities based on Japanese Castle-Towns. First, I indicate necessity of complementing by topographical map , photographs and pictures in case of using bird's-eye view pictures by YOSHIDA Hatsusaburo as research material , because characteristic of them is deformation, and examine their possibility of research material. Findings are as follows : 1) We can grasp arrangement conditions and facades of each government and municipal offices , whole construction of Civic Center and physical state of surrounding Civic Center with bird's-eye view pictures , 2) As a result of analysis 3D spatial composition of Civic Center with bird's-eye view pictures in cases of 18 cities , there was principle of 3D Urban Design answer to spatial composition of Castle Districts such as main road , moat and skirt of mountain.

THE REORGANIZATION AND URBAN DESIGN OF CIVIC CENTER BY WAR REHABILITATION PROJECT AFTER THE WORLD WAR II IN PREFECTUAL CAPITAL CITIES BASED ON JAPANESE CASTLE-TOWNS.[in Japanese], Kenjiro MATSUURA, Hirohisa NINOYU and Masuro URAYAMA: Journal of Architecture and Planning , Transactions of Architectural Institute of Japan, No. 608, p.p. 89-96, 2006.10

This paper aims to clarify reorganization and urban design of civic center by War Rehabilitation Project after the World War II , analyzing cases of 22 prefectural capital cities based on Japanese Castle-Towns. Findings are as follows : 1) governmental and municipal offices tended to be accumulated near castle area after the World War II , 2)

reorganization of civic center from before to after the World War II are grouped into three types , and most of them are the Keeping type which was kept in the same place as before the World War II and expanded , 3) in the case of forming civic center inside castle area before the World War II , civic center tended to be kept in the same place as before the World War II and seen urban design applying the elements of Japanese Castle-Towns, 4) urban design of paying attention to "Axis" tended to be kept and urban design of paying attention to "Class" tended to be disappeared after the World War II , 5) urban design of paying attention to main street built by War Rehabilitation Project after the World War II were seen in the cities of all types.

A Study of Spatial Characteristics and Urban Design of Civic Center formed in the Meiji and Taisho Era - Case Study of 39 Prefectural Capital Cities.[in Japanese],Kenjiro Matsuura , Tomohiro Iwasa and Masuro Urayama, Journal of the City Planning Institute of JAPAN, No.41, pp. 917-922, 2006.11

This Paper aims to clarify Spatial Characteristics and Urban Design of Civic Center analyzing Cases of Prefectural Capital 39 Cities formed Civic Center in the Meiji and Taisho era. Findings are as follows : 1) in Japanese Castle-Towns Civic Center were formed in Castle Districts , and in other Cities along Main Streets or behind Commercial Districts , 2) four Urban Designs used main streets were seen in Model located in Castle Districts and Model located along Main Streets , 3) four Urban Designs used side Streets crossed Main Streets were seen in Model located behind Commercial Districts , 4) Urban Design placing government and municipal offices focal point of vista was widely used regardless of Spatial Characteristics of Civic Center and cities' origin.

A Study on Shop Accumulation by Community Planning for Tourism on The Yakimono-Stroll-Road District in Tokoname City , Aichi Prefecture.[in Japanese],Shinjiro SAKAMOTO* , Kenjiro MATSUURA and Masuro URAYAMA, Journal of the City Planning Institute of JAPAN, No.41, pp. 1025-1030, 2006.11

This Paper aims to clarify Spatial Form of Shop Accumulation and Process from opening Shops to accumulating Shops paying attention to Shops for Tourists in Case of Yakimono-Stroll-Road-District in Tokoname City , Aichi Prefecture. Findings are as follows : 1) Small Shop Accumulations from three to nine were nearby Stroll-Road , 2) Shop Masters without Relationship in the Local Community were half the number and they have strong will to contribute to Stroll-Road-District, 3) Mediators encouraged opening Shops to Shop Masters , 4) Empty Factories prepared for Shops were distributed inside Stroll-Road-District , 5) Owners of Shops called out Shop Masters in selecting Shops , 6) Main Cause that make it possible to Large Shop Accumulations was Stroll-Road which was a Busy Street and has Sequence of Attractive Scenes.

A Study on Citizen's Maintenance and Use of Roads planted Street Trees with Edible Fruits.[in Japanese],Kenjiro MATSUURA and Masuro URAYAMA,Papers on Environmental Information Science No.20,p.p.223-228,2006.11

This research clarifies citizen participation in maintenance of street trees with edible fruits, using a questionnaire to local governments. Main results are as follows; Almost of the roads planted fruiterers locate in urban areas. Fruiterers require more disinfection and manure than trees without fruit, and to take those fruits. There are some roads for citizen groups, students and commerce groups to maintain and harvest them. From comparison between the Apple Street Trees and Cherry Street Trees in Iida city, street trees with fruiterers can provide citizen with chance to utilize them such as events of harvest and environmental study etc.

Development Plan of Mie prefectural Riverside Park in 1965 , Satoshi ASANO and Kenjiro MATSUURA : "Dreams of urban planning", [in Japanese], Jurinsha , p.p.134-137 , 2006.3

INABE SOGO GAKUEN Hige School,ISHIGURE Elementary School,YOKKAICHI University,OYAMADA Memorial Spa Hospital,MIE Prefectural Art Museum,MIE Center for the Arts,SENJUJI Charnel House, Kenjiro MATSUURA : " Guide Book of Modern Architectures in Tokai Area ", [in Japanese], Architectural Journal , p.p.84-87 , 2006.4

A Study on the Actual Conditions of the Reorganization and Consolidation of Municipal Offices by the Consolidation of Municipalities [in Japanese], Naoto Kanzaki, Hiroyuki Takai, Shoji Imai, Mitsumasa Nakamura: Regional Community Facilities Planning and Design, Vol.24, pp.25-32, 2006

In late years, many municipalities consolidated. When we catch the consolidation of municipalities from the architectural side, it is thought to generate the surplus facilities and spaces, and to be done the reorganization and consolidation. In that case, it is a social proposition to use them effectively today. The purpose of this study is to clarify the ideal way of effective uses in communal facilities of the future by clarifying the actual conditions of the reorganization and consolidation, and the effective uses generated in that.

A Study on the Successive Change Condition of Ashiyahama Seaside Town—From the Interview Research for Management Staffs and Homeowners Association, and Observation Research— [in Japanese], TAKAI Hiroyuki, TAKADA Mitsuo*, TONOOKA Tsubasa*, YOSHINO Masahiro, KANZAKI Naoto, BAI Jin: Journal of Papers on Housing, No. 1, pp.241-248, 2006

The aim of this research is to make clear the actual condition on successive change of the Ashiyahama Seaside Town. The research was made by the interview research for management staffs and homeowners association, and observation research. Many changes are surely occurred. For example, residents' ageing tendency has occurred, and sky-parks and open spaces are not used as the planners intended.

Passive Cooling Effect of Water Evaporation in Perspirable Building, Yukio ISHIKAWA, Proceedings of EuroSun 2006, International Solar Energy Society, pp.1-6, 2006

Spectral reflectance of ceramic tiles for exterior wall of buildings and their performances on solar heat absorption, Masato TAZAWA*, Hiroshi KAKIUCHIDA*, Ping JIN*, Toyohiko SUGIYAMA*, Yukio ISHIKAWA,, Proceedings of the World Renewable Energy Congress, pp.19-25, 2006

Spectral reflectance and Solar Absorption of Ceramic Tiles for Exterior Wall of Buildings, Masato TAZAWA*, Hiroshi KAKIUCHIDA*, Ping JIN*, Toyohiko SUGIYAMA*, Yukio ISHIKAWA,, Proceedings of Renewable Energy, pp.153-156, 2006

Mixing Model for Thermal Energy Storage Water Tank of Multi-connected Mixing Type, H. Kitano, T. Iwata, S. Ichinose*, Y. Ishikawa and K. Sagara* : Proc. of 10th International Conference on Thermal Energy Storage (ECOSTOCK 2006), pp.71-77, 2006.6

A Study on the Heat Load Characteristics of Underground Structures, Part 1. Field Experiment of Underground Structure under Internal Heat Generation, Kyung-Soon Park, Hisaya Nagai and Takeshi Iwata, Journal of Asian Architecture and Building Engineering, Vol.5, No.2, pp.421-428, November 2006

The purpose of this study is to clarify the heat load characteristics of underground structures. In order to achieve this purpose, it is necessary to clarify the heat and moisture behavior of underground basements and the surrounding ground, and to acquire the basic data for computational analysis. Accordingly, this paper presents the measurement results of about one year of field experiments begun in October, 2004, related to an underground experimental basement under internal heat generation conditions. Analysis results related to the heat and moisture behavior of the experimental basement and ground, the influence that internal heat generation had on the surrounding ground, condensation behavior, the interrelationship between precipitation and the fluctuation of moisture content in the ground, and the annual mean heating load per unit area, etc., are also presented.

Assessment Report on Damaged Prambanan World Heritage Compounds, Central Java, Satoshi YAMATO, Toshikazu HANAZATO, Kunihiko ONO et. al., July 2007

This report was published as a reconnaissance report of the Prambanan, World Heritage in Indonesia, damaged seriously damaged by the Central Java Earthquake of May 27, 2006. The authors were sent by Japanese Government to conduct the survey of the earthquake damage to the architectural heritages in the epicentral area near Yogyakarta. The report was based on this field survey performed in the middle of July 2007, focusing on both the structural damage and the historical documents/drawings of the Prambanan that would be essential for planning to restore the damaged the masonry heritages.

Fundamentals and a Few Recent Applications of Environmentally Friendly Porous Concrete, Shigemitsu HATANAKA, Naoki MISHIMA, Yukihisa YUASA*, Akihiro MAEGAWA, Takeshi NAKAGAWA and Moe KURODA : International Conference on Pozzolan, Concrete and Geopolymer, pp.20-36, 2006.5

Experimental Study on Permeability Coefficient of Fresh Mortar, Toshitsugu INUKAI, Naoki MISHIMA, Eisuke SAKAMOTO and Shigemitsu HATANAKA : Proceedings of the Japan Concrete Institute, Vol 28, No.1, pp.1109-1114, 2006.6 (in Japanese)

Study on Quality Improvement in Vacuum Processed Full-Scale Slab Concrete, Eisuke

SAKAMOTO, Naoki MISHIMA, Mamoru FURUICHI and Shigemitsu HATANAKA : Proceedings of the Japan Concrete Institute, Vol 28, No.1, pp.1325-1330, 2006.6 (in Japanese)

Experimental Study on Properties of Small Particle Size Porous Concrete, Akihiro MAEGAWA, Akira YAMAMOTO, Naoki MISHIMA and Shigemitsu HATANAKA : Proceedings of the Japan Concrete Institute, Vol 28, No.1, pp.1397-1402, 2006.6 (in Japanese)

Roof Planting with Water Culture Using Light Weight Porous Concrete, Moe KURODA, Naoki MISHIMA, Ken MATSUDA and Shigemitsu HATANAKA : Proceedings of the Japan Concrete Institute, Vol 28, No.1, pp.1409-1414, 2006.6 (in Japanese)

Strength Evaluation of Hardened Cement by a Drill Type of Surface Strength Measurement Apparatus, Tetsuya HASEGAWA, Shigemitsu HATANAKA, Naoki MISHIMA and Yasuo TANIGAWA : Proceedings of the Japan Concrete Institute, Vol 28, No.1, pp.1877-1882, 2006.6 (in Japanese)

FEM Analyses on Compressive Failure of Prismatic Concrete with Internal Defect, Eiji MIZUNO*, Tomonori TANASE*, Atsushi ITOH* and Shigemitsu HATANAKA : Proceedings of the Japan Concrete Institute, Vol 28, No.2, pp.109-114, 2006.6 (in Japanese)

Investigation on Preservation and Repairs of the Sukhothai-Ayutthaya Ruins (World Cultural Heritage Site) in Thailand, HATANAKA,S., PRINYA,C.*, HASEGAWA,T., THANUDKIJ,C.* : Bulletin of Center for International Education and Research, Mie University, Vol.2, pp.75-85, 2007.3

Fundamentals and Few Recent Applications of Environmentally Friendly Porous Concrete, HATANAKA,S., MISHIMA,N., YUASA,Y., MAEGAWA,A., NAKAGAWA,T., KURODA,M. : Bulletin of Center for International Education and Research, Mie University, Vol.2, pp.113-124, 2007.3

Strength Evaluation of Hardened Cement Paste by Small Diameter Drill-Type Test Machine, T.HASEGAWA, N.MISHIMA, S.HATANAKA, N.HASEGAWA and Y.TANIGAWA : Proceedings of The 2nd Symposium on Prospects of Nondestructive Testing Method for Concrete Structure, pp.421-426, 2006.8

Evaluation of Surface Strength of Terra-Cotta and Effect of Penetration-Type Chemical Agent by Small Diameter Drill Type Test Machine, T.HASEGAWA, S.HATANAKA, N.MISHIMA, N.HASEGAWA and Y.TANIGAWA : Proceedings of The 2nd Symposium on Prospects of

Nondestructive Testing Method for Concrete Structure, pp.441-446, 2006.8

Department of Information Engineering

*nonmember

The reachability and related decision problems for monadic and semi-constructor TRSs, Ichiro MITSUHASHI, Michio OYAMAGUCHI, Toshiyuki YAMADA: Information Processing Letters, Vol.98, pp.219-224, 2006

This paper shows that reachability is undecidable for confluent monadic and semi-constructor TRSs, and that joinability and confluence are undecidable for monadic and semi-constructor TRSs. Here, a TRS is monadic if the height of the right-hand side of each rewrite rule is at most 1, and is semi-constructor if all defined symbols appearing in the right-hand side of each rewrite rule occur only in its ground subterms.

The Confluence Problem for Flat TRSs, Ichiro MITSUHASHI, Michio OYAMAGUCHI, Florent JACQUEMARD*: KOKYUROKU of Research Institute for Mathematical Sciences Kyoto University, New Trends in Theory of Computation and Algorithm, vol.1489, pp.250-255, 2006

We prove that confluence is undecidable for flat TRSs. Here, a TRS is flat if the heights of the left and right-hand sides of each rewrite rule are at most one.

The Joinability and Related Decision Problems for Semi-constructor TRSs, Ichiro MITSUHASHI, Michio OYAMAGUCHI, Yoshikatsu OHTA and Toshiyuki YAMADA: Trans. IPS Japan, Vol.47, No.5, pp.1502-1514, 2006

The word and unification problems for term rewriting systems (TRSs) are most important ones and their decision algorithms have various useful applications in computer science. Algorithms of deciding joinability for TRSs are often used to obtain algorithms that decide these problems. In this paper, we first show that the joinability problem is undecidable for linear semi-constructor TRSs. Here, a semi-constructor TRS is such a TRS that all defined symbols appearing in the right-hand side of each rewrite rule occur only in its ground subterms. Next, we show that problem is decidable both for confluent semi-constructor TRSs and for confluent semi-monadic TRSs. This result implies that the word problem is decidable for these classes, and will be used to show that unification is decidable for confluent semi-constructor TRSs in our forthcoming paper.

The Confluence Problem for Flat TRSs, Ichiro MITSUHASHI, Michio OYAMAGUCHI and Florent JACQUEMARD*: Proceedings of the 8th International Conference on Artificial Intelligence and Symbolic Computation (AISC 2006), Lecture Notes in Artificial Intelligence 4120, pp.68-81, 2006

We prove that the properties of reachability, joinability and confluence are undecidable for flat TRSs. Here, a TRS is flat if the heights of the left and right-hand sides of each rewrite rule are at most one.

Scheduling support hardware for multiprocessor system and its evaluations, Takahiro SASAKI, Tetsuo HIRONAKA*, Naoki NISHIMURA*, Noriyoshi YOSHIDA*: Systems and Computers in Japan, Vol.37, No.2, pp.79-95, 2006

It is important to write portable programs while concealing various latencies that would be problematic in

getting the optimal performance out of a parallel processing environment. Fine Grain Parallelism is one of the methods for implementing this. However there is a problem in achieving Fine Grain Parallelism using a conventional OS. This is because, as the granularity becomes finer, the frequency of context switching, scheduling and the like increases, leading to an increase in the overhead due to those factors, and there would be a risk of causing severe performance degradation. Therefore, we propose a multiprocessor architecture using a Scheduling Support Hardware (SSH), which aims to achieve high speed context switching and scheduling while utilizing fine grain parallelism, by having the hardware support the thread scheduling and the allocation / release of the CPU resources, which are part of the function of the OS. In this paper, we designed a multi-processor system with SSH using the Verilog-HDL and showed the effectiveness of our approach in an evaluation by a computer simulation. In the evaluation, we found that the scheduling time could be reduced by using the SSH, and thus it became possible to use a parallelism with a finer granularity.

Motion Estimation Using Adaptively Hierarchical Spiral Search [in Japanese], Motoki MIYAMAE, Takahiro SASAKI, Kazuhiko OHNO, Toshio KONDO: Trans. of the Institute of Electronics, Information and Communication Engineers, Vol.J89-D, No.3, pp.482-491, 2006

Motion estimation is computationally complicated task in video coding process. Block-matching-based fast algorithms reduce the computational complexity of motion estimation at the expense of accuracy. However, the improvement of the accuracy of motion estimation is attached to importance for the high quality video coding. This paper proposes a new motion estimation algorithm executing adaptively two-stage hierarchical spiral search. The proposed algorithm a little better average image quality (PSNR) than the full-search for the evaluation image. Moreover, the quality for the worst condition image was improved from 0.46dB to 0.19dB in comparison with a current superior spiral search.

A Design and Evaluation of Low Energy Processor by Variable Stages Pipeline Technique [in Japanese], Yuji ICHIKAWA*, Takahiro SASAKI, Tetsuo HIRONAKA*, Kazuya TANIGAWA*, Toshiaki KITAMURA*, Toshio KONDO: IPSJ Trans. on Advanced Computing Systems, Vol.47, No.SIG7(ACS14), pp.231-242, 2006

Recently, in the field of mobile computing, the achievement of low energy computing and high performance computing is required simultaneously. DVS (Dynamic Voltage Scaling) is a current major technique to realize that. However, the lower the chip voltage becomes in the future, the less energy saving we get by DVS. So we propose VSP (Variable Stages Pipeline) processor by a unifying pipeline stages in the use of flip-flop called LDS-cell which has an ability to act as a latch or flip-flop. VSP can achieve low energy computing without any dependence on chip voltage. We show that VSP processor can achieve lower energy computing and higher performance computing than the DVS processor in low energy mode.

Evaluation of Bank-Based Multiport Memory Architecture with Blocking Network, Tomohiro INOUE*, Tetsuo HIRONAKA*, Takahiro SASAKI, Seiji FUKAE*, Tetsushi KOIDE*, Hans J. MATTAUSCH*: Electronics and communications in Japan (Part 3), Vol.89, No.6, pp.22-33, 2006

The bank-based multiport memory is better composition approach to realizing realistic chip area and high access bandwidth than a conventional N-Port memory cell approach. However this method is unsuitable for large numbers of ports and banks because the hardware resources of the crossbar network which connects the ports and banks increase in proportion to the product of the numbers of ports and banks. In order to solve this problem, this paper

proposes a new bank-based multiport memory architecture using a blocking network instead of a crossbar network. Many blocking networks have been researched so far. However, these researches evaluated hardware resources based on the number of switches, but the compositions and circuit scale of the switches used in crossbar network and blocking network are different. Hence, this paper compares the number of transistors to show that the bank-based multiport memory using the blocking network achieves high access bandwidth with smaller hardware resources than the conventional approach. According to our results, our approach achieves the same access bandwidth with half the number of transistors, for 512 ports and 512 banks.

A User-Level Extension Scheme for a Task Parallel Script Language [In Japanese], Yusuke SAKAGUCHI, Kazuhiko OHNO, Takahiro SASAKI, Toshio KONDO, Hiroshi NAKASHIMA*: IPSJ Transactions on Advanced Computing Systems, Vol. 47, No. SIG 12 (ACS 15), pp.296-307, 2006

We are developing a task-parallel script language named *MegaScript* for mega-scale parallel processing. MegaScript regards existing sequential/parallel programs as tasks, and controls them for massively parallel execution. Although MegaScript runtime and task programs should be specialized to the target application and platform to obtain high performance, it is undesirable for portability and reusability. To satisfy these conflicting requirements, we propose a user-level runtime extension scheme named *Adapter*. This scheme enables programmers to extend and optimize behavior of the application without modifying the runtime nor task programs. The evaluation of our implementation achieved both efficient programming and enough performance for practical use.

Structure Monitoring by Optical Fiber [in Japanese], Hiroshi NARUSE: Journal of the Japan Society of Mechanical Engineers, Vol.109, No.1048, pp.22-23, 2006

The Entire Solution Path of Kernel-based Nonparametric Conditional Quantile Estimator, Ichiro TAKEUCHI, Kaname NOMURA and Takafumi KANAMORI*: Proceedings of the 2006 IEEE World Congress on Computational Intelligence (WCCI 2006) / International Joint Conference on Neural Networks, pp.153-158, 2006

The goal of regression analysis is to describe the relationship between an output y and a vector of inputs x . Least squares regression provides how the mean of y changes with x , i.e., it estimates the conditional mean function. Estimating a set of conditional quantile functions provides a more complete view of the relationship between y and x . *Quantile regression* [1] is one of the promising approaches to estimate conditional quantile functions. Several types of quantile regression estimator have been studied in the literature. In this paper, we are particularly concerned with kernel-based nonparametric quantile regression formulated as a quadratic programming problem similar to those in support vector machine literature [2].

A group of conditional quantile functions, say, at the orders $q = 0.1, 0.2, \dots, 0.9$, can provide a nonparametric description of the conditional probability density $p(y|x)$. This requires us to solve many quadratic programming problems and it could be computationally demanding for large-scale problems. In this paper, inspired by the recently developed *path following strategy* [3][4], we derive an algorithm to solve a sequence of quadratic programming problems for the entire range of quantile orders $q \in (0, 1)$. As well as the computational efficiency, the derived algorithm provides the full nonparametric description of the conditional distribution $p(y|x)$. A few examples are given to illustrate the algorithm.

Nonparametric Quantile Estimation, Ichiro TAKEUCHI, Quoc V. LE*, Timothy D. SEARS*, Alexander J. SMOLA*: Journal of Machine Learning Research, Vol.7, pp.1231-1268, 2006

In regression, the desired estimate of $y|x$ is not always given by a conditional mean, although this is most common. Sometimes one wants to obtain a good estimate that satisfies the property that a proportion, τ , of $y|x$, will be below the estimate. For $\tau=0.5$ this is an estimate of the *median*. What might be called median regression, is subsumed under the term *quantile regression*. We present a nonparametric version of a quantile estimator, which can be obtained by solving a simple quadratic programming problem and provide uniform convergence statements and bounds on the quantile property of our estimator. Experimental results show the feasibility of the approach and competitiveness of our method with existing ones. We discuss several types of extensions including an approach to solve the *quantile crossing* problems, as well as a method to incorporate prior qualitative knowledge such as monotonicity constraints.

A Reconstruction Method of 3-D Surface Topography Using Evolutionary Computation in the SEM, Tetsuji KODAMA, Xiaoyuan LI* and Kenji NAKAHIRA*: Proceedings of the 16th International Microscopy Congress (IMC 16), p.955, 2006

Casualty Insurance Pure Premium Estimation Using Two-Stage Regression Tree, Kumiko NISHI, Ichiro TAKEUCHI: Proceedings of the International Workshop on Data-Mining and Statistical Science (DMSS 2006), pp.159-166, 2006

We study a regression tree algorithm tailored to casualty insurance pure premium estimation problem. Casualty insurance premium is mainly determined by the expected amount that the insurance companies have to pay for the contract. Therefore, casualty insurance companies have to estimate the expected insurance amount on the basis of insurance risk factors. This problem is formulated as a regression problem, i.e. estimation of conditional mean $E[Y|x]$, where Y is insurance amounts and x is risk factors. In this paper, we aim to implement the regression problem in regression tree framework. The difficulty of the problem lies in the fact that the distribution of insurance amount $P(Y|x)$ is highly skewed and exhibits a long-tail toward positive direction. Conventional least-square-error regression tree algorithm is notoriously unstable under such long-tailed error distribution. On the other hand, several types of robust regression trees, such as least-absolute-error regression tree, are neither appropriate in this situation because they yields significant bias to conditional mean $E[Y|x]$. In this paper, we propose a two-stage tree fitting algorithm. In the first stage, the algorithm constructs a quantile tree, a kind of robust regression tree, which is stable but biased to conditional mean $E[Y|x]$. In the second stage, the algorithm corrects the bias using least-square error regression tree. We discuss the theoretical background of the algorithm and empirically investigate the performances. We applied the proposed algorithm to a car insurance data set of 318, 564 records provided from a north-american insurance company and obtained significantly better results than conventional regression tree algorithm.

Underground Mine monitoring Using Distributed Fiber Optic Strain Sensing System, Hiroshi NARUSE, Hideki UEHARA*, Taishi DEGUCHI*, Kazuhiko FUJIHASHI*, Yasuhiko ISHIKURA*, Masatoshi ONISHI*, Raul ESPINOZA*, Cesar GUZMAN*, Cesar PARDO*, Cesar ORTEGA*, Manuel PINTO* and Francisco GALVEZ*: Proceedings of the 18th International Optical Fiber Sensors Conference (OSA 18), ThD5, CD-ROM, 2006

We demonstrated the applicability of a distributed fiber optic strain sensing system for monitoring changes in an underground mine through a half-year field trial. This paper outlines the mine structure and the monitoring system and presents monitoring results.

Effectiveness of Relative Expressions for Trend Information Extraction, Hiroki IMAOKA, Fumito MASUI, Atsuo KAWAI and Naoki ISU: *Journal of Japan Society for Fuzzy Theory and Intelligent Informatics*, Vol.18, No.5, pp.735-744, 2006

In this paper, we discuss effectiveness of “relative expressions” for trend information extraction. Relative expressions, for example, “12% increase”, “last year”, “the first place” and so forth, show relative difference and variation of numerical value implicitly. To extract more trend information from newspaper articles, one of possible means would be to utilize relative expressions. We investigated functions and statistical trend of the relative expressions in newspaper articles. And rules to extract basic elements were generated for trend information extraction. To evaluate effectiveness of the extraction rules, we experimented on newspaper articles. The result shows 0.8 or more F-measure. It was confirmed that relative expression-based extraction should well-performed.

An Automatic Relevance Estimation of Property Values and Its Feedback based on World Wide Web for Metaphor Recognition [in Japanese], Fumito MASUI, Jun'ichi FUKUMOTO* and Kenji ARAKI*: *IEICE Transactions on Information and Systems*, Vol.J89-D, No.9, pp.860-870, 2006

This paper proposes a method which estimates the relevance of closed-up property values as salience features during the metaphor recognition process and feeds the estimation results back to a property value set to deal with an evaluation cost problem of metaphor recognition. Evaluating the relevance of closed-up property values, the specific expressions(a comparative expression and an adnominal expression) which was generated with a pair of concepts and each closed-up property value between these concepts are retrieved from the World Wide Web (WWW). In case of a non-relevant result, it is fed back to the property ranking by reconstructing a property value set with the retrieved information. Some experiments have been conducted and those experimental results showed that our method performs human-level estimation, as about 80% of the estimation results were the same with human judgments. Also by adding a feedback process we achieved about a 20% increase of property ranking accuracy.

WoZ Simulation of Interactive Question Answering, Tsuneaki KATO*, Jun'ichi FUKUMOTO*, Fumito MASUI and Noriko KANDO*: *Proceedings of Workshop on Interactive Question Answering at HLT-NAACL2006*, 2006

Question answering (QA) systems that can be used in interactive environments are need in various applications. It is important to develop proper evaluation frameworks in order to guide the direction of research, based on a proper understanding of what functions and abilities are needed for such interactive QA systems and also what range of language phenomena should be handled by them. QACIAD (Question Answering Challenge for Information Access Dialogue) is one of such evaluation frameworks and assumes that users interactively collect information using a QA system for writing a report on a given topic and evaluates, among other things, the abilities needed under such circumstances. In this research, in order to examine the assumptions made by QACIAD, dialogues under the situation that it assumes are collected using WoZ (Wizard of Oz) simulating, which is frequently used for collecting dialogue data for designing speech dialogue systems, and then analyzed. The results indicate that the setting of QACIAD is real and appropriate and that one of the important abilities for future interactive QA systems is providing cooperative and helpful responses.

Countermeasures Against Carsickness Enhanced by Watching an Onboard Video Display, Akihiro MORIMOTO, Tomohiro OKUMURA, Noritaka HIDAKA, Dan PIAO, Yusuke ARAKI, Fumito MASUI, Atsuo KAWAI, Naoki ISU: *Information Technology Letters*, Vol. 5, pp. 323-326, 2006

Three approaches were proposed for reducing carsickness while watching an onboard display in a vehicle. The approaches are based on the sensory conflict theory to reduce a conflict of sensory information between the vestibular and the visual systems. Visual stimulus along with the original content is presented on the onboard display to provide optokinetic sensation of yaw rotation of a vehicle. Experimental study showed that the carsickness severity was remarkably reduced by the proposed approaches.

Recognizing Errors in English Writing Based on the Mass Count Distinction, [in Japanese], R.NAGATA*, T.WAKANA, A.KAWAI, K.MORHIRO*, F.MASUI, N.ISU: *Trans. of the Institute of Electronics, Information and Communication Engineers*, J89-D, pp.1777-1790, 2006

This paper proposes a method for detecting errors in article usage and singular plural usage based on the mass count distinction. First, it learns decision lists from training data generated automatically to distinguish mass and count nouns. Then, it detects errors by applying rules(the decision lists) to the mass count distinction. Experiments show that it achieves a recall of 0.648 and a precision of 0.747 and outperforms other methods(a recall of 0.564 and a precision of 0.528).

Recognizing article errors using prepositional information, R.NAGATA*, T.IGUCHI, K.WAKIDERA, F.MASUI, A.KAWAI, and N.ISU: *Systems and Computers in Japan*, vol.37, pp. 17-26, 2006

In this paper, the authors propose a method to recognize article errors often seen in English text written by Japanese learners of English. In this method, article errors are recognized using prepositional information. The results of experiments confirm that the performance of the author's method is a F-measure of 0.72 and superior to our earlier method(F-measure of 0.53).

A Feedback-augmented method for detecting errors in the writing of learners of English, R.NAGATA*, A.KAWAI, K.MORHIRO*, and N.ISU: *Proceedings of the 21st International Conference on Computational Linguistics and 44th Annual Meeting of the Association for Computational Linguistics*, pp.241-248, 2006

This paper proposes a method for detecting errors in article usage and singular plural usage based on the mass count distinction. First, it learns decision lists from training data generated automatically to distinguish mass and count nouns. Then, in order to improve its performance, it is augmented by feedback that is obtained from the writing of learners. Finally, it detects errors by applying rules to the mass count distinction. Experiments show that it achieves a recall of 0.71 and a precision of 0.72 and outperforms other methods used for comparison when augmented by feedback.

Reinforcing English countability prediction with one countability per discourse property, R.NAGATA*, A.KAWAI, K.MORHIRO*, and N.ISU: *Proceedings of the 21st International Conference on Computational Linguistics and 44th Annual Meeting of the Association for Computational Linguistics Main Conference Poster Sessions*, pp.595-602, 2006

Countability of English nouns is important in various natural language processing tasks. It especially plays an important role in machine translation since it determines the range of possible determiners. This paper proposes a method for reinforcing countability prediction by introducing a novel concept called *one countability per discourse*. It claims that when a noun appears more than once in a discourse, they will all share the same countability in the discourse. The basic idea of the proposed method is that mispredictions can be correctly overridden using efficiently the one countability per discourse property. Experiments show that the proposed method successfully reinforces countability prediction and outperforms other methods used for comparison.

The Impact of OCR Accuracy and Feature Transformation on Automatic Text Classification, Mayo MURATA, BUSAGALA, L.S.P., Wataru OHYAMA, Tetsushi WAKABAYASHI, Fumitaka KIMURA: Document Analysis Systems VII by Bunke, H. and Spdz, A.(Eds.) DAS 2006, pp.506-517, 2006

Digitization process of various printed documents involves generating texts by an OCR system for different applications including full-text retrieval and document organizations. However, OCR-generated texts have errors as per present OCR technology. Moreover, previous studies have revealed that as OCR accuracy decreases the classification performance also decreases. The reason for this is the use of absolute word frequency as feature vector. Representing OCR texts using absolute word frequency has limitations such as dependency on text length and word recognition rate consequently lower classification performance due to higher within-class variances. We describe feature transformation techniques which do not have such limitations and present improved experimental results from all used classifiers.

Automatic Assembling of Cadastral Maps Based on Generalized Hough Transformation, Fei LIU, Wataru OHYAMA, Tetsushi WAKABAYASHI, Fumitaka KIMURA: Document Analysis Systems VII by Bunke, H. and Spdz, A.(Eds.) DAS 2006, pp.593-603, 2006

There are numerous cadastral maps generated by past land surveying. The raster digitization of these paper maps is in progress. For effective and efficient use of these maps, we have to assemble the set of maps to make them superimposable on other geographic information in a Geographic Information System. The problem can be seen as a complex jigsaw puzzle where the pieces are the cadastre sections extracted from the map. We present an automatic solution to this geographic jigsaw puzzle, based on the generalized Hough transformation that detects the longest common boundary between every piece and its neighbors. The experiments have been conducted using the map of Mie Prefecture, Japan and the French cadastral map. The results of the experiment with the French cadastral maps show that the proposed method, which consists of extracting an external area and extracting and regularizing the north arrow, is suitable for assembling the cadastral map. The final goal of the process is to integrate every piece of the puzzle into a national geographic reference frame and database.

Facial Feature Extraction Using Gradient Features and MQDF Matching, Wataru OHYAMA, M.SHRIDHAR* and Paul WATTA*: Proceedings of Eighth IASTED International Conference Signal and Image Processing, pp.329-334, 2006

We propose a novel approach for the extraction of facial features from frontal face images. The proposed approach involves 3 main processing stages. In the first stage, a bounding box is placed over the face. In the second stage, candidate positions for the facial features are identified using a set of MQDF-based distance functions. Finally, in

the third stage, the candidate feature positions are evaluated using an MQDF-based verification function, and an optimal configuration is chosen. Results on the FERET database indicate that with a proper setting of parameters, the proposed algorithm can accurately extract facial features over many different scales.

Recognition of handwritten Tamil characters, N.SHARMA*, U.PAL* and F.KIMURA: In Proc. National Conference on Recent Trends in Information Systems, pp.180-183, 2006

Recognition of Handwritten characters is challenging task because of the variability involved in the writing styles of different individuals. This paper deals with the recognition of off-line Tamil handwritten characters using the quadratic classifier based on the features obtained from directional chain code histogram. The bounding box of a character is segmented into blocks and the chain code histogram is computed in each of the blocks. This chain code features are fed to the quadratic classifier for recognition. We used 50687 numbers of samples comprising all the class of the Tamil script for the present work. We obtained 90.95% recognition accuracy.

Recognition of English Multi-oriented Characters, U.PAL*, F.KIMURA, K.ROY* and T.PAL*: In. Proc International Conference on Pattern Recognition, pp. 873-876, 2006

There are some printed artistic documents where text lines may be curved in shape. As a result, characters of a single line may be multi-oriented. To handle such artistic documents, in this paper, we present a scheme towards the recognition of multi-oriented and multi-sized English characters. The features used here are invariant to character orientation and computed based on the angular information of the border points of the characters. We used modified quadratic discriminant function (MQDF) for recognition. We tested our proposed scheme on a dataset of 18232 characters and obtained 98.34% accuracy from the system.

A Lexicon Driven Method for Unconstrained Bangla Handwritten Word Recognition, U.PAL*, K.ROY* and F.KIMURA: In Proc. 10th International Workshop on Frontiers in Handwriting Recognition (IWFHR), pp. 601-606, 2006

In this paper a lexicon driven segmentation-recognition scheme for unconstrained Bangla handwritten word recognition is proposed for Indian postal automation. In the proposed method, at first, binarization of the input document is done and slant correction of the individual words is performed. Next, using water reservoir concept words are pre-segmented into possible primitive components (characters or its parts). In order to merge these primitive components into characters and to find optimum character segmentation, dynamic programming (DP) is applied using total likelihood of characters as the objective function. To compute the likelihood of a character, modified quadratic discriminant function (MQDF) is used for the purpose. The features used in the MQDF are mainly based on the directional features of the contour points of the components. We tested our system on Bangla city-name images and at present an overall accuracy of 87.21% is obtained from the proposed system.

Recognition of Handwritten Kannada Numerals, N.SHARMA*, U.PAL* and F.KIMURA: Proc. 9th International Conference on Information Technology (ICIT-2006), IEEE Computer Society Press, pp.133-136, 2006

This paper deals with a quadratic classifier based scheme for the recognition of off-line handwritten numerals of

Kannada, an important Indian script. The features used in the classifier are obtained from the directional chain code information of the contour points of the characters. The bounding box of a character is segmented into blocks and the chain code histogram is computed in each of the blocks. Here we have used 64 dimensional and 100 dimensional features for a comparative study on the recognition accuracy of our proposed system. This chain code features are fed to the quadratic classifier for recognition. We tested our scheme on 2300 data samples and obtained 97.87% and 98.45% recognition accuracy using 64 dimensional and 100 dimensional features respectively, from the proposed scheme using five-fold cross-validation technique.

Recognition of Offline Handwritten Devnagari Characters using Quadratic Classifier, N.SHARMA*, U.PAL*, F.KIMURA and S.PAL*: Indian Conference on Computer Vision Graphics and Image Processing (ICVGIP), LNCS, Springer Verlag, pp. 805-816, 2006

Recognition of handwritten characters is a challenging task because of the variability involved in the writing styles of different individuals. In this paper we propose a quadratic classifier based scheme for the recognition of off-line Devnagari handwritten characters. The features used in the classifier are obtained from the directional chain code information of the contour points of the characters. The bounding box of a character is segmented into blocks and the chain code histogram is computed in each of the blocks. Based on the chain code histogram, here we have used 64 dimensional features for recognition. These chain code features are fed to the quadratic classifier for recognition. At present we obtained 95.81% and 80.36% recognition accuracy on Devnagari numerals and characters, respectively, from the proposed scheme.

Quadratic Classifier Based approach for Recognition of Handwritten Kannada Numerals, U.PAL*, F.KIMURA, and N.SHARMA*: 41st National Annual Convention, Computer Society of India (CSI-2006), Tata McGraw Hill, pp.159-163, 2006

Recognition of handwritten characters is a challenging task because of the variability involved in the writing styles of different individuals. In this paper we propose a quadratic classifier based scheme for the recognition of off-line Kannada handwritten numerals. The features used in the classifier are obtained from the directional chain code information of the contour points of the characters. The bounding box of a character is segmented into blocks and the chain code histogram is computed in each of the blocks. Here we have used 64 dimensional and 400 dimensional features for a comparative study on the recognition accuracy of our proposed system. This chain code features are fed to the quadratic classifier for recognition. At present we modified the parameters of the classifier and obtained 98.54% and 98.98% recognition accuracy using 64 dimensional and 400 dimensional features respectively from the proposed scheme.

Offline Handwritten Kannada Character Recognition, U.PAL*, N.SHARMA*, F.KIMURA and S.PAL*: IEEE International Conference on Signal and Image Processing (ICSIP), Macmillan Advanced Research, Vol.-1, pp.174-177, 2006

Recognition of handwritten characters is challenging task because of the variability involved in the writing styles of different individuals. In this paper we propose a quadratic classifier based scheme for the recognition of off-line Kannada handwritten Characters. The features used in the classifier are obtained from the directional chain code information of the contour points of the characters. The bounding box of a character is segmented into blocks and

the chain code histogram is computed in each of the blocks. Here we have used 64 dimensional features for high speed recognition and 400 dimensional features for high accuracy recognition in our proposed system. This chain code features are fed to the quadratic classifier for recognition. At present we obtained 80.87% and 85.71% recognition accuracy using 64 dimensional and 400 dimensional features respectively from the proposed scheme.

Extraction of English Multi-oriented and Curved Text line, U.PAL*, N.SHARMA*, N.TRIPATHY*, and F.KIMURA: IEEE International Conference on Signal and Image Processing (ICSIP), Macmillan Advanced Research, Vol.-2, pp.581-586, 2006

There are many printed artistic documents where text lines of a single page may have different orientations or they may be curved in shape. For the OCR of such documents we have to extract individual text lines from the documents. Extraction of individual text lines from multi-oriented and/or curved text document is a difficult problem. In this paper, we propose a bottom-up approach to extract individual text lines from English artistic document pages and the method is based on the foreground and background information of the characters of the text lines. Here at first, individual components are detected and grouped into candidate clusters using the positions of the center of gravity (CG) of the components and the background information obtained from the components using water reservoir concept. From each candidate cluster we find some candidate points based on the water flow level of the reservoirs obtained from the components of the cluster. Finally, based on these candidate points, individual clusters are grouped to extract different text lines from a document.

Department of Physics Engineering

*nonmember

Successive Phase Transitions in Antiferroelectric Liquid Crystal Systems -An Axial Next-Nearest-Neighbor XY Model with Biquadratic Interaction, M. Koroishi, M. Torikai and M. Yamashita: *Ferroelectrics* 344, 125-132, 2006

An axial next-nearest-neighbor XY model is studied as a model of chiral liquid crystals which exhibit many ferro-, ferri- and antiferroelectric tilted smectic phases. Depending on the values of interaction parameters, this model exhibits Ising symmetric (i.e., the tilt directions of directors are parallel or anti parallel) phases or XY symmetric phases. Phases with each type-of-symmetry show the character of devil's staircase, which has been observed in experiments.

Symmetry of Nematic Phase and Oblique Axial Order, M. Yamashita and M. Torikai: *J. Phys. Soc. Jpn.*, 75, 104601-1-6, 2006

Nematic order is usually described by a uniaxial order parameter, or occasionally by a biaxial order parameter together with the uniaxial one, in a typical configuration. In a general case of a system exposed to two different types of external fields, e.g., an electric field and a magnetic field, an additional order parameter, here called an oblique axial order parameter, is shown to be necessary, in addition to the above order parameters, to describe transition phenomena of the system correctly. The symmetry of the phase with the triplet of the order parameters is discussed. Effect of the oblique axial order are demonstrated practically in two phenomena: (i) qualitative change of the phase transition when the oblique axial order is neglected; (ii) disappearance of phase transition between ordered phases with different ordering axes when an oblique axial field conjugate to the oblique axial order parameter exists.

Nematic and Smectic Orderings and Commensurability at Thin Liquid Crystal System, S. Murayama, S. Taira, M. Torikai, T. Miyazaki and M. Yamashita: *Proceedings of the 13th Tri-University International Joint Seminar & Symposium 2006*, 364-367, 2006

Liquid crystalline ordering at a very thin system is simulated to study an effect of boundary walls, especially, due to a thickness of the system. The system is composed of Gay-Berne particles of standard values of force parameters, which is sandwiched by parallel walls of homeotropic anchoring. Molecular dynamics simulation is carried out at an NVT ensemble. The system exhibits isotropic, nematic and smectic phases successively as a temperature is decreased. The transition temperature between the nematic phase and the smectic one is shown to change oscillatory as the thickness of the system is increased, and this phenomenon is interpreted as an outcome of a commensurability of the thickness to a layer spacing of the smectic structure.

An empirical potential approach to wurtzite-zinc blende polytypism in group III-V semiconductor nanowires, Toru AKIYAMA, Kosuke SANO, Kohji NAKAMUARA, Tomonori ITO: *Japanese Journal of Applied Physics*, 45, pp.L275-L278, 2006.

The relative stability between wurtzite and zinc blende structures in group III-V semiconductor nanowires is systematically investigated based on an empirical potential, which incorporates electrostatic energy due to

valence-bond and ionic charges. The energy differences between wurtzite and zinc blende structures of 12 compound nanowires with diameter of 1–22 nm show that the wurtzite nanowires are stabilized for small diameter. This structural trend is found to be due to the contribution of two- and three-coordinated atoms on the nanowire facets to the system energy. We also find that the critical diameters, where the nanowires turn out to be bistable forming both wurtzite and zinc blende structures, exist at the diameter of 12–32 nm depending on the ionicity of semiconductors. The bistability implies the synthesis of nanowires exhibiting polytypes, and supports the experimental results in GaP, GaAs, InP, and InAs nanowires.

Mechanism of oxide deformation during silicon thermal oxidation, Hiroyuki KAGESHIMA*, Masashi UEMATSU*, K. AKAGI*, Shinji TSUNEYUKI*, Toru AKIYAMA, Kenji SHIRAIISHI*: *Physica B*, 376-377, pp.407-410, 2006.

Mechanisms of oxide deformation during silicon thermal oxidation are studied by investigating the energetics of intrinsic point defects in the bulk silicon oxide and in the oxide film of the silicon oxide/silicon interface with first-principles calculations. The results suggest that the SiO_2 and the SiO interstitials are thought to relate to the deformation of the silicon oxide. Especially, during the silicon oxidation, the SiO interstitial is suggested to be important because it can be formed in the oxide film neighboring to the interface and can enhance the deformation of the oxide films.

A simple approach to polytypes of SiC and its application to nanowires, Tomonori ITO, Kosuke SANO, Toru AKIYAMA, Kohji NAKAMURA: *Thin Solid Films*, 508, pp.243-246, 2006.

SiC polytypes in bulk form and nanowire are systematically investigated using our empirical potential that is based on a simple approach, and which incorporates electrostatic energies due to bond charges and ionic charges. Using the empirical potential, the system energies of 3C (zinc blende), 6H, 4H and 2H (wurtzite) structured SiC in bulk form are calculated and compared with ab initio calculations and experimental results. Our calculated results reveal that 3C–SiC is the most stable while 2H–SiC is unstable among these structures at 0 K. This is consistent with experimental results. The appearance of polytypes in bulk form is qualitatively discussed by considering ionicity of semiconductors based on our simple approach. Furthermore, we clarify the versatility of our simple approach to nanostructures considering SiC nanowire. Hexagonal SiC nanowire stabilizes a 2H structure in the diameter range of $D < 20$ (nm), whereas 3C–SiC is stabilized only at a large diameter range beyond 20 (nm). This is also consistent with experimental findings for InAs and InP nanowires. SiC polytypes in nanowire are discussed in terms of the ratio of the number of surface dangling bonds to the total number of interatomic bonds.

A first-principles study of O_2 incorporation and its diffusion in compressively strained high-density silicon oxides, Toru AKIYAMA, Keiichi KAWAMOTO, H. KAGESHIMA*, M. UEMATSU, Kohji NAKAMURA, Tomonori ITO: *Thin Solid Films*, 508, pp.311-314, 2006.

The microscopic mechanisms of O_2 diffusion in compressively strained high-density silicon oxides are investigated based on first-principles total-energy calculations. It is found that, both in high-density α -quartz and in α -cristobalite, the calculated incorporation energies and energy barriers increase with increase of oxide density. Independent of the structure of oxides, the calculated activation energies increase with increasing density. Furthermore, the calculated activation volumes suggest that the oxidation retardation by the oxidation-induced strain is due to the retardation of O_2 diffusion in the high-density region, qualitatively consistent with experimental results.

Spin-spiral structures in free-standing Fe(110) monolayers, Kohji NAKAMURA, Naoki MIZUNO, Toru AKIYAMA, Tomonori ITO, A. J. FREEMAN*: *Journal of Applied Physics*, 99, pp.08N501-1-3, 2006.

Electronic and magnetic structures in spin-spiral structures of free-standing Fe(110) monolayers with lattice constants, a , matching those of bulk bcc Fe (2.87 Å) and W (3.16 Å), were investigated by means of first-principles film full-potential linearized augmented-plane-wave calculations including intra-atomic noncollinear magnetism. For $a=2.87$ Å, the spin-spiral structures with wavelength around $7a$ are energetically favored over the collinear ferromagnetic state while those for $a=3.16$ Å turn out to be less favorable. The formation of the spin-spiral structures are found to result from a Fermi-surface nesting that leads to an instability of the ferromagnetic state. In addition, the spin-orbit coupling is found to play an important role to determine the magnetization rotation. These results offer an important step in understanding complex noncollinear spin-spiral magnetism in thin films.

Structural stability and electronic structures of InP nanowires: Role of surface dangling bonds on nanowire facets, Toru AKIYAMA, Kohji NAKAMUR, Tomonori ITO: *Physical Review B*, 73, pp.235308-1-6, 2006.

The structural stability and electronic properties of InP nanowires (NWs) are investigated based on first-principles pseudopotential calculations. In contrast to the bulk phase, zinc-blende (ZB) NWs are found to be less favorable over wurtzite (WZ) NWs, in which the surface dangling bonds (DBs) on the NW facets play a crucial role to stabilize the WZ structure. Our analysis of the NW cohesive energy based on the number of DBs also suggests the bistability forming both ZB and WZ NWs around 120 Å diameter and the formation of rotational twin structures around 400 Å diameter being consistent with experiments. Furthermore, the stable WZ NWs are found to be semiconducting whose characteristics are dependent on the surface DBs as well as the NW size and shape. The estimated oscillator strength also indicates the possibility of efficient light emission originating from the direct gap and geometrically restricted excitonic effects.

Stacking sequence preference of pristine and hydrogen-terminated Si nanowires on Si(111) substrates, Toru AKIYAMA, Kohji NAKAMURA, Tomonori ITO: *Physical Review B*, 74, pp.033307-1-4, 2006.

The hexagonal versus cubic structural preference in vertically grown silicon nanowires on Si(111) substrates is systemized by using first-principles pseudopotential calculations. The calculated formation energy for pristine and H-terminated silicon nanowires with both hexagonal and cubic stacking sequences demonstrates that the stability depends on hydrogen chemical potential and the hexagonal-type nanowires are energetically favorable over a wide range of hydrogen chemical potential. This preference offers a possible origin for little detection of the [111]-oriented silicon nanowires with small diameters, qualitatively consistent with experimental findings.

Thermodynamic stability of $\text{In}_{1-x-y}\text{Ga}_x\text{Al}_y\text{N}$ on GaN and InN, Yoshihiro KANGAWA*, Koichi KAKIMOTO*, Tomonori ITO, Akinori KOUKITSU*: *Physica Status Solidi (c)*, 3, pp.1700-1704, 2006.

Monte Carlo simulations of InGaN MOVPE were carried out to investigate the relationship between growth conditions and atomic arrangement in thin films grown on (0001) and (11 0). In the case of small input partial pressures of indium, it was found that compositional instability was enhanced during the site exchanging process

instead of the adsorption process. Moreover, it was found that compositional fluctuation in thin films grown on (11 0) is smaller than that in thin films grown on (0001). This suggests that accumulated stress near the growth surface influences the compositional fluctuation.

Theoretical study on atomic structures of thermally grown silicon oxide/silicon interfaces, Hiroyuki KAGESHIMA*, Masashi UEMATSU*, K. AKAGI*, Shinji TSUNEYUKI*, Toru AKIYAMA, Kenji SHIRAIISHI*: e-Journal of Surface Science and Nanotechnology, 4, pp.584-587, 2006.

The reason why previous researchers have reported many different atomic structures such as cristobalite, tridymite, and quartz for the thermally grown silicon oxide/silicon interfaces is studied by following the possible interface structures during the oxidation processes using the first-principles calculations. The results show that the cristobalite-like structures can be easily formed from the silicon diamond structure. Proceeding with the oxidation, compressive strains are accumulated in these cristobalite-like regions. To significantly release these accumulated strains, it is considered that the cristobalite-like regions change into less strained tridymite-like structures and finally more relaxed quartz-like structures. If the transformation occurs without lateral ordering, then the transformed interfacial structure does not have any order and should be amorphous. This explanation provides us with a unified understanding of the interfacial atomic structures.

Oxygen trap hypothesis in silicon oxide, Hiroyuki KAGESHIMA*, Masashi UEMATSU*, Toru AKIYAMA, Tomonori ITO: Japanese Journal of Applied Physics, 45, pp.7672-7674, 2006.

A hypothesis on the atomic structure of silicon oxide is proposed to explain the discrepancy between theoretical and experimental studies on the oxygen diffusion and the interfacial reaction during the thermal silicon oxidation process. The hypothesis says that silicon oxide contains “oxygen traps”, in which the molecular oxygen can be located with almost 0 dissolving enthalpy. The density of the “traps” is $\sim 10^{16} \text{ cm}^{-3}$. A possible local structure is also proposed based on the first-principles calculations.

Magnetic and electronic structures of zinc-blende ferromagnetic/antiferromagnetic Interfaces, Yoshinori KATO, Toru AKIYAMA, Kohji NAKAMURA, Tomonori ITO: e-Journal of Surface Science and Nanotechnology, 4, pp. 58-62, 2006.

Magnetic structures at zinc-blende ferromagnetic (FM) and antiferromagnetic (AFM) interfaces, CrAs/Cr, CrAs/GaAs/Cr, and CrSe/MnSe, were investigated by means of the full-potential linearized augmented plane-wave method in order to search the half-metallic exchange bias interfaces. The CrAs/Cr structure is found to lose the half-metallicity at the CrAs interface while the CrAs/GaAs/Cr structure retains the half-metallicity but the energy difference between parallel and antiparallel moment alignments of the FM and AFM layer at the interface significantly reduces. In contrast, the CrSe/MnSe interface induces an excellent half-metallicity, which importantly offers a key ingredient as a promising half-metallic exchange bias.

Half-metallic exchange bias ferromagnetic/antiferromagnetic interfaces in transition-metal chalcogenides Kohji NAKAMURA, Yoshinori KATO, Toru AKIYAMA, Tomonori ITO, A. J. FREEMAN: Physical Review Letters, 96, (4), pp. 047206-1-4, 2006.

To investigate half-metallic exchange bias interfaces, magnetic structures at ferromagnetic (FM)/antiferromagnetic (AFM) interfaces in the zinc blende transition-metal chalcogenides, CrSe/MnSe and CrTe/MnTe with compensated and uncompensated AFM interfaces, were determined by the full-potential linearized augmented plane-wave method. With the uncompensated AFM interface, an antiparallel alignment of the Cr and Mn moments induces an excellent half-metallicity. More striking still, in the compensated AFM interface the Cr moments in the FM layer lie perpendicular to the Mn moments in the AFM layer but the Mn moments strongly cant to induce a net moment so as to retain the half-metallicity. These findings may offer a key ingredient for exchange biased spintronic devices with 100% spin polarization, having a unidirectional anisotropy to control and manipulate spins at the nanoscale.

Transport mechanism of interfacial network forming atoms during silicon oxidation, Hiroyuki KAGESHIMA*, Masashi UEMATSU*, K. AKAGI*, Shinji TSUNEYUKI*, Toru AKIYAMA, Kenji SHIRAISHI*: Japanese Journal of Applied Physics, 45, pp. 694-699, 2006.

A first-principles study on the energetics of the structural transformation at the interfaces revealed that oxygen vacancies can accompany the high density oxide regions formed during the silicon oxidation. The vacancies can also promote the effective out-migration of these regions, which allows the easier oxide viscous flow to release the interfacial strain. Compared with this mechanism, self-interstitials are rarely formed in the silicon substrate. These results also suggest defect formation mechanisms around the interfaces.

Development of a Super Broadband RF Splitter Using Bead Type Ferrite Core Transformers, T. KANIE*, H. KATO, Y. NORO and T. TAKEO: Proc. of 11th International Ceramic Congress Advances in Science and Technology 45, pp.2576-2581, 2006

Recent developments in information technologies require various communication devices to operate at a higher speed and in a wider frequency range in order to accommodate a vast amount of data. A RF Splitter whose function is to divide an input signal into multiple outputs is the most popular passive device in CATV networks and consists of transformers using ferromagnetic materials such as ferrite. Nowadays, because of the circumstances stated above, the RF splitter for CATV systems must operate in an extremely wide frequency range in order to transmit a large number of channels multiplexed with a frequency division technique. In other words, its loss should be as small as possible in that region. We have studied the broadening of the operative frequency by investigating how the ferrite core parameters including the magnetic permeability, shape, surface mounting of the core, etc. affect the transmission characteristics. We examined the relationship between each of these parameters and the transmission characteristics through a computer simulation and fabricated a device based on the calculations. It was found that by selecting the appropriate parameters, excessive splitter loss could be suppressed to less than 3.5dB in the range of 10MHz to 3,000MHz.

Preparation of Magnetic Tunnel Transistors with Double Tunnel Junctions, Haruki NAKANISHI, Haruki OMAE, Yuji FUJIWARA, Mutsuko JIMBO*, Tadashi KOBAYASHI, Shigeru SHIOMI: J. Magn. Soc. Jpn., 30, pp.188-191, 2006.

Magnetic tunnel transistors (MTTs) with double tunnel junctions were prepared in order to investigate the emitter voltage dependence of a magneto-current (MC). A three-terminal structure was fabricated, using metal shadow masks. It was observed that hot

electrons contributed to a collector current. A transfer ratio of over 10^3 was obtained in an MTT with double tunnel junctions. The MC decreased gradually with increasing emitter voltage. The emitter voltage at which the MC decreased to half its original value was over 1.5 V.

Magnetics Education in Companies, Magnetics Education in Universities, Tadashi KOBAYASHI: *Magn. Jpn.*, 1, pp.370-374, 2006.

It seems that some gap exists between magnetics education in companies and in universities. To bridge the gap, if necessary, universities should deliver lectures to companies. Furthermore, universities should educate students to obtain an exact understanding of physical phenomena. For this purpose, experience is very important. Various teaching materials for experiments are introduced, e.g. diamagnetic substances and magnets to demonstrate repulsion, paramagnetic substances and magnets to demonstrate attraction, speakers made from corrugated boxes, and microphones. It is also important to show that how theory is put to practical use.

Oil Solidified High-Pressure Traction Curve Estimation with Spin by Elastic Contact Mechanics, Yuichi NAKAMURA and Masane FUNAHASHI: *Trans. of JSME, Ser. C*, 72-717, pp. 1653-1659, 2006

Traction curves are fundamental data for the design of traction-type continuously variable transmission (tCVT) of automobiles, in which maximum hertzian contact pressure exceeds 3GPa. Under such high contact pressure, oils seems to behave like solid lubricants and elastic contact mechanics (creep theory) seems to be appropriate for evaluation of traction curves similar to that of railway wheels. In the present study, oil-solidified high-pressure traction curves with spin were roughly and simply calculated up to 3 GPa based on creep theory together with maximum traction coefficients of pure roll experimental data of reference. Calculated curves were almost consistent with several reference experimental ones of various conditions (speed, geometry of test machine). This consistency proved that main factor of oil-solidified high-pressure traction curves with spin is creep theory and main rheological property of oils is the limiting shear stress.

High-Pressure Viscosity Measurements of Vegetable Based Biodegradable Lubricant Oils up to 2.5 GPa and Tribological Characteristics, Y. Nakamura, H. Matsubo, K. Yoshizaki and H. Komiya,; *Proc. Int. Tribology Conf., Austrib 2006*, CD, 108, pp. 1-6, 2006

In order to provide environmentally friendly lubrication with high-pressure rheological and tribological data of several biodegradable vegetable oils, their viscosity and phase transition were evaluated up to 2.5 GPa at up to 200°C employing a falling sphere method in a diamond-anvil pressure cell. Also, friction and wear properties for these oils were evaluated employing a SRV tribo-tester. Similar high-pressure viscosity characteristics of 7 oils including rapeseed oil, soybean oil and polyol ester (POE) were observed. The pressure-viscosity coefficients of all the oils around the maximum pressure were 12 /GPa at 0.2-0.4 GPa and at 40°C, 7 /GPa at 0.5-1.4 GPa and at 100 °C, 3-4 /GPa at 1.8-2.7 GPa and at 200°C. For most oils, the sphere stopped falling over about 10 Pa·s at all temperatures and pressures evaluated. Finally, lubricant oils, except POE, were observed to transit to polycrystal-like phase. Friction coefficients for the vegetable oils were evaluated between 0.09 and 0.12, and between 0.12 and 0.14 for POE. The wear amount of POE was observed to be more than twice larger than that of the vegetable oils.

Fabrication of LSMO Single Layers and LSMO/YBCO Double Layers, Hong ZHU, Masanori OKADA, Atsushi KAMIYA, Ajay Krishno SARKAR, Masahito MATSUI, Md. Motin SEIKH and Tamio ENDO: International Journal of Nanoscience, 5–4 & 5, pp. 511–515, 2006

(La, Sr)MnO₃ (LSMO) single-layer and LSMO/YBCO double-layer films have been grown on LAO and MgO substrates using ion beam sputtering. For LSMO single-layer films, the highly epitaxial films can be grown at lower substrate temperatures down to 500°C. The epitaxy of the films, which is degraded with increasing TS, can be restored by supply of plasma oxygen. Smaller lattice mismatch of LSMO on LAO gives two-dimensional step-and-terrace type growth, whereas on MgO grain type growth is observed due to larger mismatch. For the double-layer films, LSMO layer can be grown epitaxially on a-oriented YBCO underlayer, but a part of the underlying a-YBCO is changed into c-YBCO during the deposition of overlayer. For c-YBCO underlayer, a part of the underlying c-YBCO is changed into (110)-oriented phase after the deposition of overlayer. Then it is necessary to deposit the overlayer at lower temperatures.

Abstracts of Books and Reviews (2006)

Department of Mechanical Engineering

*nonmember

Fundamentals of Jet Flow Phenomena, Toshihiko SHAKOUCHI, *Journal of Refrigeration*, 81-941, pp.213-219, 2006.

Control of Jet Flow Phenomena and the Advanced Application Technology, Toshihiko SHAKOUCHI, *Journal of Science of Machine*, 58-10, pp.1023-1030, 2006.

JSME Mechanical Engineer's Handbook, Fundamentals-α4: Fluids Engineering, * 10.4 Liquid Oscillation in Container, Toshihiko SHAKOUCHI, joint work, Japan Society of Mechanical Engineers, Maruzen, pp.α4- 118-120, 2006.

Department of Electrical and Electronic Engineering

*nonmember

Lattice Constants of Semiconductors [in Japanese], Kazumasa HIRAMATSU: Widegap Semiconductors Optical and Electronic Devices, pp.84-88, 2006

AlGa_N, AlN and AlGa_N/Ga_N Heterostructures [in Japanese], Kazumasa HIRAMATSU: Widegap Semiconductors Optical and Electronic Devices, pp.368-374, 2006

Department of Chemistry for Materials

* nonmember

Fullerene Reactivity — Fullerene Cations and Open-Cage Fullerenes, Toshikazu KITAGAWA, Yasujiro MURATA*, and Koichi KOMATSU*: Carbon-Rich Compounds. From Molecules to Materials, Wiley-VCH, Weinheim, pp. 383-420, 2006

Rapid and Selective Production of Hybridoma Cells Secreting Novel Monoclonal Antibodies Based on Short-Term Immunization, Masahiro TOMITA, Yoshiharu ASAOKA, Takatomi FUKUDA, Takanobu TANIGUCHI, Jun-ichiro TANAKA, Shin OGATA*, Tian Yow TSONG*, Tetsuro YOSHIMURA: Human Antibodies, 15 (1,2), pp. 33-35, 2006

Stabilities and Chemical Mechanical Polishing Properties of Ceria Particles [in Japanese], Norifumi SHIMONO, Masami KAWAGUCHI: Polymer Processing, 55 (2), pp. 72-76, 2006

Structure and Property Measurements of Polymers at Surfaces and Interfaces [in Japanese], Masami KAWAGUCHI: A Laboratory Guide to Structure and Property Measurements of Organic Compounds and Polymers for Young Chemists, Kohdansha Scientific, Part 3, Chapter 24, pp. 322-329, 2006

Added Polymer Effects on Stabilization of Dispersion Systems [in Japanese], Masami KAWAGUCHI: Science and Technology on Dispersion of Nano-particle, CMC Books, Chapter 9, pp. 125-134, 2006

Ekogarasu to Serufukuriningugarasu no Kaihatsu [in Japanese], Tadanori HASHIMOTO: Kinouseigarasu·Nanogarasu no Saishingizyutsu, NTS, pp. 291-303, 2006

Treating Technology of Waste PVC [in Japanese], Franck DUMEIGNIL, Weihua QIAN, Atsushi ISHIHARA: Petrotech 29(6), pp.422-427, 2006

Survey of Treating Technology of Waste PVC [in Japanese], Franck DUMEIGNIL, Weihua QIAN, Atsushi ISHIHARA: Kagakukougyo, 58(1), pp.65-73, 2007

Journal of artificial organs 2005: the year in review, Yoshiki SAWA, Takashi HORIUCHI, Akio KISHIDA, Toru MASUZAWA, Kazumi MIZUGUCHI, Motonobu NISHIMURA, Takafumi OKOSHI, Takehiro SHINZATO, Eisuke TATSUMI, Yasuko TOMIZAWA, Hiroshi WATANABE, J Artif Organs 9:1-7, 2006

医用材料工学、共著：堀内 孝、村林 俊、コロナ社 2006年2月